INTO THE HEART OF DARKNESS

THEORY AND PHENOMENOLOGY OF REGULAR BLACK HOLES

Jacopo Mazza

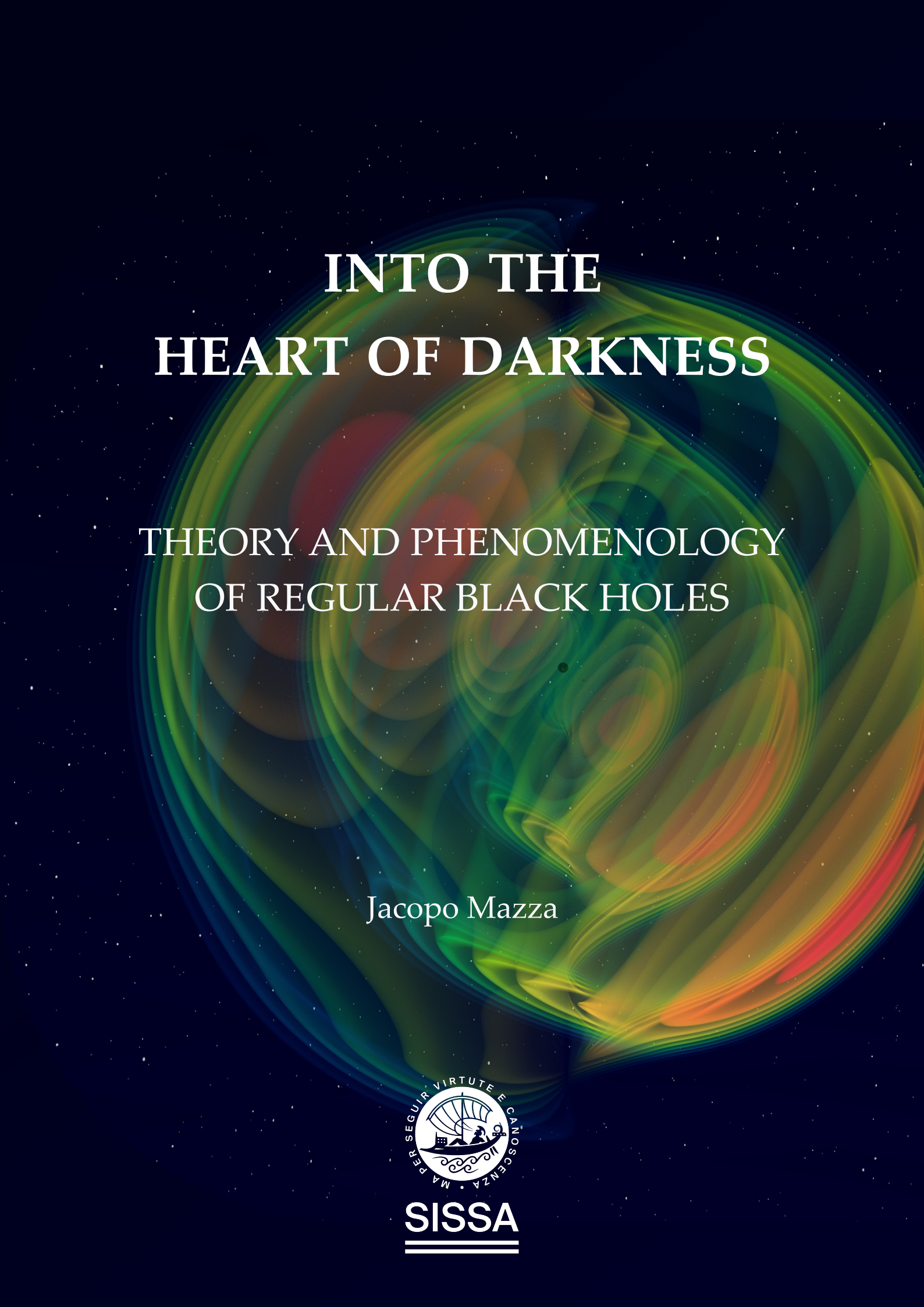

SISSA

The cover is drawn over a still from a simulation by

N. Fischer, H. Pfeiffer, A. Buonanno (Max Planck Institute for Gravitational Physics), Simulating eXtreme Spacetimes (SXS) Collaboration

https://www.ligo.caltech.edu/image/ligo20200420a

INTERNATIONAL SCHOOL FOR ADVANCED STUDIES
PHYSICS AREA
PHD COURSE IN ASTROPARTICLE PHYSICS

DOCTORAL THESIS

INTO THE HEART OF DARKNESS

THEORY AND PHENOMENOLOGY OF REGULAR BLACK HOLES

CANDIDATE:
JACOPO MAZZA

ADVISOR:
STEFANO LIBERATI

ACADEMIC YEAR 2022-2023

We knew the world backwards and forwards
So small it fit in a handshake
So easy it could be described in a smile
As plain as the echoes of old truths and a prayer

History did not greet us with triumphant fanfare
It flung dirty sand in our eyes
Ahead of us were distant roads leading nowhere
Poisoned wells, bitter bread

The spoils of war is our knowledge of the world
So large it fits in a handshake
So hard it could be described in a smile
As strange as the echoes of old truths and a prayer.

— Wisława Szymborska, 1945
translated by Joanna Trzeciak

ABSTRACT

Spacetime singularities are a generic prediction of general relativity. They are believed to mark the breakdown of the theory and, for this reason, they represent one of the main drivers for the search for alternative theories of gravity; in particular, it is commonly expected that the formation of singularities will be prevented in a full theory of quantum gravity. In this view, it is reasonable to assume that non-singular — or *regular* — metrics can provide an effective description of the outcome of gravitational collapse and a credible alternative to general-relativistic black holes.

In this thesis, we explore such hypothesis by providing strategies for constructing regular geometries of various kinds: simply and multiply connected, with and without horizons — thus exhausting all of the qualitatively different alternatives. The approach is largely theory-agnostic, with particular emphasis being placed on rotating models.

Ample room is devoted to a specific family of regular geometries known as *black bounces*. They represent wormholes that may or may not exhibit horizons, depending on the value of one parameter. The thesis describes the construction of the black-bounce counterparts to the Kerr and Kerr–Newman geometries; scalar test-field perturbations to one of these metrics are then examined by computing the quasi-normal modes and the superradiant amplification factors.

The discussion is then specialised to the context of a compelling candidate quantum theory of gravity: non-projectable Hořava gravity. In particular, regular black holes and horizonless ultra-compact objects are constructed under the assumption of staticity and spherical symmetry, and analysed through the lenses of the theory's low-energy limit. In preparation to the addition of rotation, a Kerr black hole solution is then examined in the closely related Einstein–æther theory.

This thesis thus contributes to the investigation of alternative descriptions for astrophysical black holes beyond general relativity, particularly with regards to regular black holes and horizonless black-hole mimickers. Therefore, it naturally aligns with the research programme of quantum gravity phenomenology.

PUBLICATIONS

The thesis is based on the following publications.

[P1] Edgardo Franzin, Stefano Liberati and Jacopo Mazza. *The Kerr Black Hole in Einstein–Æther Gravity*. In preparation. 2023.

[P2] Edgardo Franzin, Stefano Liberati, Jacopo Mazza, Ramit Dey and Sumanta Chakraborty. 'Scalar Perturbations around Rotating Regular Black Holes and Wormholes: Quasi-Normal Modes, Ergoregion Instability and Superradiance'. Phys. Rev. D **105**.12 (2022), p. 124051. arXiv:2201.01650.

[P3] Edgardo Franzin, Stefano Liberati, Jacopo Mazza, Alex Simpson and Matt Visser. 'Charged Black-Bounce Spacetimes'. J. Cosmol. Astropart. Phys. **2021**.07 (2021), p. 036. arXiv:2104.11376.

[P4] Edgardo Franzin, Stefano Liberati, Jacopo Mazza and Vania Vellucci. 'Stable Rotating Regular Black Holes'. Phys. Rev. D **106**.10 (2022), p. 104060. arXiv:2207.08864.

[P5] Jacopo Mazza, Edgardo Franzin and Stefano Liberati. 'A Novel Family of Rotating Black Hole Mimickers'. J. Cosmol. Astropart. Phys. **2021**.04 (2021), p. 082. arXiv:2102.01105.

[P6] Jacopo Mazza and Stefano Liberati. 'Regular Black Holes and Horizonless Ultra-Compact Objects in Lorentz-Violating Gravity'. J. High Energ. Phys. **2023**.3 (2023), p. 199. arXiv:2301.04697.

ACKNOWLEDGMENTS

With this thesis' defence my educational path is formally over. The road has been bumpy at times — as for everybody, and perhaps less so for me than for others —, but I can confidently say I walked it with pleasure. Clearly, this is not my exclusive merit. On the contrary, reaching this goal would not have been possible without the constant support of many people, whom I shall thank in person; and without the occurrence of multiple circumstances, often fortuitous in nature and largely beyond my control.

I believe that publicly acknowledging (at least some of) these circumstances is a useful exercise in intellectual honesty. Hence, I write these few lines, hoping they will offer some food for thought to whomever might read them.

Finding myself in a welcoming, healthy and supportive work environment has been crucial. For this, I have to thank first of all my advisor, Stefano, who was able to orient my (our) research while nurturing my independence. I should then thank all my collaborators, especially Edgardo: interacting with them I could acquire and refine the technical competences that made me a practitioner of scientific research. Finally, an honourable mention goes to SISSA, which — though still with some deficiencies — shows an attention to the workers' wellbeing that is not quite common.

Even within such an environment, the PhD can be an extremely stressful experience. I had the luck of facing it surrounded by people who, with affection and intelligence, could offer me their support. These relationships constituted a safety net that always empowered me throughout this journey.

Finally, I cannot ignore a fact: I was born and raised in a cultural, social and economic context in which my interest towards the sciences could arise; I then had access to the material means I needed to pursue such interest, to the point of making a passion my profession.

Judging those who accomplish such goal as "deserving" — in contrast to those who "did not measure up" — seems to me a gross and inappropriate oversimplification. Indeed, such judgement ignores important context information and, most importantly, it diverts the attention away from the profound distortions that afflict the world of academia. Hence, I wished to pay tribute to the seinsibility and humanity of the people I met, hoping those will inspire similarly positive behaviours in everybody — me included.

RICONOSCIMENTI

Con la difesa di questa tesi si conclude formalmente il mio percorso di studi: la via è stata a volte accidentata – come per tutti, e anzi per me forse meno che per tanti –, ma posso dire di averla percorsa con piacere. Ciò non è evidentemente mio merito esclusivo. Al contrario, non sarebbe stato possibile raggiungere questo traguardo senza il supporto costante di molte persone, che ringrazierò di persona; e senza il realizzarsi di molteplici circostanze, più o meno fortuite e in larga parte fuori dal mio controllo.

Ritengo che riconoscere pubblicamente (almeno alcune di) queste circostanze sia un utile esercizio di onestà intellettuale e perciò scrivo queste righe, sperando offrano interessanti spunti di riflessione a chi le leggerà.

Trovare attorno a me un ambiente di lavoro accogliente, sano e solidale è stato cruciale. Per questo devo ringraziare prima di tutto il mio relatore, Stefano, che ha saputo orientare la mia (la nostra) attività di ricerca, nutrendo allo stesso tempo la mia indipendenza. E, in secondo luogo, tutte le persone con cui ho collaborato, specialmente Edgardo: confrontandomi con loro ho potuto acquisire ed affinare le competenze tecniche che mi hanno reso un praticante della ricerca scientifica. Una menzione particolare va alla SISSA, realtà che pur ancora con alcune carenze dimostra un'attenzione per il benessere di lavoratori e lavoratrici non del tutto comune.

Anche in un tale ambiente, il dottorato di ricerca rimane un'esperienza potenzialmente molto stressante. Io ho avuto la fortuna di affrontarla circondato da persone che, con affetto e intelligenza, hanno saputo offrirmi il loro supporto: una vera e propria rete di sicurezza, fatta di robuste relazioni familiari e amicali, la cui presenza mi ha sempre dato forza.

Infine, non posso ignorare un fatto: sono nato e cresciuto in un contesto culturale, sociale ed economico nel quale il mio interesse per le scienze è potuto sorgere; mi sono poi trovato nelle condizioni materiali di poter perseguire tale interesse, fino al punto di fare di una passione la mia professione.

Giudicare chi porta a termine un tale percorso come "meritevole" – in contrapposizione a chi invece "non è stato all'altezza" – appare perciò una semplificazione grossolana e, a mio avviso, fuori luogo. Tale giudizio ignora infatti importanti condizioni di contesto e, soprattutto, distoglie l'attenzione dalle profonde storture che affliggono il mondo accademico. Ho quindi voluto rendere omaggio alla sensibilità ed all'umanità delle persone che ho incontrato, nella speranza che queste possano ispirare comportamenti virtuosi in tutte e tutti – me per primo.

CONTENTS

LIST OF FIGURES

ACRONYMS

ADM	Arnowitt–Deser–Misner
BH	black hole
RBH	regular black hole
GR	general relativity
KH	Killing horizon
UH	universal horizon
ISCO	innermost stable circular orbit
NJP	Newman–Janis procedure
MNJP	modified Newman–Janis procedure
QNM	quasi-normal mode
dS	de Sitter
AdS	anti de Sitter
SV	Simpson–Visser
WKB	Wentzel–Kramers–Brillouin

1 INTRODUCTION

E ora noi lo vediamo. Non staccare l'occhio dal telescopio, Sagredo. Quello che stai vedendo è che non esiste differenza tra il cielo e la terra. Oggi, 10 gennaio 1610, l'umanità scrive nel suo diario: abolito il cielo!
— Vita di Galielo, Bertolt Brecht

The first two decades of the XXI century have been generous in momentous achievement for gravitational physics. On the wave of these successes, expectations are high for the coming years, as the near future has the potential for breaking current records.

Gravitational waves are the prime source of this excitement. The groundbreaking first detection [126] has been a watershed: there was physics *before* GW150914, and there is physics *after* GW150914. The new physics is characterised by multimessenger observations, starting with GW170817 [123–125]; and rich catalogues of gravitational-wave transients [2, 127, 128], comprising 90 events to date. Meanwhile, as LIGO, Virgo and KAGRA enter their fourth observing run, the planning of future ground-based [76, 217, 254, 299, 302, 311] and space-born [18, 40] gravitational-wave detectors is well under way.

Furthermore, recent results from NANOGrav [337–341] and other pulsar timing array collaborations provide evidence for a low-frequency background of gravitational waves.

Most gravitational-wave events — including, most likely, those sourcing the stochastic background — are associated to astrophysical BHs. These dark and ultra-compact objects are characterised by the most intense curvatures found in the present-day universe, and for this reason they represent the best hope for testing our current understanding of gravity [365].

Notably, BHs can additionally be probed through electromagnetic observations. In this cases, the BHs are surrounded by matter, e. g. in an accretion disk [6], that emits radiation at different wavelengths [28], from the X-ray [30] all the way to the millimetre and below. By studying such emission, the Event Horizon Telescope collaboration managed to compose the first "picture" of (the shadow of) the supermassive BH M87* [329–336]; soon thereafter, the same techniques were applied to our own Sgr A* [155–160].

The centre of the Milky Way is particularly well observed, since the innermost stars orbiting Sgr A* — the S-star cluster — have been tracked for decades. Notably, the passage of the star S2 by its pericentre, located at a distance of approximately 1400 Schwarz-

schild radii from Sgr A*, allowed to measure two hallmark gravitational effects, namely redshift of light [121, 142] and pericentre precession [122].[1]

Hence, there is hope that the next decades will bring new *observational* insight [8, 35, 59] to guide the research on the many *theoretical* and *conceptual* issues that the existence of BHs, as general relativity (GR) conceives them, brings about. One such issue is the prediction that BHs conceal a spacetime singularity and that such singularities unavoidably form during gravitational collapse under mild and generic assumptions.

Despite its observational successes, reasons to doubt GR abound. One among the many: GR cannot be quantised perturbatively in any way similar to other fundamental interactions and, as of yet, there is no fully consistent and "definitive" theory of quantum gravity. For this reason, there is a widespread belief within the community of researchers who specialise in gravity that whatever "new physics" lies beyond GR, it will solve the puzzles pertaining spacetime singularities.

Though such solution might come in different forms, considerable effort has been directed into investigating the simplest of such forms: namely, that singularities will be *regularised* through mechanisms that can be captured effectively within the standard tools of differential geometry. In this view, astrophysical BHs should be better described by non-singular — or *regular* — models. These models may display horizons, hence describe regular black holes (RBHs), or not, in which case they represent horizonless (exotic) compact objects [107].

This thesis is devoted to exploring this hypothesis and its consequences. We will do so by providing general guiding principles for building regular models; then construct and analyse at length few specific examples.

Countless other examples exist, as the past years have witnessed the birth of a thriving industry around the construction of regular models that could mimic astrophysical BHs — among which, RBHs and wormholes will be particularly relevant for what follows. Providing a comprehensive account of the numerous alternatives, if ever possible, lies beyond the scope of the thesis. The bibliography we provide will thus not do justice to the richness of the current literature.

The thesis comprises three parts: part i collects background material on the topic of spacetime singularities and explains how these can be avoided in the simplest settings; part ii is devoted to the analysis of a specific family of regular models known as *black bounces*, which describe a wormhole possibly with horizons; finally, part iii contextualises regular models in the framework of specific modifications of

1 Cf. the motivation for the 2020 Nobel prize in physics to Reinhard Genzel and Andrea Ghez.

GR characterised by violations of local Lorentz invariance, namely Hořava gravity and Einstein–æther theory.

Specially, chapter 2 reviews different notions and rigorous definitions of spacetime singularities. It then recalls the reasons why singularities are a generic prediction of GR and the multiple ways in which their existence is "problematic". The chapter closes by addressing the (putative) role that new physics beyond GR might play in resolving the issue: remarkably, under the fairly generic assumption that such new physics will regularise singularities, a complete taxonomy of regular geometries can be compiled. Such taxonomy happens to be surprisingly short, as it consists of essentially two large classes: *simply connected* geometries, representing exotic star-like objects or RBHs with multiple horizons; and *multiply connected* geometries, representing wormholes whose throat might be cloaked by one or multiple horizons.

Chapter 3 introduces some common strategies to build regular models. It focuses on the simplest settings of all by assuming staticity and spherical symmetry. On the basis of said taxonomy, it describes well-known examples of simply and multiply connected regular geometries — including the so called Simpson–Visser (SV) metric, the prototypical black-bounce spacetime.

Chapter 4 addresses the issue of rotation — a key feature of any model that aims at describing the phenomenology of astrophysical BHs. It presents a technique, known as the Newman–Janis procedure (NJP), for endowing the models of the previous chapter with spin. The chapter closes with a brief review of past applications of this technique, focusing on open issues.

Chapter 5 opens part ii by presenting the construction of the rotating counterpart to the SV metric: the black-bounce–Kerr geometry. The resulting spacetime is explored and described at length. The chapter follows very closely [270].

Chapter 6 expands the previous chapter by discussing the inclusion of an electric charge. The chapter is based on [166].

Chapter 7 furthers the analysis of the black-bounce–Kerr geometry by investigating its stability against small scalar perturbations. Quasinormal modes (QNMs) and superradiance amplification factors are computed. The chapter follows [165].

This part is closed by chapter 8, which collects a few appendices to the previous chapters.

The following chapter 9 is an interlude. It remains on the issue of stability analysed in chapter 7 but detaches from the main line of reasoning by leaving black bounces aside. Rather, it focuses on the phenomenon of mass inflation, which notoriously renders inner horizons unstable and is therefore particularly relevant for simply connected RBHs. After introducing the topic, the chapter describes a proof-of-concept example of simply connected RBH whose inner horizon is

engineered so to be stable against mass inflation. The chapter follows [167].

Chapter 10 opens part iii by discussing the construction of static and spherically symmetric regular geometries, BHs or exotic horizonless compact objects, in the context of non-projectable Hořava gravity and specifically of its low-energy version, khronometric theory. Focusing on Hořava gravity is motivated by the fact that this theory is constructed to be manifestly power-counting renormalisable; however, its equations of motion are extremely complicated and searching for regular solutions with standard methods is so far out of reach. For this reason, we focus on the low-energy regime and construct regular models following the strategies of chapter 3. The chapter is based on [271].

Extending the results of chapter 10 to include rotation would be tempting and logically the obvious next step. However, this research programme faces an immediate obstacle in that no rotating BH solution is known, as of yet, in khronometric theory. Rotating BHs have been constructed numerically in the closely related Einstein–æther theory, a scalar-vector-tensor extension of GR characterised by the addition of a vector field called æther. These solutions however present the puzzling feature that their horizons are not KHs.

Chapter 11 thus examines a configuration in which the metric is that of Kerr and the æther is determined so that the two give a solution of Einstein–æther theory in a specific corner of the parameters space. The discussion in this chapter is based on ongoing work and is therefore open-ended.

Finally, chapter 12 collects our final comments and closes the thesis.

CONVENTIONS The signature of the metric is $(-,+,+,+)$ except for chapter 10, in which the opposite signature is used. The Riemann tensor is defined as in Wald's book [359]. Spacetime indeces run from 0 to 3 and are denoted with Greek letters μ, ν, ...

We use "geometrodynamics units" units in which $c = G = 1$. However, the effective stress-energy tensor is typically defined through $G_{\mu\nu} = T^{\text{eff}}_{\mu\nu}$, i. e. with a factor of 8π mismatch with respect to the usual stress-energy tensor; chapter 6 is an exception, since the factor 8π is restored there. Anyhow, the appropriate convention is specified in the text whenever needed.

ON COMPUTER ALGEBRA SOFTWARE This thesis would have been much shorter had all computations be done by hand. Fortunately, researchers can now rely on several pieces of software to aid their work [248]. In particular, the current author has extensively employed the `xAct` bundle for Mathematica, specifically the packages `xTensor`, `xCoba`, and to a minor extent `xPert` [78, 258–260].

Part I

BACKGROUND

2

SPACETIME SINGULARITIES IN METRIC THEORIES OF GRAVITY

This thesis is mostly concerned with the regularisation of spacetime singularities, particularly those arising from the gravitational collapse of a localised distribution of matter beyond a trapping horizon — i. e. BH singularities.

It thus seems wise to start the discussion by addressing two fairly basic questions: (i) What are spacetime singularities? and (ii) Why are they believed to be "probemeatic"? Though seemingly innocent at first glance — after all, the topic of singularities is touched upon in most introductory textbooks on BHs —, these questions soon reveal their non-trivial character.

These questions will be addressed in section 2.1, drawing from several standard references [120, 184, 212, 359]. The following section 2.2 will deal with the (putative) role of quantum and/or modified gravity in solving the puzzles of singularities.

2.1 WHAT ARE SINGULARITIES AND WHY ARE THEY PROBLEMATIC?

Our intuition on the subject of spacetime singularities arises from the analysis of a few simple examples, such as the Schwarzschild solution, and the analogy with other (classical) theories of long-range interactions, such as Maxwell's electrodynamics.

In both of these examples, there exist some local observable quantities whose (position-dependent) value "blows up" in the vicinity of a certain point. In the Schwarzschild case, one such quantity is the Kretschmann scalar $R^{\mu\nu\rho\sigma}R_{\mu\nu\rho\sigma}$, which is $\propto r^{-6}$; in the Maxwell's case, one can think of the energy density associated to the electrostatic field of a point charge, whose magnitude is $\propto r^{-4}$. Both quantities diverge in the limit $r \to 0$.

It is generally believed, with reason, that infinity cannot be the outcome of a physical measurement process. So, the fact that these theories predict an infinite value for some observables should be considered as a pathology, a *singularity*, pointing to a deficiency in the theory.

2.1.1 *Curvature singularities*

The previous intuition can be translated into a technical definition.

In GR, all the relevant information pertaining the geometry is encoded in the metric tensor. Because of the theory's invariance under diffeomorphisms, however, one cannot build any (non-trivial) local[1] observable out of the metric alone, nor out of its first derivatives. In fact, the components of the metric and of its first derivatives at a given point are entirely contingent on the choice of coordinates; in particular, one can always find Riemann normal coordinates in a neighbourhood of a point $\overline{x}$ such that

$$g_{\mu\nu}(\overline{x}) = \eta_{\mu\nu} \quad \text{and} \quad \partial_\rho g_{\mu\nu}(\overline{x}) = 0\,. \tag{1}$$

The second derivatives of the metric, instead, cannot be trivialised by a change of coordinates, and indeed it is these derivatives that carry information on the local curvature of spacetime.

Hence, the local observables whose unboundedness will be the telltale of a singularity must be built out of the second derivatives of the metric. More specifically, they will be built out of the Riemann tensor.

Clearly, these arguments apply equally well to alternative theories of gravity in which the metric remains the only carrier of information: we will refer to such theories as *metric* theories , to distinguish them from theories in which additional ingredients are needed in order to fully describe the geometry. So, for instance, higher-derivative theories like $f(R)$ are metric; while metric–affine gravity is not, since the connection is there an independent field. Other notable examples of non-metric theories are the Lorentz-violating Einstein–æther and khronometric theories, to which part iii is devoted. As it will become clear in due time, these cases require a dedicated discussion.

One possibility is to look directly at the components of the Riemann tensor. Consider a curve, and an orthonormal frame that is parallely propagated along the curve;[2] the components of the Riemann tensor in this frame are the tidal forces, experienced by a putative observer moving along the curve, in the direction of the frame's legs. If any of these components is unbounded along the curve, we say that the curve reaches a *p. p. curvature singularity* ("p. p." for "parallely propagated").

The above definition is independent on the choice of frame, since any two frames are related by a Lorentz transformation and unboundedness in one frame implies unboundedness in all frames; but it is quite laborious in practice. An alternative is to look at the scalars built out of the Riemann tensor, the metric and the Levi-Civita completely antisymmetric tensor. If any of them becomes unbounded along a curve, we say that the curve approaches an *s. p. curvature singular-*

1 Clearly, one can build diff-invariant non-local observables out of the metric alone: the length of a curve connecting two points is an example.

2 If the curve is not a geodesic, the proper way of propagating the frame would be Fermi, rather than parallel, transport; using parallel transport, however, seems the standard choice.

ity ("s. p." for "scalar polynomial", since these scalars are, roughly speaking, polynomials in the Riemann).

The relationship between the two definitions is subtle. Clearly, if the components of the Riemann and of the metric are bounded, so are all scalar polynomials. In contrast, it is possible to have diverging components with bounded scalars.

2.1.2 *Curve incompleteness*

Neither of the previous intuitive definitions is very useful in proving theorems concerning singularities. As is well known, a definition in terms of the incompleteness of certain classes of curves turns out to be much more effective.

In particular, an inextendible spacetime is said to be singular if it contains at least one incomplete curve. By inextendible spacetime we mean one that is not isometric to a proper subset of a larger spacetime; by incomplete curve we mean one of finite generalised affine length which has no endpoint in the spacetime, i. e. one which cannot be extended beyond a finite value of its generalised affine parameter.

A spacetime that is singular in this sense is said to be *b-incomplete* ("b" for "bundle"). Clearly, when the curve is a geodesic the definition above reduces to the usual definition of e. g. [359], in terms of which the singularity theorems are formulated. However, for future reference we shall let the curve be arbitrary.

Note that the notion of b-incompleteness brings about a very different way of looking at singularities. Indeed, in the curvature approach the singularity is a genuine point in spacetime, at which some (combinations) of the dynamical fields entering the theory happen to be ill-behaved.[3] Here, instead, the incomplete curve reaches an end, corresponding to the maximum (finite) value of its generalised affine parameter, that *does not belong* to the spacetime. In this view, the singularity is a "missing point" at which spacetime is not defined.

(It is possible to extend the spacetime by complementing it with a suitable boundary, containing the endpoints of curves that are incomplete in the spacetime, which would make it possible to speak of singularities as points in some manifold. This can be achieved in several ways, one being the so called b-boundary construction; all of which are somewhat problematic.)

This difference notwithstanding, it would be desirable that the two notions of singularity, based on unbounded curvatures and incomplete curves respectively, agreed in general. A little hope seems to be provided by a paper by Clarke [119], whose abstract reads:

3 A note is in order. Usually, one defines curvature singularities as unboundedness along an incomplete curve. In this perspective, singularities would always be defined in terms of curve incompleteness and curvature singularities would constitute a particular subcase. Our definition is thus somewhat loose from a technical point of view, but it serves the purpose of the discussion.

"A singularity reached on a timelike curve in a globally hyperbolic space-time must be a point at which the Riemann tensor becomes infinite (as a curvature or intermediate singularity) or is of type D and [electrovacuum]."

However, the Schwarzschild, Reissner–Nordström, Kerr and Kerr–Newman solutions are all electrovacuum and type D everywhere; actually, all spherically symmetric spacetimes are type D, an so are all the Kerr-like spacetimes that are usually used to model RBHs — see section 4.3 and [343, 345] —; in fact, the only non-type-D spacetimes mentioned in this thesis are those belonging to the rotating black bounce family.

So, unfortunately, this theorem rarely applies; indeed, for all practical purposes, the two notions are to be considered different.

2.1.3 *Singularity theorems*

The definition based on curve incompleteness, and more specifically on geodesic incompleteness, is particularly well-suited for a mathematical investigation of singularities.

Such investigation, which started during the so-called renaissance of GR [67] and stretched throughout the 1960s and '70s, consolidated the notion that spacetime singularities are not born out of unphysically restrictive symmetry assumptions; rather, they are a genuine prediction of GR under reasonable and generic assumptions.[4]

The main results are distilled into a series of *singularity theorems*, a set of statements in the form "if…then …" that clarify under what circumstances the formation of a singularity is inevitable [315].

Here, we shall focus on the first of said theorems (by Penrose in 1965 [295]), since it deals with BHs and is reasonably simple. Our goal is not to report the proof of the theorem, which is textbook material [184], but rather to point out some key points that will become relevant later, when we will discuss the possibility of avoiding the formation of singularities.

The statement of the theorem is the following [184, p. 263]:

A spacetime $(\mathcal{M}, g_{\mu\nu})$ cannot be null geodesically complete if:

1. $R_{\mu\nu}k^\mu k^\nu \geq 0$ *for all null vectors* k^μ*;*
2. *there is a non-compact Cauchy surface;*
3. *there is a closed trapped surface.*

Assumption 1. is sometimes referred to as the "convergence condition" [316]. Using Einstein's equations, it can be translated into a condition on the matter content of the spacetime: the energy density

4 Cf. the motivation for the 2020 Nobel Prize in Physics awarded to Sir Roger Penrose.

measured along any null curve must be non-negative (null energy condition).

Assumption 2. is equivalent to saying that the spacetime is globally hyperbolic, i. e. its complete history is predictable given appropriate Cauchy data local to an achronal surface.

Assumption 3. means, roughly speaking, that a BH horizon has formed. A trapped surface is a closed two-dimensional spacelike surface such that the two null congruences, ingoing and outgoing, orthogonal to the surface have both negative expansions. It is trapped in the sense that its area shrinks as one moves along *both* congruences.

The proof of the theorem comprises two parts: the first is "kinematical" while the second is "geometrical".

The kinematical part consists in a lemma that often goes by the name of *focusing* or *convergence theorem* [316]. It entails proving, by means of Raychaudhuri's equation, that if a closed trapped surface exists, then the null geodesic congruences that cross it must reach a point of finite affine parameter at which they focus. Such focusing point is a caustic, i. e. a point of infinite negative expansion. This kinematical part will play a central role in the classification and construction of non-singular geometries in subsection 2.2.1.

The geometric part, instead, consists in proving, by contradiction, that if the focusing point were part of the manifold, hence not a singularity, the boundary of the causal future of the trapped surface would be compact and without boundary, which is incompatible with assumption 2.

Note that the only use of Einstein's equations is in translating assumption 1. into a statement on the matter content of the spacetime, which is a non-essential step. So, Penrose's theorem actually holds in all of the theories that we called metric, irrespective of their field equations, and with suitable adaptations also in non-metric theories. This remark constitutes the foundations for the discussion in subsection 2.2.1 and, in fact, for the rest of this thesis.

2.1.4 *Conceptual issues with singularities*

Having spelled out some definitions of singularities and discussed their ubiquity, we are now in the position to elaborate on the conceptual issues that the existence of singularities entails [131, 132]. The problematic aspects touched upon herein serve as a motivation for the following section 2.2, in which we will investigate the possibility that some new physics, possibly related to quantum gravity, might play a role in solving them.

Let us start with the curvature approach. As already commented before, the fact that there exist local measurements of curvature that become unbounded along some curves is clearly problematic: curvature is a legitimate observable in the theory and it is hard to think how

the statement "infinite curvature" could be given a sensible meaning in any operational sense.

One might argue in favour of a permissive attitude, whereby unboundedness on non-causal curves could be tolerable, since these curves do not correspond to physical trajectories; moreover, unboundedness on non-geodesic causal curves might also be acceptable, since these trajectories are "artificially" accelerated in the context of GR. A p. p. singularity along a timelike geodesic, on the other hand, entails that a freely falling observer would measure infinite tidal forces — what this might mean is unclear.

On a more technical note, an s. p. singularity strongly suggests that the gravitational action might not be finite when evaluated on shell. In GR, the action contains the Einstein–Hilbert term

$$S_{\mathrm{EH}} = \frac{1}{16\pi} \int \mathrm{d}^4x \, \sqrt{-g} R \,, \tag{2}$$

where the Ricci scalar R can possibly blow up: it does not for e. g. the Schwarzschild solution, which is a vacuum solution, but it will in more general situations.[5]

Furthermore, if one extends GR in an effective-field-theory spirit, one is forced to add to eq. (2) all the terms compatible with diffeomorphism invariance and up to a given order in a derivative expansion. In the case of a s. p. singularity, some of these terms will diverge and the finiteness of the action becomes a fine tuning problem.

The incompleteness approach brings about issues that are even more disturbing. In this setting, the singularity does not belong to the spacetime, so in principle one might avoid warring about the possible unboundedness of observables. (Although it is not clear how that problem could be avoided in practice.)

As before, incompleteness of non-causal curves, and to a lesser extent of causal non-geodesic curves, could arguably be tolerated. But the incompleteness of timelike geodesics really means that observers can reach the singularity in a finite amount of proper time, and then *disappear from existence*, since their worldlines cannot be extended past that value of proper time. (We assumed that the singularity is at the future endpoint. Observers might also "pop up", seemingly out of nowhere, if it is at the past endpoint.) In other words, curve incompleteness entails a loss of predictability of the theory.

These and similar motivations, presented here filtered through the present author's personal views, are what leads many practitioners to believe that spacetime singularities represent a breakdown of GR and of our understanding of gravity.

5 Even in Ricci-flat spacetimes, if the manifold has a boundary, one needs to "renormalise" the gravitational action, since the Gibbons–Hawking–York term typically diverges. Such renormalisation is usually achieved by subtracting the contribution one would find in a flat spacetime, but if the Lagrangian density diverges this might not be sufficient.

2.2 THE ROLE OF "NEW PHYSICS"

The (not completely explained) coincidence between the two approaches to singularities, curvature- and incompleteness-based, is particularly suggestive. If one treats GR in the spirit of effective field theories, this coincidence entails that singularities appear in a regime, that of high curvatures, in which the higher-order "corrections" to GR are strong.

This suggests that the formation of singularities might be avoided in beyond-GR theories. Indeed, the equations of motion of these theories can typically be cast in the form[6]

$$R_{\mu\nu} - \frac{1}{2} R g_{\mu\nu} = T^{\text{eff}}_{\mu\nu} \,, \tag{3}$$

where $T^{\text{eff}}_{\mu\nu}$ is an *effective* stress-energy tensor encoding the effect of higher-order terms. Such effective stress-energy tensor can, in general, violate the null energy condition [91], which is one of the assumptions in Penrose's theorem. Hence, singularity theorems as they are usually formulated might be evaded and the end state of gravitational collapse might be a geometry that is regular, i. e. free of singularities.

This possibility seems even more convincing when pondering about quantum effects. Indeed, it seems reasonable to expect that quantum gravity, whatever that might be, will shed light on the issues related to singularities. Clearly, there is no guarantee that this will be the case: quantum gravity might very well have nothing to say on the matter; and, even if it were the case, it might not be possible to phrase the answer in the usual language of differential geometry.

(Actually, one might argue for a strong stance in the opposite direction and *demand* that quantum gravity "solves" singularities, in some sense — meaning that a candidate theory that did *not* address the issues would have to be considered unviable.)

Nonetheless, a scenario as the one we just presented does seem a sensible working assumption — which we will adopt for the rest of this thesis. Specifically, we will work under the following hypotheses:

1. GR is extended by the inclusion of some "new phyics", possibly but not necessarily related to quantum gravity;

2. gravitational phenomena can be described, in an effective sense, in terms of the usual tools of pseudo-Riemannian geometry, namely a spacetime manifold and a Lorentzian metric;[7]

3. the spacetime is geodesically complete and free of curvature singularities.

6 We omit the conventional 8π factor in the Einstein's equations.

7 The manifold is assumed to be four-dimensional, connected, Hausdorff and paracompact; it is equipped with a metric-compatible connection. All structures are assumed to be suitably differentiable.

We shall not dwell much longer on this point, but we wish to stress that these are assumptions and that the possible alternatives might look counter intuitive. For instance, [194] has argued that not all singularities should be cured, since some of them are useful in that they allow to discard unphysical solutions.

Notably, however, several approaches to quantum gravity seem to converge in supporting a scenario based on the aforementioned assumptions. Representative examples are loop quantum gravity [182, 308] and asymptotic safety [70].

2.2.1 *Classification of geodesically complete geometries*

The assumptions above are useful insofar as they allow for a classification of all possible non-singular geometries. Such classification was carried out first in [97, 98] (see also [140]; cf. [100] for an extension to Lorentz-violating theories of gravity) and is purely kinematical, i. e. oblivious to the dynamics of the regularisation.

Specifically, the authors of [97, 98] assume

- the assumptions above;
- global hyperbolicity;
- spherical symmetry.

They then turn their attention to the kinematical part of Penrose's singularity theorem and discuss how it can be evaded.

The first obvious possibility is that no closed trapped surface exists, i. e. there is no BH. The formation of a trapping horizon in GR typically happens in a regime of relatively low curvature, at which the effects of new physics are expected to be negligible — at least at the classical level. Yet, the inclusion of semiclassical effects (in the sense of quantum field theory in curved spacetimes) might drastically alter the picture, possibly leading to the formation of an *horizonless compact object* [15–17, 55, 92, 297]. A notable particular example of similar objects are gravastars [244, 267–269, 278, 355, 357]. Such horizonless (exotic) compact objects thus remain viable alternatives to GR BHs [107]

If, on the other hand, a closed trapped surface exists, the only option is to violate the assumption on the convergence condition (i. e. the null energy condition, assuming Einstein's equations). Then the outgoing null congruence is not bound to reach a focusing point in a finite affine distance anymore; there are therefore three alternatives:

1. the focusing point is pushed to infinite affine distance;
2. the focusing point is replaced by a defocusing point, which is reached at infinite affine distance;

3. the focusing point is replaced by a defocusing point, which is reached at finite affine distance;

A defocusing point is one at which the expansion of the outgoing congruence becomes zero. These cases can be further subdivided into subcases according, roughly speaking, to the sign of the expansion of the other (ingoing) congruence at the defocusing point — for further details, see [97].

The outcome of this analysis is that, under the assumptions, the taxonomy of non-singular geometries is remarkably short. Moreover, one can argue that most options are to be discarded for reasons that are spelled out in [97]. The taxonomy essentially comprises only two options: "evanescent horizons" and "one-way hidden wormholes" — and limiting cases thereof.

EVANESCENT HORIZONS The defocusing point is reached at finite affine distance and the ingoing congruence has negative expansion there. An *inner* trapping horizon forms inside of the *outer* trapping horizon; the two horizons merge in a finite time, leaving no BH behind. This scenario thus corresponds to a BH that lives for a finite amount of time and remains regular throughout. The limiting case in which the two horizons merge in infinite time is dubbed *everlasting horizon* in [97].

ONE-WAY HIDDEN WORMHOLES The defocusing point is reached at finite affine distance, as before, but the expansion of the ingoing congruence is non-negative there, meaning that it must be zero somewhere along the congruence between the closed trapped surface and the defocusing point. This means that the two-spheres orthogonal to the two null congruences cannot be shrunk to a point; rather their radius has a local minimum as a function of the affine parameters along the two congruences. Such minimum is a (dynamical) wormhole throat but, since the throat lies behind a trapping horizon, the wormhole is "hidden" (and the throat can only be traversed in one way). The limiting case in which the throat is infinitely far away is dubbed *asymptotic hidden wormhole* in [97].

These two classes can encompass geometries that are quite complex. For instance, in the evanescent horizon case there could be more than two horizons, nested one inside the other; still, these horizons must come in pairs and disappear in a finite amount of time. Similarly, the hidden wormhole scenario could display multiple horizons (on both sides of the throat), as well as multiple throats. However, the key features of these classes are well displayed by two "minimal" representatives: a geometry with one outer/inner horizon pair for the evanescent horizons class; and a geometry with one horizon enclosing a single throat for the hidden wormhole case.

One crucial difference between these two cases is the overall topology of the spacetime. This is always assumed to be path-connected and in the case of evanescent horizons it is also *simply connected*; i. e. the topology is the same as Mikowski spacetime. In the hidden wormhole case, instead, the existence of a throat entails that the spacetime cannot be simply connected, since a closed path that winds around the throat cannot be shrunk to a point; the spacetime is said to be *multiply connected*.

Since these geometries are assumed to result from gravitational collapse, the topology of the constant-time slices is assumed to be simply connected in the far past. In order to form an hidden wormhole, therefore, a change of topology has to take place. Whether this is at all possible, at least in quantum gravity, is an open issue (see [353] for some discussion and further references on the topic), hence we take an agnostic stance and explore this option as a viable possibility. (Note, in passing, that simply connected RBHs too typically imply a change of topology of some sort [74].)

Horizonless geometries can still be, in principle, either simply or multiply connected, so we will make this distinction even in that case.

The taxonomy of viable non-singular geometries arising from gravitational collapse can therefore be summarised, under the assumptions, in the following two-entry table:

Horizon	**Topology**	
	simply con.	multiply con.
with	multihorizon evanescent RBH	hidden wormhole
without	(exotic) compact object	naked wormhole

Table 1: Taxonomy of viable non-singular geometries.

2.2.2 *Towards phenomenology*

The classification we just presented is remarkably short and, although it could encompass arbitrarily complicated geometries, its key features are well captured by two fairly simple alternatives. This suggest that explicit examples could be built without excessive hurdles. By studying such "effective models" of regular geometries, then, one might hope to gain new insights into the process of singularity regularisation.

Ideally, these models would have to be reasonably *simple*, since phenomenological applications typically add layers of complexity and one would wish to keep as much control over the computations as possible. In practice, we will assume a high degree of symmetry (e. g. spherical or axial symmetry).

Moreover, since this classification is intended as a taxonomy of viable outcomes of gravitational collapse, these models should not differ too drastically from the astrophysical BHs that we observe in the sky — i. e. they should be reasonably *good "mimickers" of* GR BH.[8] Specifically, they should be asymptotically flat and with a well-defined Newtonian limit, so that at large distances test particles move in a Newtonian potential; furthermore, they should be compact enough to possess a light ring. Preferably, they ought to account for *rotation*.

In the spirit of simplicity, we will further assume that these models are *stationary*. This seems a reasonable assumption, since one would expect all the dynamical "hair" carrying information on the details of the collapse to be quickly radiated away, thus leaving behind an object that is not evolving anymore. This is what happens in GR, and indeed stationary geometries (namely, the Kerr geometry) provide a good description of isolated astrophysical BHs — at least as far as current observations can tell. (In this sense, stationarity is an additional requirement for a "good" mimicker.)

Yet, this assumption is less innocuous than it seems, since the taxonomy of table 1 comprises geometries that are intrinsically non-stationary (viz. the evanescent horizons). Hence, the description provided by stationary models should be regarded as approximate and valid only over appropriate timescales. Interestingly, the models will "remember" such pitfall in that globally hyperbolicity will be in doubt. In particular, the stationary counterpart of the evanescent horizons is going to be a RBH with "eternal" outer and inner horizons: similarly to the Reissner–Nordström and Kerr solutions, the inner horizon will also be a Cauchy horizon and these spacetimes will not be globally hyperbolic. In the multiply connected case, global hyperbolicity will also be quite subtle. For this reason, some care is needed when considering global characterisations of eternal spacetime, such as Carter–Penrose diagrams.

Finally, since astrophysical BHs are never really in a vacuum, one should make sure that the addition of a small amount of matter does not result in a disruptive change in the geometry. For instance, an initially small perturbation should not be allowed to grow indefinitely in amplitude as time progresses. In other words, these models should be *stable* — at least on astrophysical timescales.

The following chapters in this part expand this line of reasoning by explaining how effective models that satisfy the aforementioned *desiderata* can be built in practice: chapter 3 focuses on the simplest situation possible, in which staticity and spherical symmetry are assumed; chapter 4 describes a recipe for adding rotation to spherically

8 This represents an additional requirement that some might want to lift because they consider more exotic possibilities at least as appealing: surely this is an option, which however lies outside of the scope of this thesis.

symmetric metrics and discusses some examples that have appeared in the literature.

3

BUILDING MODELS OF REGULAR BLACK HOLES

As explained in subsection 2.2.1, if there exists some new physics that prevents the formation of spacetime singularities, gravitational collapse may possibly result in only two classes of geometries, simply and multiply connected, which may or may not exhibit horizons (cf. table 1).

In this chapter, we show how explicit examples of each kind can be built. We focus on the simplest possible situation by assuming staticity and spherical symmetry. We start with a rather general discussion in section 3.1. Soon enough, it will become clear that the simplest way to build models that satisfy the *desiderata* of subsection 2.2.2 is to "regularise" a singular solution of GR, i. e. to apply some specific changes to the metric in order to obtain a regular one — the obvious starting point is going to be Schwarzschild. Section 3.2 will explain how to do so maintaining the spacetime simply connected; section 3.3 will do the same for the multiply connected alternative.

The subject matter of this chapter, in particular with regards to simply connected RBHs, has been at the centre of great scientific activity. Apart from the cited literature, the interested reader may consult the newly published collection [29], or the reviews [12, 232, 249, 313].

3.1 A SPACETIME OF SUFFICIENT GENERALITY

Staticity means that the spacetime can be foliated by hypersurfaces orthogonal to the Killing vector field that is timelike at infinity, which we will call χ^μ. Spherical symmetry entails that these hypersurfaces can themselves be foliated by two-dimensional spheres. One can therefore choose a coordinate t associated to the orbits of χ^μ, and two coordinates θ and ϕ analogous to the usual spherical coordinates on the spheres.

One can then introduce a fourth coordinate r to label the different spheres within a constant-t hypersurface (see [359, ch. 6.1]). Such coordinate will be called "radius", for obvious reason, although in general it has no direct physical interpretation. Consistently with this terminology, the asymptotically far limit is assumed to be $|r| \to \infty$, and the point $r = 0$ is interpreted as the "centre" of the spacetime.

In these coordinates the metric is diagonal and reads

$$ds^2 = -f(r)\mathrm{d}t^2 + \frac{\mathrm{d}r^2}{g(r)} + h(r)\,\mathrm{d}\Omega^2 \,, \tag{4}$$

where $\mathrm{d}\Omega^2 = \mathrm{d}\theta^2 + \sin^2\theta\,\mathrm{d}\phi^2$ is the usual round metric on the two-sphere, while $f(r)$, $g(r)$ and $h(r)$ are free functions.

This form of the metric is quite redundant, since one can always redefine the radial coordinate to "gauge away" one between g and h.

A very common choice consists in measuring the radius in terms of the area of two-spheres. Since, according to eq. (4), such area is given by $4\pi h(r)$, this choice amounts to setting $h(r) = r^2$ — the resulting radius is known as *aerial radius*. However, since we wish to give a unified description of simply and multiply connected spacetimes, it is more useful to let $h(r)$ appear as an arbitrary function in the metric. We will only assume $h(r) \geq 0$, to ensure that the area of spheres is never negative.

Often, we will instead set

$$g(r) = f(r)\,. \tag{5}$$

This condition is such that the resulting Ricci tensor has vanishing radial null-null component [199]; our motivation for imposing it, however, is merely simplicity and analogy with the Schwarzschild solution.

The requirement of asymptotic flatness and that there exists a well-defined Newtonian limit translate into simple conditions on the free functions f, g and h. Specifically, we demand that at large $|r|$

$$\begin{aligned} & f(r) = 1 - \frac{2M}{|r|} + \mathcal{O}\left(|r|^{-2}\right) = g(r) \\ \text{and} \quad & h(r) = |r|^2 \left[1 + \mathcal{O}\left(|r|^{-3}\right)\right], \end{aligned} \tag{6}$$

where M is a positive constant that plays the role of the Newtonian mass and can be identified with the Arnowitt–Deser–Misner (ADM) or Komar masses (they coincide in this simple setting).

3.1.1 *Horizons*

Intuitively, horizons should be given by the zeroes of $g(r)$. In order to formally characterise them, we introduce two null congruences, one ingoing and one outgoing, and study their focusing properties. Though somewhat of an overkill, this method is very close in spirit to the reasoning involved in the singularity theorems.

The two congruences are specified by their tangent vectors l^μ and n^μ, which are null and taken to be future-pointing and normalised as $l^\mu n_\mu = -1$.

For consistency with chapters 4 and 5, we take

$$l^\mu \partial_\mu = \frac{1}{\sqrt{fg}} \partial_t + \partial_r \overset{|r|\to\infty}{\longrightarrow} \partial_t + \partial_r\,, \tag{7}$$

$$n^\mu \partial_\mu = \frac{1}{2}\sqrt{\frac{g}{f}} \partial_t - \frac{g}{2} \partial_r \overset{|r|\to\infty}{\longrightarrow} \frac{\partial_t - \partial_r}{2}\,, \tag{8}$$

so l^μ is outgoing and n^μ ingoing. These vectors are geodetic, although in general they are not affinely parametrised,[1] and parallely transported one along the other up to the non-affine parametrisation, i. e.

$$l^\nu \nabla_\nu n^\mu \propto n^\mu \quad \text{and} \quad n^\nu \nabla_\nu l^\mu \propto l^\mu \,. \tag{9}$$

Their expansions are defined as

$$\theta^{(X)} = p^{\mu\nu} \nabla_\mu X_\nu \quad \text{with} \quad X \in \{l,\ n\}\,, \tag{10}$$

where

$$p^{\mu\nu} = g^{\mu\nu} + l^\mu n^\nu + l^\nu n^\mu \tag{11}$$

is the projector onto the two-dimensional surfaces orthogonal to both l^μ and n^μ.[2] These surfaces are spacelike and closed; they are nothing but the constant-t and -r spheres.

When the expansion of a given congruence is positive, the area of such spheres increases as one moves along the congruence; we say that the congruence is diverging or expanding. If instead the expansion is negative, the spheres shrink along the congruence, which is then said to be converging or focusing.

A quick computation gives

$$\theta^{(l)} = \frac{h'(r)}{h} \quad \text{and} \quad \theta^{(n)} = -\frac{g(r)h'(r)}{h(r)} \tag{12}$$

(the prime stands for a derivative with respect to r, here and throughout this chapter). Two other interesting quantities are the Lie derivatives

$$\mathfrak{L}_{n^\mu}\left[\theta^{(l)}\right] = -\frac{g}{2}\left(\frac{h'(r)}{h(r)}\right)', \tag{13}$$

$$\mathfrak{L}_{l^\mu}\left[\theta^{(n)}\right] = -\left(\frac{g(r)h'(r)}{h(r)}\right)'. \tag{14}$$

Let us first consider the case in which $h(r)$ is a monotonic function of the radius, so that $h'/h > 0$. The outgoing congruence is always expanding; the ingoing congruence, instead, is converging when $g > 0$ but becomes diverging if $g < 0$. Hence, all the two-spheres with radii such that $g < 0$ are *past* trapped surfaces [185]. The spheres corresponding to $g(r) = 0$, in particular, are marginally trapped surfaces; there, we have

$$\mathfrak{L}_{l^\mu}\left[\theta^{(n)}\right]\Big|_{\text{MTS}} = -g'\frac{h'}{h}\,, \tag{15}$$

1 l^μ is affinely parametrised if $f(r) = g(r)$ [199].

2 Note that if l^μ and n^ν were affinely parametrised, it would be $\theta^{(X)} = \nabla_\mu X^\mu$.

so the marginally trapped surface is outer or inner if g' evaluated at the surface is positive or negative, respectively. The three dimensional hypersurfaces foliated by marginally trapped surfaces are then trapping horizons.

Our choice of null vector (eq. (7)) allowed us to identify past trapping horizons, i. e. white-hole horizons. However, since the spacetime is static, it is symmetric under time inversion, and the past trapping horizons have a future counterpart as well — i. e. BH horizons. We could have avoided this slight complication by choosing different null vectors.

If $h(r)$ is not monotonic, the expansions have additional zeroes at its local extrema. In general, *both* congruences change sign at points in which $h' = 0$: this is a local characterisation of a wormhole throat [186, 342]. Further details on wormhole geometries can be found e. g. in [27, 33, 85, 133, 134, 193, 257, 276, 277, 327].

Note that the condition $f(r) < 0$ only determines an ergoregion, i. e. a region in which the Killing vector χ^μ becomes spacelike. In principle, this notion is unrelated to the trapping of light rays; however, in spherical symmetry we can always pick a gauge such that $f = g$, in which the ergoregion and the trapped region trivially coincide. By doing so, however, the interpretation of the radial coordinate might change. This proves, incidentally, that under the assumption of staticity and spherical symmetry the trapping horizons are KHs — a conclusion that holds true also under the weaker assumption of stationarity, as per Hawking's rigidity theorem [117].

3.1.2 *Effective matter content*

According to the assumptions of section 2.2, the effective models we aim at constructing need not be solutions of GR. However, Einstein's equations can still be used to characterise the geometries and, in particular, to quantify the deviations from vacuum GR. Indeed, our models are supposed to describe, to a first degree of approximation, *isolated* astrophysical objects and any deviation from vacuum GR should be attributed to the putative new physics that is assumed to prevent the formation of the singularity — not, for instance, to the presence of ordinary matter.

Hence, in the following we will often compute the Einstein's tensor and equate it to the stress-energy tensor of what we will call *effective sources*. This terminology is chosen because it is handy and intuitive, but it should be clear that we never assume the existence of any actual matter source. So, in particular, one should not be alarmed if the effective sources were found to be "exotic", for instance because some energy conditions were violated. Indeed, from our point of view, the violation of the energy conditions is not a drawback but rather a necessary feature of singularity regularisation.

When the metric is that of eq. (4), the Einstein's tensor is diagonal. Its components can therefore be interpreted as the energy density ε and the pressures $p_\parallel$ and $p_\perp$ of an anisotropic fluid, as measured in a frame associated to the coordinates one is using. Specifically, we have

$$p_\perp = G^\theta{}_\theta = G^\phi{}_\phi \,, \tag{16}$$

while

$$-\varepsilon = \begin{cases} G^t{}_t & \text{in untrapped regions} \\ G^r{}_r & \text{in trapped regions} \end{cases} \tag{17a}$$

and

$$p_\parallel = \begin{cases} G^r{}_r & \text{in untrapped regions} \\ G^t{}_t & \text{in trapped regions} \end{cases} \quad ; \tag{17b}$$

the distinction between trapped and untrapped regions is necessary because the energy density is typically associated to the timelike eigenvector of the stress-energy tensor: in an untrapped region, such eigenvector is the one associated to the t-t eigenvalue, while in a trapped region the eigenvector is the one associated to the r-r direction. (As mentioned, we will usually omit the conventional 8π factor in the Einstein's equations, i. e. we will write

$$G_{\mu\nu} = T^{\text{eff}}_{\mu\nu} \,; \tag{18}$$

however, we will not be entirely consistent with this choice, since the 8π's will appear explicitly in chapter 6.)

Note that, in the absence of spherical symmetry, the simple interpretation in terms of energy density and pressures is not always possible. Indeed, in rotating spacetimes $G_{\mu\nu}$ will typically be non-diagonal, at least in the coordinates that are most often used. As a matrix, $G_{\mu\nu}$ is real and symmetric in its indeces, so one might be tempted to diagonalise it and interpret the eigenvalues as energy density and pressures. However, the eigenvactors one would find in this way are not covariant vectors and the eigenvalues are not generally covariant scalars. Such characterisation is therefore highly reliant on the coordinates chosen.

To write a generally covariant eigenvector equation, one needs to rise an index:

$$G^\mu{}_\nu \, v^\nu = \lambda v^\mu \,, \tag{19}$$

but now $G^\mu{}_\nu$, when seen as a matrix, needs not be symmetric, hence its eigenvalues might be complex. Usually, the eigenvectors are normalised so as to form an orthonormal tetrad.

For this reason, Hawking and Ellis have introduced a classification of stress-energy tensors based on the character of their eigenvalues

[184, ch. 4] (see also [262]). The classification results in four different types: type-I stress-energy tensors, in particular, have four real eigenvectors — this is the familiar case that admits a fluid interpretation, to which most "reasonable" matter fields belong.

In this thesis, we will therefore often refer to the "Hawking–Ellis type" when analysing a given spacetime. However, we will also investigate alternative ways of characterising the effective matter content, for instance by focusing on specific observers and computing the energy density as measured by them.

As mentioned already, in the models considered in this thesis the effective sources will always violate at least some of the (classical) *energy conditions*. The terminology we will follow is standard [184, 353]. Specifically, the null energy condition is the requirement that

$$T_{\mu\nu}k^\mu k^\nu \geq 0 \tag{20}$$

for all null vectors k^μ; i. e. $\varepsilon + p_i \geq 0$ for all energy densities and principal pressures. The weak energy condition is the same as eq. (20) with k^μ a timelike vector; i. e. $\varepsilon + p_i \geq 0$ and $\varepsilon \geq 0$. The strong energy condition requires

$$\left(T_{\mu\nu} - \frac{1}{2}Tg_{\mu\nu}\right)k^\mu k^\nu \geq 0\,, \tag{21}$$

with T being the trace of $T_{\mu\nu}$, for all timelike k^μ; i. e. $\varepsilon + p_i \geq 0$ and $\varepsilon + \sum p_i \geq 0$. Finally, the dominant energy condition is the weak energy condition plus the requirement that

$$T_{\mu\nu}k^\mu \geq 0 \tag{22}$$

for all timelike k^μ; i. e. $\varepsilon \geq 0$ and $|p_i| \leq \varepsilon$ for all principal pressures. Note that if the null energy condition is violated, all pointwise energy conditions are violated too. These pointwise definitions can be integrated to yield *averaged* energy conditions [353].

In closing this discussion on effective sources, we point out that it is often possible to find classical theories that have these effective models as solutions. Typically, these theories are GR supplemented with some version of non-linear electrodynamics, i. e. one whose Lagrangian is a non-linear function of the Maxwell's scalar $F_{\mu\nu}F^{\mu\nu}$; and possibly a phantom scalar field, i. e. one whose kinetic terms has the opposite sign with respect to the usual scalar fields [19, 20, 25, 68, 69, 79, 80, 83, 86, 89, 135, 244, 306]. Moreover, solutions as these have been obtained in some explicit alternative theories of gravity [154, 214, 215, 280, 288]. This is an interesting line of research which however we will not pursue here.

3.1.3 *Assessing regularity*

In static and spherically symmetric spacetimes, the Kretschmann scalar is a sum of squares and is therefore non-negative definite. In can be

shown that this entails the following: in a static and spherically symmetric spacetime, the Kretschmann scalar is bounded if and only if all the components of the Riemann tensor in an orthonormal frame are bounded [245, 320].

Therefore, in a spacetime described by eq. (4), the boundedness of the Kretschmann scalar is enough to ensure that *all* the scalar polynomials built out of the Riemann tensor (plus the metric and the Levi-Civita completely antisymmetric tensor) are bounded too.

As soon as the stationarity and axisymmetry assumptions are lifted, things become decisively more complicated. In a generic spacetime, there exist seventeen (or sixteen, depending on how they are counted) algebraically independent curvature invariants [325, sec 9.1]. A complete set was given by Zakhary and McIntosh [370]. (See also [147, app. A.1] and references therein, as well as [318].) In principle, the boundedness of all of them should be checked before claiming that the spacetime is free of scalar polynomial curvature singularities.

Luckily, the effective models considered in this thesis are highly symmetric and this tedious exercise will usually not be necessary. For example, the most common simply connected rotating RBHs are of Petrov type D and Segre type $[(1,1),(1\ 1)]$: for these spacetimes, the number of independent invariants is reduced to four — see section 4.3 and [343]. Similarly, in multiply connected models the regularisation is typically performed in such a way that boundedness is immediate: usually (e. g. in part ii), some curvature invariants are reported for completeness but the result extends trivially to all of them.

Note, however, that if one resolves to extend GR in a way that entails higher derivatives, one might have to check that invariants built out of *derivatives* of the Riemann tensor are bounded too. Not surprisingly, the number of these "higher-order" (i. e. higher than second-order) invariants grows with the number of derivatives. This is therefore a stronger version of regularity, which will translate into more restrictive regularity conditions than those we will consider in the following.

3.2 SIMPLY CONNECTED REGULARISATION

Having set the stage with the previous section, we can now move on to discuss the first class of non-singular models: simply connected geometries.

Without loss of generality, we choose coordinates so that $g(r) = f(r)$. For convenience and in analogy with the Schwarzschild metric, we will write

$$f(r) = 1 - \frac{2m(r)}{r}\,. \tag{23}$$

The function $m(r)$ is usually called Misner–Sharp mass function, since it measures the amount of "mass" within a sphere of radius r. By asymptotic flatness, we require that

$$\lim_{r\to\infty} m(r) = M\,. \tag{24}$$

The defining characteristic of a simply connected spacetime is that any closed path can be contracted to a point; therefore, the spheres centred at the origin will also be contractible to a point, which cannot be anything but the origin $r = 0$. Hence, it must be $h(0) = 0$.

Consistently with this remark, and in the spirit of simplicity, we further set $h(r) = r^2$. This is however *not* a gauge choice and it entails a loss of generality. The examples of simply connected regular geometries that we present herein, therefore, are "minimal", in the sense that they most resemble the Schwarzschild metric; by making different choices on the function $h(r)$ one can build non-minimal models.

An explicit computation yields $G^t{}_t = G^r{}_r$. In the anisotropic fluid interpretation, we thus have

$$-\varepsilon = p_\parallel = -\frac{2m'(r)}{r^2}\,, \tag{25a}$$

$$p_\perp = -\frac{m''(r)}{r}\,. \tag{25b}$$

An equation of state of this kind can be mimicked by a non-linear version of Maxwell's electrodynamics [19, 20, 25, 69, 79, 83, 161, 306].

The Kretschmann scalar evaluates to

$$R^{\mu\nu\rho\sigma}R_{\mu\nu\rho\sigma} = \left[f''(r)\right]^2 + 4\frac{\left[f'(r)\right]^2}{r^2} + 4\frac{\left[1-f(r)\right]^2}{r^4}\,. \tag{26}$$

As argued in subsection 3.1.3, in spherical symmetry the boundedness of the Kretschmann scalar is all that is needed to ensure the absence of curvature singularities. Hence, the demand of regularity translates on a condition on the behaviour of the Misner–Sharp mass close to $r = 0$. Specifically, one needs

$$m(r) = c\ell^{-2}r^3 + \mathcal{O}\left(r^4\right); \tag{27}$$

here c is a dimensionless number of order one and ℓ is a (non-negative) length scale. Deep in the core, i. e. at small r, the metric reads

$$\begin{aligned} ds^2 = &-\left[1 - 2c\ell^{-2}r^2 + \mathcal{O}\left(r^3\right)\right]\mathrm{d}t^2 \\ &+\left[1 + 2c\ell^{-2}r^2 + \mathcal{O}\left(r^3\right)\right]\mathrm{d}r^2 + r^2\,\mathrm{d}\Omega^2\,, \end{aligned} \tag{28}$$

which is the metric of a de Sitter (dS), if $c > 0$, or an anti de Sitter (AdS) universe, if $c < 0$, expressed in the static patch. Indeed, the Einstein's tensor becomes that corresponding to a (effective) cosmological constant[3]

$$\Lambda^{\text{eff}} = \frac{6c}{\ell^2}\,. \tag{29}$$

3 We use again the convention $G_{\mu\nu} = T^{\text{eff}}_{\mu\nu}$ and $T^{\text{eff}}_{\mu\nu} = \Lambda g_{\mu\nu}$.

Model	$m(r)$
Bardeen [43]	$M\frac{r^3}{(r^2+\ell^2)^{3/2}}$
Hayward [187]	$M\frac{r^3}{r^3+2M\ell^2}$
Dymnikova [144]	$M\left[1-\exp\left(-\frac{r^3}{\ell^3}\right)\right]$
Fan–Wang [161]	$M\frac{r^3}{(r+\ell)^3}$
Asymptotically Minkowski [323]	$Me^{-\ell/r}$

Table 2: Some of the most popular RBH models. .

When instead $c = 0$, the curvatures vanish and the core geometry is asymptotically Minkowski.

Note, incidentally, that these geometries are certainly non-singular, in general, only for $r \geq 0$. If one allows the coordinate r to become negative, one might still encounter spacetime singularities [231, 373] — in the form of divergences in the curvatures or in the sense of geodesic incompleteness. In order to interpret these metrics as RBHs, therefore, one must limit the domain of r to $[0, +\infty)$. Clearly, this is coherent with the interpretation of r as a radius, and with the fact that $r = 0$ is, at any given v, a point (i. e. a degenerate, zero-radius sphere).

Some popular choices for $m(r)$ are summarised in table 2. More examples can be found e. g. in [173, 229, 230, 347]. All these models depend continuously on two parameters: M, the ADM mass, and ℓ, a regularisation parameter. The Schwarzschild metric is recovered for $\ell \to 0$, in which limit the regularisation is undone. For this reason, these models are said to be "regularisations" of the Schwarzschild spacetime.

Horizons are determined by the roots of $f(r) = 0$. Since $f(r) \to 1$ both at infinity and at the centre, the continuity of $f(r)$ implies that horizons generically come in pairs: any time an (outer) KH is present, an inner KH must exist too. The outer horizon is the event horizon, while the inner horizon is a Cauchy horizon. The only exception is the particular case in which the two horizons coincide. Note that this property is generic to all simply connected RBHs and does not depend on the specific choice of the model — consistently with the discussion in subsection 2.2.1.

In the models of table 2, whether $f(r) = 0$ has solutions or not depends on the value of ℓ: the metric describes a BH only if $\ell \in [0, \ell_*]$ for some model-dependent threshold ℓ_*. This means, incidentally, that these RBHs cannot have an arbitrarily small mass, since for any fixed ℓ they satisfy

$$M \geq \ell/\ell_* \,; \tag{30}$$

in other words, there is a mass gap.

For $\ell = \ell_*$ the two horizons degenerate into a single horizon, which is extremal in the sense that its surface gravity vanishes.

For $\ell > \ell_*$ there are no horizons, but the metric remains perfectly viable: it represents a spacetime containing a non-singular horizonless exotic compact object, supported by matter whose equation of state tends to that of a cosmological constant deep in the core [99]. When the core is dS, in particular, these objects closely resemble gravastars [268, 278, 279].

For the Hayward model [187]

$$m(r) = M\frac{r^3}{r^3 + 2M\ell^2}\,, \tag{31}$$

for instance, $f(r) = 0$ reduces to

$$r^3 - 2M(r^2 - \ell^2) = 0\,. \tag{32}$$

The cubic equation has real non-negative solutions for $0 \leq \ell \leq \ell_*$ with

$$\ell_* = \frac{4M}{\sqrt{27}}\,. \tag{33}$$

(The cubic polynomial always has at least one real root, which in this case is negative and for this reason we discard it; in this range of ℓ the other two roots are real and positive.)

Since, for small r,

$$m(r) = \frac{r^3}{2\ell^2} + \mathcal{O}(r^3)\,, \tag{34}$$

the core geometry is asymptotically dS. The Penrose diagram relative to this geometry can be found in the original publication [187]: it is analogous to that of the Reissner–Nordström spacetime, except for the fact that the line corresponding to $r = 0$ is not a singularity.

3.3 MULTIPLY CONNECTED REGULARISATION

As before, we work in the gauge $g(r) = f(r)$. Contrary to the previous case, however, in a multiply connected spacetime the aerial radius $\sqrt{h}$ can never be zero. We will assume that it connects two asymptotically flat regions through one global minimum, which without loss of generality we locate at $r = 0$; we thus allow r to take positive as well as negative values, i. e. $r \in (-\infty, +\infty)$, and identify the two asymptotically flat ends with $r \to \pm\infty$. Then

$$\begin{aligned} &h'(0) = 0 \quad \text{and} \quad h''(0) \geq 0 \\ &\text{but} \quad h(0) = \ell^2\,, \end{aligned} \tag{35}$$

with ℓ some length scale.

For simplicity, we further assume that

$$f(r) = 1 - \frac{2M}{\sqrt{h}}\,. \tag{36}$$

As in the previous case, this choice represents a loss of generality yielding a model that is "minimal".

The Einstein's tensor appears more messy than in the simply connected case. It evaluates to

$$G^r{}_r = \frac{(h')^2 - 4h}{4h^2}\,, \tag{37a}$$

$$G^\theta{}_\theta = G^\phi{}_\phi = -\left(1 - \frac{M}{\sqrt{h}}\right)\frac{(h')^2 - 2hh''}{4h^2}\,, \tag{37b}$$

$$G^t{}_t = G^r{}_r - \left(1 - \frac{2M}{\sqrt{h}}\right)\frac{(h')^2 - 2hh''}{2h^2}\,. \tag{37c}$$

Such Einstein's tensor arises in GR in the presence of *both* non-linear electrodynamics *and* a phantom scalar field [80].

The Kretschmann scalar is

$$\begin{aligned} R^{\mu\nu\rho\sigma}R_{\mu\nu\rho\sigma} =& \frac{3f^2\,(h')^4}{4h^4} + \left[f''\right]^2 - f(h')^2\frac{2 + f'h' + 2fh''}{h^3} \\ &+ \frac{4 + (f')^2\,(h')^2 + 2ff'h'h'' + 2f^2\,(h'')^2}{h^2}\,. \end{aligned} \tag{38}$$

The expressions above are not particularly transparent, yet it should be clear (and fairly intuitive) that no singularity appears as long as $h(r) \neq 0$. In this case, the core geometry depends on the choice of $h(r)$ but is in general not that of a maximally symmetric space.

As in the simply connected case, horizons are determined by the zeroes of $f(r)$, i. e. by the solutions of the equation

$$\sqrt{h(r)} = 2M\,. \tag{39}$$

The present case, however, displays additional features since, according to the discussion in subsection 3.1.1 and to eq. (35), the hypersurface $r = 0$ is the throat of a wormhole.

Such throat may be located outside or inside of a trapped region, depending on the sign of $f(0)$. If the throat lies in an untrapped region, it is a timelike hypersurface which can therefore be crossed in both ways by causal curves: we thus call it a *traversable throat*. If, on the other hand, the throat lies in a trapped region, it is a spacelike hypersurface and can therefore be traversed in one way only by causal curves. This case is thus better described as a (cosmological) bounce [255]; however, in order to avoid an excessive proliferation of terms, we will speak of wormhole in this case too.

In the particular case in which the throat coincides with the locus of point at which $f(r) = 0$, such hypersurface is null and therefore

traversable in only one direction. As before, with a slight abuse of terminology we will speak of a wormhole with a null throat, or *null wormhole* for short.

Note that one could have a timelike throat which happens to be shielded by an even number of horizons. Such throat would be similar to the singularity of the Reissner–Nordström (or Kerr) spacetime, which is timelike because it lies inside of the inner horizon — hence in an untrapped region. Although in this case the throat is technically traversable, an observer that crosses it in one direction and then crosses it again in the opposite direction would still never be able to reach asymptotic infinity.[4] So, for all practical purposes, this spacetime contains a BH.

We will therefore distinguish the two cases: when the throat is cloaked by horizons we will speak of a *hidden wormhole* and specify whether the throat is timelike or spacelike; when instead the (timelike) throat is "naked", we will speak of a *traversable* or *naked wormhole*. Only this last definition corresponds to the most proper notion of wormhole, the one familiar from science fiction.

A particular example of this kind of regularisation was proposed by Alex Simpson and Matt Visser in [322]. (Similar ideas appeared in [69, 81, 82].) Their choice consists in a very simple "trick": whenever a component of a singular metric has an explicit r dependence, replace that r with $\sqrt{r^2+\ell^2}$. They first applied this trick to the Schwarzschild metric, thus introducing what has become known as the SV metric:

$$ds^2 = -\left(1-\frac{2M}{\sqrt{r^2+\ell^2}}\right)\mathrm{d}t^2 + \frac{\mathrm{d}r^2}{1-\frac{2M}{\sqrt{r^2+\ell^2}}} + \left(r^2+\ell^2\right)\mathrm{d}\Omega^2 \,. \tag{40}$$

Clearly, this metric is the particular case of the general form considered so far with $h(r) = r^2+\ell^2$.

Similarly to the examples of the simply connected case, the metric depends on two real parameters: the ADM mass M, and a regularisation parameter ℓ. The Schwarzschild metric is recovered in the limit $\ell \to 0$, in which the regularisation is undone. The limit $M \to 0$ corresponds to the metric of the Ellis wormhole [152].

Eq. (40) is symmetric under the inversion $r \mapsto -r$ and therefore describes two identical "universes", corresponding to positive and negative r respectively, connected by a throat whose spherical cross sections have area $4\pi\ell^2$. We will often refer to the positive-r region as *our universe* and to the negative-r region as the *other universe*.

4 More precisely, the observer might still be able to reach *some* asymptotic infinity, but such infinity would not be the same as the one reached by observers that never crossed the outer horizon.

Horizons may exist or not, depending on the value of ℓ. Their location is determined by

$$\sqrt{r^2 + \ell^2} = 2M\,. \tag{41}$$

When $\ell > 2M$ this equation has no real root and the spacetime thus contains a traversable wormhole; when instead $\ell < 2M$ the equation has two solutions located at

$$r = \pm r_H\,, \quad \text{with} \quad r_H = \sqrt{4M^2 - \ell^2}\,; \tag{42}$$

they correspond to two horizons, one located in our universe and one in the other universe; the spacetime thus contains a (regular) BH and a hidden wormhole, called a *black bounce*[5] in the original paper [322]. In the degenerate case $\ell = 2M$ the two solutions coincide and the resulting single horizon is extremal (in the sense that it has zero surface gravity); such horizon coincides with the throat, which is therefore null.

The original paper [322] presents Penrose diagrams for each case. Roughly speaking: that of the naked wormhole is identical to the diagram of Minkowski spacetime, except that the right and left halves of the diamond correspond to different universes; that of the black bounce, in contrast, is an infinite tower of Schwarzschild-like blocks stacked one on top of the other an glued where the singularity would be.

The SV metric eq. (40) is very simple and yet surprisingly rich. For this reason, it gained a rather substantial popularity and many other applications of the "SV trick" have been investigated by numerous researchers, including the present author. Examples can be found in [86, 237, 238, 245, 246, 307, 319, 321]. For further details, Alex Simpson's PhD thesis offers an excellent overview [320].

3.4 ON THE MEANING OF ℓ

We have seen that the regularisation of the singularity typically brings about a new length scale ℓ which controls the curvature of the region close to the would-be singularity: in the simply connected case, ℓ^2 is proportional to the inverse of the effective cosmological constant that corresponds to the dS or AdS core geometry; in the multiply connected case, instead, ℓ^2 is the area of the (cross sections of the) throat that replaces the singularity.

To better understand the meaning of this regularisation scale, we can consider the gravitational collapse of some energy density and

5 In the following, we will use the term *black bounce* to refer to the family of spacetimes obtained by generalising the SV metric, regardless of whether the throat is spacelike or not.

assume, somewhat simplistically, that the collapse proceeds as predicted by GR until a certain threshold is met, after which new-physics effects become dominant.

If this new physics is related to quantum gravity, one might be tempted to identify ℓ with a quantity related to the Planck scale — which, according to common lore, is *the* scale of quantum gravity. Deciding which Planck-scale quantity to choose, however, requires making specific assumptions on the behaviour of quantum gravity.

A very natural option seems to be $\ell \sim \ell_{\rm P}$, which corresponds to a scenario whereby quantum effects become dominant when the radius of the collapsing object is of order of the Planck length. This choice is in agreement with a standard result in perturbative quantum gravity asserting that the quantum fluctuations of the metric become $\mathcal{O}(1)$ at length smaller than the Planck length — more technically, the theory becomes strongly coupled at an energy scale given by the Planck mass.

An interesting alternative, suggested by results in loop quantum cosmology, consists in identifying the threshold with the attainment of Planckian density [182, 308]. In this scenario $\ell \sim \ell_{\rm P}\,(M/m_{\rm P})^{1/3}$, where M is the mass of the collapsing matter. This choice would thus entail a substantially larger value of $\mathrm{t}\ell$, compared to the previous one.

In either scenario, however, for astrophysically relevant masses, one would expect $\ell \ll M$. Indeed, using $m_{\rm P} \simeq 2.18 \times 10^{-8}\,\mathrm{kg}$ and $M_\odot \simeq 1.99 \times 10^{30}\,\mathrm{kg}$, we find

$$\ell \sim 1.10 \times 10^{-38} M_\odot \quad \text{in the first case, and} \tag{43}$$

$$\ell \sim 4.93 \times 10^{-26} M_\odot\,(M/M_\odot)^{1/3} \quad \text{in the second.} \tag{44}$$

These should be compared with the typical masses of astrophysical BHs: between approximately $3M_\odot$ and $\mathcal{O}\left(10^2 M_\odot\right)$ for stellar BHs visible by LIGO-Virgo-Kagra, and up to $10^{10} M_\odot$ for supermassive BHs.

In scenarios of this kind, therefore, gravitational collapse will always lead to the formation of a BH whenever GR predicts it does. More precisely, some initial conditions will lead to the formation of an horizon while others will result in the dispersion of the infalling matter: the two sets of initial data coincide with the corresponding sets in GR.[6] Moreover, the geometry of the BHs is probably going to be very similar to that of the corresponding GR solutions, and deviations from GR are likely to be too small to ever be observable.

The assumptions behind these scenarios, however, might be too simplistic. For instance, a regularisation at the Planck scale might be followed by a dynamical process, after which the structure settles down to one of the configurations that we are considering [255]. If this is the case, there is no reason for ℓ to be linked to the scale of quantum

6 Note: solutions near the threshold that separates the two sets often display critical behaviour [179]. Understanding the faith of such critical behaviour in theories beyond GR would be extremely interesting.

gravity. Such process might preserve or destroy the horizon, so that the remnant object might correspondingly consist of a (regular) BH or an horizonless configuration.

Yet another possibility is that new physics, unrelated to quantum gravity, appears way before the collapse reaches a Planckian regime. If this is the case, the formation of the horizon might be prevented altogether [15–17, 55, 92, 297].

Therefore, since the goal of these regularised models is that of providing a reasonable phenomenological description of astrophysical BHs, one can (and probably should) be agnostic on the scale of new physics. In particular one can (and should) consider values of ℓ that can be large, i. e. comparable with or larger than the mass of the object.

We close this section with a side remark. The decision to consider a scale with dimensions of length is somewhat arbitrary. It is motivated by the fact that, in units $c = G = 1$, length and mass/energy have the same dimensions and it is natural to associate the new physics responsible for the regularisation with some ultraviolet — high-energy and/or small-distance — extension of GR; moreover, length is often regarded as a rather fundamental concept compared to e. g. areas or volumes. However, what the regularisation seems to require is in fact an *area* scale, ℓ^2 rather than ℓ, corresponding roughly speaking to the upper bound of the curvature.

Incidentally, this resonates with similar remarks made by Hal Haggard in his introductory lectures to loop quantum gravity, as part of the "Basics of Quantum Gravity" series by the International Society for Quantum Gravity: in his view, the natural scale of quantum gravity has dimensions of area rather than length. This and all lectures in the series are available online.

4

ADDING ROTATION: THE NEWMAN–JANIS PROCEDURE

Astrophysical BHs rotate. Though accurately measuring their spin can be tricky [303], the fact that their angular momentum is generically non-zero is now well established. Hence, any model of compact objects that aims to be phenomenologically relevant ought to include rotation [256].

Dealing with rotation, however, brings about considerable hurdles already in GR. As an example, think of the problem of finding the metric describing a star: in spherical symmetry, Birkhoff's theorem ensures that in vacuum — i. e. outside of the star — the metric is that of Schwarzschild, so one really has to solve Einstein's equations only for the interior. When the symmetry is merely axial, in contrast, one has no guarantee that the exterior metric is that of Kerr, since no equivalent of Birkhoff's theorem exists in this case. Moving away from GR, the extent of the complications can only increase, and building rotating models from scratch is indeed difficult.

Since working in spherical symmetry is comparatively simpler, it would be very appealing to find some kind of procedure whereby a given non-rotating metric can be "spun up". In this way, one could carry out the model-building in spherical symmetry, for instance by regularising a known GR solution as in chapter 3; then add rotation and study the ensuing phenomenology. Luckily, though with many caveats, one such procedure exists: it is the Newman–Janis procedure (NJP).

The NJP [286] is a five-step method for constructing stationary and axially symmetric spacetimes: given any static and spherically symmetric "seed" metric, the method provides its rotating counterpart. Such counterpart depends continuously on a real parameter a, which can be interpreted *a posteriori* with the spin, and reduces to the seed metric in the limit $a \to 0$.

The NJP was originally discovered in the 1960s as a way of relating the Schwarzschild solution with the Kerr one. Soon thereafter, it was used to construct the Kerr–Newman metric, starting from the Reissner–Nordström [285] one. In its original version, the procedure says nothing about the electromagnetic field, which had to be solved for using the electrovacuum Einstein–Maxwell's equations. An interesting historical account of the events is provided by Newman himself in the Scholarpedia article on the Kerr–Newman metric [287]; for a somewhat different perspective, cf. Kerr's version of the story [220].

Since then, several extensions have been proposed to treat gauge fields or other charges, see [153] for a summary. Notably, it has been used quite extensively to generate rotating solutions in alternative theories of gravity [90] (although see [183]) and rotating RBHs, starting with [31].

Despite its successes, the method encodes some puzzling arbitrariness — on which we will elaborate further below — and a true understanding of its working is still lacking. Some solid ground has been established in [326] and further understanding came with [51, 52, 162, 300, 301]; recently, some new insight has come from the study of scattering amplitudes [13, 178]. This notwithstanding, the status of the NJP is highly disputed to this day: while some authors consider it little more than a *trick*, or perhaps an *Ansatz*, others are ready to grant it the name of *algorithm* and employ it as a genuine solution-generating technique.

Our use of the term *procedure* is meant to signify that we take an agnostic stance on the matter: in our view, the spacetimes constructed by means of the NJP are well motivated, particularly if one reasons in "effective" terms and is mostly interested in phenomenological applications; still, the limitations inherent in the method are real and cannot be disregarded.

In the following, we will first present the "traditional" version of the NJP (section 4.1), then move on to a modern variant (section 4.2). Finally, we will briefly discuss some early day applications to RBHs (section 4.3).

4.1 TRADITIONAL NJP

The starting point of the NJP is a "seed" metric that is supposed to be static and spherically symmetric. As mentioned in chapter 3, such a metric can always be cast in the form

$$ds^2 = -f(r)\mathrm{d}t^2 + \frac{\mathrm{d}r^2}{g(r)} + h(r)\,\mathrm{d}\Omega^2\,, \tag{45}$$

which is however quite redundant, since one between g and h can be reabsorbed by redefining r.

We will present the application of the NJP to the general form eq. (45), since this will lead to an equally general stationary and axially symmetric metric that can be easily specified to any particular case. The procedure goes as follows.

As a **step I**, write the metric in outgoing (or, equivalently, ingoing) Eddington–Finkelstein coordinates (u, r, θ, ϕ). The retarded time u is defined in terms of the tortoise coordinate r_*, as usual, by

$$\mathrm{d}u = \mathrm{d}t - \mathrm{d}r_* = \mathrm{d}t - \frac{\mathrm{d}r}{\sqrt{f(r)g(r)}}\,, \tag{46}$$

so

$$ds^2 = -f\,\mathrm{d}u^2 - 2\sqrt{\frac{f}{g}}\,\mathrm{d}u\,\mathrm{d}r + h\,\mathrm{d}\Omega^2\,. \tag{47}$$

Then (**step II**) introduce a null tetrad $\{l^\mu,\ n^\mu,\ m^\mu,\ \overline{m}^\mu\}$ (the overline marks complex conjugation) satisfying

$$l^\mu n_\mu = -m^\mu \overline{m}_\mu = -1 \quad \text{and} \tag{48a}$$

$$l^\mu m_\mu = n^\mu m_\mu = 0\,, \tag{48b}$$

in terms of which the inverse metric can be written as

$$g^{\mu\nu} = -l^\mu n^\nu - l^\nu n^\mu + m^\mu \overline{m}^\nu + m^\nu \overline{m}^\mu\,. \tag{49}$$

These conditions do not determine the tetrad uniquely. For instance, one could rescale

$$l^\mu \mapsto \alpha l^\mu \quad \text{provided} \quad n^\mu \mapsto \frac{n^\mu}{\alpha}\,; \tag{50}$$

and similarly one could multiply m^μ by a complex phase, provided one multiplies $\overline{m}^\mu$ by the complex conjugate of the same phase. However, this ambiguity is inconsequential for what follows. Typically, one uses

$$\begin{aligned} l^\mu &= \delta^\mu_r\,, \quad n^\mu = \sqrt{\frac{g(r)}{f(r)}}\,\delta^\mu_u - \frac{g(r)}{2}\,\delta^\mu_r\,, \\ m^\mu &= \frac{1}{\sqrt{2h(r)}}\left(\delta^\mu_\theta + \frac{\mathrm{i}}{\sin\theta}\,\delta^\mu_\phi\right)\,. \end{aligned} \tag{51}$$

As a **step III**, define

$$\tilde{r} = r + \mathrm{i}a\cos\theta, \quad \tilde{u} = u - \mathrm{i}a\cos\theta, \quad \tilde{\theta} = \theta, \quad \tilde{\phi} = \phi\,, \tag{52}$$

where a is a real parameter to be identified, *a posteriori*, with the spin; even though $\tilde{r}$ and $\tilde{u}$ are complex, these relations define a viable change of coordinates. The usual vector transformation law thus yields a transformed tetrad:

$$\begin{aligned} \tilde{l}^\mu &= \delta^\mu_{\tilde{r}}\,, \quad \tilde{n}^\mu = \sqrt{\frac{g(r)}{f(r)}}\,\delta^\mu_{\tilde{u}} - \frac{g(r)}{2}\,\delta^\mu_{\tilde{r}}\,, \\ \tilde{m}^\mu &= \frac{1}{\sqrt{2h(r)}}\left[\delta^\mu_{\tilde{\theta}} - \mathrm{i}a\sin\tilde{\theta}\,(\delta^\mu_{\tilde{r}} - \delta^\mu_{\tilde{u}}) + \frac{\mathrm{i}}{\sin\tilde{\theta}}\,\delta^\mu_{\tilde{\phi}}\right]\,, \end{aligned} \tag{53}$$

where r is now meant as a scalar function of $\tilde{r}$ and $\tilde{\theta}$ (not a coordinate). Correspondingly, one also gets a transformed metric:

$$\begin{aligned} ds^2 = {} & -f\,\mathrm{d}\tilde{u}^2 - 2\sqrt{\frac{f}{g}}\,\mathrm{d}\tilde{u}\,\mathrm{d}\tilde{r} + h\,\mathrm{d}\tilde{\theta}^2 + 2a\sin^2\tilde{\theta}\sqrt{\frac{f}{g}}\,\mathrm{d}\tilde{r}\,\mathrm{d}\tilde{\phi} \\ & + 2a\sin^2\tilde{\theta}\left[f - \sqrt{\frac{f}{g}}\right]\mathrm{d}\tilde{u}\,\mathrm{d}\tilde{\phi} \\ & + \sin^2\tilde{\theta}\left[h + a^2\sin^2\tilde{\theta}\left(-f + 2\sqrt{\frac{f}{g}}\right)\right]\mathrm{d}\tilde{\phi}^2\,. \end{aligned} \tag{54}$$

To obtain a new, axially symmetric metric, one needs (**step IV**) to replace the old functions f, g and h with new $\tilde{f}$, $\tilde{g}$ and $\tilde{h}$; the latter are required to be real-valued, though of complex variable, and to coincide with the former when evaluated on the real axis.

This replacement, in the standard NJP, is performed in a rather particular way but is, nonetheless, arbitrary. For example, in the Schwarzschild geometry one has

$$f(r) = g(r) = 1 - \frac{2M}{r}\,, \quad h(r) = r^2\,; \tag{55}$$

to derive the Kerr solution, $\tilde{f}$, $\tilde{g}$ and $\tilde{h}$ are given by replacing ("complexifing")

$$\frac{1}{r} \mapsto \frac{1}{2}\left(\frac{1}{r} + \frac{1}{\bar{r}}\right) = \frac{1}{2}\frac{r+\bar{r}}{r\,\bar{r}} \quad \text{and} \quad r^2 \mapsto r\,\bar{r} \tag{56}$$

in f and h, i. e.

$$\begin{aligned} f(r) &\mapsto \tilde{f}\left(\tilde{r},\tilde{\theta}\right) = 1 - \frac{2M\tilde{r}}{\tilde{r}^2 + a^2\cos^2\tilde{\theta}}\,, \\ g(r) &\mapsto \tilde{g}\left(\tilde{r},\tilde{\theta}\right) = \tilde{f}\left(\tilde{r},\tilde{\theta}\right)\,, \\ h(r) &\mapsto \tilde{h}\left(\tilde{r},\tilde{\theta}\right) = \tilde{r}^2 + a^2\cos^2\tilde{\theta} \end{aligned} \tag{57a}$$

— all other prescriptions fail. These replacements have no real justification, except that, in GR, they map vacuum and electrovacuum solutions onto vacuum and electrovacuum solutions.

To improve the flow of the exposition, we presented steps III and IV as separate. In principle, however, they should be carried out at the same time, as described in [326], because the complex coordinate change of step III is, in fact, as arbitrary as the complexification of step IV. Indeed, the particular form of eq. (52) is not particularly motivated and *a priori* nothing forbids to choose a different one.

In any case, our choice is coherent with what seems to be the common practice. In fact, in most applications step III is carried out as in eq. (52), and the true ambiguity lies in the choice of $\tilde{f}$, $\tilde{g}$ and $\tilde{h}$.

The complexification produces a metric with several off-diagonal components. To eliminate all of them except one, one needs to perform an additional transformation to Boyer–Lindquist-like coordinates (**step V**). The desired change is of the form

$$\mathrm{d}\tilde{t} = \mathrm{d}\tilde{u} + F\left(\tilde{r},\tilde{\theta}\right)\mathrm{d}\tilde{r}\,, \quad \mathrm{d}\phi' = \mathrm{d}\tilde{\phi} + G\left(\tilde{r},\tilde{\theta}\right)\mathrm{d}\tilde{r}\,, \tag{58}$$

with

$$F = \frac{\sqrt{\frac{\tilde{g}}{\tilde{f}}}\tilde{h}\left(\tilde{r},\tilde{\theta}\right) + a^2\sin^2\tilde{\theta}}{\tilde{g}\left(\tilde{r},\tilde{\theta}\right)\tilde{h}\left(\tilde{r},\tilde{\theta}\right) + a^2\sin^2\tilde{\theta}}\,, \tag{59a}$$

$$G = \frac{a}{\tilde{g}\left(\tilde{r},\tilde{\theta}\right)\tilde{h}\left(\tilde{r},\tilde{\theta}\right) + a^2\sin^2\tilde{\theta}}\,. \tag{59b}$$

However, this transformation is not always possible. Indeed, to integrate the above relations one needs F and G to be independent from $\tilde{\theta}$: this is the case, for instance, in Schwarzschild and Reissner–Nordström, but examples of the contrary exist.

When a Boyer–Lindquist form exists, the resulting metric takes the form

$$\begin{aligned} ds^2 = &-\tilde{f}\,\mathrm{d}\tilde{t}^2 + \frac{\tilde{h}}{\tilde{g}\tilde{h} + a^2\sin^2\tilde{\theta}}\,\mathrm{d}\tilde{r}^2 + \tilde{h}\,\mathrm{d}\tilde{\theta}^2 \\ &- 2a\sin^2\tilde{\theta}\left(-\tilde{f} + \sqrt{\frac{\tilde{f}}{\tilde{g}}}\right)\mathrm{d}\tilde{t}\,\mathrm{d}\phi' \\ &+ \sin^2\tilde{\theta}\left[\tilde{h} + a^2\sin^2\tilde{\theta}\left(-f + 2\sqrt{\frac{\tilde{f}}{\tilde{g}}}\right)\right]\mathrm{d}\phi'^2\,. \end{aligned} \tag{60}$$

Note that the tildes and primes have been kept throughout the exposition in order to avoid confusions. However, in practical applications it is customary to change names to the coordinates, dropping all decorations already in intermediate steps.

If the spherically symmetric seed is asymptotically flat, one may want to choose a complexification that does not spoil this property. That is, the new $\tilde{f}$, $\tilde{g}$ and $\tilde{h}$ should behave, at large $|\tilde{r}|$, as the old f, g and h do for large $|r|$ — cf. eq. (6). In particular, if at large $|\tilde{r}|$

$$\tilde{f} = 1 - \frac{2M}{|\tilde{r}|} + \mathcal{O}\left(|\tilde{r}|^{-2}\right) \quad \text{and} \quad \tilde{h} = |\tilde{r}|^2\left[1 + \mathcal{O}\left(|\tilde{r}|^{-3}\right)\right], \tag{61}$$

then eq. (60) becomes

$$\begin{aligned} ds^2 = &-\left(1 - \frac{2M}{|\tilde{r}|}\right)\mathrm{d}\tilde{t}^2 + \frac{\mathrm{d}\tilde{r}^2}{1 - \frac{2M}{|\tilde{r}|}} + |\tilde{r}|^2\left[\mathrm{d}\tilde{\theta}^2 + \sin^2\tilde{\theta}\,\mathrm{d}\phi'^2\right] \\ &- \frac{4aM\sin^2\tilde{\theta}}{|\tilde{r}|}\,\mathrm{d}\tilde{t}\,\mathrm{d}\phi'\,, \end{aligned} \tag{62}$$

and we understand that aM plays the role of the spacetime's ADM angular momentum.

We will use this traditional form of the NJP to construct the rotating generalisation of the SV metric, which we will call the black-bounce–Kerr spacetime, in chapter 5.

4.2 MODIFIED NJP

Many tweaks to the original NJP have been proposed over the years, improving on some technical aspects but without affecting the overall spirit of the procedure.

One more radical modification is due to Azreg-Aïnou [21, 22] (see also [23]). His version of the procedure, which we will call modified

Newman–Janis procedure (MNJP), is such that the final metric can always be cast into a Boyer–Lindquist form, by construction. Moreover, this version does not rely on any complexification, neither of the coordinates nor of the metric components. Rather, the arbitrariness inherent in the traditional NJP is encoded in a single free function $\Psi(r,\theta)$, which appears as a multiplicative factor in front of the line element.

This free function can then be constrained invoking new physical arguments, for instance by postulating the existence of a matter source with a physically reasonable stress-energy tensor. Note that, since Ψ appears as a conformal factor, it has no effect on the motion of light [241].

For the details, we refer the reader to the original papers [21, 22]. Here we only report the final form of the rotating metric, which reads

$$\begin{aligned} ds^2 = \frac{\Psi}{\Sigma}\Big[&- \left(1 - \frac{2H}{\Sigma}\right) \mathrm{d}t^2 + \frac{\Sigma}{\Delta}\,\mathrm{d}r^2 + \Sigma\,\mathrm{d}\theta^2 \\ &+ \frac{A\sin^2\theta}{\Sigma}\,\mathrm{d}\phi^2 - \frac{4Ha\sin^2\theta}{\Sigma}\,\mathrm{d}t\,\mathrm{d}\phi\Big]\,, \end{aligned} \tag{63}$$

where

$$\begin{aligned} &\Sigma = K + a^2\cos^2\theta\,, \quad 2H(r) = K - g(r)h(r)\,, \\ &\Delta = g(r)h(r) + a^2\,, \quad A = (K+a^2)^2 - a^2\Delta\sin^2\theta\,, \\ &K(r) = h(r)\sqrt{\frac{g(r)}{f(r)}}\,. \end{aligned} \tag{64}$$

(With respect to eq. (60), we have dropped tildes and primes.)

Clearly, a very natural choice seems to be $\Psi = \Sigma$, and indeed this is what one has to impose to recover Kerr when starting from Schwarzschild. Moreover, if the seed metric can be interpreted as a solution of some non-linear electrodynamics (like the simply connected RBHs of section 3.2), the field equations imply $\Psi = \Sigma$.

More generally, one might want to impose that the original seed metric is recovered in the limit of vanishing spin, which entails

$$\lim_{a\to 0} \Psi(r,\theta) = r^2\,. \tag{65}$$

However, this condition is very loosely restrictive and different choices of Ψ are certainly allowed. Indeed, such freedom will be exploited in chapter 9 to build a rotating model of simply connected RBH in which the properties of the inner horizon are disentangled from those of the region close to $r = 0$.

4.3 SOME EARLY APPLICATIONS TO RBHS

Both versions of the NJP can be applied to the spherically symmetric RBHs of sections 3.2 and 3.3. The traditional form, in particular, has

been used several times on simply connected RBHs — see [343] for a recent review.

In this approach, the non-trivial step consists in finding a suitable complexification. Since the simply connected RBHs typically have

$$f(r) = g(r) = 1 - \frac{2m(r)}{r} \quad \text{and} \quad h(r) = r^2\,, \tag{66}$$

the most obvious choice is to take

$$\tilde{f} = \tilde{g} = 1 - \frac{2\tilde{m}(r,\theta)r}{r^2 + a^2\cos^2\theta} \quad \text{and} \quad \tilde{h} = r^2 + a^2\cos^2\theta\,, \tag{67}$$

where $\tilde{m}(r,\theta)$ is an arbitrary function of r *and* θ. The corresponding metric is therefore similar to Kerr, and can be obtained from it, formally, by replacing the mass parameter M with $\tilde{m}$.

The simplest and most frequent choice is to drop the angular dependence in $\tilde{m}$, and to maintain the same functional dependence on the radius. That is, $\tilde{m}(r,\theta)$ is taken to be $m(r)$ — though technically the meaning of r changes in passing from the static to the stationary metric. Note however that there might be good reasons to keep the angular dependence [147–149].

The result is known as Gürses–Gürsey metric [181] and it reads

$$\begin{aligned} ds^2 = &-\left(1 - \frac{2m(r)r}{\Sigma}\right)\mathrm{d}t^2 + \frac{\Sigma}{\Delta}\,\mathrm{d}r^2 + \Sigma\,\mathrm{d}\theta^2 \\ &- \frac{4m(r)a\sin^2\theta}{\Sigma}\,\mathrm{d}t\,\mathrm{d}\phi + \frac{A\sin^2\theta}{\Sigma}\,\mathrm{d}\phi^2 \end{aligned} \tag{68}$$

where

$$\begin{aligned} &\Sigma = r^2 + a^2\cos^2\theta\,, \quad \Delta = r^2 + a^2 - 2m(r)r \\ &A = (r^2 + a^2)^2 - \Delta a^2\sin^2\theta\,. \end{aligned} \tag{69}$$

The first investigation of the rotating Hayward and Bardeen models appeared in [31]; several other examples followed soon thereafter. [31, 218, 264, 345, 346] The general properties of RBHs based on eq. (68) have been investigated in [146]. Few criteria for preferring some models over others have been discussed in [249].

All these models are reasonably simple and therefore particularly amenable to phenomenological applications, e. g. the computation of the electromagnetic shadow's shape; some examples can be found in [3, 34, 174, 230, 347, 360]. Notably, when the spherical seed can be interpreted as a solution of some non-linear electrodynamics, the Gürses–Gürsey counterpart can too [145, 346, 349].

Interested readers are encouraged to consult the cited literature for further details; here, we limit ourselves to some general remark.

Spacetimes that, like eq. (68), are Petrov type D and not spherically symmetric have four independent second-order curvature invariants. So, checking that the Kretschmann scalar is bounded is not sufficient

to assess regularity. Note that, since these spacetimes are regularisations of Kerr, dangerous behaviour might arise at $r = 0$ *only* for $\theta = \pi/2$; this "point" is in fact a ring lying on the equatorial plane, as can be seen by changing to Kerr–Schild coordinates [362].

Remarkably, the conditions that guarantee regularity in the spherical case ensure regularity in the rotating case as well. In particular, one needs

$$m(0) = m'(0) = m''(0) = 0\,, \tag{70}$$

i. e. $m(r) = \mathcal{O}(r^3)$ close to $r = 0$.

However, if $m(r) = c\ell^{-2}r^3 + \mathcal{O}(r^4)$ — as in the Bardeen and Hayward case, for example —, the curvature invariants exhibit a rather bizarre behaviour at the would-be singularity (i. e. on the ring). Specifically, the results one typically finds have the form

$$\propto \frac{r^2}{r^2 + a^2\cos^2\theta} + \dots\,, \tag{71}$$

meaning that the limit $r \to 0$, $\theta \to \pi/2$ formally does not exist. Indeed, if one takes the limit $r \to 0$ at any fixed $\theta \neq \pi/2$ one gets zero; while if one takes $\theta \to \pi/2$ first and then $r \to 0$ one gets a finite non-zero results. In other words, the curvature invariants are bounded but not continuous at the would-be singularity.

Moreover, since $r = 0$ is a ring that can be traversed for all $\theta \neq \pi/2$, the maximal analytical extension of these spacetimes typically extends to the negative values of r — as it happens for the Kerr spacetime. In such region, the Killing vector associated to the rotational isometry may become timelike: since its orbits are closed by definition, this entails that the spacetime can contain closed timelike curves. Additionally, several commonly used choices of $m(r)$ formally display poles in the $r < 0$ region, which might correspond to (new) spacetime singularities [231, 373].

The non-continuity of curvature scalars and the possible existence of closed timelike curves are thus two unpleasant, yet fairly common features of such rotating simply connected RBHs [344]. Though these drawbacks might not be relevant for phenomenological applications, they render these models less appealing from a theoretical point of view and motivate us to seek alternatives.

The next chapters 5 to 8 — which together form part ii — are devoted to the investigation of one such alternative, belonging to the multiply connected class: the black bounce family of spacetimes.

Part II

THE BLACK-BOUNCE FAMILY AND ITS PHENOMENOLOGY

5

THE BLACK-BOUNCE–KERR SPACETIME

We are now in the position to construct a rotating extension of the SV metric eq. (40) — which we report here for the reader's convenience:

$$ds^2 = -\left(1 - \frac{2M}{\sqrt{r^2+\ell^2}}\right) \mathrm{d}t^2 + \frac{\mathrm{d}r^2}{1 - \frac{2M}{\sqrt{r^2+\ell^2}}} + \left(r^2+\ell^2\right) \mathrm{d}\Omega^2 \,. \tag{72}$$

Not surprisingly, such extension will be a one-parameter deformation of the Kerr metric which, with no stretch of imagination, we will call *rotating* SV or *black-bounce–Kerr*.

The presentation will start off with a step-by-step application of the NJP (section 5.1). The resulting metric, eq. (80), is the core result of this chapter. We will then investigate the causal structure in section 5.2; and characterise the effective matter content in section 5.3. Finally, in section 5.4 we will describe how some features of the external geometry differ from their Kerr counterparts. Section 5.5 will close the chapter with a few remarks.

We will often resort to the handy notation $\varrho = \sqrt{r^2+\ell^2}$ to improve the looks of long expressions.

5.1 BUILDING THE METRIC

To apply the NJP to the SV metric eq. (72), we need to specify the steps described in section 4.1 to the particular case

$$f(r) = 1 - \frac{2M}{\sqrt{r^2+\ell^2}} = g(r), \quad h(r) = r^2+\ell^2 \,. \tag{73}$$

The definition of the null coordinate u (step I), the introduction of the null tetrad $\{l^\mu,\ n^\mu,\ m^\mu,\ \overline{m}^\mu\}$ (step II) and the complex coordinate transformation to $(\tilde{u},\ \tilde{r})$ (step III) are immediate.

Step IV instead is non-trivial: we need to provide a prescription for the complexification that will yield the new functions $\tilde{f}$ and $\tilde{h}$ and, in turn, the new metric. This prescription is arbitrary but, as we discussed, in GR only one actually works.

Here, however, we are not solving any equations and we have no way of telling if a choice is "right". Luckily, there is one choice that seems *natural*. Indeed, since the components of the SV metric are derived from those of Schwarzschild by writing $\sqrt{r^2+\ell^2}$ instead of r, one is tempted to use $\varrho = \sqrt{r^2+\ell^2}$ and complexify it as would be appropriate for Schwarzschild's radial coordinate. Namely

$$\varrho \mapsto \tilde{\varrho} = \varrho + \mathrm{i}a\cos\theta, \tag{74}$$

so that

$$h(r) = \varrho^2 \to \tilde{h}(\tilde{r}) = \tilde{\varrho}\bar{\tilde{\varrho}} = \tilde{r}^2 + \ell^2 + a^2\cos^2\theta \tag{75}$$

and

$$\begin{aligned} f(r) = 1 - \frac{2M}{\varrho} \to \tilde{f}(r') &= 1 - M\left(\frac{1}{\tilde{\varrho}} + \frac{1}{\bar{\tilde{\varrho}}}\right) \\ &= 1 - \frac{2M\sqrt{\tilde{r}^2+\ell^2}}{\tilde{r}^2 + \ell^2 + a^2\cos^2\theta}. \end{aligned} \tag{76}$$

Assuming this complexification, we are only left with step V, the transformation

$$\mathrm{d}\tilde{t} = \mathrm{d}\tilde{u} + F\,\mathrm{d}\tilde{r}\,, \quad \mathrm{d}\phi' = \mathrm{d}\tilde{\phi} + G\,\mathrm{d}\tilde{r} \tag{77}$$

to Boyer–Lindquist-like coordinates. Plugging the right expressions into eq. (59), we find

$$F = \frac{\tilde{r}^2 + \ell^2 + a^2}{\tilde{r}^2 + \ell^2 + a^2 - 2M\sqrt{\tilde{r}^2+\ell^2}}\,, \tag{78}$$

$$G = \frac{a}{\tilde{r}^2 + \ell^2 + a^2 - 2M\sqrt{\tilde{r}^2+\ell^2}}\,; \tag{79}$$

these expressions do not depend on θ and one can safely integrate them to get $\tilde{t}(u,\tilde{r})$, $\phi'(u,\tilde{r})$. (From now on we drop tildes and primes.)

Thus, the metric obtained by applying the NJP to the SV seed does have a Boyer–Lindquist form. Note that this is obvious, in hindsight, since the functions F, G above are the same that one would get starting from a Schwarzschild seed, provided one replaces the coordinate radius r with $\sqrt{r^2+\ell^2}$, and a Boyer–Lindquist form certainly exists in that case.

The metric ensuing from the application of the NJP with the choices above is our proposal for the rotating counterpart to the SV metric eq. (72):

$$\begin{aligned} \mathrm{d}s^2 = &-\left(1 - \frac{2M\sqrt{r^2+\ell^2}}{\Sigma}\right)\mathrm{d}t^2 + \frac{\Sigma}{\Delta}\,\mathrm{d}r^2 + \Sigma\mathrm{d}\theta^2 \\ &- \frac{4Ma\sin^2\theta\sqrt{r^2+\ell^2}}{\Sigma}\,\mathrm{d}t\mathrm{d}\phi + \frac{A\sin^2\theta}{\Sigma}\,\mathrm{d}\phi^2 \end{aligned} \tag{80}$$

with

$$\begin{aligned} &\Sigma = r^2 + \ell^2 + a^2\cos^2\theta\,, \qquad \Delta = r^2 + \ell^2 + a^2 - 2M\sqrt{r^2+\ell^2}\,, \\ &A = (r^2 + \ell^2 + a^2)^2 - \Delta a^2\sin^2\theta\,. \end{aligned}$$

It reduces to the SV metric when $a = 0$ and to the Kerr metric when $\ell = 0$. Formally, its components can be derived from those of the Kerr metric by replacing the Boyer–Lindquist radius r with $\sqrt{r^2+\ell^2}$, but

without changing dr; i. e. the metric eq. (80) is *not* related to Kerr by a change of coordinates.

The result eq. (80) obtained with the standard NJP is confirmed by the application of the MNJP, provided the arbitrary function Ψ be fixed equal to Σ. This choice is coherent with requiring that the spinning metric coincides with Kerr when $\ell = 0$, as it must.

We can now move on to characterise the metric eq. (80) and the spacetime it describes.

5.2 METRIC ANALYSIS AND SPACETIME STRUCTURE

As in the non-spinning case, r may take positive *as well as negative* values. Our negative-r region, however, should not be confused with the one deriving from analytically extending the Kerr spacetime beyond its ring singularity: indeed, the metric eq. (80) is symmetric under the reflection $r \mapsto -r$ and the spacetime it describes is thus composed of two identical portions glued at $r = 0$.

Some intuition can be gained by noting that the surface $r = 0$ is an oblate spheroid of size (Boyer–Lindquist radius) ℓ. When $\ell = 0$, the spheroid collapses to a ring at $\theta = \pi/2$ and the usual singularity of the Kerr geometry is recovered. When instead $\ell \neq 0$ the singularity is excised and $r = 0$ is a regular surface of finite size, which observers may cross: the metric eq. (80) thus describes a wormhole with throat located at $r = 0$. The nature of such throat (timelike, spacelike or null) depends on ℓ and a. Actually, $|a|$ is the relevant parameter, thus, without loss of generality, we only consider $a > 0$ here and throughout.

The values of ℓ and a also determine whether the metric has coordinate singularities. When this is the case, the singularities are given by $\Delta = 0$ and located at

$$r_\pm = \left[\left(M \pm \sqrt{M^2 - a^2}\right)^2 - \ell^2\right]^{1/2} . \tag{81}$$

By calling

$$\varrho_\pm = M \pm \sqrt{M^2 - a^2} , \tag{82}$$

we immediately see that r_+ is real only if $\ell \leq \varrho_+$ and, similarly, r_- is real only if $\ell \leq \varrho_-$. Thus, depending on the values of the parameters, we may have two (if $a < M$ and $\ell < \varrho_-$), one (if $a < M$ and $\varrho_- < \ell < \varrho_+$) or no singularity at all (if $a < M$ and $\ell > \varrho_+$, or if $a > M$). The cases in which equalities hold are extremal or limiting versions of the above. As the analysis in the following subsection will prove, these coordinate singularities are horizons of the spacetime.

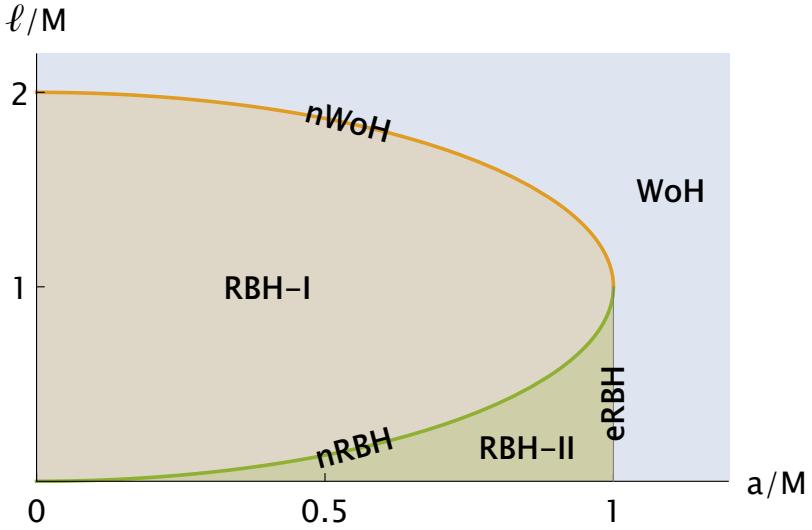

Figure 1: Parameter space and corresponding spacetime structure. Acronyms are spelled out in the text.

5.2.1 *Phase diagram*

For the sake of practicality, we summarise the spectrum of possible cases with the aid of a "phase diagram" in figure 1: each spacetime structure is associated with a region in (a constant-M slice of) the parameter space under consideration. We defer a thorough discussion of each case to subsection 5.2.3, but lay out our terminology here:

WOH traversable wormhole;

NWOH null WoH, i. e. one-way wormhole with null throat;

RBH-I RBH with one horizon (in the $r > 0$ side, plus its mirror image in the $r < 0$ side);

RBH-II RBH with an outer and an inner horizon (per side);

ERBH extremal RBH (one extremal horizon per side);

NRBH null RBH-I, i. e. a RBH with one horizon (per side) and a null throat.

We point out, in passing, that a similar "phase diagram" has been derived in [75] by applying the NJP to a seed metric inspired by loop quantum gravity.

5.2.2 *Null rays and horizon structure*

To check that the singularities at $\Delta = 0$ are coordinate artefacts, one can introduce ingoing null coordinates

$$\mathrm{d}v = \mathrm{d}t + \frac{\varrho^2 + a^2}{\Delta}\,\mathrm{d}r\,, \qquad \mathrm{d}\psi = \mathrm{d}\phi + \frac{a}{\Delta}\,\mathrm{d}r\,, \tag{83}$$

and notice that the resulting metric is indeed regular at $r = r_\pm$ except perhaps when $v = \pm\infty$; equivalently, one could adopt outgoing null coordinates

$$\mathrm{d}u = \mathrm{d}t - \frac{\varrho^2 + a^2}{\Delta}\,\mathrm{d}r\,, \qquad \mathrm{d}\tilde{\psi} = \mathrm{d}\phi - \frac{a}{\Delta}\,\mathrm{d}r\,, \tag{84}$$

and confirm the same result except perhaps at $u = \pm\infty$. Either patch covers the region on which the other is not defined, thus proving that geodesics can be extended beyond $r = r_\pm$. The same deduction holds for $-r_\pm$.

We further investigate the nature of the surfaces $r = \pm r_\pm$ by plotting the null rays $v = \mathrm{cst}$, $u = \mathrm{cst}$, in figure 2. We choose for simplicity $\theta = 0$. The horizontal axes represents the Boyer–Lindquist radius r, while the time coordinate on the vertical axes t^v_* is defined by

$$\mathrm{d}t^v_* = \mathrm{d}v - \mathrm{d}r\,, \tag{85}$$

so that

$$v = \mathrm{cst} \Rightarrow t^v_* = -r + \mathrm{cst}\,, \tag{86}$$

$$u = \mathrm{cst} \Rightarrow t^v_* = -\int^r \left(1 - 2\,\frac{\varrho^2 + a^2}{\Delta}\right)\mathrm{d}r' + \mathrm{cst}\,. \tag{87}$$

The peeling of outgoing rays shows that the surfaces $v = \mathrm{cst}$ and $r = \pm r_\pm$ are indeed horizons: r_+ and $-r_-$ are black-hole horizons, while r_- and $-r_+$ are white-hole horizons. An analogous analysis adapted to outgoing rays, in which these appear as straight lines while ingoing rays present peeling, shows that the surfaces $\pm r_\pm$ and $u = \mathrm{cst}$ have the opposite nature with respect to their $v = \mathrm{cst}$ counterparts: r_+ is a white-hole horizon, r_- a black-hole horizon, etc.

5.2.3 *Carter–Penrose diagrams*

The analytical extension of the metric eq. (80) across the horizons can be performed by standard methods (see e. g. [113]), by changing to suitable Kruskal-like coordinates U, V (a redefinition of ϕ is also required), defined in terms of u, v by an exponential mapping involving the surface gravity of the horizon under consideration and compensating for the peeling of null rays off of it.

The only practical difference between the textbook case of Kerr and our own lies in the functional relation between, e. g. the Boyer–Lindquist radius r and the tortoise coordinate r_*. Such difference is inconsequential as far as analytic continuation is concerned; for instance, curves $UV = \mathrm{cst}$ correspond to curves $r = \mathrm{cst}$ in Kerr as well as in this case.

We construct Carter–Penrose diagrams for the maximal extension of the six cases identified in section subsection 5.2.1 and report them in figures 3 and 4. A detailed description of each case follows.

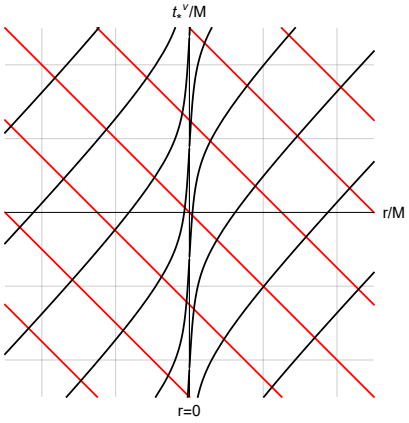

(a) Traversable wormhole (WoH).

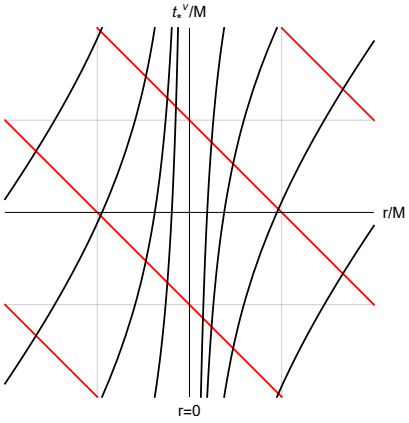

(b) Null wormhole (nWoH).

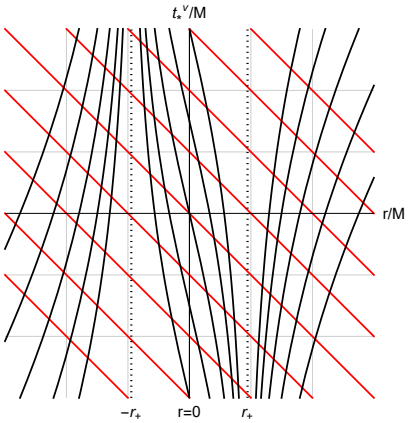

(c) Regular black hole, one horizon (RBH-I).

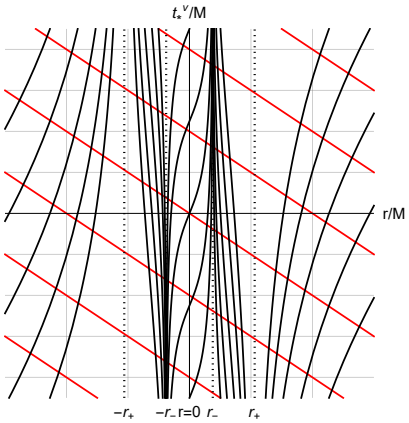

(d) Regular black hole, two horizons (RBH-II).

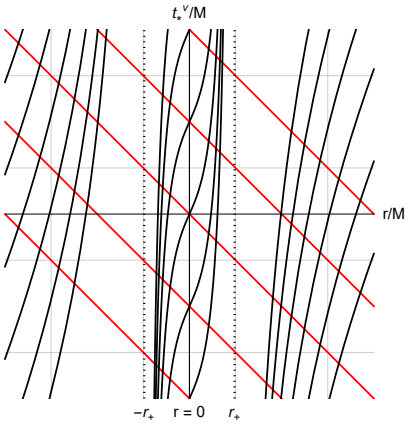

(e) Extremal regular black hole, one horizon (eRBH).

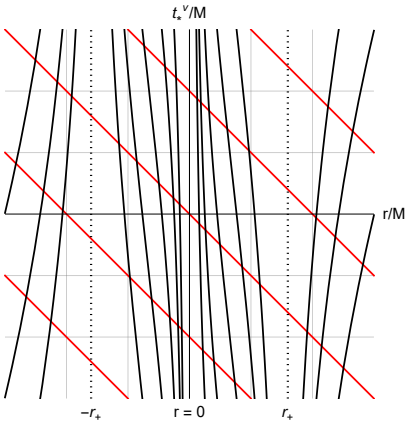

(f) Null regular black hole, one horizon (nRBH).

Figure 2: Ingoing (red) and outgoing (black) null rays close to $\pm r_\pm$ for the different cases in the phase diagram. Particular values of a and ℓ have been picked.

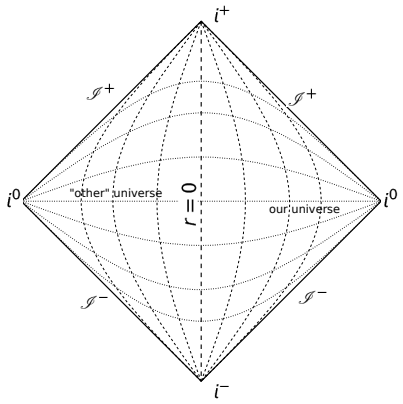

(a) WoH, corresponding to $\ell > \varrho_+$ and $a < M$, or $a > M$. The throat $r = 0$ is a timelike surface, traversable in both ways.

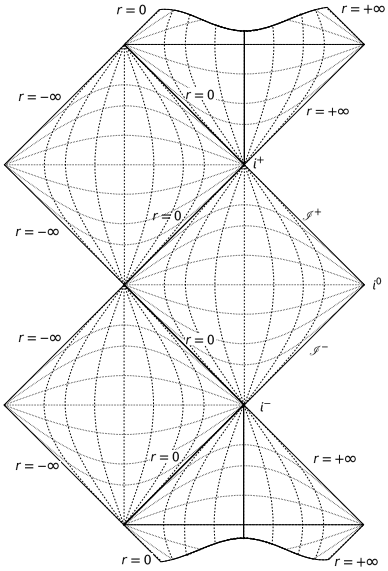

(b) nWoH, corresponding to $\ell = \varrho_+$ (and $a < M$). The throat $r = 0$ is a null surface and is an extremal event horizon.

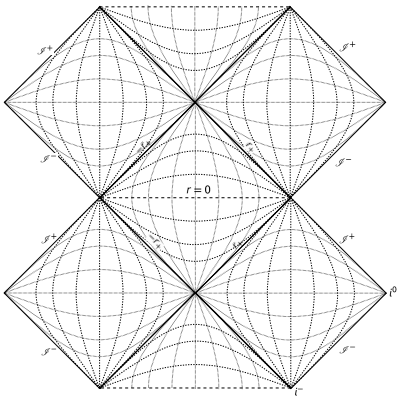

(c) RBH-I, corresponding to $\varrho_- < \ell < \varrho_+$ (and $a < M$). The throat is spacelike and cloaked by an event horizon.

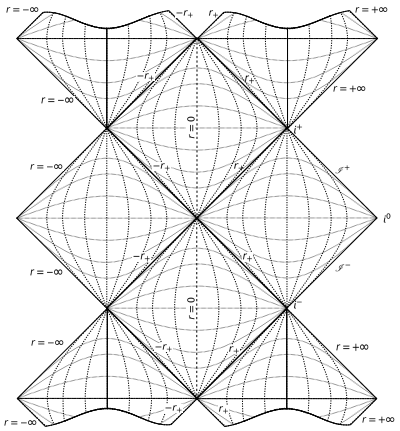

(d) eRBH, corresponding to $a = M$ and $\ell < \varrho_- = \varrho_+$. The throat is timelike and the event horizon is extremal.

Figure 3: Carter–Penrose diagrams for different spacetimes represented by the metric (80). The lines $r = 0$ correspond to the throat of the wormhole, which is a regular surface of finite area.

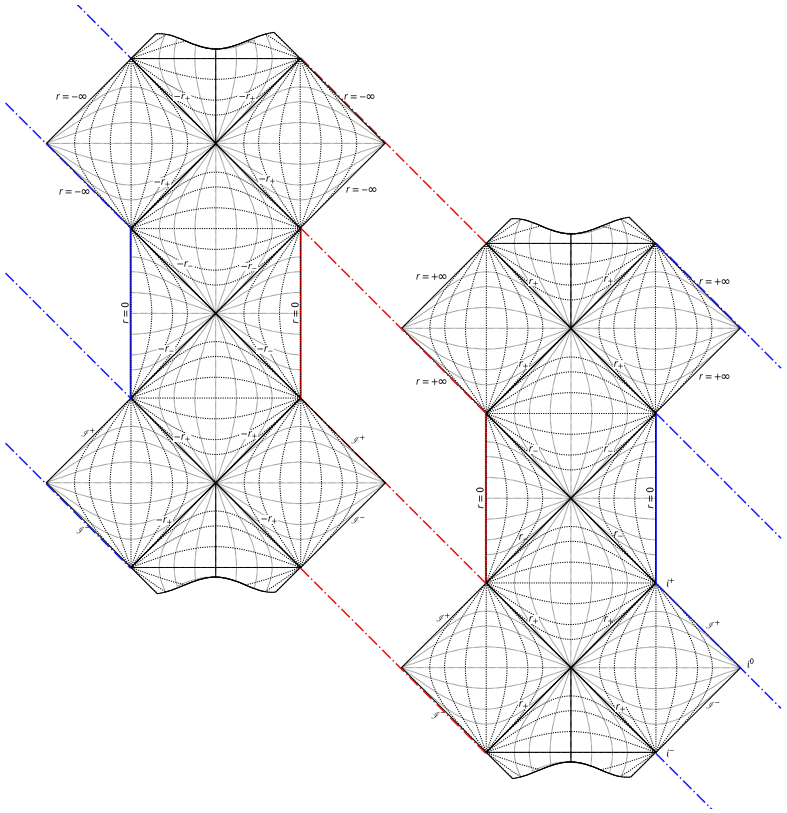

(a) RBH-II, corresponding to $\ell < \varrho_-$ (and $a < M$). $r = 0$ lines of the same colour, representing the wormhole throat, are identified.

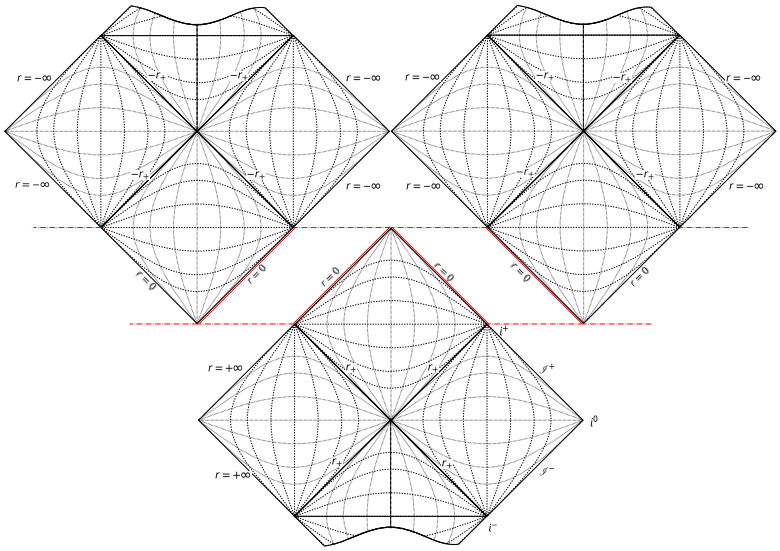

(b) nRBH, corresponding to $\ell = \varrho_-$ (and $a < M$). Coloured $r = 0$ lines are identified as indicated by dotted-dashed lines: they represent the wormhole throat, which in this case is also an extremal (inner) horizon.

Figure 4: Carter–Penrose diagrams (cont.). As in figure figure 3, $r = 0$ corresponds to the regular, finite area throat.

WOH is a traversable, two-way wormhole with a timelike throat. The Penrose diagram of this spacetime is the same as Minkowski's, provided one distinguishes the regions $r > 0$ — "our universe" — and $r < 0$ — the "other universe" —, since *a priori* they are different.

NWOH is a one-way wormhole with a null throat, which is an extremal event horizon. The analytically extended diagram continues indefinitely above and below the portion we show.

RBH-I is a spacetime containing an eternal black hole whose singularity is replaced by the (regular) throat of a spacelike wormhole. The diagram consists of infinitely many Schwarzschild-like blocks stacked one on top of the other and glued at the throats.

RBH-II is a regular black hole with two horizons per side. The Carter–Penrose diagram consists of two Kerr-like patches glued at the throats. The throats are timelike and can thus be traversed in both ways, yet the horizons are event horizons and an observer that crosses the throat twice can in no case return to the asymptotically flat region from which they left. Note that, from the point of view of an observer in "our universe", the inner horizon appears as a Cauchy horizon, as it does in the Kerr spacetime; here however, initial data cannot be specified in "our universe" only: Cauchy surfaces must be defined as disjoint unions of hypersurfaces that would be Cauchy in each of the Kerr-like patches. When one does so, one realises that r_- (and $-r_-$) is not a Cauchy horizon and the spacetime is indeed globally hyperbolic.

ERBH is the extremal version of RBH-II, i. e. a regular black hole whose two horizons coincide. The surface gravity of the ensuing horizon is zero.

NRBH is the limiting case of RBH-I in which the throat becomes null; equivalently, it can be seen as the limiting case of RBH-II in which the throat coincides with the inner horizon. The diagram however looks markedly different from either case: it continues indefinitely above and below, as well as to the right and left; it consists of infinitely many fundamental blocks glued together at the throat. The null throat is an extremal (inner) horizon.

Note that the first three cases have already been analysed in [322], while the last three are inherent to the rotating generalisation.

5.2.4 *Algebraic properties and surface gravity*

The tetrad $\{l^\mu,\ n^\mu,\ m^\mu,\ \overline{m}^\mu\}$ resulting from the NJP coincides, in the case $\ell = 0$, with the well-known Kinnersleay tetrad of the Kerr spacetime. The vector l^μ, in particular, is geodetic and indeed tangent to the outgoing null rays analysed previously. n^μ is also geodetic but not affinely parametrised. One can use these vectors to build the tensor

$$K^{\mu\nu} = \Sigma\,(l^\mu n^\nu + l^\nu n^\mu) + \varrho^2 g^{\mu\nu}\,. \tag{88}$$

In Kerr, this is a Killing tensor; one can easily verify that it remains Killing even when $\ell \neq 0$. When contracted with a geodetic vector, it gives rise to a quantity that is conserved along the geodesic and can be used to define a generalisation of the Carter constant — see section 8.2 for details. As a consequence, the equations of motion for test particles are separable.

One can further contract the tetrad with the Weyl tensor in order to determine the algebraic properties of this spacetime. We find[1] [325]

$$\Psi_0 = C_{\mu\nu\alpha\beta} l^\mu m^\nu l^\alpha m^\beta = 0 \tag{89}$$

(which agrees with [326], see proof of Theorem 2) and

$$\Psi_4 = C_{\mu\nu\alpha\beta} n^\mu \overline{m}^\nu n^\alpha \overline{m}^\beta = 0\,, \tag{90}$$

but

$$\Psi_1 = C_{\mu\nu\alpha\beta} l^\mu n^\nu l^\alpha m^\beta = \frac{a\ell^2\sqrt{1-\chi^2}}{\sqrt{2}\mathrm{i}\Sigma^2(\varrho + \mathrm{i}a\chi)}, \tag{91a}$$

$$\begin{aligned}\Psi_2 = C_{\mu\nu\alpha\beta} l^\mu m^\nu \overline{m}^\alpha n^\beta = &-\frac{M}{\varrho\Sigma^3}\left[\varrho^2\left(\varrho^2 - 3a^2\chi^2\right)\right.\\ &\left. + \mathrm{i}a\chi\sqrt{\varrho^2 - l^2}\left(3\varrho^2 - a^2\chi^2\right)\right] + \frac{\ell^2}{6\varrho^3\Sigma^3}\left[2a^2\varrho^2(\chi^2(\varrho\right.\\ &\left. - 4M) - 2\varrho) - a^4 M\chi^4 + \varrho^4(9M - 2\varrho)\right],\end{aligned} \tag{91b}$$

$$\Psi_3 = C_{\mu\nu\alpha\beta} l^\mu n^\nu \overline{m}^\alpha n^\beta = -\frac{a\ell^2\sqrt{1-\chi^2}\Delta}{2\sqrt{2}\mathrm{i}(\varrho - \mathrm{i}a\chi)\Sigma^3}, \tag{91c}$$

where $\chi = \cos\theta$. Thus this spacetime is not algebraically special.

The surface gravity that enters the analytic extension of subsection 5.2.3 is

$$\kappa_\pm = \frac{1}{2}\frac{\mathrm{d}}{\mathrm{d}r}\left(\frac{\Delta}{\varrho^2 + a^2}\right)\bigg|_{r_\pm} = \kappa_\pm^{\text{Kerr}}\left.\frac{\mathrm{d}\varrho}{\mathrm{d}r}\right|_{r_\pm} = \kappa_\pm^{\text{Kerr}}\sqrt{1 - \frac{\ell^2}{\varrho_\pm^2}}\,. \tag{92}$$

The expression above gives the so-called *peeling* surface gravity. One can easily check that it agrees with the alternative, *normal* definition

$$\kappa^\pm_{\text{normal}}\,\Xi_\mu\Big|_{\mathcal{H}^\pm} = -\frac{1}{2}\nabla_\mu\left(\Xi^\nu\Xi_\nu\right)\Big|_{\mathcal{H}^\pm}, \tag{93}$$

1 The expression appearing in [270] (eq. 3.7) has a typo.

where $\mathcal{H}^{\pm}$ are the horizons and

$$\Xi^{\mu}\partial_{\mu} = \partial_t + \Omega\,\partial_{\phi}, \quad \text{with} \quad \Omega = \frac{a}{\varrho^2 + a^2}, \tag{94}$$

is null and Killing at the horizons. Note in particular that the horizons are Killing and hence such coincidence of different definitions of surface gravity is expected [130].

5.3 STRESS-ENERGY AND ENERGY CONDITIONS

In the context of GR, wormholes are typically associated with violations of the energy conditions [353]. We thus characterise the distribution of "effective" matter entailed by the metric eq. (80) via the Einstein equations. We do so in two complementary ways: by focusing on particular geodesics (first a null congruence, then those of a timelike observer) and by diagonalising the Einstein tensor. The former method is more physical, in the sense that it sheds light on the energy density that actual observers would measure when orbiting these compact objects; the latter method is more systematic, in that it does not hinge on the particular choice of observer.

Note that the throat is an extremum for the energy density, however defined. Indeed, for any $\varepsilon(r)$,

$$\frac{\mathrm{d}\varepsilon}{\mathrm{d}r} = \frac{\mathrm{d}\varrho}{\mathrm{d}r}\frac{\mathrm{d}\varepsilon}{\mathrm{d}\varrho} = \frac{r}{\varrho}\frac{\mathrm{d}\varepsilon}{\mathrm{d}\varrho} \tag{95}$$

and $r = 0$ is automatically a zero when $\mathrm{d}\varepsilon/\mathrm{d}\varrho$ is finite. The sign of the second derivatives determines whether the extremum is a (local) minimum or maximum: denoting with a prime differentiation with respect to ϱ, we have

$$\frac{\mathrm{d}^2\varepsilon}{\mathrm{d}r^2} = \frac{r^2}{\varrho^2}\,\varepsilon'' + \frac{\ell^2}{\varrho^3}\,\varepsilon'\,. \tag{96}$$

5.3.1 *Energy density for infalling observers*

NULL GEODESICS Consider again the congruence l^{μ}: being null and geodetic, these vectors are tangent to trajectories that fall towards the centre. Assuming GR holds, the contraction $G_{\mu\nu}l^{\mu}l^{\nu}$ is the energy density measured along these trajectories. A straightforward computation shows that

$$G_{\mu\nu}l^{\mu}l^{\nu} = -\frac{2\ell^2}{\Sigma^2}\,. \tag{97}$$

This quantity is negative, hence the null energy condition is violated. Thus exotic matter is encountered everywhere in the spacetime, in an amount that decreases as $1/r^4$ and is maximal at $r = 0$. Note

that the limit $\ell \to 0$ is zero at all radii and angles but $r = 0,\ \theta = \pi/2$, where it is infinite; in fact

$$G_{\mu\nu} l^\mu l^\nu \Big|_{r=0} = -\frac{2\ell^2}{\left(\ell^2 + a^2 \cos^2\theta\right)^2}\,. \tag{98}$$

Such behaviour is not surprising, since in the limit $\ell \to 0$ one recovers, at $r = 0,\ \theta = \pi/2$, the standard ring singularity of the Kerr geometry.

TIMELIKE OBSERVER Consider now a timelike observer moving along a geodesic with tangent vector u^μ. Because of the symmetries of this spacetime, the components $u_t = -E$ and $u_\phi = L_z$ are constants of motion, corresponding respectively to the observer's energy per unit mass and to the projection along the rotation axis of the observer's angular momentum per unit mass. Moreover, the existence of the Killing tensor eq. (88) yields a third constant of motion, in terms of which u_θ can be expressed. The remaining component u_r is fixed by the normalisation $u_\mu u^\mu = -1$.

We can restrict for definiteness to motion on the equatorial plane $\theta = \pi/2$, and compute again the double contraction with the Einstein tensor. We find:

$$\begin{aligned}\varepsilon_u = G_{\mu\nu} u^\mu u^\nu \Big|_{\theta=\pi/2} = -\frac{\ell^2}{\varrho^7}\big[&M(L_z - aE)^2 - 2\varrho(L_z^2 - a^2E^2) \\ &- \varrho^3(1 - 2E^2)\big].\end{aligned} \tag{99}$$

Thus — assuming GR holds — observers with, say, $L_z = aE$ measure a negative energy density at all radii when their energy is such that $E^2 > 1/2$. The weak energy condition is therefore violated (and, consequently, the dominant energy condition too). Again, the limit $\ell \to 0$ yields zero except at the throat.

The sign of the second derivative of ε_u at $r = 0$ is the sign of $(x = L_z - aE)$

$$\varepsilon_u' \Big|_{r=0} = \ell^2 \left.\frac{7Mx^2 - 4\varrho[6axE + 3x^2 + \varrho^2\left(1 - 2E^2\right)]}{\varrho^8}\right|_{\varrho=\ell}\,. \tag{100}$$

Thus, observers with $x = 0$ and $E^2 > 1/2$ measure at $r = 0$ a (local) maximum of the energy density.

5.3.2 *Eigenvalue analysis*

To characterise the distribution of stress-energy in an observer-independent way, we diagonalise the Einstein tensor in mixed form — cf. eq. (212) in section 8.1. We find four distinct real eigenvectors, which in Boyer–Lindquist coordinates and up to multiplicative dimensionful constants are:

$$v_0^\mu = (a + \varrho^2/a, 0, 0, 1)\,, \qquad v_1^\mu = (0, 1, 0, 0)\,, \tag{101a}$$

$$v_2^\mu = (0, 0, 1, 0)\,, \qquad v_3^\mu = (a\sin^2\theta, 0, 0, 1)\,. \tag{101b}$$

We identify as minus the energy density $-\varepsilon$ the eigenvalue relative to the timelike eigenvector (v_0^μ when $\Delta > 0$, v_1^μ otherwise); and as pressures p_i ($i = 1,2,3$) the other eigenvalues. We find

$$\varepsilon = \frac{\ell^2}{\Sigma^3}\left\{\frac{\varrho\Sigma - 2a^2M\chi^2}{\varrho} - 2\Delta H(\Delta)\right\}, \tag{102a}$$

$$p_1 = \frac{\ell^2}{\Sigma^3}\left\{\frac{a^2[2M\chi^2 - \varrho(\chi^2-2)] + \varrho^2(\varrho-4M)}{\varrho} - 2\Delta H(\Delta)\right\}, \tag{102b}$$

$$p_2 = -\frac{\ell^2}{\Sigma^3}\left\{\frac{a^2\varrho^2[4M\chi^2 + \varrho(\chi^2-2)] + a^4M\chi^4}{\varrho^3} + \varrho(M-\varrho)\right\}, \tag{102c}$$

$$p_3 = \frac{\ell^2}{\Sigma^3}\left\{\frac{-M(2a^2\chi^2\varrho^2 + \Sigma^2) + \Sigma\varrho^3}{\varrho^3}\right\}, \tag{102d}$$

where $H(\cdot)$ is Heaviside's function. Note that the density and pressures so defined are continuous at the horizon, but their derivatives are generically not.

In the remainder of this section, we will analyse the null ($\varepsilon + p_i \geq 0$) and weak (null + $\varepsilon \geq 0$) energy conditions. Note however that

$$\varepsilon + p_1 = -\frac{2|\Delta|\ell^2}{\Sigma^3} \leq 0 \tag{103}$$

and this suffices to prove that all energy conditions are violated (except possibly at the horizons). The other $\varepsilon + p_i$ have less wieldy expressions and we therefore not report them here.

Note that the expressions in eq. (102) depend on the polar angle θ in a rather involved way but only through $\chi^2 = \cos^2\theta \in [0,1]$. We do not expect this dependence to induce dramatic features in the angular profiles of ε and p_i; in particular, such dependence should be marked only at small radii and rapidly die out at spatial infinity.

We confirm this intuition by studying ε, p_i as functions of χ, both analytically and graphically. The energy density, for instance, has an extremum at $\chi = 0$ (either a minimum or a maximum, depending on the values of the parameters); in addition, it may have at most two more extrema, symmetric with respect to $\chi = 0$. Similar considerations apply to $\varepsilon + p_i$: $\chi = 0$ is always an extremum and at most two other extrema, symmetric with respect to $\chi = 0$, can exist. For $\varepsilon + p_1$, in particular, $\chi = 0$ is the only extremum; at large radii it is a minimum — but can become a maximum at smaller radii, depending on the parameters.

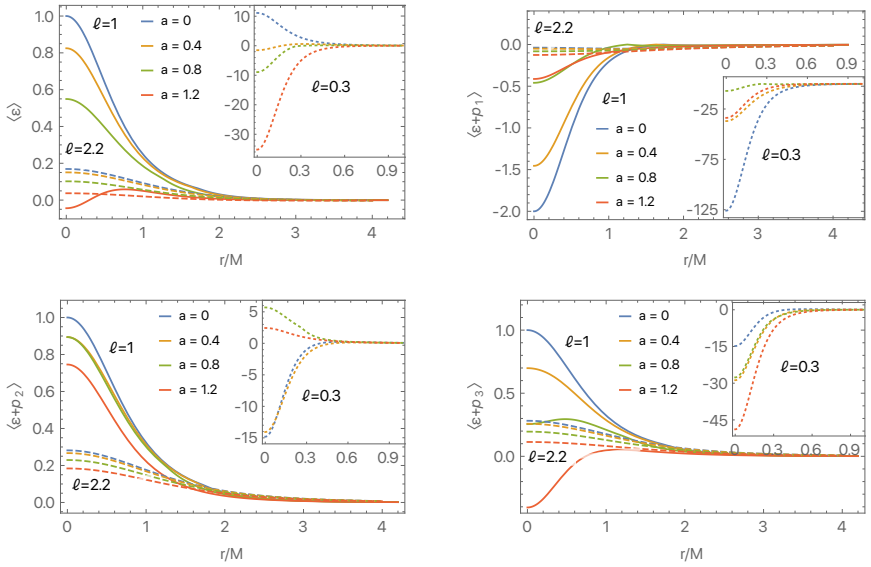

Figure 5: Energy conditions, averaged over the polar angle, as a function of r. Different colours represent different choices for the spin a, while different line styles stand for different values of ℓ. Given the difference of scales, one particular value of ℓ is plotted in an inset.

Hence, if we aim at characterising the radial distribution of stress and energy, a marginalisation over the angular variable is justified. Thus, for a generic quantity X, we resolve to consider

$$\langle X \rangle = \frac{1}{2} \int_{-1}^{+1} \mathrm{d}\chi \, X \,. \tag{104}$$

In figure 5 we plot $\langle \varepsilon \rangle$ and $\langle \varepsilon + p_i \rangle$ for selected values of a and ℓ. Notice that the stress-energy content of this spacetime is localised close to the origin: inspection of eq. (102) indeed confirms that energy density and pressures all scale as $1/r^4$.

To quantify the amount of violation of the energy conditions in the whole spacetime, we adopt the strategy proposed in [219, 282, 356]. That is, we compute the so-called volume integral quantifier

$$\mathcal{E} = \int \mathrm{d}r \, \mathrm{d}\theta \, \mathrm{d}\phi \, \sqrt{|g|} \, \varepsilon \,, \tag{105a}$$

$$\mathcal{E} + P_i = \int \mathrm{d}r \, \mathrm{d}\theta \, \mathrm{d}\phi \, \sqrt{|g|} \, (\varepsilon + p_i) \,, \tag{105b}$$

where g is the determinant of the four-dimensional metric.

We draw contour plots of these quantities for varying values of the parameters a, ℓ and report the results in figure 6. Note that the amount of effective matter varies substantially as the parameters vary and can be made very small by trimming them carefully.

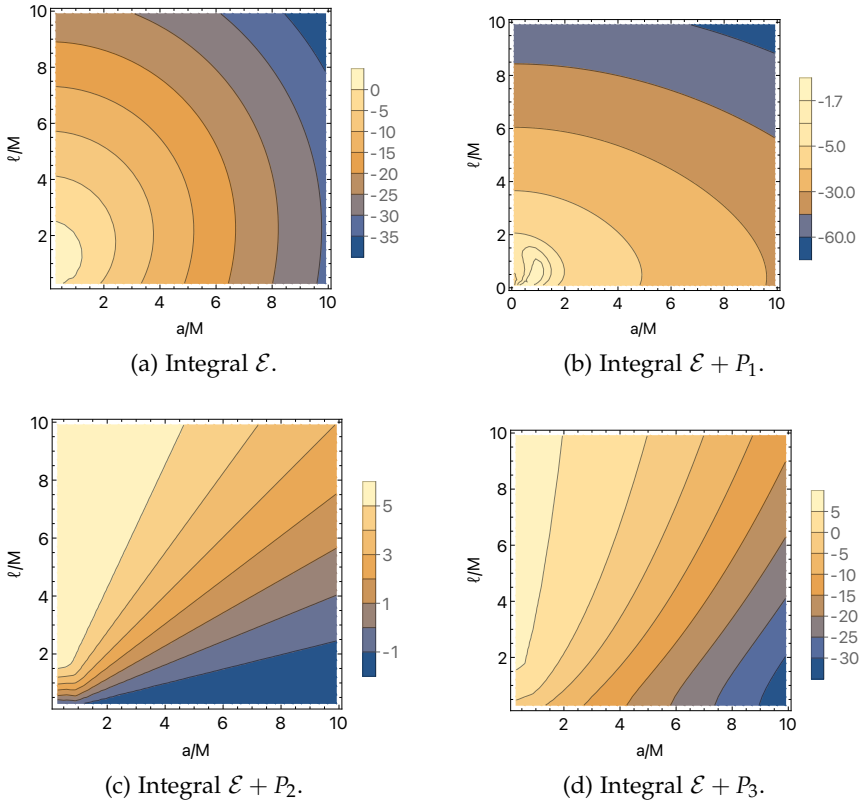

(a) Integral $\mathcal{E}$.

(b) Integral $\mathcal{E} + P_1$.

(c) Integral $\mathcal{E} + P_2$.

(d) Integral $\mathcal{E} + P_3$.

Figure 6: Contour plots of the volume integral quantifier in the (a, ℓ)-plane. Negative values of $\mathcal{E} + P_i$ entail violations of the (averaged) null energy condition; negativity of $\mathcal{E}$ or $\mathcal{E} + P_i$ further entail violations of the (averaged) weak energy condition.

5.4 FEATURES OF THE EXTERIOR GEOMETRY

The exterior of a Kerr black hole is rich in noticeable features, which largely determine the phenomenology of these objects. In this section, we focus on the exterior ($r \geq 0$ and outside any horizon) of our geometry and study how switching on the parameter ℓ affects it. In particular, we describe the ergoregion and, schematically, the orbits, focusing on equatorial light ring and innermost stable circular orbit (ISCO).

5.4.1 *Ergoregion*

An ergoregion is a region inside of which no static observer can exist. Its boundary, the ergosurface, is the locus of points where $g_{tt} = 0$. In our metric, the roots of this equation correspond to values of ϱ given by

$$\varrho^{\pm}_{\text{erg}} = M \pm \sqrt{M^2 - a^2 \cos^2\theta}\,. \tag{106}$$

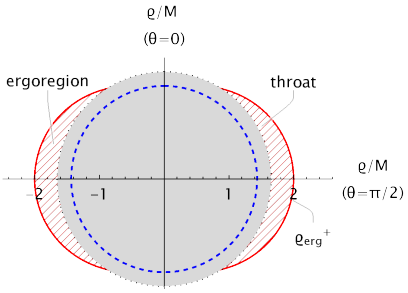

(a) WoH with $a < M$. The ergoregion is limited to a crescent-shaped region about the equator. The dashed blue line represents the would-be outer horizon and is plotted for reference: the wormhole is traversable as long as the throat is "larger than the horizon", otherwise the object is a regular black hole (figure figure 8).

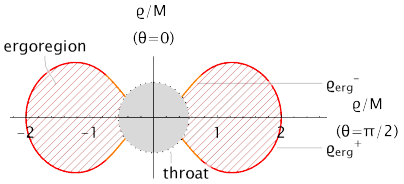

(b) WoH with $a > M$. Note that the two branches ϱ^{+}_{erg} and ϱ^{-}_{erg}, plotted in red and orange respectively, only exist for $|\cos\theta| \leq a/M$ and join smoothly, thus producing an ergoregion of such peculiar shape.

Figure 7: Traversable wormhole with ergoregion, corresponding to values of ℓ such that $\varrho_+ < \ell < \varrho^{+}_{\text{erg}}$. Each plot is a slice at fixed ϕ, the angle with the vertical axis is θ and the distance from the centre is ϱ. The hatched region is the ergoregion. The black dotted line represents the throat $r = 0$; the grey region is therefore *excised* from the spacetime.

Clearly, this expression coincides with what one finds in Kerr. Contrary to what is usually assumed in that case, however, here we do consider arbitrarily high spins. Therefore, the radicand in eq. (106) is not always positive and the ergosurface has markedly distinct shapes in the $a > M$ and $a < M$ cases. An ergosurface exists when at least one of the quantities

$$r^{\pm}_{\text{erg}} = \sqrt{\left(\varrho^{\pm}_{\text{erg}}\right)^2 - \ell^2} \tag{107}$$

is real. Note, incidentally, that

$$\min_{\theta\in[0,\pi]}\left(\varrho^{+}_{\text{erg}}\right) = \varrho_+ \quad \text{and} \quad \max_{\theta\in[0,\pi]}\left(\varrho^{-}_{\text{erg}}\right) = \varrho_- \,. \tag{108}$$

Hence, if $\ell \geq \varrho^{+}_{\text{erg}}$ there is no ergoregion. When this is the case, the object under consideration is a traversable wormhole (WoH case of section section 5.2), since $\varrho^{+}_{\text{erg}} \geq \varrho_+$; note that these wormholes may have arbitrary spin.

If, on the contrary, $\ell < \varrho^{+}_{\text{erg}}$, an ergoregion is indeed present. This eventuality encompasses all cases of section 5.2, though with marked differences.

Indeed, when the object is a traversable wormhole — i. e. if $a > M$, or $a < M$ and $\ell > \varrho_+$ —, the throat intercepts the ergosurface at some angle $\theta \neq 0,\ \pi$; therefore, the ergoregion is limited to a region that is coaxial with the wormhole and whose longitudinal section is

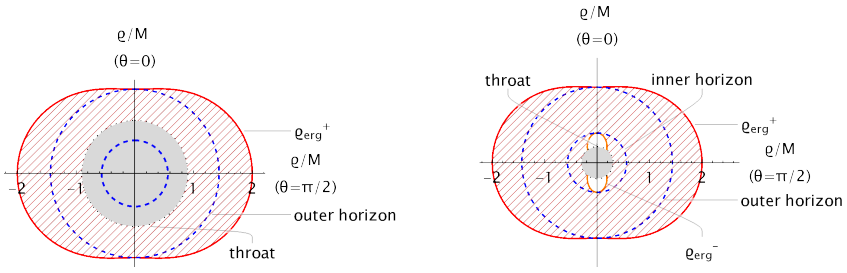

(a) RBH-I (nWoH and nRBH are qualitatively similar). The ergoregion extends across the horizon and to the throat. The innermost dashed blue line represents the would-be inner horizon and is plotted for reference: the case in which the throat is "smaller than the inner horizon" is depicted in 8b.

(b) RBH-II (eRBH is qualitatively similar: the two horizons coincide and the inner and outer ergosurfaces touch at the poles). The ergoregion extends across two horizons, and to the throat or the inner ergosurface; within the white lobes $g_{tt} < 0$, hence these regions do not belong to the ergoregion.

Figure 8: Ergoregion in regular black holes, i.e. when $\ell \leq \varrho_+$. As in figure figure 7, each plot is a slice at fixed ϕ, the angle with the vertical axis is θ and the distance from the centre is ϱ. The hatched region is the ergoregion. The black dotted line represents the throat $r = 0$; the grey region is therefore *excluded* from the spacetime.

shaped as a crescent — see figure 7a and figure 7b. (This is a common feature of other rotating traversable wormholes, cf. e. g. [327]). Note however that the throat is technically not an edge of the ergoregion, which in fact continues in the "other universe" as far as the mirrored ergosurface.

When instead the object is a RBH — i. e. if $a < M$ and $\ell \leq \varrho_+$ — , the ergoregion extends all the way to the horizon and its external portion is thus tantamount to that of Kerr.

For completeness, however, we describe the structure of the ergoregion inside the horizon, too. If $\varrho_- \leq \ell < \varrho_+$, viz. in the cases nWoH, RBH-I and nRBH, the ergoregion stretches as far as the throat — see figure 8a. If instead $\ell < \varrho_-$, that is in the RBH-II and eRBH cases, the ergoregion has an inner ergosurface; this surface is intercepted by the throat at some angle θ: thus the only portions of the spacetime, close to the throat, that do not belong to the ergoregion are lobes enclosing the poles — see figure 8b. Note that, as before, the throat is not an edge of the ergoregion, in the sense that g_{tt} does not change sign upon crossing it.

5.4.2 *Notable orbits*

The study of orbits can proceed as for the Kerr geometry. More detail can be found in section 8.2; here we focus on the most relevant case of equatorial circular motion.

Indeed, the t- and ϕ-motion are readily integrated by exploiting the conservation of the test particle's energy E and angular momentum L_z (per unit mass) along the rotation axis. Thus, setting $\theta = \pi/2$, the problem is effectively one-dimensional and governed by

$$\varrho^2 \dot{r} = \pm\sqrt{\mathcal{R}} \tag{109}$$

where the dot marks differentiation with respect to the affine parameter along the geodesic and $\mathcal{R}$ is the same potential one finds for a Kerr spacetime mapped by a Boyer–Lindquist radius that has been called ϱ:

$$\mathcal{R} = [E(\varrho^2 + a^2) - aL_z]^2 - \Delta[\mu^2\varrho^2 + (L_z - aE)^2], \tag{110}$$

with $\mu^2 = 0, +1$ for null and timelike orbits, respectively (the expression for generic θ can be found in section 8.2).

Circular orbits satisfy simultaneously

$$\mathcal{R} = 0 \quad \text{and} \quad \frac{\mathrm{d}\mathcal{R}}{\mathrm{d}r} = 0\,. \tag{111}$$

Note that

$$\frac{\mathrm{d}\mathcal{R}}{\mathrm{d}r} = \frac{\mathrm{d}\varrho}{\mathrm{d}r}\frac{\mathrm{d}\mathcal{R}}{\mathrm{d}\varrho} = \frac{r}{\varrho}\frac{\mathrm{d}\mathcal{R}}{\mathrm{d}\varrho}\,, \tag{112}$$

hence Kerr's circular orbits readily correspond to circular orbits of our spacetime. Since $r = 0$ does not generically satisfy the above relations, the mapping between Kerr equatorial circular geodesics and our own is onto.

Thus, in particular, to any pair $E_c,\ L_z^c$ there corresponds a solution ϱ_c of eq. (111) as long as

$$\varrho_c^2 - 3M\varrho_c \pm 2a\sqrt{M\varrho_c} \geq 0\,, \tag{113}$$

where the plus (minus) sign refers to prograde (retrograde) orbits. When the equality holds, the equation has formally three real solutions for $a < M$ and only one for $a > M$. In the former case, however, the smallest of such roots lies inside the horizon and, therefore, does not correspond to any orbit; the other two correspond to the familiar unstable circular photon orbits ϱ_{ph}, one prograde and one retrograde, of the Kerr spacetime. In the latter case, the corresponding orbit connects smoothly to the retrograde branch of the $a < M$ case. These orbits of the Kerr spacetime translate into orbits of our spacetime, located at

$$r_{\mathrm{ph}} = \sqrt{\varrho_{\mathrm{ph}}^2 - \ell^2}\,. \tag{114}$$

Notice that for $\ell > 3M$ we find no prograde photon circular orbit, at any spin; these wormholes however do have a retrograde circular orbit, if they spin fast enough.

Timelike circular orbits are stable as long as

$$\varrho_c^2 - 6M\varrho_c \pm 8a\sqrt{M\varrho_c} - 3a^2 \geq 0\,. \tag{115}$$

Once again, the equality gives rise to two branches of solutions for $a < M$, the prograde and retrograde branches, one of which (the retrograde) continues to the $a > M$ region. In the Kerr spacetime, these solutions represent the ISCOs. In our spacetime, they are located at

$$r_{\text{ISCO}} = \sqrt{\varrho_{\text{ISCO}}^2 - \ell^2}\,. \tag{116}$$

Note that, for $\ell > 6M$, these wormholes do not present prograde ISCO. They may have a retrograde ISCO, if they spin fast enough.

5.5 CHAPTER WRAP-UP

In this chapter, we have constructed a rotating generalisation of the SV metric, applying the NJP. Depending on the values of a and ℓ, it may represent a traversable wormhole, a RBH with one or two horizons, or three limiting cases of the above. The global properties of the ensuing spacetime have been discussed at length. We further characterised our metric by describing the violations of the energy conditions and found that the exotic matter is localised in the vicinity of the throat. Finally, we investigated some relevant features of the exterior geometry: an ergoregion exists when $\ell < 2M$, whatever the value of the spin; a (retrograde) circular photon orbit exists for $\ell < 3M$ and a (retrograde) ISCO for $\ell < 6M$, again independently on the spin.

The metric of eq. (80) thus describes a family of good mimickers of the Kerr BH, suitable for serious phenomenological inquiry. Indeed, black bounces have received considerable attention from the community and several applications have been considered. For instance, their electromagnetic shadows have been computed, and often compared with observed ones, in [177, 205, 242, 317, 350]. Other examples, including strong lensing and scattering of scalars, can be found e. g. in [26, 118, 138, 172, 195, 209, 213, 239, 348, 367–369].

Notably, X-ray emission spectra from known astrophysical BHs and gravitational-wave inspiral data have been used to put bounds on the parameter ℓ in [304, 305]. These constraints are quite impressive, as they are as strong as $\ell/M < 0.39$ (at 90% confidence level).

These and similar results raise novel questions concerning the epistemology of the stream of research that deals with RBHs and other effective models. Indeed, though there might be reasons to prefer some of these models over others, all of them — including black bounces — are constructed by hand and thus reflect the (arbitrary) choices made by their inventors. In the author's view, this means that the prior degree of belief on e. g. the black-bounce–Kerr metric — or

the rotating Hayward metric, or any other model in particular — is essentially zero. Still, analyses that use actual data to constrain and possibly rule out some specific models are extremely interesting and compelling insofar as they showcase the capabilities of current data, in terms of sensitivity and constraining power. It would be *extremely* interesting to devise strategies for constraining *classes* of models, thus bypassing the ambiguities inherent to any one of them.

Coming back to the black-bounce–Kerr, another compelling question concerns its stability against small perturbations. Indeed, the existence of an ergoregion is known to lead to interesting new phenomenology, particularly in the absence of an horizon. This question will be addressed in chapter 7; before moving to that, however, we will investigate further the ductility of the SV trick by applying it to the Kerr–Newman spacetime in chapter 6.

6

THE BLACK-BOUNCE–KERR–NEWMAN SPACETIME

Given the demonstrated existence of the black-bounce–Schwarzschild [81, 82, 245, 246, 319, 322], and the black-bounce–Kerr [240, 270, 317] geometries, it is intuitive to suspect that analogous black-bounce variants of both the Reissner–Nordström and Kerr–Newman spacetimes will exist [366]; and that they would be amenable to reasonably tractable general-relativistic analyses.

Such charged black-bounce geometries would probably be of limited phenomenological interest, since astrophysical BHs are believed to be electrically neutral. Indeed, if they did have a charge, they would preferentially accrete matter of the opposite charge until they became neutral.

Yet, charged spacetimes exhibit additional structures with respect to their neutral counterparts and for this reason they are of great theoretical interest. For instance, they exhibit a non-trivial electromagnetic field, whose faith upon regularisation is unclear.

For this reason, this chapter will present the construction and the subsequent analysis of the black-bounce–Kerr-Newman spacetime. When appropriate, we will specify results to the non-rotaing case, i. e. to the black-bounce–Reissner–Nordström spacetime.

The discussion will loosely follow that of [166], though the notations have often been adapted for coherence with the rest of the thesis.

6.1 BLACK-BOUNCE–KERR–NEWMAN GEOMETRY

To build the black-bounce–Kerr–Newman geometry, start from Kerr–Newman in standard Boyer–Lindquist coordinates [354, 362]

$$\begin{aligned} \mathrm{d}s^2_{\mathrm{KN}} = &- \left(1 - \frac{2Mr}{\Sigma_{\mathrm{KN}}}\right) \mathrm{d}t^2 + \frac{\Sigma_{\mathrm{KN}}}{\Delta_{\mathrm{KN}}} \mathrm{d}r^2 + \Sigma_{\mathrm{KN}} \mathrm{d}\theta^2 \\ &- \frac{4Mra\sin^2\theta}{\Sigma_{\mathrm{KN}}} \mathrm{d}t\mathrm{d}\phi + \frac{A_{\mathrm{KN}}\sin^2\theta}{\Sigma_{\mathrm{KN}}} \mathrm{d}\phi^2 \,, \end{aligned} \tag{117}$$

where

$$\Sigma_{\mathrm{KN}} = r^2 + a^2\cos^2\theta \,, \tag{118a}$$

$$\Delta_{\mathrm{KN}} = r^2 + a^2 - 2Mr + Q^2 \,, \tag{118b}$$

$$A_{\mathrm{KN}} = (r^2 + a^2)^2 - \Delta_{\mathrm{KN}} a^2 \sin^2\theta \,. \tag{118c}$$

Then apply the SV regularisation procedure as usual: any time the metric components have an explicit dependence on r, replace $r \mapsto \sqrt{r^2 + \ell^2}$; without touching the object $\mathrm{d}r$.

The result is the following line element:

$$\begin{aligned} \mathrm{d}s^2 = &-\left(1-\frac{2M\sqrt{r^2+\ell^2}}{\Sigma}\right)\mathrm{d}t^2+\frac{\Sigma}{\Delta}\,\mathrm{d}r^2+\Sigma\mathrm{d}\theta^2 \\ &-\frac{4Ma\sin^2\theta\sqrt{r^2+\ell^2}}{\Sigma}\,\mathrm{d}t\mathrm{d}\phi+\frac{A\sin^2\theta}{\Sigma}\,\mathrm{d}\phi^2\,, \end{aligned} \tag{119}$$

where now Σ, Δ and A are

$$\Sigma = r^2+\ell^2+a^2\cos^2\theta\,, \tag{120a}$$

$$\Delta = r^2+\ell^2+a^2-2M\sqrt{r^2+\ell^2}+Q^2\,, \tag{120b}$$

$$A = (r^2+\ell^2+a^2)^2-\Delta a^2\sin^2\theta\,. \tag{120c}$$

(Eq. (119) is formally the same as eq. (80), except the electric charge Q now appears in the definition of Δ.)

The natural domains of the angular and temporal coordinates are unaffected, while the natural domain of the r coordinate expands from $r\in[0,+\infty)$ to $r\in(-\infty,+\infty)$. Both manifest axisymmetry and asymptotic flatness are preserved by the regularisation.

Setting $a=0$ yields the static and spherically symmetric black-bounce–Reissner–Nordström geometry

$$\begin{aligned} ds^2 &= -f(r)\,\mathrm{d}t^2+\frac{\mathrm{d}r^2}{f(r)}+(r^2+\ell^2)\,\mathrm{d}\Omega^2\,, \\ f(r) &= 1-\frac{2M}{\sqrt{r^2+\ell^2}}+\frac{Q^2}{r^2+\ell^2}\,. \end{aligned} \tag{121}$$

6.2 HORIZONS, SURFACE GRAVITY AND ERGOSURFACES

Horizons are associated to the roots of Δ and they are located at

$$r_H = S_1\sqrt{\left(M+S_2\sqrt{M^2-Q^2-a^2}\right)^2-\ell^2}\,. \tag{122}$$

Here S_1, $S_2=\pm1$, and choice of sign for S_1 dictates which universe we are in, whilst the choice of sign on S_2 corresponds to an outer/inner horizon respectively.

The spacetime structures are analogous to those of the uncharged case. Specifically:

- For $\ell < M-\sqrt{M^2-a^2-Q^2}$, the geometry has two horizons in the $r>0$ region and two in the $r<0$ region; the throat is timelike and the maximally extended spacetime has the Carter–Penrose diagram of figure 9. This case is qualitatively identical to the RBH-II case of the black-bounce–Kerr spacetime, discussed in section 5.2.

- For $M-\sqrt{M^2-a^2-Q^2}<\ell<M+\sqrt{M^2-a^2-Q^2}$, there is only one horizon per universe; the throat is spacelike and the

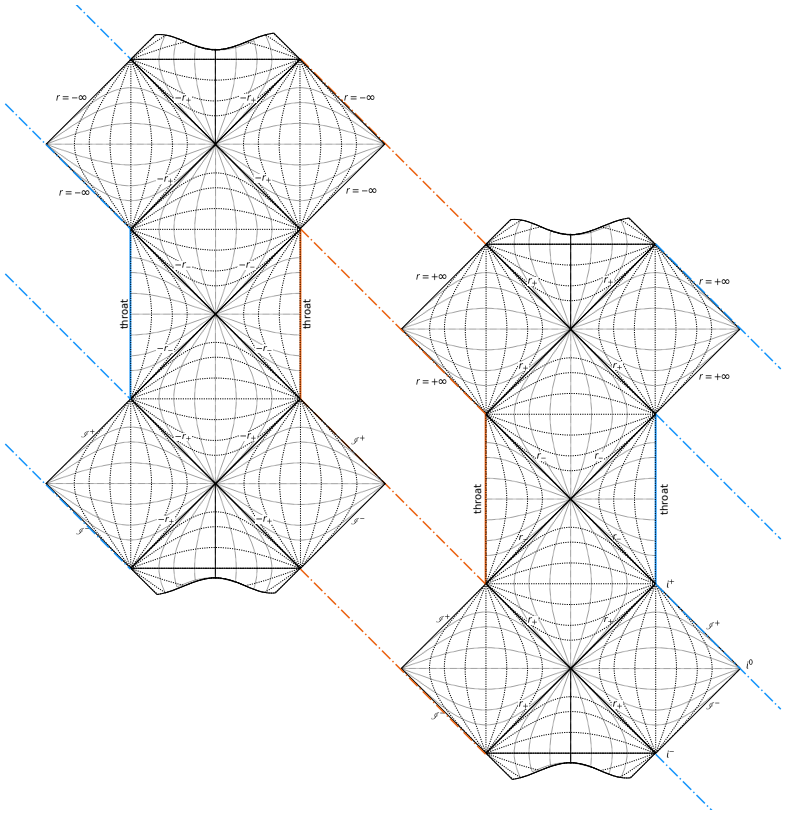

Figure 9: Penrose diagram for a regular black hole with outer and inner horizons, corresponding to $\ell < m - \sqrt{m^2 - a^2 - Q^2}$. Vertical lines of the same colour are identified, as the right-hand (left-hand) part of the diagram represents the $r > 0$ ($r < 0$) universe; the diagram continues indefinitely above and below the portion shown. Here r_+ (resp. r_-) is r_H with $S_2 = +1$ (-1); the sign in front of it is S_1.

Carter–Penrose diagram is that of figure 10. This case corresponds to the RBH-I case of section 5.2.

- For $\ell > M + \sqrt{M^2 - a^2 - Q^2}$, there are no horizons; the throat is timelike and traversable, hence the Carter–Penrose diagram resembles that of Minkowski spacetime. This case corresponds to the WoH case of section 5.2.

As usual, the intermediate cases correspond to some horizon becoming extremal.

Note that, in the Kerr–Newman geometry, one must demand $Q^2 + a^2 \leq M^2$ to avoid the possibility of naked singularities. In our case, we need not worry about this eventuality and may consider arbitrary values of spin and charge. Thus, if $Q^2 + a^2 > M^2$, the spacetime has no horizon and is therefore analogous to the case $\ell > M + \sqrt{M^2 - Q^2 - a^2}$.

This classification holds for the non-rotating case too, provided one sets $a = 0$ in the expressions above.

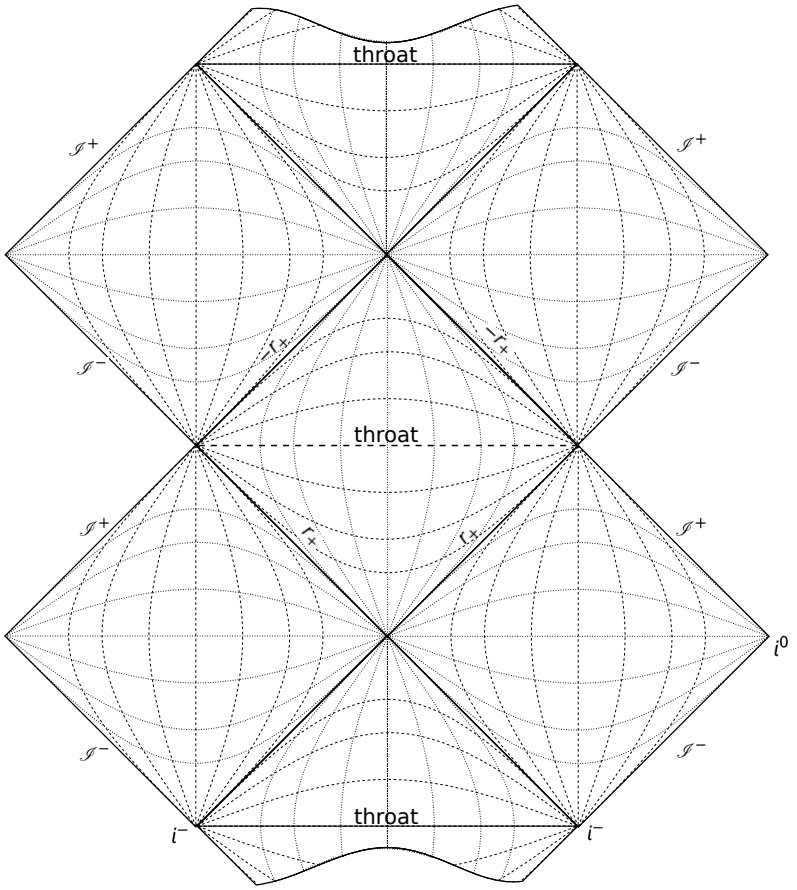

Figure 10: Penrose diagram for a regular black hole with only outer horizons, corresponding to $m - \sqrt{m^2 - a^2 - Q^2} < \ell < m + \sqrt{m^2 - a^2 - Q^2}$. The lower (upper) portion of the diagram corresponds to the $r > 0$ ($r < 0$) universe; the diagram continues indefinitely above and below the portion shown by repetition of this fundamental block. Here, r_+ is r_H with $S_2 = +1$; the sign in front of it is S_1.

If horizons are present, their surface gravity is given by

$$\kappa_{S_2} = \frac{1}{2}\frac{\mathrm{d}}{\mathrm{d}r}\left(\frac{\Delta}{r^2+\ell^2+a^2}\right)\bigg|_{r_H} = \kappa^{\mathrm{KN}}_{S_2}\sqrt{\frac{r_H^2}{r_H^2+\ell^2}}\,, \tag{123}$$

where $\kappa^{\mathrm{KN}}_{S_2}$ is the surface gravity relative to the inner, when $S_2 = -1$, or outer, when $S_2 = +1$, horizon of a Kerr–Newman black hole with mass M, spin a and charge Q.

The ergosurface is determined by $g_{tt} = 0$, which is a quadratic equation in r. The roots are given by:

$$r_{\mathrm{erg}} = S_1\sqrt{\left(M + S_2\sqrt{M^2 - Q^2 - a^2\cos^2\theta}\right)^2 - \ell^2}, \tag{124}$$

where S_1, S_2 are as before.

6.3 STRESS-ENERGY TENSOR

We can now move on to characterise the effective matter content. As usual, we will do so by assuming a specific geometrdynamics, namely that of GR.

The (mixed) Einstein tensor $G^{\mu}_{\ \nu}$ can be diagonalised over the real numbers: its four eigenvectors $\{e_{\hat{\mu}}\}_{\mu=t,r,\theta,\phi}$ form a globally defined tetrad [284] and have explicit Boyer–Lindquist components

$$\left(e_{\hat{t}}\right)^{\mu} = \frac{1}{\sqrt{\Sigma|\Delta|}}\left(r^2+\ell^2+a^2, 0, 0, a\right)\,, \tag{125a}$$

$$\left(e_{\hat{r}}\right)^{\mu} = \sqrt{\frac{|\Delta|}{\Sigma}}\,(0,1,0,0)\,, \tag{125b}$$

$$\left(e_{\hat{\theta}}\right)^{\mu} = \frac{1}{\sqrt{\Sigma}}\,(0,0,1,0)\,, \tag{125c}$$

$$\left(e_{\hat{\phi}}\right)^{\mu} = \frac{1}{\sin\theta\sqrt{\Sigma}}\left(a\sin^2\theta, 0, 0, 1\right)\,. \tag{125d}$$

Eigenvectors are defined up to multiplicative, possibly dimensionful constants. This choice of normalisation ensures that the tetrad $\{e_{\hat{\mu}}\}$ is orthonormal and that, in the limit $a \to 0$, it reduces to what one would read off directly from the black-bounce–Reissner–Nordström metric eq. (121). Components of tensors expressed in this tetrad will be denoted by hatted indeces.

The tetrad of eq. (125) may be used to characterise the distribution of stress-energy in our spacetime. Assuming standard GR holds, the Einstein tensor is proportional to the stress-energy tensor: we may thus interpret the one component of $G_{\hat{\mu}\hat{\nu}}$ that corresponds to the time-like direction as an energy density ε, and all the other non-zero components as principal pressures p_i. Contrary to other chapters, here we normalise the effective stress-energy tensor as

$$G_{\mu\nu} = 8\pi T^{\mathrm{eff}}_{\mu\nu}\,. \tag{126}$$

In particular, outside any horizon (technically, whenever $\Delta > 0$), we have

$$\varepsilon = -\frac{\ell^2\left(2a^2\varrho + 2M\Sigma - 6M\varrho^2 + 2\varrho^3 - \Sigma\varrho\right)}{8\pi\Sigma^3\varrho} - \frac{Q^2\left(3\ell^2 - \Sigma\right)}{8\pi\Sigma^3}, \tag{127a}$$

$$p_1 = \frac{\ell^2\left[\Sigma(2M-\varrho) - 2M\varrho^2\right]}{8\pi\Sigma^3\varrho} + \frac{Q^2\left(\ell^2 - \Sigma\right)}{8\pi\Sigma^3}, \tag{127b}$$

$$p_2 = \frac{\ell^2\left[-M\Sigma^2 + \Sigma\varrho^2(\varrho - 2M) + 2M\varrho^4\right]}{8\pi\Sigma^3\varrho^3} + \frac{Q^2\left(\Sigma - \ell^2\right)}{8\pi\Sigma^3}, \tag{127c}$$

$$p_3 = \frac{\ell^2\left[2a^2\varrho^3 + M\left(-\Sigma^2 - 2\Sigma\varrho^2 + 2\varrho^4\right) - \Sigma\varrho^3 + 2\varrho^5\right]}{8\pi\Sigma^3\varrho^3} + \frac{Q^2\left(\Sigma - \ell^2\right)}{8\pi\Sigma^3}. \tag{127d}$$

The expressions above prove, incidentally, that our black-bounce–Kerr–Newman spacetime is Hawking–Ellis type I [184, 261–263].

Note that

$$\varepsilon + p_1 = -\frac{\ell^2\Delta}{8\pi\Sigma^3}. \tag{128}$$

This is the same result one gets in the black-bounce–Kerr spacetime, modulo the redefinition of Δ. Thus, in particular, the null energy condition is violated. Note that on the horizon $\Delta = 0$ so $(\varepsilon + p_1)|_H = 0$. This on-horizon simplification is a useful consistency check [262, 272, 273, 352].

Since the effective sources depend explicitly on the electric charge Q, it seems reasonable to characterise the spacetime by means of some variant of curved-spacetime Maxwell-like electromagnetism, that is, by assuming that some variant of Maxwell's equations hold.

6.3.1 *Interpreting the black-bounce–Reissner–Nordström stress-energy*

We start from the non-rotating case, which is simpler. We may write

$$\frac{1}{8\pi}\,G^{\hat{\mu}}{}_{\hat{\nu}} = [T_{\text{bb}}]^{\hat{\mu}}{}_{\hat{\nu}} + [T_{\text{Q}}]^{\hat{\mu}}{}_{\hat{\nu}}, \tag{129}$$

where $[T_{\text{bb}}]^{\hat{\mu}}{}_{\hat{\nu}}$ is the stress-energy tensor for the original electrically neutral black-bounce spacetime from [322], and

$$\begin{aligned}[T_{\text{Q}}]^{\hat{\mu}}{}_{\hat{\nu}} &= \frac{Q^2r^2}{8\pi(r^2+\ell^2)^3}\,\text{diag}\left(\frac{2\ell^2}{r^2} - 1, -1, 1, 1\right)\\ &= \frac{Q^2r^2}{8\pi(r^2+\ell^2)^3}\left[\,\text{diag}\,(-1,-1,1,1) + \text{diag}\left(\frac{2\ell^2}{r^2}, 0, 0, 0\right)\right]\end{aligned} \tag{130}$$

is the charge-dependent contribution to the stress-energy.

The first term of eq. (130) above can be interpreted as the usual Maxwell stress-energy tensor [275]

$$[T_{\text{Maxwell}}]^{\hat{\mu}}{}_{\hat{\nu}} = \frac{1}{4\pi}\left[-F^{\hat{\mu}}{}_{\hat{\alpha}}F^{\hat{\alpha}}{}_{\hat{\nu}} - \frac{1}{4}\delta^{\hat{\mu}}{}_{\hat{\nu}}F^2\right], \tag{131}$$

while the second term can be interpreted as the stress-energy of a "charged dust", with the density of the dust involving both the bounce parameter ℓ and the total charge Q. Overall we have

$$[T_{\text{Q}}]^{\hat{\mu}}{}_{\hat{\nu}} = [T_{\text{Maxwell}}]^{\hat{\mu}}{}_{\hat{\nu}} + \Xi\, V^{\hat{\mu}}V_{\hat{\nu}}\,. \tag{132}$$

The vector $V^{\hat{\mu}}$ is the normalised unit timelike eigenvector of the stress-energy, which in the current situation reduces to the normalised time-translation Killing vector, while the dust density Ξ has to be determined. We obtain

$$[T_{\text{Q}}]^{\hat{t}}{}_{\hat{t}} = -\varepsilon_{\text{em}} = [T_{\text{Maxwell}}]^{\hat{t}}{}_{\hat{t}} - \Xi = -\frac{1}{8\pi}\mathscr{E}^2 - \Xi\,. \tag{133}$$

Comparing with eq. (130), we find for the electric field strength $\mathscr{E}$

$$\mathscr{E} = \frac{Qr}{(r^2+\ell^2)^{3/2}} = \mathscr{E}_{\text{RN}}\left[\frac{r^3}{(r^2+\ell^2)^{3/2}}\right], \tag{134}$$

where $\mathscr{E}_{\text{RN}}$ is the electric field strength of a Reissner–Nordström black hole. For the density of the dust Ξ we find

$$\Xi = -\frac{1}{4\pi}\frac{Q^2\ell^2}{(r^2+\ell^2)^3}\,. \tag{135}$$

All told, we have the following form for the electromagnetic stress-energy tensor for our regularised Reissner–Nordström spacetime

$$[T_{\text{Q}}]^{\hat{\mu}}{}_{\hat{\nu}} = \frac{1}{4\pi}\left[-F^{\hat{\mu}}{}_{\hat{\alpha}}F^{\hat{\alpha}}{}_{\hat{\nu}} - \frac{1}{4}\delta^{\hat{\mu}}{}_{\hat{\nu}}F^2\right] - \frac{1}{4\pi}\frac{Q^2\ell^2}{(r^2+\ell^2)^3}V^{\hat{\mu}}V_{\hat{\nu}}\,. \tag{136}$$

Finally, the electromagnetic potential is easily extracted by integrating eq. (134), and in view of asymptotic flatness we may set the constant of integration to zero, yielding

$$A_\mu = (\Phi_{\text{em}}(r), 0, 0, 0) = -\frac{Q}{\sqrt{r^2+\ell^2}}\,(1,0,0,0)\,. \tag{137}$$

Note that this really is simply the electromagnetic potential from standard Reissner–Nordström spacetime, $-Q/r$, under the map $r \mapsto \sqrt{r^2+\ell^2}$.

It is easy to verify that the electromagnetic field-strength tensor $F_{\mu\nu} = \nabla_\mu A_\nu - \nabla_\nu A_\mu$ satisfies $F_{[\mu\nu,\sigma]} = 0$. The inhomogeneous Maxwell equation is, using $\varrho = \sqrt{r^2+\ell^2}$,

$$\nabla^{\hat{\mu}}F_{\hat{\mu}\hat{\nu}} = \frac{Q\ell^2}{\varrho^6}\sqrt{\varrho^2 - 2m\varrho + Q^2}\;(1,0,0,0)\,. \tag{138}$$

The rotating case is significantly more involved. We can still isolate the Q-dependent contribution to the total stress-energy

$$[T_Q]^{\hat{\mu}}{}_{\hat{\nu}} = \frac{1}{8\pi}\frac{Q^2\left(\Sigma-\ell^2\right)}{\Sigma^3}\Bigg[\operatorname{diag}\left(-1,-1,1,1\right) + \frac{2\ell^2}{\Sigma-\ell^2}\operatorname{diag}\left(1,0,0,0\right)\Bigg]. \tag{139}$$

This is structurally the same as what we saw happening for the black-bounce–Reissner–Nordström spacetime, cfr. eq. (130), with the substitutions

$$\frac{Q^2r^2}{(r^2+\ell^2)^3} \longleftrightarrow \frac{Q^2\left(\Sigma-\ell^2\right)}{\Sigma^3} \qquad \text{and} \qquad \frac{2\ell^2}{r^2} \longleftrightarrow \frac{2\ell^2}{\Sigma-\ell^2}\,. \tag{140}$$

The first term in eq. (139) is structurally of the form of the Maxwell stress-energy tensor, and the second term is structurally of the form of charged dust. At first sight this seems to suggest that a similar treatment as the one presented for the black-bounce–Reissner–Nordström spacetime should lead to a consistent picture. However, as we shall soon see below, the rotating case will prove much trickier.

6.3.2 *Black-bounce–Kerr–Newman electromagnetic potential*

The first step in carrying on the same interpretation for the stress-energy tensor as in the non-rotating case is to introduce the electromagnetic potential. Clearly, there is no obvious way to derive such potential, since we are not *a priori* specifying the equations of motion for the electromagnetic sector. Therefore, we shall choose to modify the Kerr–Newman potential in a minimal way, as we did for the black-bounce–Reissner–Nordström, i. e. we shall perform the usual substitution $r \mapsto \sqrt{r^2+\ell^2}$. Thus, our proposal in Boyer–Lindquist coordinates reads

$$A_\mu = -\frac{Q\sqrt{r^2+\ell^2}}{\Sigma}\left(1,0,0,-a\sin^2\theta\right). \tag{141}$$

In the orthonormal basis one has

$$A_{\hat{\mu}} = e_{\hat{\mu}}{}^{\nu}\,A_\nu = -\frac{Q\sqrt{r^2+\ell^2}}{\sqrt{\Sigma|\Delta|}}\left(1,0,0,0\right). \tag{142}$$

This is a minimal modification in the sense that, when we put $a \to 0$, the corresponding electrostatic potential is that of the black-bounce–Reissner–Nordström spacetime eq. (137), and when $\ell \to 0$ we regain the usual result for standard Kerr–Newman. The potential eq. (141) is also compatible with the NJPs as outlined in [153] and as applied to the black-bounce–Reissner–Nordström geometry.

We can now compute the electromagnetic field-strength tensor $F_{\mu\nu}$. In the orthonormal basis, its only non-zero components are

$$F_{\hat{t}\hat{r}} = -F_{\hat{r}\hat{t}} = -\frac{Q}{\Sigma^2}\sqrt{\frac{r^2}{r^2+\ell^2}}(r^2+\ell^2-a^2\cos^2\theta)\,, \tag{143a}$$

$$F_{\hat{\theta}\hat{\phi}} = -F_{\hat{\phi}\hat{\theta}} = \frac{2aQ\cos\theta\sqrt{r^2+\ell^2}}{\Sigma^2}\,. \tag{143b}$$

The homogeneous Maxwell equation is trivially satisfied $F_{[\mu\nu,\sigma]} = 0$. For the inhomogeneous Maxwell equation we find

$$\begin{aligned}\nabla^{\hat{\mu}}F_{\hat{\mu}\hat{\nu}} &= J_{\hat{\nu}}\\ &= \frac{Q\ell^2}{\Sigma^{7/2}\varrho}\left(-\frac{\Delta\left(\Sigma^2+2\Sigma\varrho^2-4\varrho^4\right)}{\varrho^2\sqrt{|\Delta|}},0,0,2a\sin\theta\left(\Sigma-2\varrho^2\right)\right).\end{aligned} \tag{144}$$

We interpret the right-hand side of eq. (144) as an effective electromagnetic source. Note that in terms of the (orthonormal) components of the electric and magnetic fields we have $\mathscr{E}_{\hat{r}} = F_{\hat{t}\hat{r}}$ and $\mathscr{B}_{\hat{r}} = F_{\hat{\theta}\hat{\phi}}$. It is then easy to check that this implies that the Maxwell stress-energy tensor eq. (131) is diagonal in this orthonormal basis and that

$$[T_{\text{Maxwell}}]^{\hat{\mu}}{}_{\hat{\nu}} = \frac{\mathscr{E}_{\hat{r}}^2+\mathscr{B}_{\hat{r}}^2}{8\pi}\,\text{diag}\,(-1,-1,1,1) \tag{145}$$

independently of the specific values of $E_{\hat{r}}$ and $B_{\hat{r}}$. It is also useful to check that

$$\mathscr{E}_{\hat{r}}^2+\mathscr{B}_{\hat{r}}^2 = \frac{Q^2}{\Sigma^2}\frac{r^2}{r^2+\ell^2}+\frac{4Q^2\ell^2a^2\cos^2\theta}{\rho^8}\,. \tag{146}$$

6.3.3 *Interpreting the black-bounce–Kerr–Newman stress-energy*

All of the above treatment is a relatively straightforward generalisation of the Reissner–Nordström case and also provides the correct limits for $\ell \to 0$ and/or $a \to 0$. However, when one attempts to interpret eq. (139) as the sum of the Maxwell stress-energy tensor eq. (145) and a charged dust, an inconsistency appears in the form of extra terms. Assuming some generalisation of the energy density of the charged dust and working out the needed electromagnetic potential also does not lead to satisfactory results.

In what follows, we shall present two alternative interpretations of the stress-energy tensor, one based on a generalisation of the Maxwell dynamics to a non-linear one, the other consisting of a generalisation of the charged dust fluid to one with anisotropic pressure.

NON-LINEAR ELECTRODYNAMICS An alternative to identifying a Maxwell stress-energy tensor in eq. (139) consists in generalising the

decomposition of the charged part of the stress energy tensor adopted in the Reissner–Nordström case to

$$[T_Q]^{\hat{\mu}}{}_{\hat{\nu}} = \mathcal{A}\,[T_{\text{Maxwell}}]^{\hat{\mu}}{}_{\hat{\nu}} + \Xi\, V^{\hat{\mu}} V_{\hat{\nu}}\,. \tag{147}$$

The multiplicative factor $\mathcal{A}$ will soon be seen to be position-dependent, and to depend on the spin parameter a and regularisation parameter ℓ, but to be independent of the total charge Q. This sort of behaviour is strongly reminiscent of non-linear electrodynamics where quite generically one finds $[T_{\text{NLED}}]^{\hat{\mu}}{}_{\hat{\nu}} \propto [T_{\text{Maxwell}}]^{\hat{\mu}}{}_{\hat{\nu}}$. The contribution $\Xi\, V^{\hat{\mu}} V_{\hat{\nu}}$ is again that appropriate to charged dust. The 4-velocity $V^{\hat{\mu}}$ is now the (non-geodesic) unit vector parallel to the timelike leg of the tetrad.

If we now compare eq. (145) with $[T_Q]^{\hat{\mu}}{}_{\hat{\nu}}$ as defined in eq. (147) we identify

$$\mathcal{A} = \frac{Q^2(\Sigma-\ell^2)/\Sigma^3}{\mathscr{E}_{\hat{r}}^2 + \mathscr{B}_{\hat{r}}^2} = \frac{\Sigma(\Sigma-\ell^2)(r^2+\ell^2)}{\Sigma^2 r^2 + 4a^2\ell^2(r^2+\ell^2)\cos^2\theta}\,. \tag{148}$$

We note that at small ℓ

$$\mathcal{A} = 1 - \frac{a^2\cos^2\theta\left(3r^2 - a^2\cos^2\theta\right)}{r^2(r^2+a^2\cos^2\theta)^2}\,\ell^2 + \mathcal{O}\left(\ell^4\right). \tag{149}$$

So in the limit as $\ell \to 0$, we see that $\mathcal{A} \to 1$, restoring standard Maxwell electromagnetism as would be expected for ordinary Kerr–Newman.

Also, we observe the large distance limit

$$\mathcal{A} = 1 - \frac{3\ell^2 a^2\cos^2\theta}{r^4} + \mathcal{O}\left(r^{-6}\right). \tag{150}$$

That is, at sufficiently large distances, $[T_Q]^{\hat{\mu}}{}_{\hat{\nu}}$ can safely be approximated as a Maxwell-like contribution plus a charged dust, while at small r we have

$$\mathcal{A} = \frac{\ell^2 + a^2\cos\theta^2}{4\ell^2} + \mathcal{O}\left(r^2\right). \tag{151}$$

This indicates a simple rescaling of the Maxwell stress-energy, (similar to what happens in non-linear electrodynamics), deep in the core of the black bounce.

Indeed, it is possible to further characterise the departure from Maxwell-like behaviour by decomposing $\mathcal{A} = 1 - a^2\ell^2\mathcal{F}$, where

$$\mathcal{F} = \frac{\cos^2\theta\left[4(r^2+\ell^2) - \Sigma\right]}{\Sigma^2 r^2 + 4a^2\ell^2\cos^2\theta(r^2+\ell^2)}\,. \tag{152}$$

The motivation for doing so is to make utterly transparent the correct limiting behaviour for $\mathcal{A}$ both for $a \to 0$, and for $\ell \to 0$.

ANISOTROPIC FLUID As an alternative to the non-linear electrodynamics interpretation, we can instead generalise the pressureless dust fluid we had introduced in the Reissner–Nordström case and impose

$$[T_Q]_{\hat{\mu}\hat{\nu}} - [T_{\text{Maxwell}}]_{\hat{\mu}\hat{\nu}} = \text{diag}\left(\varepsilon_f, -p_f, p_f, p_f\right) , \tag{153}$$

which can be satisfied if

$$\begin{aligned} \varepsilon_f &= \frac{Q^2\ell^2}{\varrho^2\Sigma^4}\left(4\varrho^4 - 7\varrho^2\Sigma + \Sigma^2\right), \\ p_f &= \frac{Q^2\ell^2}{\varrho^2\Sigma^4}\left(4\varrho^4 - 5\varrho^2\Sigma + \Sigma^2\right) . \end{aligned} \tag{154}$$

This implies that the right-hand side of eq. (153) can be interpreted, formally, as the stress-energy of an anisotropic fluid. Specifically, it can be written as

$$\varepsilon_f V_{\hat{\mu}} V_{\hat{\nu}} + \frac{p_f}{3}\left(g_{\hat{\mu}\hat{\nu}} + V_{\hat{\mu}} V_{\hat{\nu}}\right) + \pi_{\hat{\mu}\hat{\nu}} \tag{155}$$

with $V^{\hat{\mu}} = (1,0,0,0)$ — i. e. $(e_{\hat{t}})^{\hat{\mu}}$ — the velocity of the fluid and

$$\pi_{\hat{\mu}\hat{\nu}} = \frac{2p_f}{3}\,\text{diag}\,(0,-2,1,1) \tag{156}$$

the (traceless) anisotropic shear [184]. Note that

$$p_f \propto \left(4\varrho^4 - 5\varrho^2\Sigma + \Sigma^2\right) = \left(4\varrho^2 - \Sigma\right)\left(\varrho^2 - \Sigma\right) \propto a^2\cos^2\theta. \tag{157}$$

So in the limit $a \to 0$ this anisotropic fluid reduces to the usual charged dust.

6.4 GEODESICS AND EQUATORIAL ORBITS

Having characterised the spacetime in terms of the effective matter content, we shall now describe few notable orbits.

Consider a test particle with mass μ, energy E, component of angular momentum (per unit mass) along the rotation axis L_z and zero electric charge. Its trajectory $x^\mu(\tau)$ is governed by the following set of first-order differential equations (see e. g. ref. [169]):

$$\begin{aligned} \Sigma\frac{\mathrm{d}t}{\mathrm{d}\tau} &= a(L_z - aE\sin^2\theta) \\ &\quad + \frac{(r^2+\ell^2)+a^2}{\Delta}[E(r^2+\ell^2+a^2) - L_z a]\,, && \text{(158a)} \\ \Sigma\frac{\mathrm{d}r}{\mathrm{d}\tau} &= \pm\sqrt{\mathcal{R}}, && \text{(158b)} \\ \Sigma\frac{\mathrm{d}\theta}{\mathrm{d}\tau} &= \pm\sqrt{\Theta}\,, && \text{(158c)} \\ \Sigma\frac{\mathrm{d}\phi}{\mathrm{d}\tau} &= \frac{L_z}{\sin^2\theta} - aE + \frac{a}{\Delta}[E(r^2+\ell^2+a^2) - L_z a]\,, && \text{(158d)} \end{aligned}$$

where

$$\mathcal{R} = [E(r^2+\ell^2+a^2) - L_z a]^2 \\ - \Delta[\mu^2(r^2+\ell^2) + (L_z - aE)^2 + \mathcal{Q}], \tag{159}$$

$$\Theta = \mathcal{Q} - \cos^2\theta\left[a^2(\mu^2 - E^2) + \frac{L_z^2}{\sin^2\theta}\right], \tag{160}$$

and $\mathcal{Q}$ is a generalised Carter constant associated to the existence of a Killing tensor discussed in subsection 6.4.1 below.

In view of the existence of the Killing tensor, there exist orbits that lie entirely on the equatorial plane $\theta = \pi/2$. Exploiting the conserved quantities, their motion is effectively one-dimensional and governed by the effective potential $\mathcal{R}$: circular orbits, in particular, are given by

$$\mathcal{R} = 0 \qquad \text{and} \qquad \frac{\mathrm{d}\mathcal{R}}{\mathrm{d}r} = 0\,; \tag{161}$$

when, in addition,

$$\frac{\mathrm{d}^2\mathcal{R}}{\mathrm{d}r^2} > 0\,, \tag{162}$$

the orbits are stable.

Solutions to eq. (161) can be easily found by exploiting known results on the Kerr–Newman geometry [111, 285, 354, 362]. Indeed, writing eq. (159) in terms of $\varrho = \sqrt{r^2+\ell^2}$, one immediately recognises the textbook result for a Kerr–Newman spacetime in which the Boyer–Lindquist radius has been given the uncommon name ϱ. Moreover,

$$\frac{\mathrm{d}\mathcal{R}}{\mathrm{d}r} = \frac{\mathrm{d}\varrho}{\mathrm{d}r}\,\frac{\mathrm{d}\mathcal{R}}{\mathrm{d}\varrho}\,, \tag{163}$$

so

$$\frac{\mathrm{d}\mathcal{R}}{\mathrm{d}\varrho} = 0 \quad \Longrightarrow \quad \frac{\mathrm{d}\mathcal{R}}{\mathrm{d}r} = 0\,. \tag{164}$$

Furthermore, at the critical point

$$\frac{\mathrm{d}^2\mathcal{R}}{\mathrm{d}r^2} = \left(\frac{\mathrm{d}\varrho}{\mathrm{d}r}\right)^2 \frac{\mathrm{d}^2\mathcal{R}}{\mathrm{d}\varrho^2}\,. \tag{165}$$

So stability (or lack thereof) is unaffected by the substitution $r \leftrightarrow \varrho$. Therefore, suppose ϱ_c is such that

$$\mathcal{R}(\varrho_c) = 0 \qquad \text{and} \qquad \frac{\mathrm{d}\mathcal{R}(\varrho_c)}{\mathrm{d}\varrho} = 0\,; \tag{166}$$

that is, suppose the Kerr–Newman spacetime has a circular orbit at radius $\varrho = \varrho_c$, then the black–bounce-Kerr–Newman spacetime has a circular orbit at $r = r_c = \sqrt{\varrho_c^2 - \ell^2}$. Clearly, this mapping is allowed only if $\varrho_c \geq \ell$.

As a particular example, we report the coordinate location of the light ring and the ISCO in the non-rotating limit, since these can easily be found analytically — for the details of the computations, see [166]. For the light ring, we find (in our universe):

$$r_{\rm ph} = \sqrt{\frac{M}{2}\left(9M + 3\sqrt{9M^2 - 8Q^2}\right) - 2Q^2 - \ell^2}\,; \tag{167}$$

in the limit as $Q,\ \ell \to 0$ we reproduce the standard Schwarzschild result, $r_{\rm ph} = 3M$, as expected. For the ISCO (again, in our universe), we find:

$$r_{\rm ISCO} = \frac{1}{MB}\left[9M^4Q^4 - 6M^2Q^2\left(B^2 + 2BM^2 + 4M^4\right) + \left(B^2 + 2BM^2 + 4M^4\right)^2 - B^2\ell^2M^2\right]^{1/2} \tag{168}$$

where now

$$B = \left[2M^2Q^4 + M^2\left(\pm C - 9M^2\right)Q^2 + 8M^6\right]^{\frac{1}{3}}\,,$$
$$C = \sqrt{4Q^4 - 9M^2Q^2 + 5M^4}\,; \tag{169}$$

it is easily verified that in the limit as $Q,\ \ell \to 0$, $r_{\rm ISCO} \to 6M$, as expected for Schwarzschild.

Non-circular and non-equatorial orbits, instead, require a more thorough analysis: see section 8.2 for some further details.

6.4.1 *Killing tensor and non-existence of the Killing tower*

The existence of the generalised Carter constant $\mathcal{Q}$ introduced in the previous section is guaranteed by the fact that the tensor

$$K_{\mu\nu} = \Sigma\left(l_\mu n_\nu + l_\nu n_\mu\right) + \left(r^2 + \ell^2\right)g_{\mu\nu} \tag{170}$$

is a Killing tensor; it is easy to explicitly check that $K_{(\mu\nu;\lambda)} = 0$. Here

$$l^\mu = \left(\frac{r^2 + \ell^2 + a^2}{\Delta}, 1, 0, \frac{a}{\Delta}\right)$$
$$\text{and}\quad n^\mu = \frac{1}{2\Sigma}\left(r^2 + \ell^2 + a^2, -\Delta, 0, a\right) \tag{171}$$

are a pair of geodesic null vectors belonging to a generalised Kinnersley tetrad — see subsection 5.2.4.

Based on proposition 1.3 in [175], it has been established [24] that when one defines the Carter operator $\mathcal{K}\Phi = \nabla_\mu\left(K^{\mu\nu}\nabla_\nu\Phi\right)$ and wave operator $\Box\Phi = \nabla_\mu\left(g^{\mu\nu}\nabla_\nu\Phi\right)$ one has

$$[\mathcal{K}, \Box]\,\Phi = \frac{2}{3}\left(\nabla_\mu\,[R, K]^\mu{}_\nu\right)\nabla^\nu\Phi\,. \tag{172}$$

This operator commutator will certainly vanish when the tensor commutator $[R,K]^{\mu}{}_{\nu} = R^{\mu}{}_{\alpha}K^{\alpha}{}_{\nu} - K^{\mu}{}_{\alpha}R^{\alpha}{}_{\nu}$ vanishes, and this tensor commutator certainly vanishes for the black-bounce–Kerr–Newman spacetime considered herein. Hence the wave equation (not merely the Hamilton–Jacobi equation) separates on the black-bounce–Kerr–Newman spacetime.

In the Kerr–Newman spacetime we started from, the Killing tensor is part of a "Killing tower" which ultimately descends from the existence of a closed conformal Killing–Yano tensor — called a *principal tensor* for short [171]. Such a principal tensor is a rank-2, antisymmetric tensor $h_{\mu\nu}$ satisfying (in four spacetime dimensions) the equation:

$$\nabla_{\mu} h_{\nu\alpha} = \frac{1}{3}\left[g_{\mu\nu}\nabla^{\beta}h_{\beta\alpha} - g_{\mu\alpha}\nabla^{\beta}h_{\beta\nu}\right]. \tag{173}$$

In the language of forms, $\mathbf{h} = h_{\mu\nu}\,\mathrm{d}x^{\mu}\wedge\mathrm{d}x^{\nu}$ is a non-degenerate two-form satisfying

$$\nabla_{\mathbf{Y}}\mathbf{h} = \mathbf{Y}\wedge\mathbf{X}, \qquad \mathbf{X} = \frac{1}{3}\boldsymbol{\nabla}\cdot\mathbf{h} \tag{174}$$

with $\mathbf{Y}$ any vector. (The equation above implies, incidentally, that $\mathbf{h}$ is closed: $\mathrm{d}\mathbf{h} = 0$, so that locally $\mathbf{h} = \mathrm{d}\mathbf{b}$.) The Hodge dual of a principal tensor is a Killing–Yano tensor, i. e.

$$\mathbf{f} = *\mathbf{h} \qquad \text{is such that} \qquad \nabla_{\mu}f_{\nu\alpha} + \nabla_{\nu}f_{\mu\alpha} = 0\,. \tag{175}$$

A Killing–Yano tensor, in turn, squares to a tensor

$$k_{\mu\nu} = f_{\mu\alpha}f_{\nu}{}^{\alpha} \tag{176}$$

that is a Killing tensor; $k_{(\mu\nu;\lambda)} = 0$.

We may thus wonder whether the Killing tensor eq. (170) derives from a principal tensor, as in the Kerr–Newman case. Naively, one may want to apply the usual trick $r \mapsto \sqrt{r^2+\ell^2}$ to the Kerr–Newman principal tensor, or to the potential $\mathbf{b}$ (the two options are not equivalent). By adopting the first strategy, one finds a "would-be" Killing–Yano tensor that does indeed square to eq. (170) but fails to satisfy eq. (175). The second approach also fails.

In fact, one can prove that no principal tensor can exist in this spacetime. The system eq. (173) is overdetermined and has a solution only if a certain integrability condition is satisfied: this condition implies that the corresponding spacetime be of Petrov type D. However, the discussion in subsection 5.2.4 proves that the black-bounce–Kerr spacetime is not algebraically special, hence neither can the black-bounce–Kerr–Newman spacetime be algebraically special. More prosaically, the non-existence of the Killing tower can be seen as a side effect of the fact that our black-bounce–Kerr–Newman geometry does not fall into Carter's "off shell" two-free-function distortion of Kerr [171].

For reference, here is the would-be Killing–Yano tensor:

$$f_{\mu\nu} = \begin{pmatrix} 0 & -a\cos\theta & 0 & 0 \\ a\cos\theta & 0 & 0 & -a^2\cos\theta\sin^2\theta \\ 0 & 0 & 0 & 0 \\ 0 & a^2\cos\theta\sin^2\theta & 0 & 0 \end{pmatrix} + \varrho\sin\theta \begin{pmatrix} 0 & 0 & a & 0 \\ 0 & 0 & 0 & 0 \\ -a & 0 & 0 & (\varrho^2+a^2) \\ 0 & 0 & -(\varrho^2+a^2) & 0 \end{pmatrix}. \tag{177}$$

This would-be Killing–Yano tensor is taken from [171, eq. (3.22), p. 47], with coordinates changed to Boyer–Lindquist form, and with the substitution $r \mapsto \sqrt{r^2+\ell^2}$ in the tensor components. It is easy to check that "$f^2 = K$", but

$$\nabla_{(\mu} f_{\nu)\alpha} = \left(\sqrt{r^2+\ell^2} - r\right) \times [\text{tensor, finite as } \ell \to 0]\,. \tag{178}$$

(This manifestly vanishes when $\ell \to 0$, as it should to recover the Killing–Yano tensor of the Kerr–Newman spacetime.) Its divergence is in fact particularly simple:

$$\nabla_\mu f^{\mu\nu} = \left[\left(\sqrt{r^2+\ell^2} - r\right)\frac{2a\cos\theta}{\Sigma}\right](1,0,0,0)\,. \tag{179}$$

(This again manifestly vanishes when $\ell \to 0$, as it should.)

Note that if one instead takes

$$b_\mu \mathrm{d}x^\mu = -\frac{1}{2}(r^2+\ell^2-a^2\cos^2\theta)\mathrm{d}t - \frac{1}{2}\left[-r^2-\ell^2+(r^2+\ell^2+a^2)\cos^2\theta\right]a\mathrm{d}\phi, \tag{180}$$

as in ref. [171, eq. (3.21), p. 47], converted to Boyer–Lindquist coordinates, and subjected to the substitution $r \mapsto \sqrt{r^2+\ell^2}$, one finds

$$f_{\mu\nu} \neq \nabla_\mu b_\nu - \nabla_\nu b_\mu\,. \tag{181}$$

(This is not surprising since derivatives are involved.)

6.5 CHAPTER WRAP-UP

We have seen that adding an electromagnetic charge to the black-bounce–Kerr metric leads to the black-bounce–Kerr–Newman metric, which is a minimal, one-parameter deformation of the entire Kerr–Newman family with the desirable properties that it simultaneously (i) passes all weak-field observational tests, (ii) is globally regular (no curvature singularities), and (iii) neatly interpolates between a RBH and a charged traversable wormhole.

While adding an electromagnetic charge to the black-bounce–Kerr spacetimes in this manner is maybe not of direct astrophysical importance (since in any plausible astrophysical situation $|Q|/M \ll 1$), it is of considerable theoretical importance, as it gives us an entirely new class of relatively clean everywhere regular BHs to work with. Indeed, we have seen that such geometries present interesting theoretical features such as the existence of a Killing tensor without the presence of the full Killing tower (principal tensor, Killing–Yano tensor) or the fact that the charge-dependent component of the stress-energy for the black-bounce–Kerr–Newman spacetime has a rather non-trivial physical interpretation. In particular, we found that it can either be interpreted as charged dust together with a non-linear modification to standard Maxwell electromagnetism, or as standard Maxwell electromagnetism together with an anisotropic fluid.

While there is no simple way to remove this ambiguity, we can however notice that it appears at least problematic to justify from a physical point of view the introduction of a non-linear electrodynamics for the black-bounce–Kerr–Newman spacetime, given that the latter is not required for consistency with GR of the black-bounce–Reissner–Nordström or the black-bounce–Kerr spacetime. This seems to suggest that the anisotropic fluid interpretation might be more natural.

7

SCALAR PERTURBATIONS ON BLACK-BOUNCE–KERR SPACETIMES

At the end of chapter 5 we mentioned that one compelling question concerning the black-bounce–Kerr is whether it can be stable over astrophysical timescales when perturbed by a small amount of matter. Indeed, as hinted to at the end of subsection 2.2.2, observations suggest that isolated astrophysical BHs, though never really in a vacuum, are well described by vacuum solutions of GR, meaning that the back-reaction of matter onto the geometry is often negligible. Hence, we said that stability is a necessary requirement for any effective model that aims to be phenomenologically viable.

A simple and popular test of stability consists in the computation of quasi-normal modes (QNMs) [56, 222, 225, 253, 289]. Such computation is typically performed in the context of perturbation theory, whereby a test perturbation field is made to propagate "on top" of a fixed background geometry, and is therefore relatively insensitive to the specific theory the geometry is a solution of. It is however sensitive to the boundary conditions one imposes at infinity and at the horizon (or at the throat, in the case of a wormhole). Hence any modification to the near-horizon geometry is expected to affect the QNM spectrum.

In Kerr BHs, all QNMs are decaying functions of time, meaning that in this geometry small perturbations are dissipated away — the Kerr spacetime is therefore perturbatively stable. That the same is true for other BHs is not obvious; even less so if the spacetime is horizonless but possesses an ergoregion. This is because, in the absence of an horizon, negative-energy modes are (partially) reflected by the object and can therefore accumulate inside the ergoregion — producing the so-called *ergoregion* or *superradiance instability* [9, 77, 102, 168, 191, 298]. For instance, a very compact and rapidly rotating BH mimicker with a highly reflective surface would be prone to such instability [108, 109, 139, 250, 251, 292, 372], although absorption by the object's surface might quench the effect.

Notably, QNMs are also of great observational interest, since they describe a geometry's response to a localised perturbation. Moreover, they characterise the ringdown following the merger of multiple objects. In this respect, the most (and so far the only) interesting QNMs are those of gravitational (helicity-2) perturbations, which can be detected in gravitational-wave signals. However, vector (helicity-1) and scalar (helicity-0) perturbations are often considered too, because they

are simpler to deal with and their behaviour often mirrors that of gravitational perturbations.

Measuring multiple QNMs originating from the same object, such as a remnant resulting from a binary merger, would thus allow for testing GR and deviations thereof, as well as the no-hair conjecture and the Kerr hypothesis — a program that goes by the name of BH *spectroscopy* [5, 60, 105, 110, 112, 227, 252, 254]. Moreover, QNMs from an horizonless object might get repeatedly reflected by the surface and by the potential barrier, thus generating a train of "echoes" that could in principle be detected in ringdown signals [4, 11, 84, 87, 103, 104, 106, 107, 274, 281, 351].

The BH spectroscopy programme has recently come into question, as it was realised that the QNM spectrum is generically unstable, i. e. small changes in the geometry, possibly due to environmental effects, can result in very large changes in the frequencies [115, 207, 208]. The relevance of this findings for time-domain gravitational-wave signals is however still debated [58].

This chapter is thus devoted to the study of scalar test-field perturbations on top of a black-bounce–Kerr spacetime. Specifically, we first describe some general properties of the scalar wave equation on this background in section 7.1. Then, in section 7.2, we compute the QNMs for massless perturbations; when the background is a traversable wormhole, we further search for unstable modes. Finally, in section 7.3, we endow the field with a mass and study superradiance by computing the spectrum of the amplification factors.

7.1 SCALAR PERTURBATIONS

In studying perturbations, it is convenient to upgrade the quantity $\varrho = \sqrt{r^2 + \ell^2}$ to a coordinate and work with the following form of the metric

$$\begin{aligned} \mathrm{d}s^2 = &- \left(1 - \frac{2M\varrho}{\Sigma}\right) \mathrm{d}t^2 + \frac{\Sigma}{\delta\Delta}\,\mathrm{d}\varrho^2 + \Sigma\,\mathrm{d}\theta^2 \\ &- \frac{4Ma\varrho\sin^2\theta}{\Sigma}\,\mathrm{d}t\,\mathrm{d}\phi + \frac{A\sin^2\theta}{\Sigma}\,\mathrm{d}\phi^2 \end{aligned} \tag{182}$$

with now

$$\Sigma = \varrho^2 + a^2\cos^2\theta, \quad \Delta = \varrho^2 - 2Mr + a^2, \quad \delta = 1 - \frac{\ell^2}{\varrho^2}, \tag{183a}$$

$$A = \left(\varrho^2 + a^2\right)^2 - \Delta a^2\sin^2\theta\,. \tag{183b}$$

With these coordinates $(t, \varrho, \theta, \phi)$ we recognise the metric in eq. (182) as a particular case of the Johannsen family [210, 211]. Recall that $\varrho \geq \ell$, with $\varrho = \ell$ representing the wormhole throat; and that horizons, if any, are located at $\varrho = \varrho_\pm$ with

$$\varrho_\pm = M \pm \sqrt{M^2 - a^2}\,. \tag{184}$$

As discussed in chapter 5, the deviations from GR, quantified by the effective sources, fall off very quickly as one moves away from the object. Namely, the effective energy density and pressures all scale as $\sim \varrho^{-4}$ (technically, as $r^{-4} = (\varrho^2 - \ell^2)^{-2}$). Therefore, for all practical purposes the spacetime is effectively vacuum.

This means that a test scalar field Φ, with mass $m_\Phi = \hbar\mu$, will evolve according to the Klein–Gordon equation $\Box\Phi = \mu^2\Phi$ — where d'Alembert's $\Box$ operator is determined by eq. (182).

Assuming the decomposition[1] $\Phi = e^{\mathrm{i}m\phi}e^{-\mathrm{i}\omega t}S(\theta)R(\varrho)$, with m and ω being the azimuthal number and the frequency of the perturbation, the Klein–Gordon equation separates (cf. the discussion in chapter 6) into an angular equation

$$\frac{1}{\sin\theta}\frac{\mathrm{d}}{\mathrm{d}\theta}\left(\sin\theta\frac{\mathrm{d}S}{\mathrm{d}\theta}\right) + \left(a^2\left(\omega^2-\mu^2\right)\cos^2\theta + A_{lm} - \frac{m^2}{\sin^2\theta}\right)S = 0\,, \tag{185}$$

which is the spheroidal harmonics equation, whose eigenvalues A_{lm} are characterised by the harmonic number l; and a radial equation

$$\sqrt{\delta}\,\frac{\mathrm{d}}{\mathrm{d}\varrho}\left(\sqrt{\delta}\Delta\frac{\mathrm{d}R}{\mathrm{d}\varrho}\right) + \left(\frac{K^2}{\Delta} - \mu^2\varrho^2 - \lambda\right)R = 0\,, \tag{186}$$

where $K = \left(\varrho^2 + a^2\right)\omega - am$ and $\lambda = A_{lm} - 2am\omega + a^2\omega^2$. Eq. (185) is exactly what one would find in the Kerr geometry, while eq. (186) is a distortion of its Kerr analogue due to the presence of δ.

In the non-rotating limit, eq. (185) reduces to the spherical harmonics equation with eigenvalues $A_{lm} = l(l+1)$. More generally, eq. (185) must be solved perturbatively in $a\omega$ or numerically [57]. In our computations, we have evaluated the angular eigenvalue both numerically with the Leaver method [234] and approximately with a high-order expansion in $a\omega$.

For the radial equation, on the other hand, two limits are worth considering: one corresponding to spatial infinity, i. e. $\varrho \to \infty$, and one to the near-horizon or near-throat region, depending on the background geometry.

At spatial infinity, the radial function has the following asymptotic behaviour

$$R(\varrho) \sim \frac{1}{\varrho}\,e^{q\varrho}\varrho^{M\left(\mu^2-2\omega^2\right)/q}\,, \quad q = \pm\sqrt{\mu^2-\omega^2}\,. \tag{187}$$

The sign of the real part of q determines the behaviour of the wavefunction at $\varrho \to \infty$. If $\mathrm{Re}(q) > 0$ the solution diverges, while for

1 Contrary to other chapters, here the symbol R denotes the radial wavefunction and not the Ricci scalar; similarly, the symbol S stands for the angular wavefunction and not the action. These minor inconsistency should not generate confusion, as the meaning of the symbols is clear from context.

$\mathrm{Re}(q) < 0$ the solution tends to zero. The general solution will be a linear combination of both cases.

In the massless case, eq. (187) reduces to a simpler form,

$$R(\varrho) \sim \frac{1}{\varrho}\, e^{\pm \mathrm{i}\omega\varrho}\varrho^{\pm 2\mathrm{i}M\omega} \tag{188}$$

where the plus (minus) sign corresponds to outgoing (ingoing) waves. It is to be noted that the asymptotic solution at spatial infinity is independent of the parameter ℓ, but for determining the near-horizon or near-throat asymptotic solution, ℓ would play an important role, which we explore now.

When the regularisation parameter ℓ satisfies $\ell < \varrho_+$, the metric in eq. (182) describes a RBH and the two independent solutions close to the event horizon behave as

$$\begin{aligned} R(\varrho) &\sim (\varrho - \varrho_+)^{\pm \mathrm{i}\sigma}\,, \\ \sigma &= \frac{am - 2M\omega\varrho_+}{\gamma\,(\varrho_+ - \varrho_-)}\,, \quad \gamma = \sqrt{1 - \frac{\ell^2}{\varrho_+^2}}\,. \end{aligned} \tag{189}$$

For traversable wormholes with regularisation parameter $\ell > \varrho_+$, close to the throat the two linearly independent solutions are asymptotic to

$$\begin{aligned} R(\varrho) &\sim \exp\left(\pm \frac{\mathrm{i}\tilde{\omega}\,(a^2+\ell^2)\,\sqrt{2\ell(\varrho-\ell)}}{\Delta(\ell)}\right), \\ \tilde{\omega}^2 &= \left(\omega - \frac{am}{a^2+\ell^2}\right)^2 - \frac{\Delta(\ell)\,(\ell^2\mu^2+\lambda)}{(a^2+\ell^2)^2} - \frac{\Delta(\ell)^2}{(a^2+\ell^2)^3}\,, \end{aligned} \tag{190}$$

where $\Delta(\ell)$ means Δ evaluated at $\varrho = \ell$.

In the particular case in which the throat of the wormhole becomes a null surface and coincides with the black-hole horizon, i. e. for $\ell = \varrho_+$, the corresponding solutions are of the form

$$R(\varrho) \sim \exp\left(\pm \mathrm{i}\frac{am - 2M\omega\varrho_+}{\varrho_+ - \varrho_-}\sqrt{\frac{2\ell}{\varrho - \ell}}\right). \tag{191}$$

In eqs. (189) to (191) the plus (minus) sign corresponds to outgoing (ingoing) waves.

7.1.1 *Boundary conditions*

For determining the QNMs or the superradiant amplification factors, one needs to supplement eq. (186) with appropriate boundary conditions. Such boundary conditions define the physical problem at hand and depend on whether the spacetime contains a BH or not.

QNMs encode the scalar's late-time response to an initial perturbation that is localised in space. For this reason, we demand purely

outgoing waves at spatial infinity. In the RBH case, we further demand that no radiation comes out of the horizon. The null throat case is analogous to the RBH, in this respect: As can be deduced by inspecting the conformal diagrams of figure 3b, in this case the wormhole throat coincides with the horizon and is therefore a causal boundary. (The only causal curves that reach $\varrho = +\infty$ after having crossed $\varrho = \ell$ originated from the "other universe" in the past analytical extension of the spacetime.) Hence, we impose purely ingoing boundary conditions at the null throat. When $\ell > \varrho_+$, instead, the throat is traversable in both directions and the "two universes" are causally connected. Since the geometry on the two sides of the wormhole is symmetric, we assume that the scalar field will inherit the symmetry of the background. This assumption translates into perfect reflection at the throat, which we implement by demanding $R(\ell) = 0$. Alternatively, one can require the derivative of the radial function to vanish at the throat; such Neumann boundary conditions are associated to another family of QNMs, whose computation is beyond our scope.

Superradiance is, in essence, a scattering experiment whereby an ingoing wave is sent in from infinity, it scatters off the compact object and is then measured again at infinity. As both ingoing and outgoing radiation must be present at spatial infinity, we allow for both solutions of eq. (190). For RBHs and null wormholes, the conditions at the inner boundary (i. e. at the horizon) are the same we impose for the QNMs computation. In the traversable wormhole case, however, the assumption of perfect reflection at the throat is no longer justified. Indeed, that assumption would entail that the same scattering experiment is performed simultaneously in the "two universes". We rather resolve to study superradiance from the perspective of "our universe" alone, thus assuming no ingoing radiation at infinity in the "other universe"; of course, it is possible to do otherwise, but that investigation lies beyond the scope of this chapter. Under this circumstance, a simple argument — which we report in section 7.3 — ensures that no superradiant amplification can occur, regardless of the exact boundary conditions imposed at the throat. Our choice of boundary conditions is summarised in table 3.

Clearly, other choices of boundary conditions are possible. For instance, the symmetry between the "two universes" could easily be broken, e. g. by the presence of some matter on one side of the wormhole but not the other; if this were the case, perfect reflection at the throat could not be justified. Alternatively, one could imagine a situation in which the background is still symmetric but the perturbation is not, as in a scattering problem whereby a wavepacket is prepared in "our universe" and sent towards the object; in such a case, boundary conditions at the throat might not be needed at all. Finally, one might envisage a scenario in which the exotic matter that keeps the worm-

Inner boundary	
regular black hole ($\ell < \varrho_+$)	pure absorption, cf. eq. (189)
null-throat wormhole ($\ell = \varrho_+$)	pure absorption, cf. eq. (191)
traversable wormhole ($\ell > \varrho_+$)	(QNMs) pure reflection, $R(\ell) = 0$
Infinity, cf. eqs. (187) and (188)	
QNMs	purely outgoing
superradiance	ingoing and outgoing

Table 3: Behaviour of the radial function close to the inner boundary, i. e. the horizon for regular black holes and the throat for wormholes, and asymptotically, according to the physical problem under investigation.

hole open is not transparent to the perturbation; this would make the dynamics non-conservative even at the test-field level. All these possibilities, though interesting, lie beyond the scope of this work.

7.2 QNMS AND (IN)STABILITY

QNMs can be obtained by various analytical methods but the complicated form of the potential makes it difficult to solve the perturbation equation without added assumptions or imposing restrictions on the parameter space. In this section, we focus on obtaining the QNMs numerically by the direct integration and shooting techniques. This approach is valid both for the BH and the wormhole branches. For the RBHs, the QNMs can also be approximated using the more analytic Wentzel–Kramers–Brillouin (WKB) approach [197, 312], and its generalisation to rotating backgrounds [221, 314]. Below we first detail the two methods, then present our results.

7.2.1 *Methods*

7.2.1.1 *Direct integration*

The direct integration technique [114] works as follows. First, consider the non-rotating case. For the BH, we integrate eq. (186) supplied with the correct boundary conditions both from infinity and from the horizon to an intermediate point (typically the maximum of the scalar potential) and then we shoot for the value of ω such that the radial function and its derivative are continuous at the intermediate point. The same procedure is followed for the null-throat wormhole, though this case is technically more subtle — we provide more detail

in section 8.4. For the wormhole, we only integrate from infinity and shoot for the value of ω such that the solution is zero at the throat.

In practice, infinity is taken to be at some large value of ϱ — e. g. $75M$. Similarly, the integration must start or stop a small distance away from the horizon or the throat, since the coefficients of the differential equation diverge there. These parameters, along with the location of the intermediate point, are varied by small amounts in order to assess the stability of our numerical results, which are stable within a numerical accuracy of, typically, order 10^{-3} or less. Moreover, shooting requires an initial guess for the value of the QNM frequency ω. In the BH case, we looked for solutions in the vicinity of the tabulated value of the corresponding fundamental QNM of Kerr. The wormhole case requires a more thorough mapping of the solutions to the eigenvalue problem.

For the rotating case, starting with a small value of a/M, we start by considering the non-rotating QNM frequencies as initial guess values and then we solve for the angular eigenvalue. Next, we integrate the radial equation as in the non-rotating case and we shoot for the frequency ω. We repeat this procedure as long as the frequency ω converges to a constant value; in practice, this is often achieved within five iterations. The QNM frequencies for configurations with higher values of a/M are determined by using the previous frequency as initial guess and following their behaviour as a function of the spin parameter.

7.2.1.2 WKB

Alternatively, for RBHs and null-throat wormholes, the QNMs can be determined with the WKB approach.

Let us begin with the non-rotating case again. In a nutshell, the WKB approximation connects two solutions in a matching region, and gives the best results when the matching region is around the maximum of the scalar potential, which in this case does not depend on the frequency of the perturbation. Hence, the potential can be Taylor-expanded around the maximum of the potential and, at leading order, the QNM frequencies are given by

$$\omega^2 = V_0 - \mathrm{i}\sqrt{-2V_0''}\left(n + \frac{1}{2}\right), \quad n = 0, 1, \dots , \tag{192}$$

where a prime represents a derivative with respect to the tortoise coordinate, and the subscript "0" means evaluated at the maximum of the potential. The integer n is the overtone number and the QNM with $n = 0$ is called the fundamental mode. Higher-order corrections to this equation have been computed, as well as approaches to increase its accuracy [196, 197, 223, 226, 266]. In our computations, good agreement with the numerical results are achieved considering a fourth-order approximation. This is also motivated by the fact that

for scalar perturbations in a Kerr background, especially for the lowest l values, agreement of order 3% with numerical results requires at least a fourth-order WKB approximation [226].

The rotating case is more involved, as the scalar potential and the angular eigenvalues *do* depend on the frequency. The strategy in this case is to work perturbatively in powers of $a\omega$. For $a\omega$ sufficiently small, we expect to obtain good accuracy with this truncated series. In our computations, we have considered orders up to the sixth — the highest for which analytical results are available. This choice allows us to explore intermediate values of the spin parameter. The procedure to determine the QNM frequency is then, in essence, equivalent to the WKB method in the non-rotating case, and we need to numerically solve an equation of the form

$$\omega^2 = f\left(a, \omega, \ell, n, l, m\right), \tag{193}$$

in order to determine ω, given a, ℓ, n, l and m. Generically, eq. (193) will contain a number of spurious roots which we discard by starting with the well-defined solution for $a = 0$ and following the roots for increasing a/M.

7.2.2 *Results*

7.2.2.1 *Regular black holes*

Some of our results are presented in figure 11, where solid lines are obtained with the direct integration method, while dashed lines come from the WKB method. We verified that the results are not affected significantly by changes in the parameters entering our numerical routines (i. e. the locations of the numerical infinity, of the numerical horizon and of the intermediate point). Clearly, the two methods are in good agreement for $a \lesssim 0.5M$, although less so for the $l = m = 0$ mode. This is not surprising, as the WKB approximation is expected to hold best for values of l larger than the spin of the perturbation ($l > 0$ in this case). In the non-rotating limit, our results are also in agreement with those in [118], obtained both with the WKB and time-domain methods. The fundamental QNM frequencies, as presented in figure 11, show a clear dependence on the regularisation parameter ℓ, though the relative variations in their magnitude are rather mild. Each fundamental mode is accompanied by a whole tower of overtones which can in principle be computed with the same methods.

7.2.2.2 *Null-throat wormholes*

As mentioned before and as explained in detail in section 8.4, the null-throat case is technically more involved than the RBH one. The structure of the space of solutions is also more complex, as multiple modes (all stable) lie close to one another. As a result, we need higher

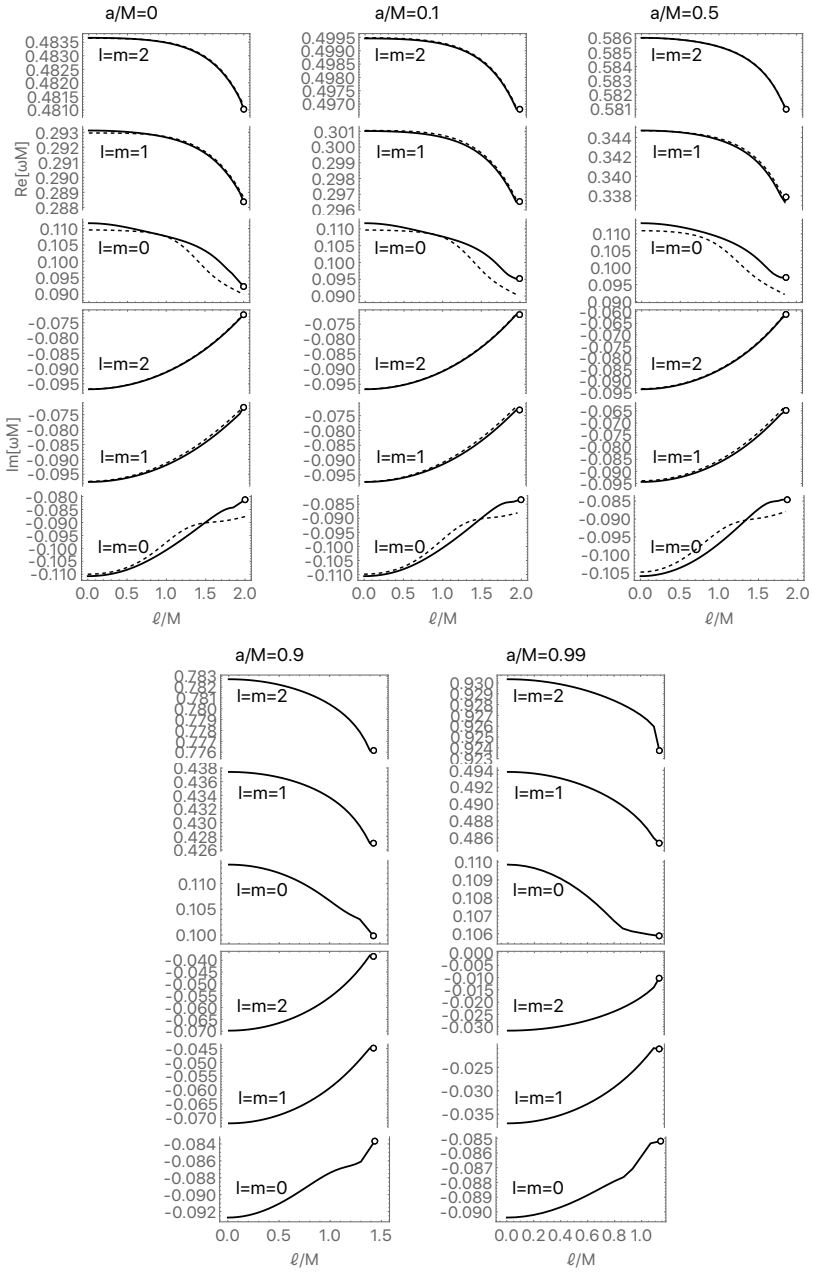

Figure 11: QNMs for RBHs and null-throat wormholes (empty circle for the $\ell = r_+$ case): real (top panels) and imaginary parts (bottom panels) of the QNM frequencies have been plotted as functions of the dimensionless regularisation parameter (ℓ/M), for the first few $l = m$ modes, for selected values of the spin parameter. The solid lines arise out of the direct integration scheme; while the dashed lines correspond to the WKB approximation, valid up to $a/M \lesssim 0.5$.

accuracy in our numerical routines and very precise initial guesses for the shooting. Otherwise, it is possible for small variations in the spacetime and in the integration parameters to cause the numerical

routine to "jump" between nearby modes, e. g. from the fundamental mode to an overtone.

Despite the hurdles, a solid qualitative picture does emerge: wormholes with a null throat are stable, in the sense that their QNMs have negative imaginary part; and in all of the cases we have studied there exists a mode that can be reached along the curves of figure 11, the empty circle, in the limit $\ell \to \varrho_+$[2]. In other words, wormholes with a null throat seem to be phenomenologically akin to RBHs, and a limiting case thereof, in all respects hereby considered.

7.2.2.3 *Wormholes*

Given the different boundary conditions, there is no reason to expect that the curves of figure 11 will cross over smoothly to the wormhole branch. Lacking guidance from known results, the frequency space had to be spanned more broadly in order to confidently identify the QNMs. More specifically, we considered a rectangular grid of points in the $\mathrm{Im}(\omega)$-$[\mathrm{Re}(\omega) > 0]$ space, wide enough to enclose our rough expectations for the QNM frequency, and computed the quantity $\arg[R(\ell)]$. A plot of this quantity permits to visually locate the zeroes of $R(\ell)$ in the frequency space, since the argument yields a recognisable pattern around them.[3] In this way, we were able to pick accurate guesses for our shooting routine.

As a result of this investigation, we were able to pinpoint a "fundamental" QNM, which we tracked under changes of the rotation parameter a and regularisation parameter ℓ — see figure 12. This mode is stable and is the least damped of a family of stable modes, which we identify as the overtones.

In addition to these, for high enough values of the spin parameter, and for $\mathrm{Re}(\omega) < m\Omega_{\mathrm{H}}$, being Ω_{H} the would-be horizon angular velocity, a second family of QNMs appears. All of the modes in this second family are *unstable*; the imaginary parts of their QNM frequencies are very small, but *positive*, and span several orders of magnitude, between approximately $10^{-6}/M$ and $10^{-15}/M$, corresponding to instability timescales in the approximate range 10 to $10^{10}\,(M/M_{\odot})$ s. For some specific cases, a few of these modes have been presented in figure 13.

Once again, the qualitative picture presented herein is unaffected by changes in the parameters that specify the numerical routines (the values of the numerical infinity and of the numerical throat). However, as in the null-throat wormhole case, high accuracy and precise initial guesses for the QNM frequencies are required in our numerical routine, otherwise the numerical value of the QNM frequencies found with the shooting technique could not converge. Furthermore,

2 In same cases, the empty circle seems not to lie on the BH curve: this is due solely to numerical precision.

3 This is analogous to what the MATHEMATICA's `ComplexPlot` function does.

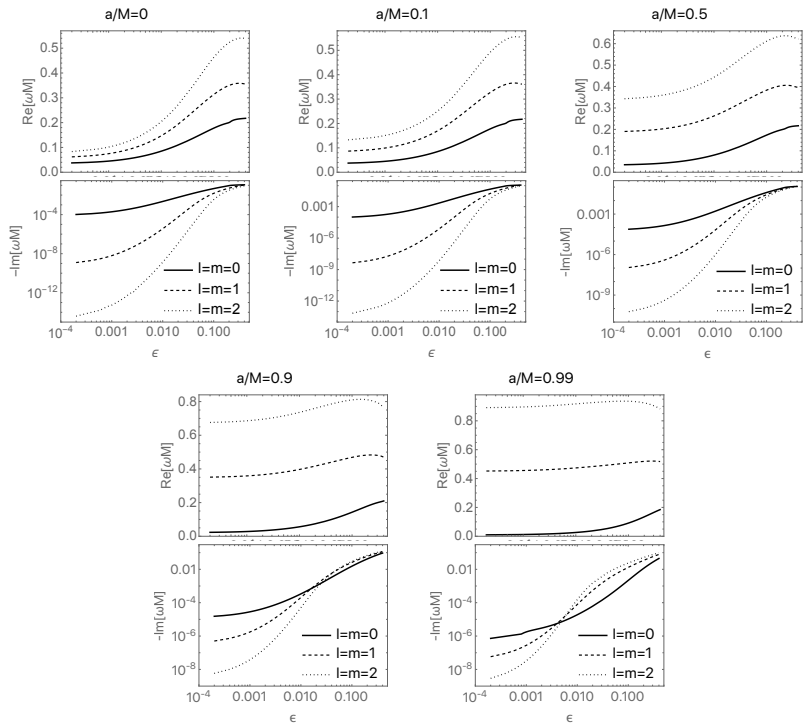

Figure 12: QNMs for rotating wormholes: real (top panels) and imaginary parts (bottom panels) of the QNM frequencies have been plotted as a function of the dimensionless parameter $\epsilon = (\ell/\varrho_+) - 1$, depicting how much the wormhole throat is shifted from the would-be black-hole horizon. We have presented the QNM frequencies for the first few $l = m$ modes, for selected values of the spin parameter.

when changing the spacetime parameters for not-so-close-by configurations, the shooting can jump from the fundamental mode to an overtone, meaning that we had to consider a quite narrow parameters grid. Despite these numerical difficulties, our results clearly show that there are unstable modes for the traversable wormhole configurations.

Our results on the instability timescale are compatible with those in [109], where Kerr-like wormholes are modelled by the Kerr metric with a mirror at finite Boyer–Lindquist radius larger than the would-be horizon.

7.3 SUPERRADIANCE FOR REGULAR BLACK HOLES

The existence of an ergoregion, and the fact that some of its features depend on ℓ, motivate an investigation into the phenomenon of superradiance: bosonic waves propagating on top of a Kerr BH background can get amplified at the expense of the hole's rotational energy. It is reasonable to expect that the same will happen in a black-bounce–Kerr background, though to a different degree — cf. [168]. In what

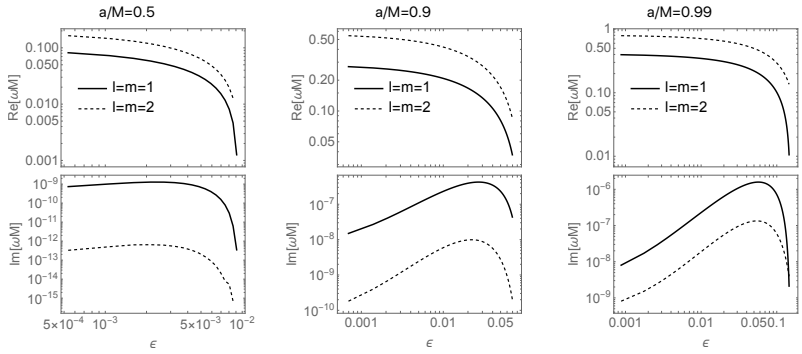

Figure 13: Unstable QNMs for rotating wormholes: real (top panels) and imaginary parts (bottom panels) of the QNM frequencies have been presented as a function of the dimensionless regularisation parameter $\epsilon = (\ell/\varrho_+) - 1$, for the first few unstable $l = m$ modes for selected values of the spin parameter. As evident, the imaginary part of the QNM frequencies are positive, signalling instability.

follows we first build an intuition on the relevant physics by analysing the Penrose process in the vicinity of a black-bounce–Kerr RBH, then compute the spectrum of superradiant amplification, for massless and massive scalar fields and for different values of ℓ.

We do not repeat the same analysis for the wormholes, as these are known to yield no supperadiant amplification according to an argument presented in [224]. To understand why, think of a scattering experiment whereby a monochromatic wave, with amplitude $\mathfrak{I}$, is sent from past null infinity in our universe towards the wormhole: part of the radiation will be reflected and part will be transmitted, will cross the throat and reach the future null infinity in the other universe. Let the amplitudes of the reflected and transmitted waves — as read off at infinity — be $\mathfrak{R}$ and $\mathfrak{T}$, respectively. As a consequence of the equation of motion, one can write the following relation

$$-\mathrm{i}\omega_{\text{our}}(|\mathfrak{I}|^2 - |\mathfrak{R}|^2) = -\mathrm{i}\omega_{\text{other}}|\mathfrak{T}|^2 \tag{194}$$

(the two sides of the equation are nothing but the Wronskian, which is ϱ-independent, computed at infinity in our universe, on the left, and in the other, on the right). Crucially, because of the symmetry of the spacetime the frequency of the wave at infinity in our and in the other universe coincide, $\omega_{\text{our}} = \omega_{\text{other}}$. Hence $|\mathfrak{R}|^2 \leq |\mathfrak{I}|^2$, i. e. superradiant amplification cannot happen. As already mentioned in discussing boundary conditions in subsection 7.1.1, alternative scenarios can be conceived; their exploration however lies beyond the scope of this chapter.

7.3.1 *The Penrose process around regular black holes*

Classical analyses of the *maximal* efficiency of the Penrose process [294] are summarised in [113] — see also [44, 228, 358]. In this framework, one typically considers particles on the equatorial plane and splitting at their turning points, i. e. with vanishing radial velocities; and further notices that the most efficient extraction of energy requires both decay products to be photons. One finds

$$\eta = \frac{E_{\text{output}} - E_{\text{input}}}{E_{\text{input}}} = \frac{1}{2}\left(\sqrt{1+g_{tt}} - 1\right), \tag{195}$$

where g_{tt} must be evaluated at the point of splitting. Hence, the maximal efficiency is achieved for particles splitting at the inner edge of the ergoregion and its value is governed by the magnitude of g_{tt} at that point. (For an extremal Kerr black hole one finds $\eta \approx 20\%$.)

Since in our spacetime the component g_{tt} is the same as in Kerr, we must conclude

$$\eta_{\max} = \frac{1}{2}\left(\sqrt{\frac{2M}{\tilde{\varrho}}} - 1\right) \quad \text{where} \quad \tilde{\varrho} = \max(\varrho_+, \ell); \tag{196}$$

i. e. the maximal efficiency of the Penrose process is completely insensitive to ℓ as long as this is smaller than ϱ_+.

This argument, however, does not provide a complete picture of the energetics of the Penrose process. Indeed, if we aim at using it to gain insight into other processes linked to the ergoregion, we cannot limit our attention to its *maximal* efficiency and the many assumptions that this brings about. In particular, we should consider decays that take place at any point in the ergoregion, not just its inner edge, and — crucially — away from the turning point.

Let us stick to equatorial motion. Take a particle with energy (per unit mass) E and angular momentum (per unit mass) along the rotation axis L_z; let $\mu = 1$ if the particle is massive and $\mu = 0$ if it is massless. Its motion is effectively one-dimensional and governed by

$$\frac{\varrho^2 \dot{\varrho}^2}{\delta} = T \tag{197}$$

where the dot denotes differentiation with respect to an affine parameter along the geodesic and

$$T = \tau_1 E^2 - 2\tau_2 E + \tau_3\,, \tag{198}$$
$$\tau_1 = \varrho^4 + a^2(\varrho^2 + 2M\varrho), \tag{199}$$
$$\tau_2 = 2aML_z\varrho, \tag{200}$$
$$\tau_3 = L_z^2 a^2 - \Delta(\mu^2\varrho^2 + L_z^2)\,. \tag{201}$$

We may write eq. (197) as

$$\tau_1 E^2 - 2\tau_2 E + \tilde{\tau}_3 = 0 \tag{202}$$

with $\tilde{\tau}_3 = \tau_3 - \varrho^2\dot{\varrho}^2/\delta$, which has formally two roots

$$V_\pm = \frac{\tau_2 \pm \sqrt{\tau_2^2 - \tau_1\tilde{\tau}_3}}{\tau_1} = \Omega L_z \pm \sqrt{\Omega^2 L_z^2 - \tilde{\tau}_3/\tau_1}\,; \tag{203}$$

here $\Omega = -g_{t\phi}/g_{\phi\phi}$ is the angular velocity of frame dragging. Actually, only the root V_+ is acceptable, since it must be $E > \Omega L_z$ for the particle's momentum to be future-directed.

Since $\delta \leq 1$, we have that $\tilde{\tau}_3 \leq \tilde{\tau}_3\big|_{\ell=0}$ and therefore $V_+ \geq V_+\big|_{\ell=0}$. Thus, particles moving in this spacetime are generically *more energetic* than their counterparts in Kerr. When in particular $E < 0$, i. e. for Penrose's negative energy states, $|E| \leq |E|\big|_{\ell=0}$: these are "less negative" than their Kerr counterparts, *ceteris paribus*.

We would like to emphasise that the above analysis involving the Penrose process is a warm up exercise, while our main aim is to study superradiance. Our results demonstrate that there are certain quantities associated with the Penrose process, e. g. maximal efficiency, which are independent of the parameter ℓ, while some others, e. g. energy extraction by a particle in radial motion with a fixed angular momentum, predict smaller values, in the same coordinate chart as Kerr. Of course, this is not conclusive and does not exhaust all possible scenarios involving the Penrose process, but is one indication towards less amount of energy being extracted from such RBHs. This prompts us to study the superradiance of the black-bounce–Kerr spacetime in detail.

7.3.2 *Numerical results*

Consider first an incident massless wave with amplitude $\mathfrak{I}$ coming from infinity and producing a reflected wave with amplitude $\mathfrak{R}$. The asymptotic solution to eq. (186) can be written as

$$R \sim \mathfrak{I}\, e^{-\mathrm{i}\omega\varrho}\varrho^{-2\mathrm{i}M\omega-1} + \mathfrak{R}\, e^{\mathrm{i}\omega\varrho}\varrho^{2\mathrm{i}M\omega-1}\,. \tag{204}$$

The black-bounce–Kerr spacetime is asymptotically indistinguishable from the Kerr spacetime, hence the energy fluxes of scalar fields at infinity can be defined by the above asymptotic behaviour exactly as in the Kerr spacetime [328]. In particular, the ingoing and outgoing fluxes are proportional to the modulus of the amplitudes, and we can define a quantity $Z_{0,l,m}$ which gives the amplification or absorption factor for scalar waves with quantum numbers (l, m) off a BH. In this case,

$$Z_{0,l,m} = \frac{\mathrm{d}E_{\text{out}}}{\mathrm{d}E_{\text{in}}} - 1 = \frac{|\mathfrak{R}|^2}{|\mathfrak{I}|^2} - 1\,. \tag{205}$$

In the Kerr spacetime, for massless scalar fields, this quantity can be positive only for frequencies satisfying [77]

$$\omega < m\Omega_{\text{H}}\,, \tag{206}$$

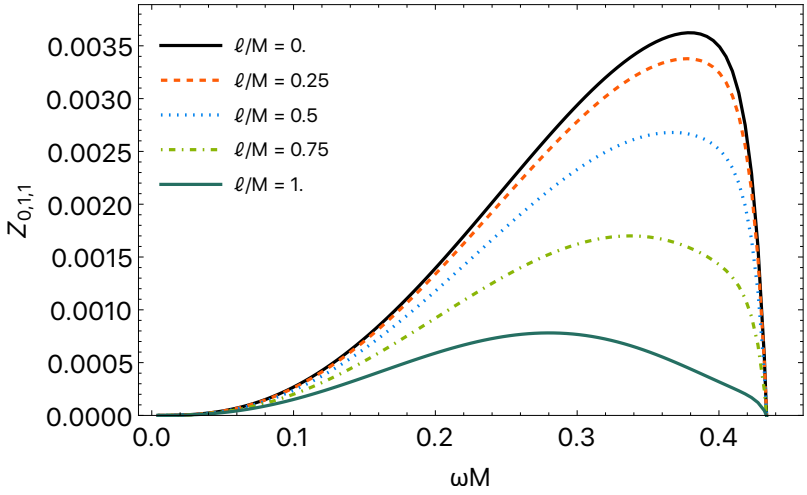

Figure 14: Spectra of the amplification factor for a massless scalar with $l = m = 1$ off a RBH with $a = 0.99M$ for selected values of the regularisation parameter.

where Ω_H is the horizon angular velocity. The same reasoning can be applied to our case yielding an identical result. The angular velocity of the horizon of the RBH in the black-bounce–Kerr scenario, is still given by

$$\Omega_H = \frac{a}{2M\varrho_+}, \tag{207}$$

as in Kerr. Thus, we expect the superradiant interval not to depend on ℓ.

For generic values of the frequency, the angular and radial equation must be integrated numerically. For each couple (l, m) and value of $a\omega$ we first compute the angular eigenvalue and then we integrate the radial equation for a fixed value of ℓ from the horizon with ingoing boundary conditions until a sufficiently large radius. Our numerical solution is compared to the expansion in eq. (204) to extract the amplitudes and finally determine the amplification factor $Z_{0,l,m}$. To increase the accuracy of these computations, we have used a higher-order expansion near the horizon and at infinity.

To obtain a spectrum of the amplification factor, we repeat the routine for several values of ω for different values of the BH parameters and the scalar field quantum numbers. An example of our results is shown in figure 14 for an $l = m = 1$ scalar wave scattered off a highly spinning BH with $a/M = 0.99$ and selected values of the regularisation parameter ℓ.

Similarly to what happens for a Kerr BH, the amplification factor is larger for higher values of the spin parameter and for the minimum allowed value of $l = m$, i. e. $l = m = 1$. Modes with $m \leq 0$ are not superradiant while the phenomenon is less pronounced for other values of (l, m). Figure 14 confirms the general arguments in subsection 7.3.1

on the Penrose process and shows that superradiance is reduced for $\ell \neq 0$ and vanishes for $\ell \to \varrho_+$. Note, incidentally, that this behaviour disproves the intuition according to which the spatial extent of the ergoregion determines the amount of superradiance. Indeed, as shown in section 8.3, both the volume of the ergoregion and the area of the ergosurface actually *increase* with ℓ. We also notice that, although the superradiant threshold frequency does not depend on ℓ, the position and the maximum value of $Z_{0,l,m}$ do. In particular we observe a drift of position of the maximum towards smaller frequencies for larger values of ℓ/M. For values of the frequency larger than the superradiant threshold, the amplification factor approaches rapidly the value -1.

In the non-rotating limit superradiance disappears and our results agree with those of [239] on the scalar absorption cross section.

These results can easily be extended to massive scalar fields. Once the appropriate boundary conditions are taken into account, the numerical procedure is identical. In figure 15 we show spectra of the amplification factor for an $l = m = 1$ scalar wave scattered off a RBH with $a/M = 0.99$ and selected values of the regularisation parameter ℓ and the mass parameter μ. Massive waves can be superradiant in the frequency range $\mu < \omega < m\Omega_{\rm H}$, while they are trapped near the horizon and exponentially suppressed at infinity for $\omega < \mu$. We notice that even in this case superradiance is reduced both for larger values of ℓ/M and μM. Moreover, there could be a degeneracy in the sense that the spectrum of a massive wave off a Kerr BH might look like the spectrum of a massive (but also massless) wave off a RBH with the same spin.

7.4 CHAPTER WRAP-UP

In this chapter we have studied and analysed some phenomenological aspects of scalar test-field perturbations on top of the black-bounce–Kerr spacetime.

First, we have computed the QNMs for massless perturbations. For the RBH spacetime, we have used both the WKB approximation, as well as the direct integration of the scalar perturbation equation. Our analysis demonstrates that there is a deviation of the QNM spectrum from that of Kerr BHs due to the non-zero value of the regularisation parameter ℓ. Wormholes with a null throat (which coincides with the horizon) phenomenologically behave as BHs and their QNMs are in continuity with those of RBHs. On the other hand, the presence of the throat for traversable wormholes modifies the boundary conditions, and hence the QNM spectra. In particular, we have imposed Dirichlet boundary conditions at the throat obtaining QNM frequencies with greatly suppressed imaginary parts as compared to the BH case; in some scenarios, the imaginary parts were found to be positive. This

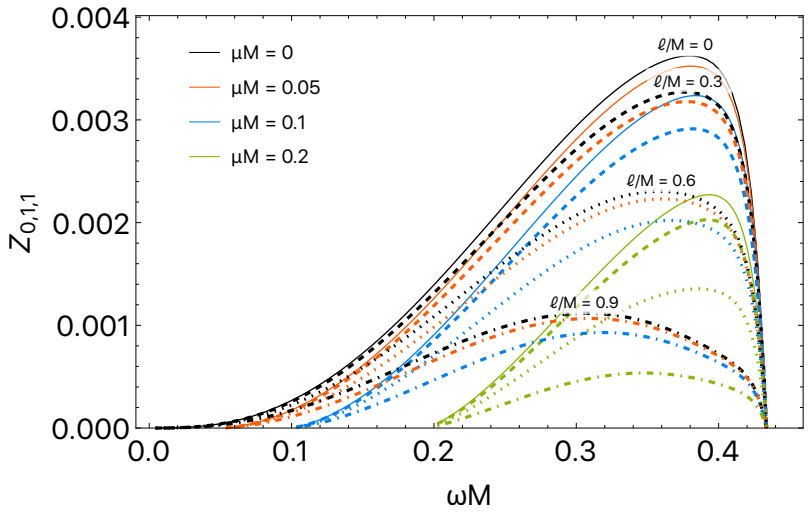

Figure 15: Spectra of the amplification factor for a massive scalar with $l = m = 1$ off a RBH with $a = 0.99M$: different colours distinguish among choices of the mass parameter, while linestyles mark the values of the regularisation parameter (solid $\ell/M = 0$, dashed $\ell/M = 0.3$, dotted $\ell/M = 0.6$, dash–dotted $\ell/M = 0.9$).

seems to indicate that rotating traversable wormholes are unstable to small perturbations. This is somewhat expected for rotating horizonless objects, albeit this instability could be tamed by relaxing the purely reflective conditions at the throat and allowing for partial absorption.

Second, we have studied the phenomenon of superradiance for both massless and massive test scalar fields around rotating RBHs. It turns out that both the Penrose process and superradiance are suppressed by the regularisation parameter ℓ. For example, in the Penrose process, the particles' energies become less negative, compared to their counterparts in Kerr, as ℓ gets larger. Similarly, for superradiance, the amplification of the modes depends on ℓ: the larger ℓ/M the smaller the amplification factor, meaning that ℓ actually stabilises the BH against superradiant instability. In the BH-to-wormhole limit $\ell \to \varrho_+$, the amplification factor gets suppressed and it vanishes for the null-throat wormhole, while in the wormhole branch there cannot be superradiant amplification, at least as long as the wormhole is symmetric and the throat can be modelled by a purely reflective surface. Relaxing these conditions at the throat and allowing for partial absorption, might also resolve the instability of traversable wormholes against small perturbations. Clarifying this issues is however beyond the scope of this thesis.

8

APPENDICES ON BLACK BOUNCES

This chapter gathers a few additional results concerning the black-bounce family of spacetimes. Its purpose is not to further the discussion in any way, but rather to complement what has already been said so far. Indeed, most of these sections' material has appeared as appendices to [165, 166, 270].

8.1 CURVATURES

In the black-bounce–Kerr–Newman spacetime, the Ricci scalar is given by (recall $\varrho = \sqrt{r^2 + \ell^2}$)

$$R = 2\ell^2 \frac{M\left(\Sigma^2 - 2\varrho^4\right) + Q^2\varrho^3 + \varrho^3\left(\Sigma - 2\Delta\right)}{\Sigma^3\varrho^3}\,. \tag{208}$$

It is clearly finite in the limit $r \to 0$, i. e. $\varrho \to \ell$. So are the Kretschmann scalar and the invariants $R^{\mu\nu}R_{\mu\nu}$ and $C^{\mu\nu\rho\sigma}C_{\mu\nu\rho\sigma}$.

In particular, for $Q = 0$, i. e. for the black-bounce–Kerr spacetime, the Kretschmann scalar reads:

$$R^{\mu\nu\lambda\sigma}R_{\mu\nu\lambda\sigma} = \frac{48M^2}{\Sigma^6}\,\mathcal{K}_0 + \frac{16\ell^2 M}{\Sigma^6}\,\mathcal{K}_1 + \frac{4\ell^4}{\varrho^6\Sigma^6}\,\mathcal{K}_2\,, \tag{209}$$

with

$$\mathcal{K}_0 = (\varrho^2 - a^2\chi^2)\left[\left(\varrho^2 + a^2\chi^2\right)^2 - 16a^2\varrho^2\chi^2\right]\,, \tag{210a}$$

$$\begin{aligned}\mathcal{K}_1 = {}& \varrho^3\left[4a^2 + \varrho(2\varrho - 9M)\right] - 2a^2\varrho\chi^2\left[6a^2 + \varrho(4\varrho - 31M)\right] \\ & + a^4\chi^4(6\varrho - 41M)\,,\end{aligned} \tag{210b}$$

$$\begin{aligned}\mathcal{K}_2 = {}& \varrho^6\left[2a^2\varrho(2\varrho - 11M) + 4a^4 + \varrho^2\left(33M^2 - 16M\varrho + 3\varrho^2\right)\right] \\ & + 2a^2\varrho^5\chi^2\left[2a^2(5M - \varrho) - 26M^2\varrho + 5M\varrho^2 + \varrho^3\right] \\ & + 2a^6M\varrho^2\chi^6(6M - \varrho) + a^4\varrho^3\chi^4\big[2a^2M + \\ & \varrho\left(34M^2 - 16M\varrho + 3\varrho^2\right)\big] + a^8M^2\chi^8\,,\end{aligned} \tag{210c}$$

The only potentially dangerous behaviour arises from the denominators, which, in the $r \to 0$ limit, take the form

$$\frac{1}{\ell^2(\ell^2 + a^2\cos^2\theta)^6}\,. \tag{211}$$

As long as $\ell \neq 0$, therefore, these quantities are never infinite.

Using the tetrad eq. (125), the components of the Einstein tensor are

$$G_{\hat{t}\hat{t}} = \operatorname{sign}\Delta\left\{\frac{\ell^2\left[2M\left(\varrho^2-\Sigma\right)+\varrho\left(\Sigma-2\Delta\right)\right]}{\Sigma^3\varrho} + \frac{Q^2\varrho\left(\Sigma-\ell^2\right)}{\Sigma^3\varrho}\right\}, \tag{212a}$$

$$G_{\hat{r}\hat{r}} = -\operatorname{sign}\Delta\left\{\frac{\ell^2\left[2M\left(\varrho^2-\Sigma\right)+\Sigma\varrho\right]}{\Sigma^3\varrho} + \frac{Q^2\varrho\left(\Sigma-\ell^2\right)}{\Sigma^3\varrho}\right\}, \tag{212b}$$

$$G_{\hat{\theta}\hat{\theta}} = \frac{\ell^2\left[M\left(-\Sigma^2-2\Sigma\varrho^2+2\varrho^4\right)+\Sigma\varrho^3\right]}{\Sigma^3\varrho^3} + \frac{Q^2\varrho^3\left(\Sigma-\ell^2\right)}{\Sigma^3\varrho^3}, \tag{212c}$$

$$G_{\hat{\phi}\hat{\phi}} = \frac{\ell^2\left[M\left(-\Sigma^2-2\Sigma\varrho^2+6\varrho^4\right)+\varrho^3\left(2\Delta-\Sigma\right)\right]}{\Sigma^3\varrho^3} + \frac{Q^2\varrho^3\left(\Sigma-3\ell^2\right)}{\Sigma^3\varrho^3}. \tag{212d}$$

We note that

$$G_{\hat{t}\hat{t}} + G_{\hat{r}\hat{r}} = -\operatorname{sign}\Delta\,\frac{2\ell^2\Delta}{\Sigma^3} \tag{213}$$

which is well-behaved at $\Delta = 0$.

The Ricci tensor is clearly diagonal in this tetrad, too:

$$R_{\hat{t}\hat{t}} = \operatorname{sign}\Delta\frac{M\ell^2\left(-\Sigma^2-2\Sigma\varrho^2+4\varrho^4\right)+Q^2\varrho^3\left(\Sigma-2\ell^2\right)}{\Sigma^3\varrho^3}, \tag{214a}$$

$$R_{\hat{r}\hat{r}} = \operatorname{sign}\Delta\left\{\frac{\ell^2\left(M\left(\Sigma^2+2\Sigma\varrho^2-4\varrho^4\right)-2\Delta\varrho^3\right)+Q^2\varrho^3\left(2\ell^2-\Sigma\right)}{\Sigma^3\varrho^3} + \frac{Q^2\varrho^3\left(2\ell^2-\Sigma\right)}{\Sigma^3\varrho^3}\right\}, \tag{214b}$$

$$R_{\hat{\theta}\hat{\theta}} = \frac{Q^2}{\Sigma^2} - \frac{2\ell^2}{\Sigma^3}\left[\Delta+\frac{\Sigma(M-\varrho)}{\varrho}\right], \tag{214c}$$

$$R_{\hat{\phi}\hat{\phi}} = \frac{2M\ell^2\left(2\varrho^2-\Sigma\right)+Q^2\varrho\left(\Sigma-2\ell^2\right)}{\Sigma^3 z}. \tag{214d}$$

Similarly, we note that

$$R_{\hat{t}\hat{t}} + R_{\hat{r}\hat{r}} = -\operatorname{sign}\Delta\,\frac{2\ell^2\Delta}{\Sigma^3} \tag{215}$$

which is well-behaved at $\Delta = 0$.

From these expressions one immediately notices that the curvature tensors are rational polynomials in the variable $\varrho = \sqrt{r^2 + \ell^2}$, which is strictly positive, and their denominators never vanish. The same is true for the Riemann and Weyl tensors; we thus conclude that the spacetime is free of curvature singularities.

A notable corollary to the previous remark is that the throat $r = 0$ is an extremum point — a local maximum or minimum — for the components of the curvatures, as wall as for the scalars constructed with them. Clearly, this is a consequence of the symmetry of the metric under the parity transformation $r \mapsto -r$.

8.2 A NOTE ON GEODESICS

We focus on the black-bounce–Kerr spacetime, but everything can be translated to the black-bounce–Kerr–Newman case in a straightforward manner. Geodesics can be described in terms of the Hamilton–Jacobi method [113, 169], whereby the equations of motion descend from

$$\frac{\partial S}{\partial \tau} = -\frac{1}{2}\, g^{\mu\nu} \frac{\partial S}{\partial x^\mu} \frac{\partial S}{\partial x^\nu}\,, \tag{216}$$

with S the action and τ an affine parameter along the geodesic. Separability, foretold in subsection 5.2.4, motivates the Ansatz

$$S = \frac{1}{2}\,\mu^2 \tau - Et + L_z \phi + S_r(r) + S_\theta(\theta)\,; \tag{217}$$

here μ^2, E and L_z are arbitrary constants: $\mu^2 = 0$ for null geodesics and $+1$ for timelike geodesics; the other two can be interpreted as the energy (per unit mass) and the projection of the angular momentum (per unit mass) along the rotation axis, respectively.

Inserting Ansatz eq. (217) in eq. (216), one obtains relations among the functions $t(\tau)$, $r(\tau)$, $\theta(\tau)$ and $\phi(\tau)$; and, differentiating with respect to τ, the following system of first-order, ordinary differential equations:

$$\Sigma \frac{\mathrm{d}t}{\mathrm{d}\tau} = a(L_z - aE\sin^2\theta) + \frac{\varrho^2 + a^2}{\Delta}[E(\varrho^2 + a^2) - L_z a]\,, \tag{218a}$$

$$\Sigma \frac{\mathrm{d}r}{\mathrm{d}\tau} = \pm\sqrt{\mathcal{R}}\,, \tag{218b}$$

$$\Sigma \frac{\mathrm{d}\theta}{\mathrm{d}\tau} = \pm\sqrt{\Theta}\,, \tag{218c}$$

$$\Sigma \frac{\mathrm{d}\phi}{\mathrm{d}\tau} = \frac{L_z}{\sin^2\theta} - aE + \frac{a}{\Delta}[E(\varrho^2 + a^2) - L_z a]\,, \tag{218d}$$

where

$$\mathcal{R} = [E(\varrho^2 + a^2) - L_z a]^2 - \Delta[\mu^2 \varrho^2 + (L_z - aE)^2 + \mathcal{Q}], \tag{219}$$

$$\Theta = \mathcal{Q} - \cos^2\theta \left[a^2(\mu^2 - E^2) + \frac{L_z^2}{\sin^2\theta}\right], \tag{220}$$

Here $\mathcal{Q}$ is the Carter constant already hinted to in subsection 5.3.1. Its existence derives from the Killing tensor eq. (88) via the constant

$$\mathcal{K} = K_{\mu\nu}\frac{\mathrm{d}x^\mu}{\mathrm{d}\tau}\frac{\mathrm{d}x^\nu}{\mathrm{d}\tau}\,, \tag{221}$$

as $\mathcal{Q} = \mathcal{K} - (aE - L_z)^2$. Its expression in this spacetime coincides with its Kerr homonym's:

$$\mathcal{Q} = u_\theta^2 + \cos^2\theta\left[a^2(1-E)^2 - \frac{L_z}{\sin^2\theta}\right]. \tag{222}$$

Note that the system (eq. (219)–eq. (220)) looks almost identical to its Kerr analogue: indeed, the right-hand sides are precisely those one would find performing the same analysis in a Kerr spacetime, charted by the Boyer–Lindquist coordinates $(t,\ \varrho,\ \theta,\ \phi)$.

Hence, one might expect that our metric and Kerr's share the same geodesics. Namely, given a Kerr geodesic $\big(t(\tau),\ \varrho(\tau),\ \theta(\tau),\ \phi(\tau)\big)$, one could guess that the curve $\big(t(\tau),\ r(\tau) = \sqrt{\varrho(\tau)^2 - \ell^2},\ \theta(\tau),\ \phi(\tau)\big)$ might be a geodesic of our spacetime (charted by r as Boyer–Lindquist-like radius) — at least as long as $\varrho(\tau) \geq \ell$.

This however is not true, in general. Clearly, the reason is that the relation between r and ϱ is not a mere shift:

$$\frac{\mathrm{d}r}{\mathrm{d}\tau} = \frac{\mathrm{d}\varrho}{\mathrm{d}\tau}\frac{\mathrm{d}r}{\mathrm{d}\varrho} = \frac{\mathrm{d}\varrho}{\mathrm{d}\tau}\frac{\varrho}{r} \tag{223}$$

and therefore

$$\begin{aligned} \Sigma\frac{\mathrm{d}\varrho}{\mathrm{d}\tau} &= \pm\sqrt{\mathcal{R}} \quad \text{(Kerr geodesic)} \\ \not\Rightarrow\ \Sigma\frac{\mathrm{d}r}{\mathrm{d}\tau} &= \pm\sqrt{\mathcal{R}} \quad \text{(rotating SV geodesic).} \end{aligned} \tag{224}$$

Rather, using the Kerr-like coordinate ϱ, test particles in our spacetime feel a distorted effective potential in the radial direction:

$$\Sigma\frac{\mathrm{d}\varrho}{\mathrm{d}\tau} = \pm\sqrt{1 - \frac{\ell^2}{\varrho^2}}\sqrt{\mathcal{R}}\,. \tag{225}$$

Note however that, analogously to what happens in Kerr, circular orbits do exist on the equator $\theta = \pi/2$ with $\mathcal{Q} = 0$ — hence our analysis in subsection 5.4.2 is justified.

8.3 PROPERTIES OF THE ERGOREGION

Superradiance and the ensuing instability are linked to the existence of an ergoregion, i. e. a portion of the spacetime in which the Killing vector associated to time translations — which is timelike at spatial infinity — becomes spacelike. With this appendix, we aim at spelling

out some of its relevant details in Kerr–black-bounce spacetimes. A quick inspection of the metric in eq. (182) allows to identify the ergoregion with the locus of points for which $\Sigma - 2M\varrho \leq 0$. Equality is met at

$$\varrho = \varrho^{\pm}_{\text{erg}}(\theta) = M \pm \sqrt{M^2 - a^2\cos^2\theta}\,. \tag{226}$$

When $a > M$ — a case we usually neglect — there are no horizons and the curves $\varrho^{\pm}_{\text{erg}}(\theta)$, along with the throat $\varrho = \ell$, mark the boundary of the ergoregion; note that for $\ell > 2M$ no ergoregion exists. When instead $a \leq M$, the ergoregion stretches between $\varrho^{+}_{\text{erg}}(\theta)$ and the horizon, if there is one, or the wormhole throat. When $\ell > \varrho_+$, in particular, the ergosurface does not extend to the poles but is limited to polar angles $\theta \in [\theta_*,\ \pi - \theta_*]$, with

$$\theta_* = \arccos\left(\frac{\sqrt{\ell(2M-\ell)}}{a}\right); \tag{227}$$

i. e. it is a solid of revolution whose section is shaped as a crescent and whose axis coincides with the axis of symmetry of the spacetime. At any given time, the area of the ergosurface is given by the integral [293]

$$A_{\text{erg}} = \int \mathrm{d}\theta\,\mathrm{d}\phi\,\sqrt{\mathscr{A}} \tag{228}$$

where $\phi \in [0, 2\pi]$, $\theta \in [0, \pi]$ or $\theta \in [\theta_*, \pi - \theta_*]$ when $\ell > \varrho_+$ and $\mathscr{A}$ is the determinant of the two-dimensional induced metric. Specifically, we have

$$\begin{aligned}\mathscr{A} &= \left[g_{\varrho\varrho}\left(\frac{\mathrm{d}\varrho_{\text{erg}}}{\mathrm{d}\theta}\right)^2 + g_{\theta\theta}\right] g_{\phi\phi} \\ &= \Sigma\left[1 + \frac{a^2\cos^2\theta}{\delta(\varrho^2_{\text{erg}} - M^2)}\right] 2\sin^2\theta\left(M\varrho_{\text{erg}} + a^2\sin^2\theta\right),\end{aligned} \tag{229}$$

which should be evaluated at $\varrho = \varrho_{\text{erg}}$.

Since $\delta \leq 1$, as long as $\ell < \varrho_+$, we expect $A_{\text{erg}} \geq A_{\text{erg}}\big|_{\ell=0}$, i. e. that the area be larger than its Kerr analogue; for $\ell > \varrho_+$, instead, A_{erg} is a continuously decreasing function of ℓ that reaches zero for $\ell = 2M$. Note, incidentally, that surfaces of constant ϱ, such as the horizon, have the same area in our spacetime as they have in Kerr: the ℓ-dependence comes in as soon as different radii are spanned.

The volume of a constant-t slice of the ergoregion is given by

$$V_{\text{erg}} = \int \mathrm{d}\varrho\,\mathrm{d}\theta\,\mathrm{d}\phi\,\sqrt{h} \tag{230}$$

where $\varrho \in \left[\max(\varrho_+, \ell), \varrho_{\text{erg}}\right]$, $\theta \in [0, \pi]$ when $\ell \leq \varrho_+$ or $\theta \in [\theta_*, \pi - \theta_*]$ otherwise, and $\phi \in [0, 2\pi]$. We have

$$h = g_{\varrho\varrho}g_{\theta\theta}g_{\phi\phi} = \frac{\Sigma A\sin^2\theta}{\Delta\delta}\,. \tag{231}$$

The integrand in eq. (230) has poles at $\varrho = \varrho_+$ and $\varrho = \ell$, i.e. along the inner edge of the ergoregion. The integral itself is usually convergent, unless $\ell = \varrho_+$: in this case the two poles coincide and the integral diverges logarithmically. Something analogous happens for extremal Kerr BHs, see [292]. In any case, since $\delta \leq 1$, the volume of the ergoregion will be larger than that of the corresponding Kerr as long as $\ell < \varrho_+$; for larger values of ℓ, instead, the volume will strictly decrease and reach zero for $\ell = 2M$.

The fact that both the area of the ergosurface and the volume of the ergoregion increase with increasing ℓ, while superradiant amplification gets tamed (cf. section 7.3), disproves the intuitive notion that a larger ergoregion entails "more superradiance". A better understanding of the physics of this phenomenon is provided by the analysis of the Penrose process in the equatorial plane given in subsection 7.3.1.

8.4 SINGULARITIES OF THE RADIAL EQUATION FOR SCALARS

In this appendix, we elucidate some subtleties concerning the behaviour of the solution to the radial eq. (186) close to its singular points. (Note: in this subsection, as in chapter 7, the symbol R denotes the radial wavefunction of a test scalar field, not the Ricci scalar.) First of all, write eq. (186) in canonical form:

$$R'' + \alpha(\varrho) R' + \beta(\varrho) R = 0\,, \tag{232}$$

where

$$\alpha(\varrho) = \frac{\left(\sqrt{\delta}\Delta\right)'}{\sqrt{\delta}\Delta}\,, \tag{233}$$

$$\beta(\varrho) = \frac{1}{\delta\Delta^2}\left(\frac{\left[\left(\varrho^2 + a^2\right)\omega - am\right]^2}{\Delta} - \lambda - \mu^2\varrho^2\right)\,. \tag{234}$$

Note that

$$\alpha(\varrho) = \frac{1}{2}\left[\frac{1}{\varrho+\ell} + \frac{1}{\varrho-\ell}\right] - \frac{1}{\varrho} + \frac{1}{\varrho-\varrho_+} + \frac{1}{\varrho-\varrho_-}\,. \tag{235}$$

The poles of the coefficients α and β are singular points for the differential equation. Following standard terminology [53], we call *irregular* those singular points where $\alpha(\varrho)$ or $\beta(\varrho)$ have a pole of order higher than one or two, respectively, and *regular* the singular points where the divergences of $\alpha(\varrho)$ and $\beta(\varrho)$ are less severe. According to this convention, we find

- regular singular points at $\varrho = \varrho_+,\ \varrho_-,\ 0,\ +\ell$ (and $-\ell$, technically) when $\ell \neq \varrho_\pm$, and
- an irregular singular point at $\varrho = \infty$.

As $\ell \to 0$, the three poles of α located at $\varrho = \pm\ell,\ 0$ exactly cancel each other out and the two poles $\varrho = \pm\ell$ in β also disappear; the resulting equation (second-order ordinary differential equation with two regular and one irregular singular points) is of the confluent Heun type. The "confluent" case in which $\ell = \varrho_\pm$ is particularly nasty, as two regular singular points merge into an irregular singular point.

Using the throat-penetrating coordinate r instead of the Johannsen coordinate ϱ does not change the picture: δ disappears from the equation but Δ is not a polynomial of degree two and its zeroes have a more complicated structure.

In the vicinity of a regular singular point ϱ_0, the equation admits a (possibly divergent) power-series solution of the form (Frobenius' method)

$$R(\varrho) = (\varrho - \varrho_0)^s \sum_{n\in\mathbb{N}} a_n (\varrho - \varrho_0)^n \tag{236}$$

with s satisfying the *indicial equation*

$$s(s-1) + \alpha_0 s + \beta_0 = 0\,; \tag{237}$$

here

$$\alpha_0 = \lim_{\varrho\to\varrho_0} (\varrho - \varrho_0)\alpha(\varrho) \quad \text{and} \quad \beta_0 = \lim_{\varrho\to\varrho_0} (\varrho - \varrho_0)^2 \beta(\varrho)\,. \tag{238}$$

Close to $\varrho = \varrho_+$, we have $s = \pm\mathrm{i}\frac{am - 2M\omega\varrho_+}{(\varrho_+ - \varrho_-)\gamma}$, hence eq. (189). Similarly, close to $\varrho = \ell$, we find $s = 0,\ 1/2$, although $s = 0$ must be excluded since it does not give rise to a solution.

Close to an irregular singular point, one can construct a generalisation of Frobenius' series. The solution will consist of an exponential prefactor, encoding the leading divergent behaviour, and a power series in the variable $(\varrho - \varrho_0)^c$, with c some number. Proceeding in this way, one can recover the standard result of eq. (187). More interestingly, in the particular case $\ell = \varrho_+$, close to $\varrho = \ell$ the solution turns out to be

$$R(\varrho) = \exp\left(\pm\mathrm{i}\frac{am - 2M\omega\varrho_+}{\varrho_+ - \varrho_-}\sqrt{\frac{2\ell}{\varrho - \ell}}\right) \sum_{n\in\mathbb{N}} a_n (\varrho - \ell)^{n/2}\,, \tag{239}$$

(hence, in particular, $c = 1/2$). Such behaviour renders the numerical integration of the null-throat wormhole case particularly difficult.

9 INTERLUDE: MASS INFLATION INSTABILITY

The discussion of chapter 7 represents an example of stability analysis: by studying the dynamics of test perturbations, we found that they decay in time when the background is a BH, but we also found evidence for exponentially growing modes when the background is a rapidly rotating wormhole.

Technically, the computations of chapter 7 are specific to the black-bounce–Kerr metric and the results do not necessarily carry over to other spacetimes. Yet, if we understand the physical origin of a given behaviour, stable or unstable, we might be able to formulate general arguments with reasonable confidence. For instance, we have argued that the unstable behaviour of rotating wormhole is most likely due to the existence of an ergoregion and the concomitant lack of an horizon; and for this reason it is probably general to all geometries that share the same features.

Clearly, in order to prove this statement quantitatively one would have to repeat the same computations for virtually all conceivable models — an impossible and uninteresting task. When dealing with instabilities, however, the qualitative argument is sufficient and, being more general, it is also more interesting.

The *mass inflation instability*, to which this chapter is devoted, involves a similar kind of reasoning. It is a phenomenon related to the infinite blueshift experienced by matter perturbations at an inner BH horizon: since all simply connected RBHs have an inner horizon, they are all generically plagued by this instability. The quantitative details of such phenomenon depend on the model, but the qualitative character of the instability does not. (See also [101] for possible phenomenological consequences of this phenomenon.)

The goal of this chapter — which is slightly off the thesis's main line of reasoning — is to discuss how the instability related to mass inflation could be quenched. We will do so by constructing a rotating model of a RBH whose inner horizon has been appropriately engineered. The resulting "inner-extremal" RBH is admittedly somewhat artificial, and it should be considered as a proof of concept that models of RBHs without mass inflation are in principle viable.

We will start by recalling some basic notions on mass inflation in section 9.1, then discuss a "new" strategy for regularising the singularity (section 9.2) — slightly different from those presented in chapter 3. Section 9.3 explains how the properties of the inner horizon can be trimmed; the metric of our "inner-extremal" RBH is reported in eq. (270). Finally, section 9.4 analyses and describes the spacetime.

9.1 PRELIMINARIES

The term mass inflation refers to the unbounded growth of the mass due to the presence of perturbations at an inner horizon. Computations are often carried out in either of two simplified models: the "double-shell" model due to Poisson and Israel [296] and a variant due to Ori [291].

In the double-shell scenario, perturbations to a spherically symmetric background geometry are modelled as two null shells, one ingoing and the other outgoing. The two shells cross at some point, where one imposes junction conditions on the components of the metric to ensure their continuity. Such junction conditions, together with an assumption on the late-time behaviour of the ingoing shell (e. g. that they satisfy Price's law), suffice to prove that the Misner–Sharp mass in the region between the two shells blows up as the crossing point approaches an inner horizon. Such divergence, which percolates to the curvatures, is exponential and its timescale is set by the inner horizon's surface gravity.

In the Ori model, the ingoing null shell is replaced by a somewhat more realistic continuous influx of null dust. The analysis is similar and leads to analogous results. Hence, it is generally believed that, in GR, the backreaction of the perturbations onto the geometry makes the inner horizon shrink all the way to $r = 0$.

Both models were devised to investigate the stability of Reissner–Nordström's inner horizon, but they apply equally well to RBHs with inner horizons. As we have said multiple times, all simply connected RBHs fall in this class and are therefore potentially unstable.

Some authors [71] have claimed that *some* RBHs exhibit a divergence that is not exponential but merely polynomial — hence much milder; this seems to be even more true when one takes into account Hawking evaporation [72, 73]. Other authors have repeatedly pointed out that, although the divergence might look polynomial at late times, it is always preceded by a phase in which it proceeds exponentially [94, 95, 141].

It is beyond the scope of this thesis to delve deeper into this debate; the present author's take is that, very likely, simply connected RBHs cannot be considered stable end states of gravitational collapse; at most, they could be approximations valid in an intermediate (likely short) stage of a process that is truly dynamical. This is in accord, by the way, we the discussion of subsection 2.2.1.

Moreover, the classical mechanism described herein has a semiclassical counterpart that seems to be leading to drastically different conclusions [41, 42]. Indeed, when accounting for the backreaction of quantum perturbations onto the geometry, the inner horizon appears to be pushed outwards. Hence, the fate of perturbed inner horizons is far from clear.

The fact that the timescale of the mass inflation instability is set by the inner horizon's surface gravity suggests a possible way by which the instability could be quenched: if the surface gravity happens to be very small, the instability will correspondingly take longer to develop. If the surface gravity is exactly zero, the instability is absent — at least when analysed through the two models mentioned above.

Ideally, one would like to turn off the inner horizon's surface gravity without disrupting the outer horizon's properties: namely, its surface gravity should remain non-zero and the two horizons should remain separate. That is, one would like to consider situations different from an extremal BH.

In spherical symmetry a RBH model that achieves this goal can easily be constructed. The issues is thoroughly discussed in [96], which also reports the computations that show the absence of mass inflation.

Extending the result to include rotation, using a Gürses–Gürsey metric, is not quite trivial — at least if one insists in keeping $m(r) \propto r^3$ close to the centre. Moreover, these metrics suffer from the issues that we have detailed in section 4.3.

The metrics that result from the application of the MNJP, instead, have a particularly suggestive form. We remind the reader that the MNJP yields a metric that is Kerr-like — and in particular it can be written as a Gürses–Gürsey metric —, up to a free multiplicative function $\Psi(r,\theta)$:

$$ds^2 = \frac{\Psi}{\Sigma}\, ds^2_{\text{GG}}\,. \tag{240}$$

Ψ can be, and usually is, constrained by some physical arguments. In particular, if the seed metric can be interpreted as a solution of some non-linear electrodynamics, the field equations imply $\Psi = \Sigma$. Moreover, within the Newman–Janis framework, in the $a \to 0$ limit, the line element eq. (240) must reduce to the seed metric — that is, $\lim_{a\to 0} \Psi(r,\theta) = r^2$. The choice $\Psi = \Sigma$ thus seems the most natural, but it entails all the issues we discussed.

On the other hand, a large body of work in the context of conformal gravity (e. g. [32, 89, 216, 283]) has shown that appropriate choices for the conformal factor can lead to geodesically complete spacetimes. In light of this fact, eq. (240) looks particularly promising, as it encodes a significantly larger amount of freedom than the Gürses–Gürsey metric eq. (68). In particular, when $\Psi/\Sigma \neq 1$ it becomes possible to disentangle the regularisation of the central singularity from the choice of $m(r)$, which instead determines the location and properties of the horizons.

In this chapter, we will show how one can exploit such freedom to build a RBH that is free from mass inflation, and from all the issues of section 4.3. In our proposal, Ψ will be used to improve the appearances of the spacetime close to $r = 0$, while $m(r)$ will be chosen so as to trim the properties of the inner horizon.

Note, incidentally, that adding a conformal factor to eq. (68) is by no means disruptive: the spacetime described by the metric eq. (240) is of Petrov type D, exactly as eq. (68), with double null directions given by

$$l^\mu = \sqrt{\frac{\Sigma}{\Psi}}\frac{1}{\Delta}\left(r^2+a^2, \Delta, 0, a\right),$$
$$n^\mu = \sqrt{\frac{\Sigma}{\Psi}}\frac{1}{\Delta}\left(r^2+a^2, -\Delta, 0, a\right); \tag{241}$$

these two null vectors can be complemented with

$$m^\mu = \sqrt{\frac{\Sigma}{\Psi}}\frac{1}{\sqrt{2}\,(r+\mathrm{i}a\cos\theta)}\left(\mathrm{i}a\sin\theta, 0, 1, \mathrm{i}\csc\theta\right) \tag{242}$$

and its complex conjugate $\bar{m}^\mu$ to form a Kinnersley-like tetrad. When $\Psi(r,\theta) = \psi_r(r) + \psi_\theta(\theta)$ (i. e. it is "separable"), the geometry admits the non-trivial Killing tensor

$$K_{\mu\nu} = \Psi(r,\theta)\left[l_\mu n_\nu + l_\nu n_\mu\right] + \psi_r(r) g_{\mu\nu}\,. \tag{243}$$

In this case, the equations of motion for a test particle of Killing energy per unit mass E and Killing angular momentum along the axis of rotation per unit mass L are

$$\dot{t} = \frac{1}{\Psi\Delta}\left[AE - 2m(r)arL\right], \tag{244}$$
$$\dot{\phi} = \frac{1}{\Psi\Delta}\left[\frac{L}{\sin^2\theta}\left(\Sigma - 2m(r)r\right) + 2m(r)arE\right], \tag{245}$$
$$\Psi^2\dot{r}^2 = \left[(r^2+a^2)E - aL\right]^2 - \Delta\left(\mu\psi_r + K\right), \tag{246}$$
$$\begin{aligned}\Psi^2\dot{\theta}^2 &= K - \mu\psi_\theta - \left(aE\sin\theta - \frac{L}{\sin\theta}\right)^2 \\ &= Q + \cos^2\theta\left(E^2a^2 - \frac{L^2}{\sin^2\theta}\right) - \mu\psi_\theta\,,\end{aligned} \tag{247}$$

where $\mu = 0$ for massless particles and $\mu = 1$ for massive ones, while K is the conserved quantity associated to the Killing tensor of eq. (243), $K = K_{\mu\nu}\dot{x}^\mu\dot{x}^\nu$, and $Q = K - (Ea - L)^2$. Clearly, planar equatorial orbits are possible only if $\psi_\theta(\pi/2) = 0$.

In the more general case in which Ψ is not separable, the equations of motion are more involved and not separable. Motion with $\ddot{\theta} = \dot{\theta} = 0$ can take place on the equator and on the axis of symmetry if $\partial_\theta\Psi = 0$ there. Note that, if Ψ is a function of Σ only, this is always the case, since $\partial_\theta\Psi = \Psi'\partial_\theta\Sigma = 2a^2\cos\theta\sin\theta\Psi'$.

9.2 REGULARISING THE SINGULARITY WITH Ψ

In this section we discuss how the function Ψ can regularise the spacetime, regardless of the specific choice of $m(r)$. We assume such Ψ

will satisfy a very minimal set of requirements, namely: $\Psi(r,\theta) > 0$ everywhere, in order to ensure that no additional singularities are introduced; and

$$\frac{\Psi}{\Sigma} = 1 + \mathcal{O}\left(\frac{1}{r^2}\right) \quad \text{as} \quad r \to \infty\,, \tag{248}$$

so that the spacetime ADM mass and specific angular momentum are still given by the parameters $M = \lim_{r\to\infty} m(r)$ and a, respectively — this is tantamount to a slightly stricter version of the usual asymptotic flatness condition. (Note, in particular, that we do not follow the physical interpretation of [21–23] and hence we do not impose the partial differential equations that descend from that reasoning.)

Let us now look for a Ψ that regularises the singularity of the Kerr BH, i. e. one for which

$$ds^2 = \frac{\Psi}{\Sigma}\, ds^2_{\text{Kerr}} \tag{249}$$

is the line element of a spacetime free of scalar polynomial curvature singularities. The same Ψ will also regularise more general metrics characterised by a generic (analytic) $m(r)$. As will become clear momentarily, the function Ψ can also "remove" regions of the spacetime with undesirable features.

A simple example of such Ψ is

$$\Psi = \Sigma + \frac{b}{r^{2z}}\,, \tag{250}$$

with z a real number, which we will further constrain in a moment, and b a positive constant with dimensions $[M]^{2z+2}$. Note that if $b \to 0$ as $M \to 0$ or as $a \to 0$ one may recover respectively the Minkowski or the Schwarzschild metric. The Ricci scalar has the form

$$R = -\frac{6b\, r^{2z}}{r^2\Sigma^2\left(b + r^{2z}\Sigma\right)^3} P_z\left(r, \cos\theta\right)\,, \tag{251}$$

where $P_z\left(r,\cos\theta\right)$ is an expression (a polynomial in r and $\cos\theta$ when z is an integer) that goes to zero at least as fast as Σ^2 in the limit $r \to 0$, $\theta \to \pi/2$. Hence, the Ricci scalar never blows up for $z \geq 1$. However, $z = 1$ still does not yield a well-defined limit, while for $z > 1$ the limit exists and is zero, irrespective of the path taken to reach the would-be singularity in the r–θ space. Similar remarks hold for the Ricci tensor squared $R^{\mu\nu}R_{\mu\nu}$ and the Kretschmann scalar $R_{\mu\nu\rho\sigma}R^{\mu\nu\rho\sigma}$.

The Ansatz in eq. (250) can be written as $\psi_r(r) + \psi_\theta(\theta)$, i. e. it is "separable" in the terminology introduced at the end of section 9.1, and hence has the advantage of leading to separable equations of motion.

Note that, with $z > 1$, Ψ is divergent on the whole disk $r = 0$ — which will have consequences for closed timelike curves. The fact

that this divergence can in fact cancel the divergences in the curvature scalars is quite remarkable. For these reasons, eq. (250) is the choice we will mostly explore in the remainder of the chapter: in particular, we will often consider the "minimal" choice $z = 3/2$, corresponding to the smallest integer exponent of r that yields a well defined limit.

It is also worth mentioning that, if one focuses on the non-spinning case only, lower values of the exponent z are required. Indeed, in order to regularise the metric

$$ds^2 = \frac{\Psi}{r^2} ds^2_{\text{Schw}} , \tag{252}$$

with the $a \to 0$ limit of eq. (250)

$$\Psi = r^2 + \frac{b}{r^{2z}} , \tag{253}$$

one must have $z \geq 1/2$.

Finally, before moving on, let us add that an interesting alternative to eq. (250) can be represented by the Ansatz

$$\Psi = \Sigma + \frac{b}{\Sigma^z} . \tag{254}$$

In this case it is easy to check that the Ricci scalar tends to zero for $r \to 0$, $\theta \to \pi/2$ for any $z > 1$. The same holds true for the Ricci tensor squared and the Kretschmann scalar, hence eq. (254) seems equivalent to eq. (250). Notably, however, in this second case $z = 1$ too yields a well-defined, and finite, limit

$$\lim_{\Sigma \to 0} R = -\frac{24a^2}{b} \tag{255}$$

and similar results can be found for $R^{\mu\nu}R_{\mu\nu}$ and the Kretschmann.[1] With this choice, Ψ only diverges on the ring $r = 0$, $\theta = \pi/2$, but not on the disk $r = 0$, $\theta \neq \pi/2$. Eq. (254) will be juxtaposed to eq. (250) in subsection 9.2.1 to highlight the properties that make us prefer the latter.

9.2.1 *The spacetime close to $r = 0$*

Although the scalar curvatures we computed are everywhere finite, the components of the metric still diverge for $\Sigma = 0$. Previous works [32] have argued that the resulting spacetime is in fact geodesically complete, since the would-be singularity is reached in infinite proper time. Since our choice of conformal factor is slightly different from that discussed in [32], we sketch the relevant computations below.

Consider first a particle moving on the equatorial plane $\theta = \pi/2$ and falling radially towards $r = 0$. With E and L being the particle

1 To our knowledge, those built with a Ψ are the only examples of rotating RBHs whose curvature scalars are continuous and non-zero at the would-be singularity.

energy and angular momentum per unit mass, its radial velocity satisfies

$$\Psi^2 \dot{r}^2 = \mathcal{R}_{\text{Kerr}} - \mu\Delta(\Psi - r^2)\,. \tag{256}$$

Here $\mu = 0$ or 1 for massless or massive particles respectively, and $\mathcal{R}_{\text{Kerr}}$ is the right-hand side of eq. (246) with $\Psi = \Sigma$. The proper time it takes for the particle to fall from r_0 to r is

$$\Delta\tau = -\int_{r_0}^{r} \frac{\Psi}{\left[\mathcal{R}_{\text{Kerr}} - \mu\Delta(\Psi - \tilde{r}^2)\right]^{1/2}}\,\mathrm{d}\tilde{r}\,. \tag{257}$$

For both our Ansätze (eq. (250) or eq. (254)), one finds that on the equatorial plane $\Psi - r^2 = b\,r^{-2z} > 0$; therefore the infall time for massless particles ($\mu = 0$) is shorter than that for massive particles ($\mu = 1$). (Obviously, this is true as long as $\mathcal{R}_{\text{Kerr}} - \mu\Delta(\Psi - r^2) > 0$, i. e. only where the trajectory is classically allowed: where the condition is not met, such motion cannot take place.)

Let us then focus on massless particles. At $r = 0$, $\mathcal{R}_{\text{Kerr}} = a^2(Ea - L)^2$, while Ψ diverges at least as fast as $1/r^2$. We conclude that massless particles reach the would-be singularity in an infinite amount of proper time. Given the inequality above, the conclusion remains true for massive particles.

Next, consider a particle that falls along the axis of symmetry $\theta = 0$. Such particle could reach the disk $r = 0$ without encountering the would-be singularity, and potentially cross it through its centre. On-axis motion requires $L = 0$, so the radial velocity now satisfies

$$\Psi^2 \dot{r}^2 = -\mu\Psi\Delta + E^2(r^2 + a^2)^2 \tag{258}$$

where Ψ is now evaluated at $\theta = 0$. The infall proper time becomes in this case

$$\Delta\tau = -\int_{r_0}^{r} \frac{\Psi}{\sqrt{\left(\tilde{r}^2 + a^2\right)^2 E^2 - \mu\Delta\Psi}}\,\mathrm{d}\tilde{r}\,. \tag{259}$$

First of all, we can see that it is still true that massless particles fall in a shorter time than massive ones, therefore we again focus on the former. We have

$$E\Delta\tau_{\text{light}} = -\int \frac{\Psi}{r^2 + a^2}\,\mathrm{d}r \tag{260}$$

and with our Ansatz we have

$$\frac{\Psi}{r^2 + a^2} = 1 + b \begin{cases} (r^2 + a^2)^{-1} r^{-2z} & \text{for eq. (250)} \\ (r^2 + a^2)^{-(z+1)} & \text{for eq. (254).} \end{cases} \tag{261}$$

In the first case, the integrand diverges faster than r^{-2} as $r \to 0$, hence the particle will reach the would-be singularity in an infinite

time. In the second case, instead, the integrand is everywhere finite. For massive particles, one can show that the infall time remains finite in the second case but, according to the inequality above, it is infinite in the first.

Therefore, the two choices of Ψ lead to a very different structure of the region close to the would-be singularity: in the first case, the whole disk $r = 0$ is (regularised and) "sent to infinity"; in the second case, only the ring $r = 0$, $\theta = \pi/2$ is pushed away, so that particles can still cross the disk inside the ring. This is a non-negligible difference as in the case of Ansatz eq. (250) we end up precluding, to light or matter, access to that region of the Kerr geometry ($r < 0$) characterised by the presence of close timelike curves.

Let us stress that while usually such a region is taken to be non-physical in the Kerr geometry, due to the fact that it is shielded by a Cauchy horizon which is widely (albeit non-unanimously) considered unstable, the same region would represent a problem for us once we shall have proceeded to stabilise the RBH inner horizon. It is henceforth even more pressing for a stable RBH to choose an Ansatz such as eq. (250) over one like eq. (254).

9.3 STABILISING THE INNER HORIZON WITH $m(r)$

As shown in [96], the mass inflation instability can be turned off if the surface gravity of the inner horizon κ_- is made to vanish thanks to a wise choice of the mass function. The problem with extending this idea to the rotating case is that we wish to impose several conditions at the same time. Indeed, we want to: remove the ring singularity; avoid close timelike curves; have a well-defined limit at the would-be singularity; *and* have an inner horizon with vanishing surface gravity. Making all these conditions coexist seems a daunting task. While we do not have a no-go theorem in this sense, it is rather clear to a first investigation that, even if viable, such regular metrics would be too cumbersome for any phenomenological application.

We shall then pursue a different path, hinging on the realisation that if we regularise the singularity with the conformal factor as above, the functional form of $m(r)$ is left with very few constraints (namely it must be everywhere finite and it must reduce to the ADM mass M at infinity), and can be easily shaped so to stabilise the inner horizon.

The surface gravity of the inner horizon r_- depends on the mass function as

$$\kappa_- \propto \partial_r \Delta|_{r=r_-} \,. \tag{262}$$

assuming $m(r)$ is a rational function, the vanishing of κ_- is achieved if the inner horizon is a degenerate root of Δ

$$\Delta = r^2 - 2m(r)r + a^2 = 0 \Rightarrow (r - r_+)(r - r_-)^d = 0 \,, \tag{263}$$

for some $d \in \mathbb{N}_{\geq 2}$. $d = 2$ is not viable, since it implies that $m(r)$ has a pole at some positive r. Thus the minimal choice ends up being $d = 3$ which implies (given also the required asymptotic behaviour) a mass function of the form

$$m(r) = M \frac{r^2 + \alpha r + \beta}{r^2 + \gamma r + \delta} \,. \tag{264}$$

From eq. (263), it can been shown that β cannot be zero and thus the limit of $m(r)$ for $r \to 0$ is not zero but the finite value $M\beta/\delta$. In this form, $m(r)$ is parameterised by four coefficients, two of dimension $[M]$ (α and γ) and two of dimension $[M]^2$ (β and δ). However, through eq. (263), they can all be expressed as functions of the position of the two horizons

$$\alpha = \frac{a^4 + r_-^3 r_+ - 3a^2 r_- (r_- + r_+)}{2a^2 M} \,, \tag{265a}$$

$$\beta = \frac{a^2(2M - 3r_- - r_+) + r_-^2 (r_- + 3r_+)}{2M} \,, \tag{265b}$$

$$\gamma = 2M - 3r_- - r_+ \,, \tag{265c}$$

$$\delta = \frac{r_-^3 r_+}{a^2} \,. \tag{265d}$$

If we choose $r_+ = M + \sqrt{M^2 - a^2}$, i. e. the outer horizon to coincide with its Kerr analogue, our family of metrics can be parameterised in terms of r_- only.

It is quite remarkable, and very relevant for phenomenological studies, that in spite of being located beyond a trapping horizon, the position of the inner horizon can matter for observable in the outside geometry. An example of this can be exposed by looking at the large-r behaviour of the mass function:

$$m(r) \sim M + \frac{M(\alpha - \gamma)}{r} + \mathcal{O}\left(1/r^2\right) \,, \quad (r \to \infty) \,. \tag{266}$$

The second term in the above expansion could be interpreted as an electric charge, and could lead to a different quadrupole moment with respect to a Kerr BH.

The choice $\alpha = \gamma$ must be discarded as it forces the inner horizon to coincide with that of Kerr, and in turn implies a non-zero κ_- (actually the usual one for the Kerr geometry) making the conformal Kerr metric still unstable to mass inflation.

Nonetheless, we can introduce a parameter controlling the difference between the inner-horizon position in our geometry and in Kerr. This parameter will in turn control the difference $\alpha - \gamma$. Let us write then

$$r_- = \frac{a^2}{M + (1 - e)\sqrt{M^2 - a^2}} \,, \tag{267}$$

with $e \neq 0$ and $e < 2$ in order to ensure $0 < r_- < r_+$. Further requiring the mass function to have no poles implies

$$-3 - \frac{3M}{\sqrt{M^2 - a^2}} < e < 2\,, \tag{268}$$

where in the positive (negative) part of the interval r_- is larger (smaller) than the Kerr inner horizon.

With the above choice, it follows that $\alpha - \gamma = \mathcal{O}(e^3)$ — the same holds true for all the other coefficients in the large-r expansion. This suggests that sizeable deviations of r_- from its Kerr value could translate into measurable differences in the value of the quadrupole moment, or in the periastron precession and the orbital frequency in a binary system [309]. Such differences would all be $\mathcal{O}(e^3)$, which entails that values of $|e|$ close to one or smaller might be phenomenologically favoured; but the possible impact of e on astrophysical observables certainly deserves further scrutiny, which we leave for the future.

Let us also note that, with the parametrisation eq. (267), the mass function becomes $m(r) = M + \mathcal{O}(e^3)$ and in particular $m(r_+) = M$. This entails, among other things, that the outer-horizon angular velocity is the same as in Kerr, while its surface gravity is

$$\kappa_+ = \frac{\partial_r \Delta(r_+)}{2(r_+^2 + a^2)} = \kappa_+^{\text{Kerr}} + \mathcal{O}(e^3)\,. \tag{269}$$

Moreover, $e \to 2$ is an extremal limit similar to $a \to M$, since in this limit $r_- \to r_+$ and $\kappa_+ \to 0$.

Of course, choices for r_- different from eq. (267) are in principle possible but they are strongly limited by a series of sanity requirements: the inner horizon must lie within the outer horizon for all values of a; $m(r)$ must go to M asymptotically; the denominator of $m(r)$ must have no zeros (for all $r > 0$), that is $\gamma^2 < 4\delta$; all the coefficients of $m(r)$ must be finite for all values of a; the extremal limit $a \to M$ should remain thermodynamically unattainable and thus also the surface gravity of r_+ should become zero in this limit — indeed this is possible only if $r_- \to r_+$ for $a \to M$.

In conclusion, the complete form of our rotating "inner-degenerate" metric is

$$\begin{aligned} ds^2 = \frac{\Psi}{\Sigma}\Bigg[&- \left(1 - \frac{2m(r)r}{\Sigma}\right) \mathrm{d}t^2 - \frac{4a\, m(r) r \sin^2\theta}{\Sigma}\, \mathrm{d}t\, \mathrm{d}\phi \\ &+ \frac{\Sigma}{\Delta}\, \mathrm{d}r^2 + \Sigma\, \mathrm{d}\theta^2 + \frac{A \sin^2\theta}{\Sigma}\, \mathrm{d}\phi^2 \Bigg], \end{aligned} \tag{270}$$

with $m(r)$ given in eq. (264) and

$$\begin{aligned} &\Psi = \Sigma + \frac{b}{r^3}, \quad \Sigma = r^2 + a^2 \cos^2\theta, \\ &\Delta = r^2 - 2m(r)r + a^2, \quad A = (r^2 + a^2)^2 - \Delta a^2 \sin^2\theta\,, \end{aligned} \tag{271}$$

where for the power law of Ψ we have chosen the lowest integer that makes the curvature scalars continuous and finite (see section 9.2).

Fixing $r_+ = r_+^{\rm Kerr}$ and choosing r_- as in eq. (267), this metric represents a family of stable, rotating, close-timelike-curve-free, regular spacetimes with two free parameters (beyond the usual spin one): the "Kerr-deviation parameter" e and the "regularisation parameter" b. Notice that for $a \to M$ the metric becomes conformal to the extremal Kerr, while for $a \to 0$ the metric becomes conformal to Schwarzschild.

9.4 THE ROTATING "INNER-DEGENERATE" REGULAR BLACK HOLE AS A KERR BLACK HOLE MIMICKER

In this section we investigate the extent to which our metric eq. (270) can mimic a Kerr BH: first we describe the causal structure; then the effective matter content; the position of ergosurfaces; and finally the location of the light rings and the ISCOs.

9.4.1 *Causal structure*

To study the casual structure of this spacetime we introduce ingoing null coordinates

$$\mathrm{d}v = \mathrm{d}t + \frac{r^2+a^2}{\Delta}\,\mathrm{d}r\,, \quad \mathrm{d}\psi = \mathrm{d}\phi + \frac{a}{\Delta}\,\mathrm{d}r\,, \tag{272}$$

that are regular at the horizons. In figure 16 we plot the equatorial principal null geodesics in the r–t_*^v plane where t_*^v is defined as

$$\mathrm{d}t_*^v = \mathrm{d}v - \mathrm{d}r\,. \tag{273}$$

We see that, even if the inner horizon has zero surface gravity, we still have peeling of geodesics there, the difference with respect to Kerr being in the rate of peeling. Since $\kappa_- \propto \partial_r\Delta|_{r_-} = 0$ and $\partial_r^2\Delta|_{r_-} = 0$ this peeling is no longer exponential but scales as $1/\sqrt{t}$. In fact, for the principal null geodesics

$$\frac{\mathrm{d}r}{\mathrm{d}t} = \pm\frac{\Delta}{r^2+a^2}\,, \tag{274}$$

and near the inner horizon we have

$$\frac{\mathrm{d}r}{\mathrm{d}t} = \pm\frac{\partial_r^3\Delta|_{r_-}}{r_-^2+a^2}\,(r-r_-)^3 + \mathcal{O}(r-r_-)^4\,. \tag{275}$$

The causal structure of the spacetime is summarised by the Penrose diagram of figure 17. The diagram is completely analogous to that of the Kerr spacetime, except for the fact that the surface $r = 0$ — which is timelike — is not a singularity and it can be reached only after an infinite amount of proper time by any infalling observer. In order to hint at these differences, we choose to represent $r = 0$ as a branch of hyperbola instead of a straight line.

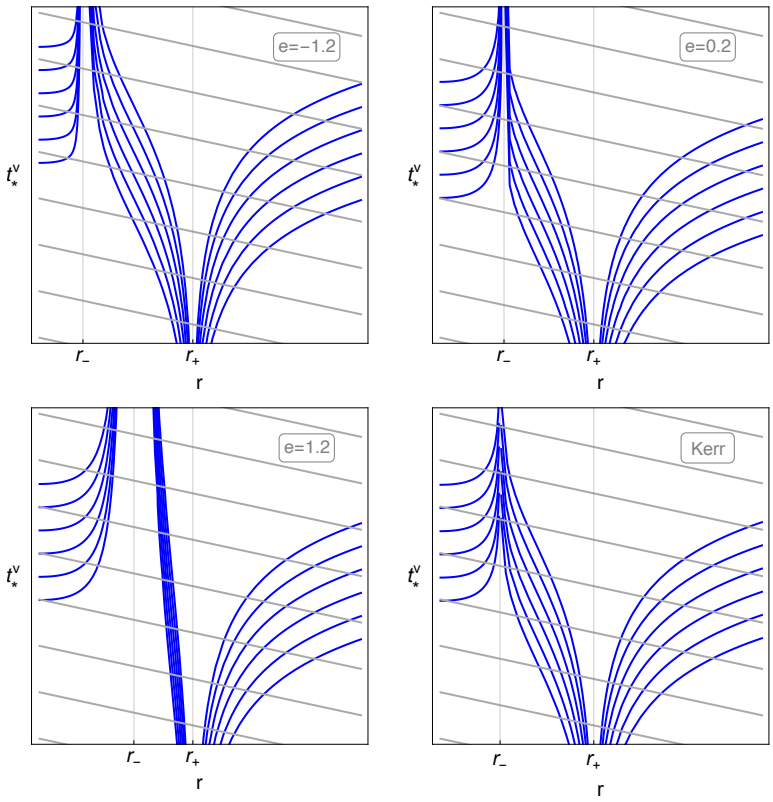

Figure 16: Ingoing (gray) and outgoing (blue) null rays near the horizons for selected values of the "Kerr-deviation parameter" e compared with the Kerr ones in the bottom right panel. The spin parameter is set to $a = 0.9M$.

9.4.2 *Effective matter content*

Clearly, the metric we are considering is not a vacuum solution of GR. Yet, as discussed, the Einstein's equations can be used to characterise the spacetime by interpreting the Einstein tensor $G^\mu_{\ \nu} = R^\mu_{\ \nu} - \frac{1}{2} R\, \delta^\mu_{\ \nu}$ as an effective stress-energy tensor; this allows to quantify deviations of our candidate spacetime from the Kerr one.

To properly characterise the effective matter content, one first needs to project the Einstein tensor onto an orthonormal tetrad, e. g. the one of [21–23]. The behaviour of the orthonormal components close to spatial infinity is particularly relevant: since the spacetime is asymptotically flat, they must all tend to zero as $r \to \infty$, but they do so at different rates.

In particular, the slowest decaying (non-zero) components are those on the diagonal, all the others being of higher order in powers of

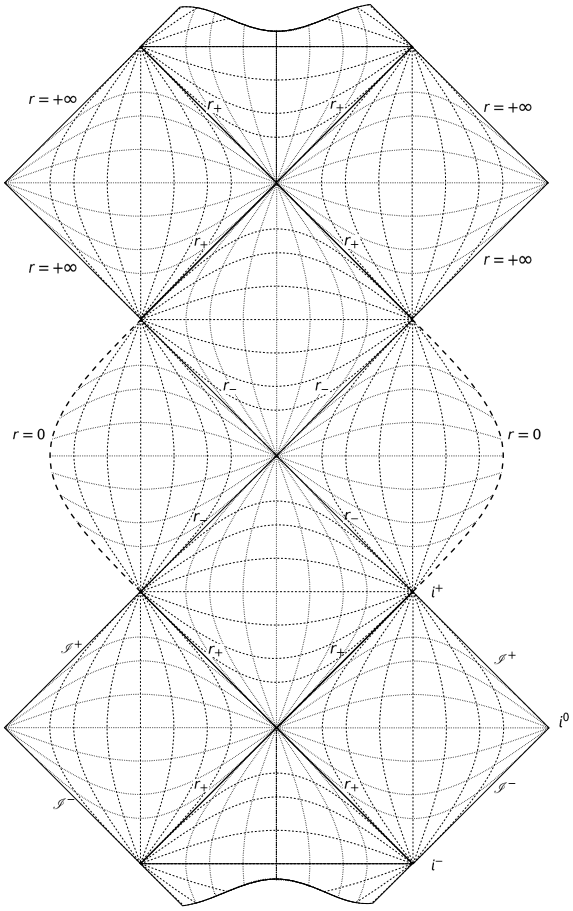

Figure 17: Penrose diagram of the rotating RBH in eq. (270). The hypersurface $r = 0$ is timelike, but reached in infinite proper time by any infalling observer: for this reason it is drawn not as a straight line but as a curve.

$1/r$. Such components, at infinity, are the effective energy density and pressures:[2]

$$\varepsilon = -p_r = p_\theta = p_\phi = -\frac{2M(\alpha-\gamma)}{r^4} + \mathcal{O}\left(1/r^5\right). \tag{276}$$

Note that these quantities fall off quickly as $r \to \infty$, meaning that deviations from vacuum GR are sizeable only in a region close to the object. Moreover, they are $\mathcal{O}\left(e^3\right)$ and do not depend on b; the next-to-leading order $\mathcal{O}\left(1/r^5\right)$ also does not depend on b.

Eq. (276) can lead to violations of the null energy condition, which requires $\rho + p_i \geq 0$, if $\alpha - \gamma > 0$. When the null energy condition

2 Technically, the energy density and pressures are defined in terms of the eigenvalues of the orthonormalised Einstein tensor, when these are real. In asymptotically flat spacetimes, this procedure and the one presented in the text agree at leading order.

is violated, all the other classical energy conditions are violated too. When instead $\gamma > \alpha$, not only the null but also the weak (null + $\rho \geq 0$) and dominant ($\rho \geq |p_i|$) energy conditions are met; the strong energy condition (null + $\rho + 3p_i \geq 0$) instead is always violated. Notice also that the above effective matter distribution does not correspond to any simple realistic matter content. This is not surprising, as this effective stress-energy tensor gives an insight into putative new physics beyond GR.

Moving closer to $r = 0$, the simple interpretation in terms of energy density and pressures is not always viable, since there are regions in which the Einstein tensor cannot be diagonalised over the real numbers: in these regions, the effective matter content is of type IV in the Hawking–Ellis classification [184]. (The existence of these regions is entirely due to the presence of the conformal factor: when $\Psi = \Sigma$, the effective stress-energy tensor is of Hawking–Ellis type I for any $m(r)$.)

In order to circumvent this problem, we select particular geodesics and investigate the effective matter content as measured along them. We focus first on null geodesics: calling k^μ their tangent vector, the contraction

$$G_{\mu\nu} k^\mu k^\nu \tag{277}$$

is always real and can be interpreted as the energy density measured along the geodesic. When this quantity is non-positive, the null energy condition is violated. For simplicity, we choose a geodesic that lies on the equatorial plane ($k^\theta = 0$) and that falls towards the BH with zero angular momentum ($L = 0$) — cf. eqs. (244) to (247). Clearly, this choice represents a loss of generality, but is sufficiently illustrative for our purposes.

The result is displayed in figure 18, for $a/M = 0.9$ and some choices of the parameters e and b. The effective energy density measured along the null geodesic is mostly negligible outside of the BH; inside the outer horizon, it becomes large and negative, signalling a substantial violation of the null energy condition; and it is exactly zero at $r = 0$ (although that point is reached only at infinite affine parameter). The plot of figure 18a is representative of all the cases $|e| \gtrsim 1$: increasing e slightly moves the negative trough to the right; increasing b, instead, tends to smooth out the trough; but the overall shape of the curve is not greatly affected. When $|e| \lesssim 1$, the curves exhibit additional features close to the inner horizon, signalling that the limit $e \to 0$ is not smooth. Lowering the spin suppresses the height of all the features just described.

We then move on to timelike geodesics, whose tangent vector we name u^μ. As before, we choose them to lie on the equatorial plane and to fall into the BH with zero specific angular momentum ($u^\theta =$

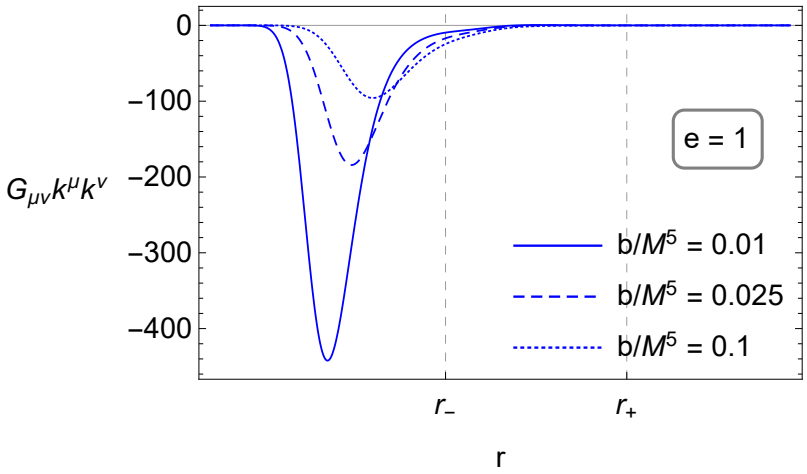

(a)

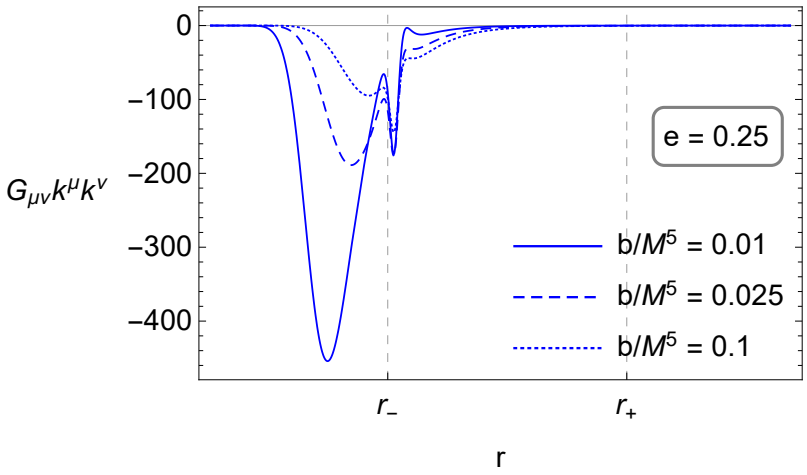

(b)

Figure 18: Effective energy density as measured along a null equatorial trajectory, with $L = 0$, that falls into a RBH with spin $a/M = 0.9$. Each plot is relative to a particular choice of the deviation parameter e and displays curves corresponding to three values of the regularisation parameter b. The two vertical lines mark the location of the inner and outer horizons.

0, $L = 0$); we further choose the radial velocity to be zero at infinity ($E = 1$). The contraction

$$G_{\mu\nu}u^\mu u^\nu \tag{278}$$

yields radial profiles that are qualitatively similar to those of figure 18 and for this reason we do not report them here. When this quantity is negative, the weak energy condition is violated. Finally, we complement the analysis by computing

$$R_{\mu\nu}u^\mu u^\nu. \tag{279}$$

Assuming the Einstein equations, $R_{\mu\nu} \propto T_{\mu\nu} - (T/2)g_{\mu\nu}$, hence when eq. (279) is negative the strong energy condition is violated. Some

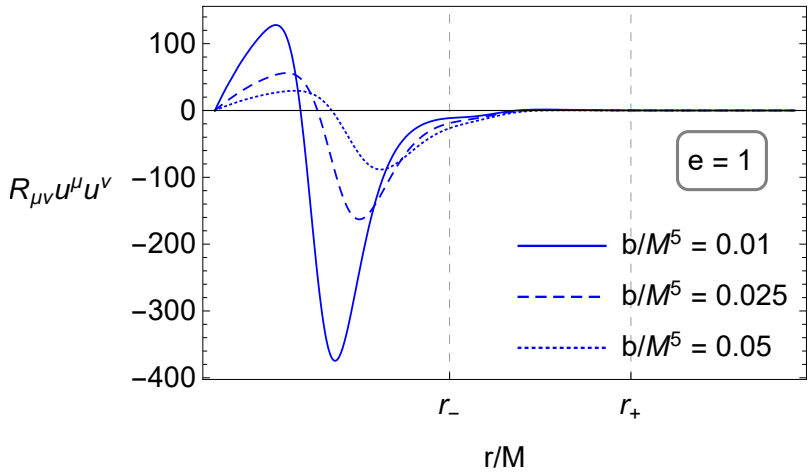

(a)

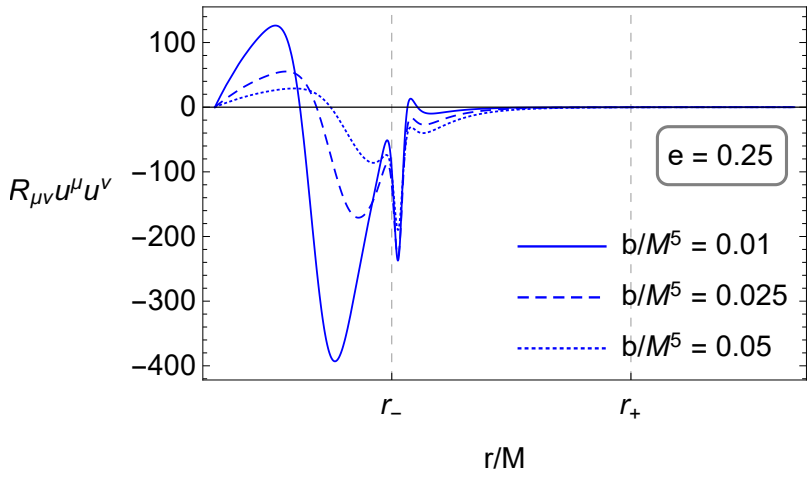

(b)

Figure 19: Contraction of the Ricci tensor with the tangent vector of a particular timelike equatorial trajectory ($L = 0$, $E = 1$) that falls into a RBH with spin $a/M = 0.9$. Each plot is relative to a particular choice of the deviation parameter e and displays curves corresponding to three values of the regularisation parameter b. The two vertical lines mark the location of the inner and outer horizons.

results are reported in figure 19, again for $a/M = 0.9$ and a few illustrative choices for e and b. As in the null case, these observers measure an effective matter content that is practically zero outside of the outer horizon. Large violations of the strong energy condition are measured inside of the inner horizon. At variance with the null case, now the curves exhibit a second positive bump before reaching zero at $r = 0$. Similarly to the previous case, increasing the value of e pushes the large negative trough to the right but does not substantially affect its depth, which is instead controlled by b; the height of the positive bump increases with e. Moreover, for $|e| \lesssim 1$ additional

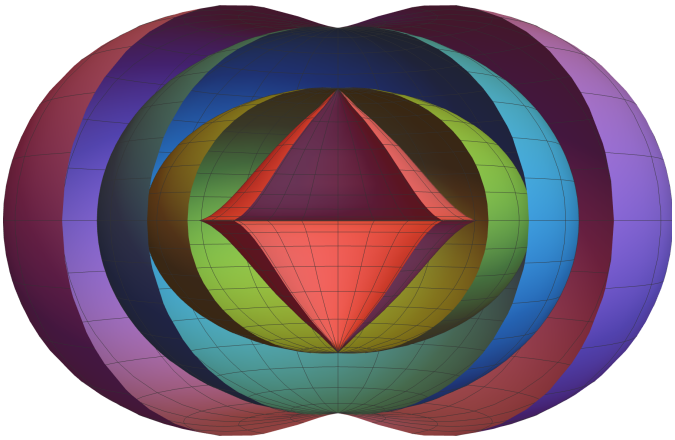

Figure 20: Embedding in Euclidean space of the horizons (green and blue surfaces) and ergosurfaces (red and purple surfaces) for $a/M = 0.95$ and $e = 1$.

features appear close to the inner horizon. As before, lowering the spin suppresses the magnitude of all these features.

9.4.3 *Ergosurfaces*

The ergosurfaces are defined by the roots of $g_{tt} = 0$, or equivalently of $r^2 - 2m(r)r + a^2\cos^2\theta = 0$, whose solution can be given in closed form. Since the result is cumbersome, in figure 20 we show the embedding in Euclidean space of the horizons and ergosurfaces for some illustrative choice of the parameters. The main difference with respect to a Kerr BH is the shape of the inner ergosurface around the poles: values of e closer to the upper and lower bounds in eq. (268) correspond to a more pronounced cuspid around the poles; for values of e closer to the lower bound, the inner horizon and ergosurface move close and eventually touch also at the equator; for values of e closer to the upper bound the horizons move closer as previously said. The conformal factor does not affect the ergosurfaces at all.

Finally, let us notice that, since with our choice $m(r_+) = M$, the textbook expression for the maximal efficiency of the Penrose process [44, 228, 294, 358] seems to yield the same result as in Kerr:

$$\eta_{\max} = 1 - \frac{2m(r_+)}{r_+} = 1 - \frac{2M}{M + \sqrt{M^2 - a^2}}\,. \tag{280}$$

Checking whether this is actually the case would require a more careful analysis of the motion of test particles in our spacetime — an interesting question which however lies outside the scope of this work.

9.4.4 *Notable equatorial orbits*

In order to characterise the spacetime and its deviations away from Kerr from a phenomenological point of view, we compute the coordinate location of the light ring and the ISCO. We focus on the equatorial plane, where the radial motion is governed by the function (cf. eq. (246))

$$\mathcal{R} = E^2 r^2 (r^2 + a^2) - r^2 L^2 + 2m(r) r (aE + L)^2 - \mu \Psi \Delta \,, \tag{281}$$

with $\mu = 0$ or 1 for null and timelike geodesics, respectively. Circular orbits correspond to $\mathcal{R} = \mathcal{R}' = 0$ and are stable if $\mathcal{R}'' \leq 0$. Since the analytical expressions are not particularly illuminating, the values of $r_{\rm LR}$ ("LR" for "light ring") and $r_{\rm ISCO}$ are computed numerically.

The location of the light ring, which is a null geodesic, does not depend on Ψ. Its fractional deviation from its Kerr anal is shown in figure 21, as a function of the spin, for some choices of the parameter e. The extrema and sign changes displayed by the curves of figure 21 are ultimately determined by the behaviour of the function $m(r)$ (and its derivative), which is not monotonic.

The analogous plot for the ISCO is reported in figure 22. Contrary to the previous case, $r_{\rm ISCO}$ depends on Ψ, hence the curves in the figure correspond to specific choices of b. In fact, varying the parameter b substantially affects the location of the ISCO, particularly for high spin. The peculiar spike associated to prograde orbits and high spins, in particular, can be entirely explained in terms of the behaviour of Ψ: since, as the spin increases, the prograde ISCO shrinks, $r_{\rm ISCO}$ enters deeper into the region where Ψ is markedly different from r^2.

In order to further explore the parameter space in the high-spin regime, we set $a = 0.998M$ (roughly the Thorne limit) and let the parameters vary in the ranges $b \in [0, 1]$ and $e \in [-3 - 3M/\sqrt{M^2 - a^2}, 2]$, thereby producing the contour plots of figure 23. Despite the much larger interval spanned by e, the gradient of the deviation is dominated by the b component: this is clear for prograde orbits (figure 23a), but is also true for retrograde orbits (figure 23b) if e is restricted to take reasonably small values as in figure 23c. Note, however, that even for spins as high as $a = 0.998M$, except for rather extreme values of the parameters, the ISCO moves less than a few percent in the prograde case and less than a few per mil in the retrograde case.

9.5 CHAPTER WRAP-UP

In this chapter, we built and studied a new regular alternative to Kerr BHs that is stable under mass inflation. To construct it, we combined two common tools for regularisation in a novel way: we used a mass function to construct a degenerate (zero-surface gravity) — and thus stable — inner horizon; and a conformal factor to regularise

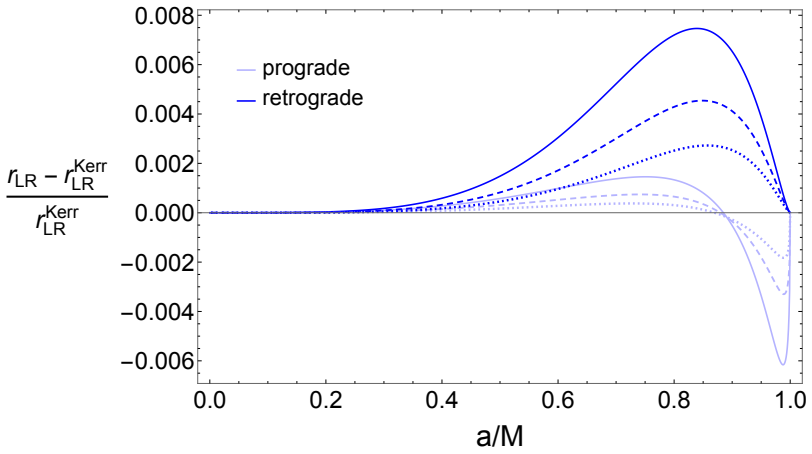

Figure 21: Relative difference in the position of the light ring as a function of the spin between Kerr and our spacetime with $e = 0.9$ (dotted lines), $e = 1$ (dashed lines) and $e = 1.1$ (continuous lines). We do not need to specify a value for the regularisation parameter b as null geodesics are insensitive to the conformal factor Υ. While we display only values of e near 1, corrections to the light-ring position actually grow very fast with e and they can be up to order 60% for $e \to 2$. Note also that the extrema and sign changes displayed by the curves are ultimately determined by the behaviour of the function $m(r)$ (and its derivative), which is not monotonic.

the singularity. In general, this procedure leads to a family of metrics, depending on the precise choice of the conformal factor and of $m(r)$.

We decided to focus on a particular form of the conformal factor that accomplishes the regularisation in a minimal way and at the same time ensures the non-existence of close timelike curves and the separability of the equations of motion for test particles. With this choice, the curvature scalars are continuous and tend to zero on the would-be singularity[3] thereby solving a long-standing issue that affects many rotating RBHs. The regularisation is controlled by a scale that we parameterise in terms of the quantity b, with dimensions $[M]^5$.

We further took an Ansatz for $m(r)$ that is again minimal, in a suitable sense, and fixed the coordinate location of the outer horizon so that it coincides with its Kerr analogue. The resulting mass function can be expressed entirely in terms of the coordinate location of the inner horizon, whose deviation from that of Kerr is encoded by the dimensionless quantity e. In the limit $e \to 0$ we obtain the conformal Kerr metric that, though regular, is characterised by the usual surface gravity at the inner horizon (as it should be, given that the surface gravity is conformally invariant) and hence is again unstable under mass inflation. However, it is important to notice that our metric cannot indefinitely deviate from the conformal Kerr one since the

3 With a slightly different choice, however, the limit can also be made non-zero.

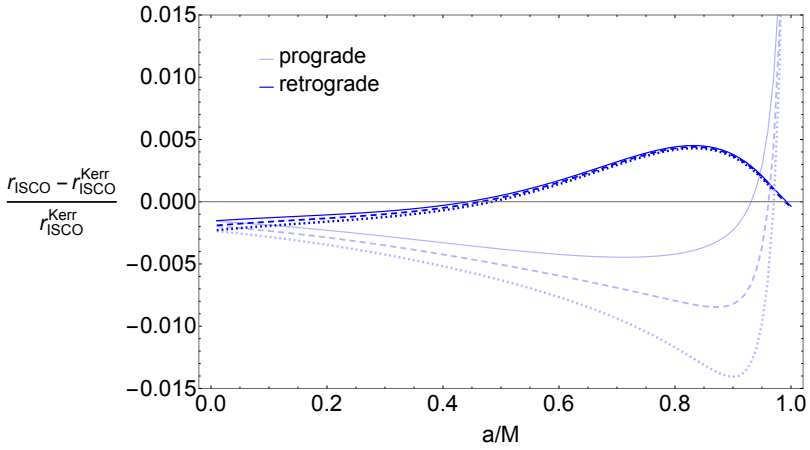

Figure 22: Difference in the position of the ISCO between Kerr and our spacetime with $e = 1$ and $b/M^5 = 0.8$ (continuous lines), $b/M^5 = 1$ (dashed lines) and $b/M^5 = 1.2$ (dotted lines). The prograde orbit, being in the more internal region of the spacetime where the conformal factor is greater, presents larger deviations, particularly for high spin.

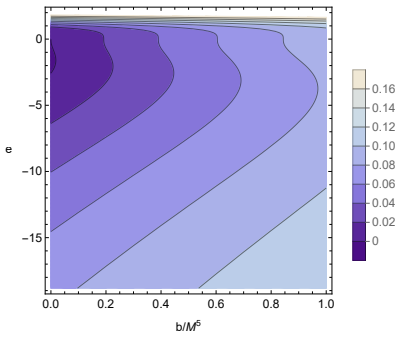

(a) Prograde orbits.

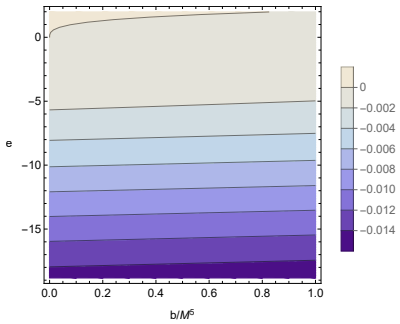

(b) Retrograde orbits.

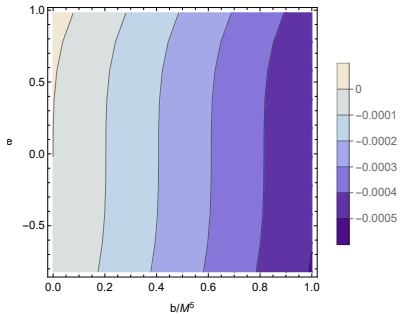

(c) Retrograde orbits, zoom to the region $|e| < 1$ of figure 23a.

Figure 23: Fractional deviation of the ISCO from its Kerr analog, computed as $r_{\rm ISCO}/r^{\rm Kerr}_{\rm ISCO} - 1$. Spin $a/M = 0.998$.

deviation parameter e must lie in a specific interval in order for the mass function to be everywhere finite and for the horizons to be well ordered ($0 < r_- < r_+$).

Our metric thus depends on a total of four real parameters: the ADM mass M, the spin a, the regularisation parameter b and the deviation parameter e. The two additional parameters b and e can be constrained by observations, at least in principle. In particular, e enters at low order in the parameterised post Newtonian expansion of this object's gravitational field and thus influences its multipolar structure; moreover, it affects the orbits of massless test particles and therefore shifts the position of the light ring. Finally e and b both affect the motion of massive test particles, with b having the dominant effect on the location of the ISCO (at least when e is taken to vary in reasonably small ranges) especially at high spins.

Part III

LORENTZ-VIOLATING THEORIES OF GRAVITY

10

REGULAR BLACK HOLES AND ULTRA-COMPACT OBJECTS IN LORENTZ-VIOLATING GRAVITY

In the previous chapters we always assumed that some new physics would regularise singularities, but we never framed the discussion within any specific proposal for extending GR. Here, we aim at rectifying such deficiency, though only partially.

We resolve to consider theories of gravity in which Lorentz invariance is broken. Admittedly, this choice looks exotic, given the astounding accuracy to which Lorentz invariance has been tested in the matter sector [235, 236]; however, several independent approaches to quantum gravity seem to point to the possibility that Lorentz invariance might be broken at high energies, only to be recovered accidentally in the infrared [265].

In particular, we focus on a few intimately related theories: (non-projectable) Hořava gravity; its low-energy limit, khronometric theory; and later on Einstein–æther theory, a close relative of the latter which however is general enough to be considered an effective field theory for all theories of gravity with a dynamical preferred frame.

The low-energy theories admit BH solutions that are singular; it is reasonable to expect that, by properly accounting for high-energy effects, those BHs will be regularised. This motivates us to carry out an analysis akin to those of previous chapters.

Note: solely for this chapter, the signature of the metric will be $(+,-,-,-)$.

10.1 INVITATION: WHY VIOLATING LORENTZ INVARIANCE?

Historically, the most important obstacle to the quantisation of gravity has probably been the perturbative non-renormalisability of GR [1, 176]. Nowadays the perspective on the issue is somewhat different [88, 143] and several other aspects of the problem, arguably deeper in nature, have been identified — see e. g. [247, 361].

Still, an approach to quantum gravity that remains actively investigated to this day consists in deforming Einstein–Hilbert's action by the addition of terms that contain higher-order derivatives of the metric — an example being quadratic gravity [310, 324]. Indeed, higher derivatives improve the ultraviolet behaviour of propagators and can ameliorate loop divergences. However, the inclusion of these terms changes the spectrum of the theory by introducing new degrees of freedom, some of which are Ostrogradski ghost [364]. These theories are therefore generically unstable, since classically their Hamiltonian is unbounded below.

To circumvent the issue, Hořava [192] proposed a field theory of gravity in which the additional terms contain higher-order *spatial* derivatives only and therefore do not give rise to ghosts. In his proposal, power-counting renormalisability is manifest; but it comes at the price of breaking diffeomorphism invariance and, locally, Lorentz invariance, as this construction distinguishes time from space at a fundamental level.

In the years following Hořava's paper, several improvements to the original idea have been proposed, including a "healthy" extension known as non-projectable Hořava gravity [63, 64, 66]. There are now strong indications — [45–50] and references therein — that this version of the theory is perturbatively renormalisable: if this property is confirmed, non-projectable Hořava gravity will represent an example of a consistent quantum theory of gravity in $(3+1)$ spacetime dimensions.

Note, incidentally, that another version of Hořava gravity, dubbed projectable in [63, 64, 66], has *already* been proven to be renormalisable [45] in $(2+1)$ [46] and $(3+1)$ [48] dimensions. So, *projectable Hořava gravity is an ultraviolet-complete quantum theory of gravity*. This statement is so remarkable it deserves to be repeated: *projectable Hořava gravity is an ultraviolet-complete quantum theory of gravity*.

However, the projectable theory is considered to be too restrictive to be able to account for the gravitational phenomena we observe in our universe. For instance, it does not admit BHs. For this reason, it is often regarded as an interesting but phenomenologically unviable example.

A recent review on the status of renormalisation in Hořava gravity can be found in [188].

10.2 HOŘAVA AND KHRONOMETRIC THEORY

Hořava's theory is most naturally written in an ADM $(3+1)$ decomposition, whereby spacetime is foliated by three-dimensional spacelike hypersurfaces. In this framework, space and time are thus distinguished explicitly and one can easily add higher spatial derivatives while being sure not to introduce ghosts. Renormalisability requires derivatives up to sixth order in $(3+1)$ dimensions — see [188] for a more accurate version of this statement.

However, the theory can be reformulated in a fully covariant fashion via the introduction of a Stückelberg compensator field $T(x)$. Such field, called *khronon*, encodes information on the "preferred" foliation, which is identified with the hypersurfaces

$$T(x) = \text{cst}\,. \tag{282}$$

The action of the theory is thus built out of the geometric quantities that describe the embedding of these hypersurfaces into spacetime.

In particular, the khronon itself will never appear in the action, which will instead be constructed out of its normalised timelike gradient

$$u_\mu = N\nabla_\mu T \quad \text{with} \quad N = \left(\sqrt{\nabla_\nu T \nabla^\nu T}\right)^{-1} ; \tag{283}$$

such (co)vector is dubbed *æther* for reasons that will become clear momentarily, while the normalisation factor N is the lapse of the preferred foliation. Note that u_μ is invariant under reparametrisations of the khronon and, being orthogonal to the constant-khronon hypersurface, it is irrotational. The æther thus identifies, at each spacetime point, a preferred time direction within the tangent space.

Schematically, the action can be written as

$$S = -\frac{1}{16\pi}\int \mathrm{d}^4x\,\sqrt{-g}\left[R + \mathcal{L}_2 + \frac{1}{M_*^2}\mathcal{L}_4 + \frac{1}{M_*^4}\mathcal{L}_6\right] , \tag{284}$$

where each of the $\mathcal{L}_n$ contains derivatives of order n and M_* is a mass scale.

At low energies, much smaller that M_*, one can neglect $\mathcal{L}_4$ and $\mathcal{L}_6$. The resulting action, which defines a theory mostly known as khronometric theory, explicitly reads

$$\begin{aligned} S = -\frac{1}{16\pi}\int \mathrm{d}^4x\,\sqrt{-g}\big[&R + \lambda(\nabla_\mu u^\mu)^2 + \beta\nabla_\mu u^\nu \nabla_\nu u^\mu \\ &+ \alpha a^\mu a_\mu\big] , \end{aligned} \tag{285}$$

where $a_\mu = u^\nu\nabla_\nu u_\mu$ is the æther's acceleration while α, β and λ are three dimensionless couplings.

The parameters α, β, λ are tightly constrained by observations [163]: $|\beta| \lesssim 10^{-15}$ and either $|\alpha| \lesssim 10^{-7}$ with λ unconstrained or $|\alpha| \lesssim 0.25 \times 10^{-4}$ with $\lambda \approx \alpha/(1-2\alpha)$. Moreover, $\lambda > 0$ to avoid ghosts. Since α and β seem both very small, one may at times consider a "minimal khronometric theory" in which they are set to zero exactly, while λ remains free.

Incidentally, note that the action eq. (285) coincides with a particular case of the scalar-vector-tensor modification of GR known as Einstein–æther theory [200, 204]. Such theory is constructed in terms of an everywhere timelike and unit-norm vector field which the authors of [204] decided to call æther; *that* æther needs not be hypersurface orthogonal, but when it is constrained to be so at the level of the action, then one gets eq. (285) [201, 203]. For this reason, the vector u_μ of khronometric theory is unanimously called æther, too.

However, hypersurface orthogonality restricts the number of physical degrees of freedom in the spectrum. The two theories are therefore different, though closely related. In particular, they happen to share *some* solutions — namely, all hypersurface-orthogonal solutions of Einstein–æther, e. g. those that are spherically symmetric, are solutions of khronometric theory too. But the two sets of solutions are

nonetheless distinct. The relationship between the two theories is therefore quite subtle [37, 38].

10.2.1 *Black holes*

Although the action eq. (284) is generally covariant, the fact that the khronon identifies a preferred foliation opens the door to the existence of non-linear dispersion relations that schematically take the form

$$\omega^2(\mathbf{k}) = \mathbf{k}^2 + \eta_4 \frac{\mathbf{k}^4}{M_*^2} + \eta_6 \frac{\mathbf{k}^6}{M_*^4} \,. \tag{286}$$

The higher powers of the spatial momentum descend directly from the higher-order spatial derivatives and are a manifestation of the anisotropic scaling that characterises Hořava gravity in the ultraviolet. Their presence entails that signals may propagate faster than light. Moreover, the theory "propagates" an istantaneous mode, i. e. one whose equation of motion has an elliptic character, which persists even at low energy [66].

There seems to be no room for BHs in such a context. Remarkably, this conclusion turns out to be incorrect. Indeed, the presence of superluminal signals simply entails that the light cones associated with the metric do not characterise the causal structure. In theories with a preferred notion of time, however, it is this preferred time that rules causality [93].

Specifically, a curve is said to be causal if it only intersects each leaf of the foliation once [62]; i. e. if it moves forward or backwards in the preferred time, without ever turning back nor standing still. In terms of these curves one can rephrase the usual definitions of casual infinities; in particular, a suitable notion of BHs does in fact exist [36–39, 54, 61, 65, 150, 206, 290].

However, the characterisations of horizons normally used in GR fail to pinpoint the boundary of such BHs. Rather, the role of the event horizon, in these theories, is played by the so-called UH. This is a constant-khronon surface, i. e. a leaf of the preferred foliation, that happens to be compact. Such leaf does not close to the same point at infinity as the non-compact ones, and neither will the leaves in its causal future — which will therefore be causally disconnected from the future causal infinity.

When the spacetime is stationary, calling χ^μ the timelike (at infinity) Killing vector, the UH is characterised by the conditions [62]

$$u_\mu \chi^\mu \Big|_{\text{UH}} = 0 \quad \text{and} \quad a_\mu \chi^\mu \Big|_{\text{UH}} \neq 0 \,. \tag{287}$$

(The latter condition amounts to saying that UHs cannot be extremal; it was introduced in [62] for technical reasons but could in principle be relaxed [164].)

UHs are thus leaves of the preferred foliation that are *orthogonal* to the Killing vector of stationarity. Further note that the quantity $u_\mu \chi^\mu$ can play the role of the lapse function of the preferred foliation [1] and its vanishing means that the preferred time infinitely "slows down" as one approaches the UH. Moreover, UHs are Cauchy horizons as defined appropriately for this context. Hence, it is not completely obvious that extending the spacetime beyond a UH makes sense — we will work under the assumption that it does.[2] If this is the case, it can be shown that the lapse must change sign upon crossing the UH [137].

UHs are different, in general, from the more familiar KHs — defined as hypersurfaces on which a Killing vector becomes null. However, the two notions are somewhat related since the existence of a UH generically implies that of a KH: roughly speaking, since u_μ is always timelike, $u_\mu \chi^\mu = 0$ entails that χ^μ must be spacelike at the UH; but since it is timelike at infinity it must also become null somewhere in between.

Note, incidentally, that dispersion relations like eq. (286) are conceivable in Einstein–æther theory, too. Thus, one might conjecture that UHs exist in that context as well. Whether the characterisation of eq. (287) makes sense in the absence of hypersurface orthogonality is, however, unclear. We will come back to this point in chapter 11.

10.2.2 *A static and spherically symmetric infrared solution*

Let us focus on the low-energy limit, i. e. khronometric theory, and investigate its static and spherically symmetric solutions.

The equations of motion obtained by varying eq. (285) with respect to $\delta g_{\mu\nu}$ and δT can be written as:

$$\mathcal{G}_{\mu\nu} = 0\,, \tag{288}$$

$$\nabla_\mu \left(N \mathcal{A}^\mu\right) = 0\,. \tag{289}$$

Eq. (288) is the equivalent of the Einstein's equation, indeed one can write $\mathcal{G}_{\mu\nu} = G_{\mu\nu} - T^{æ}_{\mu\nu}$, with $G_{\mu\nu}$ the Einstein's tensor and $T^{æ}_{\mu\nu}$ the stress-energy tensor of the æther. Eq. (289) is the equation of motion of the khronon:[3] the vector $\mathcal{A}^\mu$ is built out of u_μ and its derivatives and is orthogonal to the æther $u_\mu \mathcal{A}^\mu = 0$.

To include matter, one can add the matter action S_{mat} to eq. (285) (or eq. (284)). This yields source terms that appear on the right-hand side of eqs. (288) and (289).

1 More precisely, the quantity $u_\mu \chi^\mu$ is the lapse when one makes the gauge choice $\chi^\mu \nabla_\mu T = 1$ — cf. eq. (283).

2 More precisely, such extension seems justified — and arguably necessary — in a context like Einstein–æther theory, which is defined in terms of the æther and does not require a foliation; in khronometric theory, the issue is less transparent.

3 This equation actually follows from the Einstein's equation as a consequence of the (generalised) Bianchi identities [202].

Since in eqs. (288) and (289) the metric and the æther appear to be coupled, it is natural to expect that the isometries of the metric will extend to symmetries of u_μ. Hence, when assuming staticity and spherical symmetry, we also assume that the æther is Lie-dragged along the corresponding Killing vectors. Thus, in particular, the angular components of u_μ will vanish, and the remaining components will not depend on the Killing time.

(The terminology *static æther* has appeared in the literature, e. g. [151], to refer to an æther that is everywhere aligned with the Killing vector; however, this assumption implies the non-existence of UHs and is therefore too restrictive for our purposes.)

We will adopt in-going Eddington–Finkelstein coordinates, and write the metric and the æther as

$$ds^2 = f(r)\,\mathrm{d}v^2 - 2\,\mathrm{d}v\,\mathrm{d}r - h(r)\,\mathrm{d}\Omega^2\,, \tag{290}$$

$$u^\mu\partial_\mu = Y(r)\partial_v + y(r)\partial_r\,. \tag{291}$$

Note that, despite the change in signature, the metric is in the general form of eq. (4) with the gauge choice $g(r) = f(r)$. Moreover, since the æther has unit norm, the four functions are not all independent, as the following relation holds:

$$y = -\frac{1 - Y^2 f}{2Y}\,. \tag{292}$$

In these coordinates, the Killing vector of staticity is

$$\chi^\mu\partial_\mu = \partial_v\,, \tag{293}$$

hence its projection along the æther reads

$$\begin{aligned} u_\mu\,\chi^\mu &= \frac{1 + Y^2 f}{2Y} \\ &= fY - y \end{aligned} \tag{294}$$

(eq. (292) has been used in passing from the first line to the second).

An exact solution can be found quite easily by setting $\alpha = 0$ [54], which is compatible with current observational bounds.[4] In the parametrisation above, it is given by $f = f_{\text{sing.}}$, $h = h_{\text{sing.}}$ and $y = y_{\text{sing.}}$ with

$$f_{\text{sing.}}(r) = 1 - \frac{r_0}{r} - \beta\frac{r_{æ}^4}{r^4}\,, \qquad h_{\text{sing.}}(r) = r^2\,, \tag{295}$$

$$y_{\text{sing.}}(r) = -\frac{r_{æ}^2}{r^2}\,, \tag{296}$$

where r_0 is twice the ADM mass of the spacetime and $r_{æ}$ is another, *a priori* independent, integration constant. One can then easily compute

$$Y_{\text{sing.}}(r) = \frac{1}{f_{\text{sing.}}(r)}\left[-\frac{r_{æ}^2}{r^2} \pm \sqrt{f_{\text{sing.}}(r) + \frac{r_{æ}^4}{r^4}}\right] \tag{297}$$

4 Another exact solution can be found for $\beta + \lambda = 0$.

and

$$\left(u_\mu \chi^\mu\right)_{\text{sing}} = \pm\sqrt{f_{\text{sing}}(r) + \frac{r_{\text{æ}}^4}{r^4}}\,. \tag{298}$$

(Note that reference [54] only reports the plus sign in front of the square root, although the constraint actually allows for both. However, sticking to a single sign would lead to a kink-like behaviour at the zeroes of $u_\mu \chi^\mu$, whose derivative would thus be discontinuous. Indeed, [137] showed that the lapse must change sign upon crossing a UH.)

Depending on the relative magnitude of r_0 and $r_{\text{æ}}$, the quantity under the square root in eqs. (297) and (298) may become negative, thus rendering $\left(u_\mu \chi^\mu\right)_{\text{sing}}$ complex. This undesirable circumstance can be avoided imposing a suitable inequality between r_0 and $r_{\text{æ}}$. In particular, if one imposes the fine-tuned choice

$$r_{\text{æ}} = \frac{r_0}{4}\left(\frac{27}{1-\beta}\right)^{1/4}, \tag{299}$$

the lapse function has one isolated zero and the solution thus describes a BH. (When $r_{\text{æ}}$ is larger than this value the solution is still acceptable, but does not describe a BH; in fact, it describes a naked singularity.)

The UH is located at

$$r_{\text{UH}} = \frac{3}{4} r_0\,. \tag{300}$$

Moreover, the lapse can be written as

$$\left(u_\mu \chi^\mu\right)_{\text{sing.}} = \frac{1}{r^2}\left(r - \frac{3}{4}r_0\right)\sqrt{r^2 + \frac{r_0}{2}r + \frac{3r_0^2}{16}}\,. \tag{301}$$

The signs have been chosen so that this quantity tends to one at spatial infinity but changes sign upon crossing the UH — as it must [137]. This corresponds to choosing the plus sign in eq. (297) outside of the UH and the minus inside.

The UH has an associated surface gravity that sets the temperature of the analogue of Hawking's radiation, in a way similar to the surface gravity of horizons in GR (see e. g. [136, 137, 189] and references therein). It is defined as

$$\kappa_{\text{UH}} = -\frac{1}{2} a_\mu \chi^\mu\,, \tag{302}$$

which on the solution evaluates to

$$\kappa_{\text{UH}}^{\text{sing.}} = \frac{2\sqrt{2}}{3\sqrt{3} r_0 \sqrt{1-\beta}}\,. \tag{303}$$

The metric also exhibits a KH, associated with the zero of $f_{\rm sing}(r)$. Clearly, when $\beta = 0$ the metric reduced to that of Schwarzschild and the KH is located at $r_{\rm KH} = r_0$. More generally, one can write $f_{\rm sing}(r) = 0$ as

$$r^3(r - r_0) - \left[\frac{27}{256}\frac{\beta}{1-\beta} r_0^4\right] = 0\,; \tag{304}$$

hence, one can deduce that the KH moves towards larger values of r as β increases (we always assume $\beta < 1$), i. e. $r_{\rm KH} \geq r_0$. Thus, the KH always encloses the UH, as it must. The equation does not have any more roots. Further note that $\Upsilon_{\rm sing}(r)$ is well-behaved at the KH, as can be verified by expanding close to $r = r_{\rm KH}$:

$$\Upsilon_{\rm sing}(r) = \frac{r_{\rm KH}^2}{2r_{æ}^2} + \mathcal{O}\Big((r - r_{\rm KH})^2\Big)\,. \tag{305}$$

Notably, however, this metric is singular at $r = 0$, as one can check e. g. by evaluating the Kretschmann scalar:

$$R_{\mu\nu\rho\sigma}R^{\mu\nu\rho\sigma} = 12\frac{r_0^2 r^6 + 10\beta r_0 r_{æ}^4 r^3 + 39\beta^2 r_{æ}^8}{r^{12}}\,. \tag{306}$$

The components of the æther also seem ill-defined at that point, although this statement relies on the choice of coordinates. To check that the æther flow is in fact singular at $r = 0$ one should characterise it in terms of scalar quantities. Since the æther constitutes a timelike non-geodesic congruence, a rather natural choice is to describe it in terms of its optical scalars:[5] the expansion, the square of the symmetric shear and the square of the antisymmetric twist. The explicit computations are carried out in subsection 10.8.1.

10.2.2.1 *Causal structure*

As mentioned in subsection 10.2.1, in the presence of Lorentz violations the light cones associated to the metric do not characterise the causal structure, since signals that are superluminal in the preferred frame can still be causal. If the theory is such that there exists a finite maximum speed of propagation, then one can define a new metric whose "light" cones do characterise the causal structure. Notably, such light cones will be wider than those of the original metric.

In theories like Hořava gravity, however, there exists an istantaneous mode and the propagation speed is unbounded. In a sense, this situation can be seen as a limiting case of the former, whereby the maximum speed is sent to infinity. Correspondingly, the "light" cones of the auxiliary metric that determines causality open up to become the hypersurfaces orthogonal to the æther, i. e. the constant-khronon surfaces.

5 The term "optical scalars" is usually reserved for null geodesic congruences. We are abusing this terminology, hopefully without confusion.

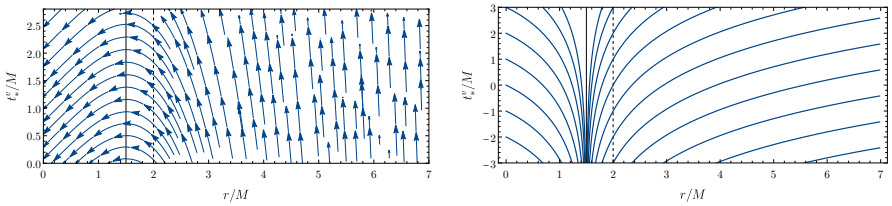

Figure 24: Causal structure for the infrared singular solution: æther flow (left) and constant-khronon surfaces (right).

Hence, one can represent pictorially the flow of the æther through spacetime, or equivalently the embedding of the preferred foliation, in order to visualise causal relationships in a way very similar to what one does in GR. Specifically, in such plots the constant-khronon surfaces will play a role analogous to light rays in GR.

In the following, we will often resort to plots of this kind. In order to ease the future discussion, we introduce them here for the particular solution eqs. (295) and (296). This case will therefore serve as a baseline, departures from which will be described in due time

Thanks to spherical symmetry, the dependence on the angles is always trivial and we can thus limit the analysis to an appropriate time–radius plane. As usual, the most natural definition of time is given in terms of the null coordinate v as

$$\mathrm{d}t^v_* = \mathrm{d}v - \mathrm{d}r \ ; \tag{307}$$

this is a (Killing-)"horizon-penetrating" Killing time. The more familiar time t, given by $\mathrm{d}t = \mathrm{d}v - \mathrm{d}r/f$, would not be appropriate, since the components of the metric and of the æther are singular at the KHs when expressed in terms of it.

The æther flow can then be portrayed as in the left panel of figure 24: a stream of arrows, whose components are proportional to those of the æther. Specifically, the æther is taken to be in its covariant form, hence the horizontal components of the arrows is $u_r = y_{\text{sing.}}$ while the vertical component is $u_{t^v_*} = \left(u_\mu \, \chi^\mu\right)_{\text{sing.}}$.

Furthermore, the right panel of figure 24 reports plots of several constant-khronon surfaces in the (t^v_*, r) plane. Since the æther is by definition orthogonal to constant-khronon hypersurfaces, the information provided by the two plots is not independent but complementary. We report both, hoping this will benefit the reader.

Looking at figure 24, we notice that at large r the æther is almost vertical, and the constant-khronon lines are also lines of constant Killing time t^v_*. This is because, at infinity, the æther is aligned with the Killing vector — whose flow would be a stream of vertical arrows, since the Killing vector is orthogonal to constant-t^v_* surfaces.

As one approaches to smaller r, however, the æther tilts inwards. Nothing remarkable happens at the KH, whose location is depicted

for reference by a dashed vertical line. Somewhere inside the KH, at a location marked by the solid vertical line, the æther becomes horizontal, hence orthogonal to the Killing vector: this defines the UH. Correspondingly, the constant-khronon lines have a vertical asymptote at the UH and exponentially recede away from it in its vicinity — i. e. they peal off, in an amount that is controlled by the surface gravity, exactly as null rays would do at a trapping horizon.

Note that behind the outer UH the æther points downwards, meaning that it flows in the opposite direction with respect to the Killing vector. These plots end at $r = 0$, which as argued is a spacetime singularity.

10.2.3 *Goal of the chapter*

The rationale guiding this chapter should now be intuitively clear. It is reasonable to think that the low-energy singular solution eqs. (295) and (296) will be regularised when the effects of the higher-order terms in $\mathcal{L}_4$ and $\mathcal{L}_6$ are taken into account.

However, $\mathcal{L}_4$ and $\mathcal{L}_6$ contain all the operators that, at that order in derivatives of the metric and the æther, are compatible with the symmetries. Since the number of such operators is very high, listing them all is already a non-trivial exercises. Therefore, solving the equations of motion for the full theory is likely going to be very difficult.

(Note that RBHs have been searched for, but not found, in the projectable version of Hořava gravity in [233]. That analysis however did not allow for the running of the couplings.)

Luckily, as parts i and ii have made clear, some progress can be made without actually solving those equations. Indeed, general arguments analogous to those of subsection 2.2.1 lead us to predict that the regular solutions of said equations will fall into one of very few classes. These classes are characterised by certain qualitative features, which can be captured by effective models like those of sections 3.2 and 3.3. Hopefully, studying examples of such effective models will guide the search for *exact* regular solutions.

The rest of the chapter is thus structured similarly to several others in this thesis: we will first describe the implementation of some common regularisation prescriptions in section 10.3; then analyse horizons (section 10.4) and the ensuing causal structure (section 10.5); finally, we will characterise the deviations from the vacuum of the infrared theory by computing the effective sources through khronometric theory's equaitions of motion (section 10.6).

10.3 REGULARISATIONS OF THE SINGULARITY

With some technical adaptions, the classification of subsection 2.2.1 applies to the case of Hořava gravity as well. Specifically, we will distinguish simply connected and multiply connected regularisations: the simply connected regularisations will generically exhibit multiple UHs; the multiply connected regularisations instead will sport a wormhole throat[6] at their centre.

The difference with respect to parts i and ii is that here the metric is not the only ingredient needed to fully characterise the geometry. Indeed, in Hořava gravity the preferred foliation plays a genuinely physical role. Consequently, ensuring that the metric is free of curvature singularities and that the spacetime is curve-complete is not enough to claim regularity — one also has to make sure that the æther field describes a well-behaved flow throughout the whole spacetime.

Somewhat surprisingly, the simple regularisation of the metric described in sections 3.2 and 3.3, suitably implemented, lead very naturally to regularisations of the æther, too.

10.3.1 *Simply connected regularisation*

As usual, to build a simply connected regularisation we replace the parameter r_0 with a function $r_0(r)$. If we assume the fine-tuned choice eq. (299), this replacement will percolated to the parameter $r_æ$, which will become a function as well:

$$r_æ(r) = \frac{r_0(r)}{4}\left(\frac{27}{1-\beta}\right)^{1/4} . \tag{308}$$

So, the æther will inherit the regularisation of the metric.

Specifically, the regularised metric and æther will be described by the general form eqs. (290) and (291) with $f = f_{SC}$, $h = h_{SC}$ and $y = y_{SC}$ with

$$f_{SC}(r) = 1 - \frac{r_0(r)}{r} - \beta\frac{r_æ^4(r)}{r^4} , \qquad h_{SC}(r) = r^2 , \tag{309}$$

$$y_{SC}(r) = -\frac{r_æ^2(r)}{r^2} , \tag{310}$$

6 Examples of wormholes in Hořava gravity are given in [116, 243].

so that

$$\Upsilon_{\text{SC}}(r) = \frac{1}{f_{\text{SC}}(r)}\left[-\frac{r_{æ}^2(r)}{r^2} + \frac{1}{r^2}\left(r - \frac{3}{4}r_0(r)\right)\sqrt{r^2 + \frac{r_0(r)}{2}r + \frac{3r_0^2(r)}{16}}\right], \tag{311}$$

$$\left(u_\mu \chi^\mu\right)_{\text{SC}} = \frac{1}{r^2}\left(r - \frac{3}{4}r_0(r)\right)\sqrt{r^2 + \frac{r_0(r)}{2}r + \frac{3r_0^2(r)}{16}}\,. \tag{312}$$

(SC stands for simply connected.)

As usual, the function $r_0(r)$ is arbitrary except for a minimum set of requirements (cf. section 3.2) [12, 170, 249, 313]:

$$\begin{cases} r_0(r) = c\ell^{-2}r^3 + \mathcal{O}\left(r^4\right) \quad \text{close to} \quad r = 0\,, \\ \lim_{r\to\infty} r_0(r) = r_0\,, \\ r_0(r) \quad \text{“well-behaved”, e.g.} \quad r_0(r) > 0\,. \end{cases} \tag{313}$$

The metric is regular, as discussed in section 3.2. The components of the æther are now manifestly regular, too. In particular,

$$y_{\text{SC}}(r) = \mathcal{O}\left(r^3\right) \quad \text{and} \quad \Upsilon_{\text{SC}}(r) = 1 + \frac{c\ell^{-2}}{2}r^2 + \mathcal{O}\left(r^3\right), \tag{314}$$

i.e. in the limit $r \to 0$ the æther coincides with the Killing vector, up to corrections of order $\mathcal{O}\left(r^2\right)$. This is precisely the trivial æther flow that one would expect in a maximally symmetric space. The first derivatives of $f_{\text{SC}}(r)$ and $\Upsilon_{\text{SC}}(r)$ are similarly well-behaved close to $r = 0$, which ensures that all the optical scalars characterising the æther congruence are regular too — details can be found in subsection 10.8.1.

In what follows, we will present calculations for Hayward's choice of $r_0(r)$ [187],

$$r_0(r) = 2M\frac{r^3}{r^3 + 2M\ell^2}\,, \tag{315}$$

but the features we will describe are generic: other well-studied examples, e.g. the Bardeen [43] or Dymnikova [144] metrics, yield very similar results.

10.3.2 *Multiply connected regularisation*

Unsurprisingly, to build a multiply connected regularisation we resort again to the SV trick and replace, in eqs. (295) and (296), any

instance of r with $\sqrt{r^2+\ell^2}$. The result takes the form of eqs. (290) and (291) with $f = f_{\rm MC}$, $h = h_{\rm MC}$ and $y = y_{\rm MC}$

$$f_{\rm MC}(r) = 1 - \frac{r_0}{\sqrt{r^2+\ell^2}} - \beta\frac{r_{æ}^4}{(r^2+\ell^2)^2}\,, \qquad h_{\rm MC}(r) = r^2+\ell^2\,, \tag{316}$$

$$y_{\rm MC}(r) = -\frac{r_{æ}^2}{r^2+\ell^2}\,, \tag{317}$$

so that (using again $\varrho = \sqrt{r^2+\ell^2}$)

$$\begin{aligned} \Upsilon_{\rm MC}(r) &= \frac{1}{f_{\rm MC}(r)}\left[-\frac{r_{æ}^2}{\varrho^2}\right. \\ &\qquad \left. + \frac{1}{\varrho^2}\left(\varrho - \frac{3}{4}r_0\right)\sqrt{\varrho^2 + \frac{r_0}{2}\varrho + \frac{3r_0^2}{16}}\right], \\ \left(u_\mu \chi^\mu\right)_{\rm MC} &= \frac{1}{\varrho^2}\left(\varrho - \frac{3}{4}r_0\right)\sqrt{\varrho^2 + \frac{r_0}{2}\varrho + \frac{3r_0^2}{16}}\,. \end{aligned} \tag{318}$$

(MC stands for multiply connected.) We are still assuming $r_{æ} = 27^{1/4}(1-\beta)^{-1/4}(r_0/4)$, without $r$dependence, as in the singular solution (eq. (299)). As usual, since the metric and the æther are invariant under $r \mapsto -r$, one can extend the domain of the coordinate r to $(-\infty, +\infty)$. We will then have the familiar "two universes", connected by a throat located at $r = 0$.

In this example, regularity is manifest, since all components of both the metric and the æther approach a finite non-zero limit as $r \to 0$. (Details on the æther's optical scalars can be found in subsection 10.8.1.)

10.4 HORIZONS

The regularised metrics introduced above, similarly to the singular solution, exhibit KHs located at the solutions of $f(r) = 0$. These horizons are still surfaces of infinite redshift/blueshift for matter that is minimally coupled to the metric and uncoupled to the æther. However, because of the breaking of local Lorentz invariance, they are not causal horizons since, as mentioned before, the presence of superluminal signals affects the causal structure [93]. The role of causal horizons is instead played by UHs.

Nonetheless, the two notions are related insofar as the existence of a UH implies that of a KH too. We hinted at this fact already in subsection 10.2.1 and argued that this is indeed the case in subsection 10.2.2. Here we have yet another example, since in both simply and multiply connected regularisations we have

$$\left(u_\mu \chi^\mu\right)^2 = f(r) + \text{positive function of } r\ : \tag{319}$$

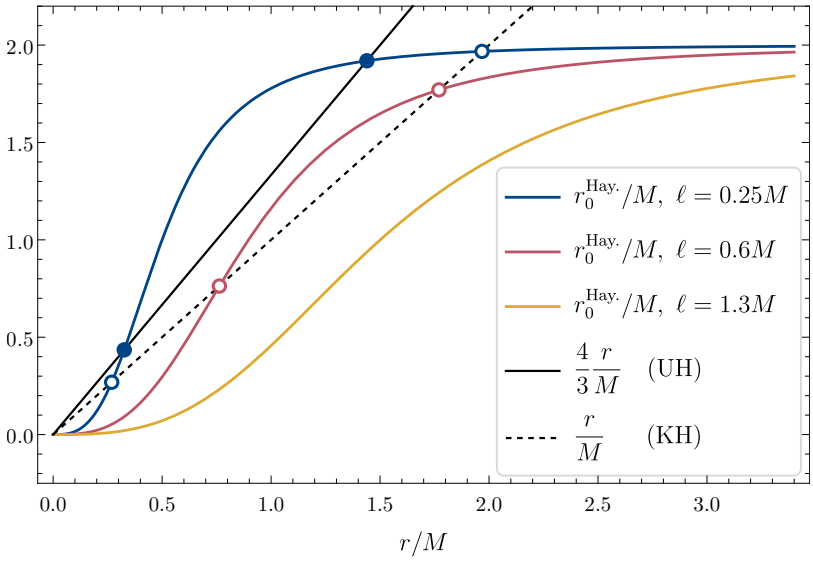

Figure 25: Plot of Hayward's choice of $r_0(r)$ for three values of the parameter ℓ. Intersections with the straight (dashed) black line correspond to UHs (KHs) in the minimal theory $\alpha = \beta = 0$.

both $u_\mu \chi^\mu$ and f are positive at infinity, hence the lapse can reach zero only in a region in which $f(r)$ is negative — i. e. in what in GR would be a trapped region.

Moreover, since in both cases $f(r)$ becomes positive again — at $r = 0$ in the simply connected case and at $r = -\infty$ in the multiply connected case — KHs *as well as* UHs generically come in pairs.

Thus, RBH geometries typically exhibit a nested structures of KHs and UHs. In the following subsections we will describe this structure in detail for the specific examples that we are exploring, but the above considerations can be proven to be general by exploiting the notion of the degree of a map. Moreover, in subsection 10.8.2 we present an alternative, local characterisation of UHs in terms of the expansions of two congruences, in a language that makes contact with [100].

10.4.1 *Horizons — Simply connected regularisation*

We start by setting $\beta = 0$, for simplicity. KHs are given by $r = r_0(r)$ and UHs by $4r/3 = r_0(r)$. Whether these equations admit solutions or not is a model-dependent question. When $r_0(r)$ is that of Hayward, eq. (315), for example, the answer depends on the value of the parameter ℓ.

As an illustration, in figure 25 we plot Hayward's $r_0(r)$ for three values of ℓ; the plot also reports two straight lines, with slope equal to one (dashed line) and 4/3 (solid line) respectively: the intersections of $r_0(r)$ with these lines determine the horizons. When ℓ is small, we can count two intersections with the dashed line and two with the solid one. Hence, this configuration presents two KHs and two UHs;

coming from infinity, they are met in the following order: outer KH, outer UH, inner UH, inner KH. As ℓ is increased, the curve relative to $r_0(r)$ moves towards the bottom-left corner of the picture: inner and outer horizons thus approach each other. They keep approaching until the two UHs merge into a single, degenerate UH; this happens at a threshold value of $\ell = M/2$ above which no UH exist. Similarly, the KHs keep approaching until they merge into a degenerate KH and then disappear: this second threshold corresponds to a higher value of $\ell_* = 4M/(3\sqrt{3})$ — cf. section 3.2.

Therefore, we can distinguish three qualitatively different regimes: a RBH regime, characterised by an inner/outer UH pair (as well as an inner/outer KH pair); an intermediate regime in which there are two KHs but no UHs; and a star-like regime with no horizons. Although technically a BH is present only in the first regime, an object in the intermediate regime would still appear "almost black", given that low energy modes would linger for an extremely long time at the KH before being able to escape to infinity.

Reinstating the parameter β does not greatly distort this picture, since its only effect is that of displacing the KHs. Eq. (304) remains valid upon replacing r_0 with $r_0(r)$, so increasing the value of β shifts the outer KH outwards. The inner KH, instead, moves inwards. That is, increasing β has the effect of pushing KHs further apart; this is the opposite effect one has by increasing the regularisation parameter ℓ, which instead pushes KHs closer together. The location of UHs is unaffected by β.

In the BH regime, the UHs each have a surface gravity. Plugging eq. (310) in the definition eq. (302), we get

$$\kappa^{\text{SC}}_{\text{UH}} = \left.\frac{4 - 3r_0'(r)}{3\sqrt{6}r_0\sqrt{1-\beta}}\right|_{UH}, \tag{320}$$

which should be evaluated at each of the UHs. Note that when $r_0' = 0$ we recover the result for the singular solution eq. (303).

In the BH and in the intermediate regime, the horizon radii provide an intuitive way of telling the "size" of the compact object. It would be useful to extend this notion to the star-like regime by defining an appropriate effective radius. A particularly simple choice is to pick the unique $r_\star$ for which $f'(r_\star) = 0$. This is the radius of maximum (metric) redshift and thus quantifies the compactness of the star. Moreover, in the limit in which ℓ approaches (from above) the threshold value for the KH's formation, $r_\star$ approaches the (degenerate) horizon radius.

Explicitly, we have

$$f'_{\text{SC}} = -\left(\frac{r_0}{r}\right)'\left[1 + 4\frac{27}{256}\frac{\beta}{1-\beta}\left(\frac{r_0}{r}\right)\right], \tag{321}$$

hence $f'_{\rm SC} = 0$ reduces to

$$r_0(r) - r\, r_0'(r) = 0\,, \tag{322}$$

independently on β. For Hayward's choice, we find

$$r_\star = \left(4M\ell^2\right)^{1/3}\,. \tag{323}$$

10.4.2 *Horizons — Multiply connected regularisation*

As in the previous case, the existence and location of horizons is, strictly speaking, a model-dependent question. In the simple example that we are considering, the answer is determined by the only free parameter ℓ. The discussion becomes particularly simple if one resorts to $\varrho = \sqrt{r^2 + \ell^2}$.

KHs are solutions of

$$\varrho^3(\varrho - r_0) - \left[\frac{27}{56}\frac{\beta}{1-\beta} r_0^4\right] = 0\,, \tag{324}$$

which is formally the same as eq. (304). Call $\varrho_{\rm KH}$ the (unique) solution; in the r coordinates, this corresponds to

$$r_{\rm KH}^2 = \varrho_{\rm KH}^2 - \ell^2\,. \tag{325}$$

Hence, for $\ell < \varrho_{\rm KH}$ the spacetime has one KH per each universe, located at $r = \pm r_{\rm KH}$ with $r_{\rm KH} = \sqrt{\varrho_{\rm KH}^2 - \ell^2}$; when instead $\ell > \varrho_{\rm KH}$ the spacetime has no KHs; the limiting case $\ell = \varrho_{\rm KH}$ corresponds to the two horizons coinciding with the wormhole throat, which in this case is null. Similarly to the simply connected configuration, one can easily check that increasing ℓ makes the KH shrink, while increasing β makes it larger.

For what concerns the UHs, instead, they are located at

$$\varrho_{\rm UH} = \frac{3}{4} r_0\,. \tag{326}$$

That is, when $\ell < 3r_0/4$ there is one UH per each universe, located at $r = \pm r_{\rm UH}$ with $r_{\rm UH} = \sqrt{\varrho_{\rm UH}^2 - \ell^2}$; when instead $\ell > 3r_0/4$ there are no UHs. As before, the equality corresponds to a degenerate case for which the throat of the wormhole coincides with the UH. Analogously to the previous case, increasing ℓ makes the UH shrink while β has no effect at all; note that $r_{\rm UH} < r_{\rm KH}$.

The surface gravity of the UH has a particularly simple form:

$$\kappa_{\rm UH} = \kappa_{\rm UH}^{\rm sing.} \sqrt{1 - \frac{\ell^2}{\varrho_{\rm UH}^2}}\,, \tag{327}$$

where $\kappa_{\rm UH}^{\rm sing.}$ is the surface gravity for the singular solution written in eq. (303). Thus, for $\ell = \varrho_{\rm UH} = 3r_0/4$ the UH is "degenerate" and the BH is extremal, in the sense that its UH's surface gravity vanishes.

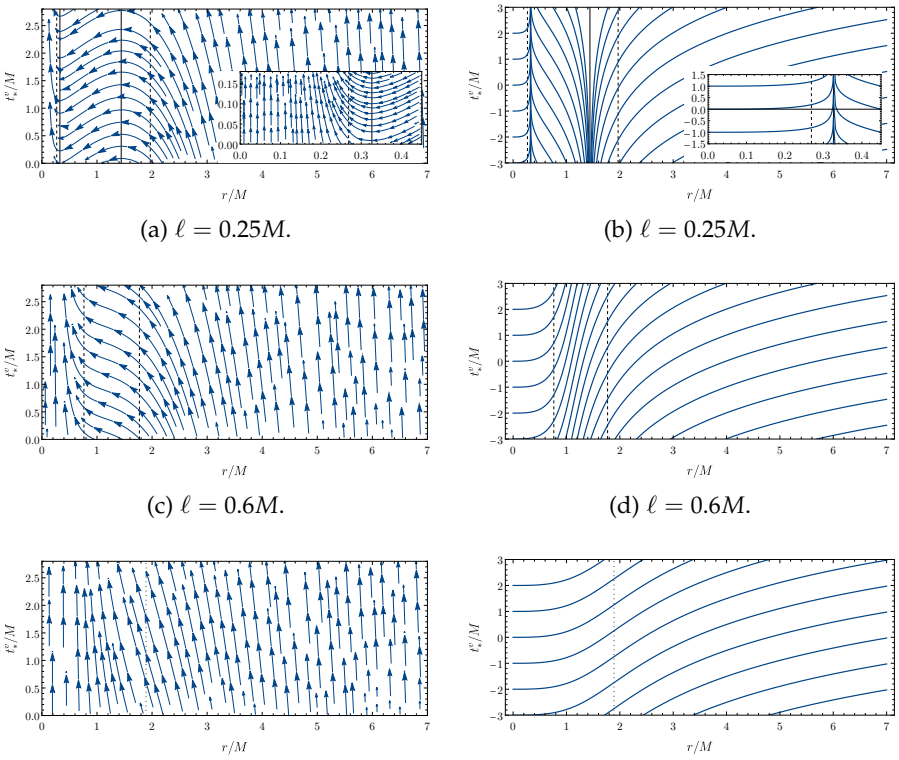

(a) $\ell = 0.25M$. (b) $\ell = 0.25M$.

(c) $\ell = 0.6M$. (d) $\ell = 0.6M$.

(e) $\ell = 1.3M$. (f) $\ell = 1.3M$.

Figure 26: Hayward RBH: æther flow (left) and constant-khronon surfaces (right). Black solid lines mark UHs, dashed lines KHs; the dotted line signals the star's effective radius. The first row depicts the case with outer and inner KHs and UHs, the middle row the case with only two KHs, the bottom row the case of an ultracompact, horizonless, object. The insets are a zoom-in to the small-r region.

10.5 CAUSAL STRUCTURE

We repeat the analysis of subsection 10.2.2.1 for both the simply and multiply connected regularisations.

10.5.1 *Causal structure — Simply connected regularisation*

The causal structure corresponding to the Hayward-like regularisation is summarised in figure 26. Each row corresponds to a different value of ℓ and therefore to a different regime: the top row represents a RBH, the second row the intermediate regime and the third row the star-like regime.

In the outer regions, these pictures are analogous to those in figure 24: at infinity the æther is aligned with the Killing vector and it tilts inwards as one moves to smaller r; then it becomes horizontal at the outer UH, where the familiar peeling structure appears.

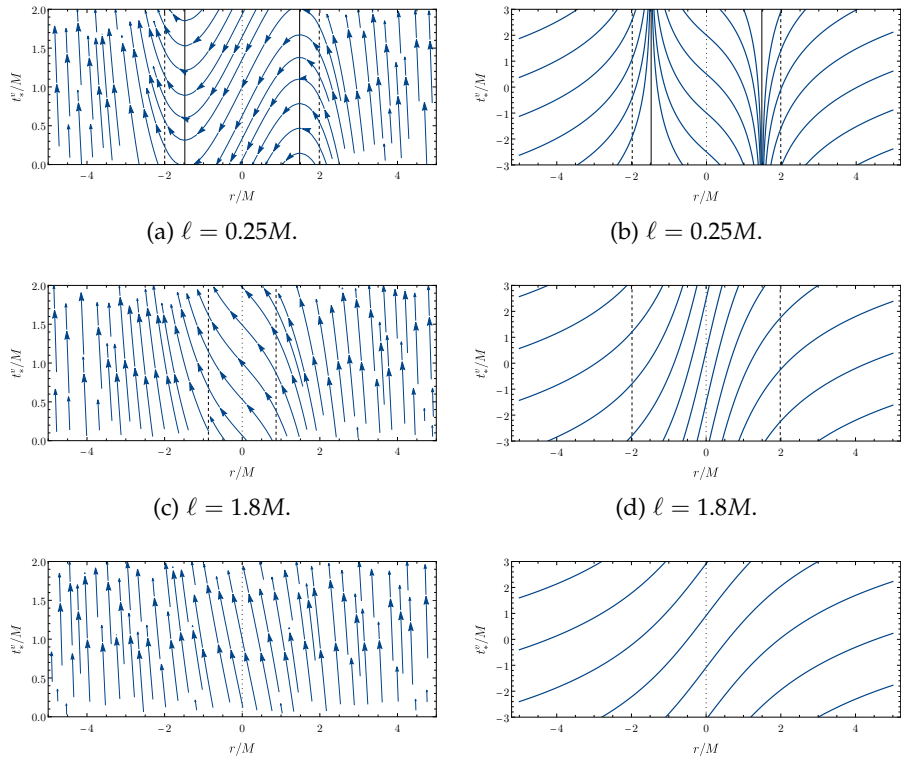

(a) $\ell = 0.25M$. (b) $\ell = 0.25M$.

(c) $\ell = 1.8M$. (d) $\ell = 1.8M$.

(e) $\ell = 2.5M$. (f) $\ell = 2.5M$.

Figure 27: Black bounce: æther flow (left) and constant-khronon surfaces (right). Black solid lines mark UHs, dashed lines KHs; the dotted line signals the throat. The first row depicts a black bounce with a UH and a KH per side, the second row represents a configuration with just one with KHs per side but no UHs, the third row portraits a naked (without horizons) traversable wormhole.

Inside the UH, the æther flows in the opposite direction with respect to the Killing vector until it becomes horizontal again at the inner UH. Correspondingly, the constant-khronon lines pile up exponentially — as null rays would do at an inner trapping horizon.

Inside the inner UH the æther points again in the same direction as the Killing vector. Close to $r = 0$, the flow becomes identical to that of large r, i. e. to that of flat space.

Nothing remarkable takes place at the either of the KHs.

10.5.2 *Causal structure — Multiply connected regularisation*

The æther flow and constant-khronon lines for the black-bounce-like regularisation are displayed in figure 27. As before, each row corresponds to a different regime: the first to a black bounce with UHs, the second to one with KHs but no UHs and the third to one without horizons.

The æther, which is aligned with the Killing vector at infinity, tilts inwards as one moves closer to $r = 0$. At the UH it becomes horizontal, it flows in the opposite direction until it becomes horizontal again at the UH in the other universe and then returns aligned with the Killing vector at $r = -\infty$. The constant-khronon curves pile off the UH in our universe and pile up at the UH in the other universe. Note that the KHs and the throat look like any other location to the æther.

10.6 EFFECTIVE SOURCES

Having described the structure of the regularisations we presented, we now wish to understand the extent to which they deviate from the vacuum of the infrared theory. As customary, we will do so by plugging the regular metrics (and æther) into khronometric theory's equations of motion.

Not surprisingly, we will find that such effective sources are sizeable only in the proximity of the would-be singularity and decay very rapidly as one moves to larger radii. For all practical purposes, therefore, the spacetime surrounding our regular objects can be considered vacuum and their phenomenology can thus be studied using standard low-energy physics.

Let us start by noticing that the equation of motion for the khronon eq. (289) can be written as

$$NJ = 0 \quad \text{with} \quad J = \left[\nabla_\mu \mathcal{A}^\mu - a_\mu \mathcal{A}^\mu\right] . \tag{328}$$

The lapse N can be chosen (almost) arbitrarily, since it depends on how the khronon is parametrised; the scalar quantity J instead only depends on the æther and can be computed unequivocally. Thus, four our purposes J will serve as the khronon's effective source.

Similar considerations hold for the Einstein's equations eq. (288). Since the components of $\mathcal{G}_{\mu\nu}$ clearly depend on the choice of coordinates, one first needs to find a coordinate-independent way of characterising the source. One way to achieve this goal would be to compute its eigenvalues, which are scalars under general coordinate transformations. When the eigenvalues are real, they can be interpreted as energy density and principal pressures of some non-perfect fluid. Unfortunately, while this characterisation works for the Einstein's tensor, it fails for the stress-energy tensor of the æther, since there are regions in the spacetime where the eigenvalues are complex (i. e. the æther's stress-energy tensor is of Type IV in the Hawking–Ellis classification [184]).

However, since in the framework of Hořava gravity there exists a preferred foliation and therefore a preferred observer, it makes sense

to characterise the effective sources as measured by such observer. Hence, we compute the projection

$$\varepsilon^{(u)} = \mathcal{G}_{\mu\nu} u^\mu u^\nu \,, \tag{329}$$

which we could interpret as the energy density measured by an observer that is comoving with the æther. We then pick another vector s_μ that is spacelike, outward-pointing, of unit norm and orthogonal to u_μ and use it to define a radial pressure as

$$p^{(s)} = \mathcal{G}_{\mu\nu} s^\mu s^\nu \,. \tag{330}$$

We use

$$s^\mu \partial_\mu = \Upsilon \partial_v + w \partial_r \quad \text{with} \quad w = + \frac{1 + \Upsilon^2 f}{2\Upsilon} \,. \tag{331}$$

Finally, we could define a tangential pressure in an analogous way, or simply as

$$p^\perp = - \mathcal{G}^\theta_{\ \theta} = - \mathcal{G}^\phi_{\ \phi} \,. \tag{332}$$

Since the parameters α, β, λ enter the action as coupling constants, all the scalars that we have just introduced share the same simple structure. Consider $\varepsilon^{(u)}$ as an example: it can be written as

$$\varepsilon^{(u)} = \varepsilon^{(u)}_G + \alpha\, \varepsilon^{(u)}_\alpha + \beta\, \varepsilon^{(u)}_\beta + \lambda\, \varepsilon^{(u)}_\lambda \,. \tag{333}$$

Here, $\varepsilon^{(u)}_G$ derives from the Einstein's tensor while each of $\varepsilon^{(u)}_\alpha$, $\varepsilon^{(u)}_\beta$, $\varepsilon^{(u)}_\lambda$ derives from the operators that appear in the action multiplied respectively by α, β and λ. Clearly, each of them still depends on β (and on ℓ), since the explicit form of the metric and of the æther does; but not on α nor λ. We will use analogous notations for the decompositions of $p^{(s)}$, $p^\perp$ and J, with the only difference that J has no "J_G part". One can check that $p^{(s)}_\alpha = - p^\perp_\alpha$ in all the cases that we consider.

A remark is in order, at this point. The singular geometry presented in eqs. (295) and (297) is a solution of the equations of motion only for $\alpha = 0$. Indeed, as will be made explicit in the next two subsections, the effective sources proportional to α generically do not vanish — not even in the limit $\ell \to 0$, in which the singular geometry is retrieved. Hence, one might worry that allowing $\alpha \neq 0$ in the analysis of the non-singular configurations is not consistent.

Here, however, we choose to keep $\alpha \neq 0$. The reason is that, in the absence of some custodial symmetry that protects it against running, the higher-order operators in the action of Hořava gravity will generically affect the value of α (as well as that of β and λ) at the level of the effective field theory. Hence, we cannot presume it to be zero at this stage.

Still, at low energies, the effect of higher-order operators is negligible and the value of α is the one set by (low-energy) observations:

$\alpha \lesssim \mathcal{O}(10^{-4})$ — cf. section 10.2. One should bear in mind, therefore, that at large distances the effective sources proportional to α are *highly* suppressed.

10.6.1 *Effective sources — Simply connected regularisation*

Here, we remain agnostic on the specific choice of $r_0(r)$ for as long as possible; however, the explicit results are often cumbersome and not particularly enlightening. For this reason, we specialise to Hayward's choice and discuss, in particular, the asymptotic behaviour of the effective sources.

KHRONON'S EQUATION One finds that $J_\beta = J_\lambda$; clearly, these are zero when $\ell = 0$. J_α instead is non-zero even in the limit in which the regularisation parameter vanishes, since the singular solution we started with is an exact (vacuum) solution only for $\alpha = 0$. The explicit expressions are not particularly enlightening and we hence omit them here. We can however get useful insights by looking at their asymptotic behaviour.

At infinity, we find

$$\begin{aligned} J &= \alpha\, J_\alpha + (\beta+\lambda) J_{\beta,\lambda} \\ &= \alpha \left[-6\sqrt{3} \sqrt{\frac{1}{1-\beta}} \frac{M^4}{r^5} + \mathcal{O}\left(r^{-6}\right) \right] \\ &\quad + (\beta+\lambda) \left[540\sqrt{3} \sqrt{\frac{1}{1-\beta}} \frac{M^3 \ell^2}{r^6} + \mathcal{O}\left(r^{-7}\right) \right] . \end{aligned} \tag{334}$$

The different scaling between J_α and $J_{\beta,\lambda}$ is not surprising, since the former does not vanish in the $\ell \to 0$ limit — as previously argued. In any case, it is easy to see from the above expression that the effective source vanishes rapidly as one moves away from the object.

The sources may be large at intermediate radii, but become very small in the opposite limit, small r, and vanish exactly at $r = 0$. Indeed, expanding around this point, we find

$$\begin{aligned} J &= \alpha \left[\frac{27\sqrt{3}}{4} \sqrt{\frac{1}{1-\beta}} \frac{r^5}{\ell^6} + \mathcal{O}\left(r^6\right) \right] \\ &\quad + (\beta+\lambda) \left[27\sqrt{3} \sqrt{\frac{1}{1-\beta}} \frac{r^3}{\ell^4} + \mathcal{O}\left(r^4\right) \right] . \end{aligned} \tag{335}$$

Hence, the connected non-singular configuration is almost a solution of khronometric theory at very large and very small distances from the centre.

EINSTEIN'S EQUATIONS Plugging in the general form of eqs. (309) and (310), we find a series of additional identities:

$$\varepsilon_G^{(u)} = -p_G^{(s)}\,, \tag{336a}$$

$$p_\lambda^\perp = p_\lambda^{(s)}\,, \tag{336b}$$

$$\varepsilon_G^{(u)} + \beta\varepsilon_\beta^{(u)} = \frac{r_0'}{r^2} + \beta\varepsilon_\lambda^{(u)}\,, \tag{336c}$$

$$p_G^{(s)} + \beta p_\beta^{(s)} = -\frac{r_0'}{r^2} + \beta p_\lambda^{(s)}\,, \tag{336d}$$

$$p_G^\perp + \beta p_\beta^\perp = -\frac{r_0''}{2r} + \beta p_\lambda^\perp \tag{336e}$$

Hence, we can write

$$\varepsilon^{(u)} = \frac{r_0'}{r^2} + (\beta+\lambda)\frac{27r_0^2}{128(1-\beta)}\left[\frac{r_0'}{r^2}\right]^2 + \alpha\,\varepsilon_\alpha^{(u)}\,, \tag{337a}$$

$$p^{(s)} = -\frac{r_0'}{r^2} - (\beta+\lambda)\frac{27r_0^2}{128(1-\beta)r^5}\left[2r(r_0')^2 + r_0(rr_0'' - 2r_0')\right] + \alpha\,p_\alpha^{(s)}\,, \tag{337b}$$

$$p^\perp = -\frac{r_0''}{2r} - (\beta+\lambda)\frac{27r_0^2}{128(1-\beta)r^5}\left[2r(r_0')^2 + r_0(rr_0'' - 2r_0')\right] - \alpha\,p_\alpha^{(s)}\,. \tag{337c}$$

The expressions of $\varepsilon_\alpha^{(u)}$ and $p_\alpha^{(s)}$ are slightly more involved and we omit them here.

Focusing on Hayward's choice, we can read off the asymptotic behaviours. At large r we have

$$\varepsilon^{(u)} = \left[\frac{12M^2\ell^2}{r^6} + \mathcal{O}\left(r^{-9}\right)\right] + (\beta+\lambda)\left[\frac{243M^6\ell^4}{2(1-\beta)r^{12}} + \mathcal{O}\left(r^{-15}\right)\right] + \alpha\left[\frac{M^2}{2r^4} + \mathcal{O}\left(r^{-5}\right)\right]\,, \tag{338a}$$

$$p^{(s)} = -\left[\frac{12M^2\ell^2}{r^6} + \mathcal{O}\left(r^{-9}\right)\right] + (\beta+\lambda)\left[\frac{243M^5\ell^2}{2(1-\beta)r^9} + \mathcal{O}\left(r^{-12}\right)\right] + \alpha\left[\frac{M^2}{2r^4} + \mathcal{O}\left(r^{-5}\right)\right]\,, \tag{338b}$$

$$p^\perp = \left[\frac{24M^2\ell^2}{r^6} + \mathcal{O}\left(r^{-9}\right)\right] + (\beta+\lambda)\left[\frac{243M^5\ell^2}{2(1-\beta)r^9} + \mathcal{O}\left(r^{-12}\right)\right] - \alpha\left[\frac{M^2}{2r^4} + \mathcal{O}\left(r^{-5}\right)\right]\,. \tag{338c}$$

Clearly, these effective sources display "tails" that extend, in principle, up to infinity; the tails however decrease very rapidly, hence for all practical purposes the spacetime surrounding the object can be considered empty. Further note that, as anticipated, these sources do not vanish in the limit $\ell \to 0$ because of the terms $\propto \alpha$. This is simply due to the fact that the singular configuration is a solution only for $\alpha = 0$.

At $r = 0$, the following expansions hold:

$$\varepsilon^{(u)} = \left[\frac{3}{\ell^2} + \mathcal{O}(r^3)\right] + (\beta+\lambda)\left[\frac{243r^6}{128(1-\beta)\ell^8} + \mathcal{O}(r^7)\right] + \alpha\left[\frac{3}{\ell^2} + \mathcal{O}(r)\right], \tag{339a}$$

$$p^{(s)} = -\left[\frac{3}{\ell^2} + \mathcal{O}(r^3)\right] - (\beta+\lambda)\left[\frac{243r^6}{64(1-\beta)\ell^8} + \mathcal{O}(r^7)\right] + \alpha\left[\frac{r^2}{2\ell^4} + \mathcal{O}(r^3)\right], \tag{339b}$$

$$p^{\perp} = -\left[\frac{3}{\ell^2} + \mathcal{O}(r^3)\right] - (\beta+\lambda)\left[\frac{243r^6}{64(1-\beta)\ell^8} + \mathcal{O}(r^7)\right] - \alpha\left[\frac{r^2}{2\ell^4} + \mathcal{O}(r^3)\right]. \tag{339c}$$

Note that the Einstein's tensor presents a dS form.

Focusing on the minimal theory ($\alpha = \beta = 0$), the analytic expressions become more tractable. We report them for completeness:

$$\varepsilon_G^{(u)} = -p_G^{(s)} = \frac{12M^2\ell^2}{(r^3+12M\ell^2)^2}, \qquad p_G^{\perp} = -\frac{24M^2\ell^2(M\ell^2-r^3)}{(r^3+2M\ell^2)^3}, \tag{340a}$$

$$\varepsilon_\lambda^{(u)} = \frac{243M^6\ell^4r^6}{2(r^3+2M\ell^2)^6}, \qquad p_\lambda^{(s)} = p_\lambda^{\perp} = \frac{243M^5\ell^2r^6(r^3-2M\ell^2)}{2(r^3+2M\ell^2)^6}; \tag{340b}$$

and provide their plots in figure 28.

In order to produce the figures, we exploit a self-similarity property that these functions enjoy: when written in terms of the variable $x = r\left(M\ell^2\right)^{-1/3}$, they only depend on ℓ through a multiplicative factor, which we can remove. Thus, the curves in figure 28 are ℓ-independent: the ℓ-dependence can be reinstated by simply rescaling the axes appropriately.

The location of the horizons in the x coordinate depends markedly on ℓ: for reference, figure 28 reports an illustrative example. It also reports the location of the star's effective radius, which is defined only for $\ell > 4M/(3\sqrt{3})$ but has an otherwise ℓ-independent x-coordinate:

$$r_\star = \left(4M\ell^2\right)^{1/3} \mapsto x_\star = 4^{1/3} \simeq 1.59\,. \tag{341}$$

The fact that $x_\star$ does not depend on the regularisation parameter might sound suspicious, as it seems to suggest that the value of the effective sources at the star's radius is always the same, irrespective of the value of ℓ. Physical intuition would suggest the opposite: the sources corresponding to large stars should be "dilute" with respect

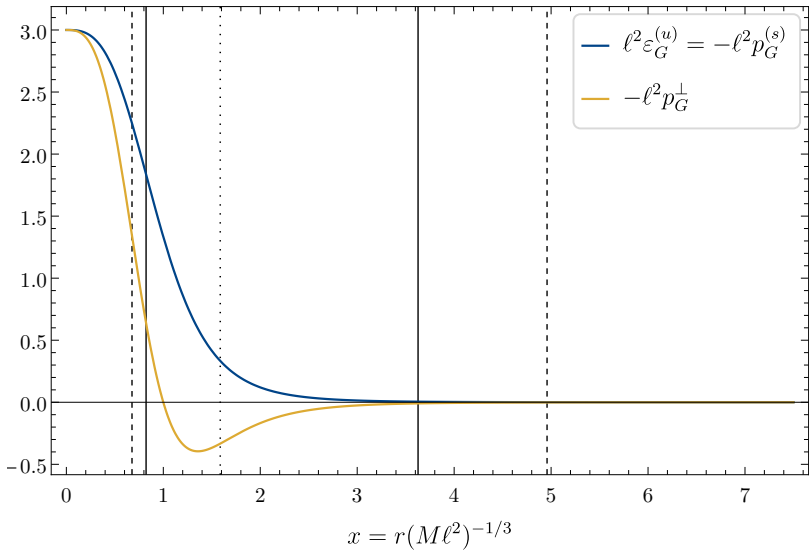

(a) Energy density and principal pressures deriving from the Einstein's tensor.

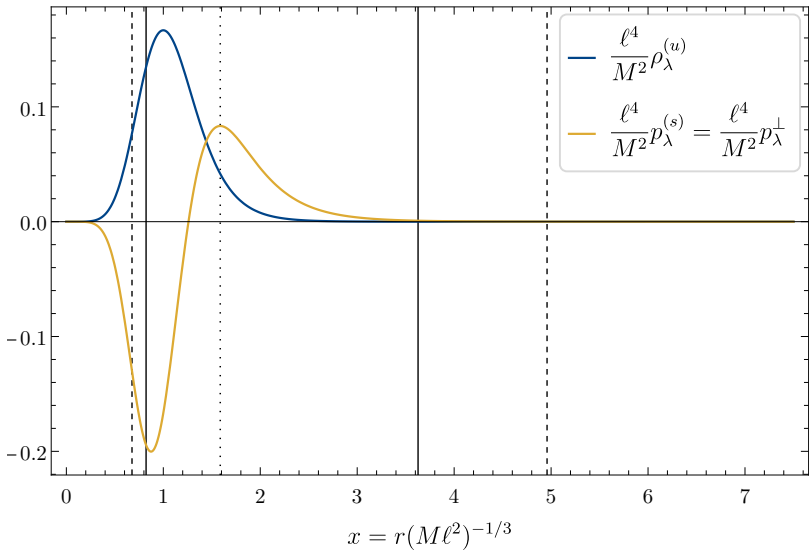

(b) Energy density and principal pressures derived from the æther's SEMT. These curves should be multiplied by λ.

Figure 28: Components of the energy density and the principal pressures, as measured by an observer comoving with the æther, for the Hayward non-singular configuration in the minimal theory $\alpha = \beta = 0$. The position of the horizons in this coordinate strongly depends on ℓ: the vertical black lines mark UH (solid) and KH (dashed) for $\ell = 0.25M$; the dotted line corresponds to the star's effective radius (which coincides with the degenerate KH in the extremal case).

to those of more compact stars. Physical intuition does indeed paint the correct picture: the value of each of the effective sources at the star's radius is given by a constant (of order one in appropriate units)

divided by ℓ^2. So increasing ℓ does suppress the deviations away from vacuum.

Inspecting the figure, we realise that the effective sources are typically negligible at the scale of the outer horizon. They are still small, though less so, at the scale of the star's radius, and become almost zero very rapidly as one moves outwards. We deduce that most of the phenomenologically relevant phenomena involving these non-singular objects take place, for all practical purposes, in vacuum.

10.6.2 *Effective sources — Multiply connected regularisation*

In the multiply connected case, we only analyse the specific example provided by the black bounce spacetime. The analytic expressions are often reasonably compact: when this is the case, we report them in full. However, as in the previous section, we will put the emphasis on the more informative asymptotic behaviours.

KHRONON'S EQUATION We find that $J_\lambda = 0$ identically. This means that, remarkably, the khronon's equation of motion is satisfied in the minimal theory $\alpha = \beta = 0$. For the more general cases, J_α and J_β can be written as

$$J_\alpha = r\left[M\varrho^2 P_5(\varrho) + \ell^2 P_6(\varrho)\right] j_\alpha(\varrho) \tag{342a}$$

$$J_\beta = r\ell^2 j_\beta(\varrho)\,, \tag{342b}$$

where j_α and j_β do not depend on ℓ while $P_5(\varrho)$ and $P_6(\varrho)$ are polynomials of degree five and six, respectively, in ϱ.

At infinity, one finds the following expansions:

$$\begin{aligned} J = {} & \alpha\left[-6\sqrt{3}\sqrt{\frac{\beta}{1-\beta}}\frac{M^4}{\varrho^5} + \mathcal{O}\left(\varrho^{-6}\right)\right] \\ & + \beta\left[12\sqrt{3}\sqrt{\frac{\beta}{1-\beta}}\frac{M^2\ell^2}{\varrho^5} + \mathcal{O}\left(\varrho^{-6}\right)\right], \end{aligned} \tag{343}$$

so even in this case the effective sources go to zero very rapidly.

As the expressions in eq. (342) make explicit, these functions are $\mathcal{O}(r)$ close to $r = 0$, for all nonzero values of ℓ. Note that the limit $\ell \to 0$ is, as expected, singular.

EINSTEIN'S EQUATIONS We find that the term proportional to λ in $\mathcal{G}_{\mu\nu}$ vanishes identically: this means that, in the minimal theory $\alpha = \beta = 0$, the only deviations from vacuum come from the Einstein tensor. In other words

$$\varepsilon_\lambda^{(u)} = p_\lambda^{(s)} = p_\lambda^{\perp} = 0\,. \tag{344}$$

The analytic expression of the effective energy density is

$$\varepsilon^{(u)} = -\frac{\ell^2}{8\varrho^8}\left(8\varrho^4 - 32\varrho^3 M + 27M^4\right) + \alpha\left[M\frac{\varrho^2 M P_4(\varrho) + \ell^2 P_5(\varrho)}{8\varrho^8\left(4\varrho^2 + 4\varrho M + 3M^2\right)}\right], \tag{345}$$

where the P_n are polynomials of degree n in ϱ; note in particular that nothing depends on β — $\varepsilon_G^{(u)}$ and $\varepsilon_\beta^{(u)}$ separately do, but the sum $\varepsilon_G^{(u)} + \beta\varepsilon_\beta^{(u)}$ does not. For the pressures, we find

$$p^{(s)} = -\frac{\ell^2}{8\varrho^8}\left(8\varrho^4 + 27M^4\right) + \alpha\left[\frac{M^2 r^2\left(4\varrho^2 + 6\varrho M + 9M^2\right)^2}{8\varrho^8\left(4\varrho^2 + 4\varrho M + 3M^2\right)}\right], \tag{346a}$$

$$p^{\perp} = \frac{\ell^2(\varrho - M)}{\varrho^5} - \alpha\left[\frac{M^2 r^2\left(4\varrho^2 + 6\varrho M + 9M^2\right)^2}{8\varrho^8\left(4\varrho^2 + 4\varrho M + 3M^2\right)}\right]; \tag{346b}$$

as before, the β-dependence cancels out.

Once again, we focus on the asymptotic behaviour. At infinity

$$\varepsilon^{(u)} = \left[-\frac{\ell^2}{\varrho^4} + \mathcal{O}\left(\varrho^{-5}\right)\right] + \alpha\left[-\frac{M^2}{2\varrho^4} + \mathcal{O}\left(\varrho^{-5}\right)\right], \tag{347a}$$

$$p^{(s)} = -p^{\perp} + \mathcal{O}\left(\varrho^{-5}\right) = \varepsilon^{(u)} + \mathcal{O}\left(\varrho^{-5}\right). \tag{347b}$$

Note that the fall-off rate of the tails is still rather fast. Again, it is easy to see that even for $\ell \to 0$ one does not recover vacuum if $\alpha \neq 0$. As in the previous case this is simply due to the fact that only for $\alpha = 0$ the considered singular BH spacetime is an exact solution of the field equations in vacuum.

At $r = 0$, instead, the values of the sources are nonzero and controlled by the regularisation parameter ℓ:

$$\varepsilon^{(u)} = -\frac{8\ell^4 + 27M^4 - 32\ell^3 M}{8\ell^6} + \alpha\left[\frac{27M^4 - 8M\ell^3}{8\ell^6}\right], \tag{348a}$$

$$p^{(s)} = -\frac{8\ell^4 + 27M^4}{\ell^6}, \tag{348b}$$

$$p^{\perp} = \frac{\ell - M}{\ell^3}. \tag{348c}$$

For symmetry reasons, the throat is an extremal point (either a local minimum or maximum) for these functions.

Finally, we again focus on the minimal theory and provide plots of the nonzero sources. As the analytic expressions make clear, once the coordinate ϱ is employed the dependence on ℓ is trivial, since this parameter only enters as a multiplicative factor. For this reason, we decide to plot, in figure 29, the ℓ-independent part only, as a function

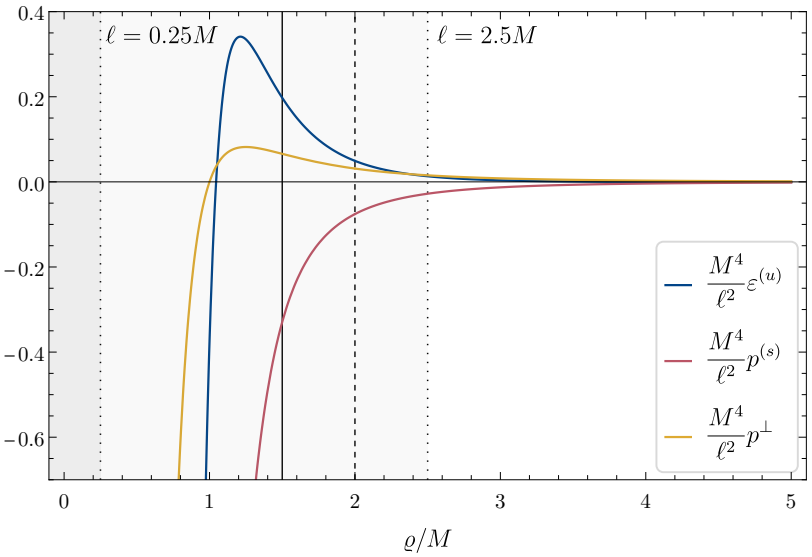

Figure 29: Energy density and principal pressures, as measured by an observer comoving with the æther, for the black-bounce nonsingular metric in the minimal theory $\alpha = \beta = 0$. The black vertical lines mark the UH (solid) and KH (dashed), which may be present or not depending on the value of ℓ. Dotted lines signal the position of the mouth for two choices of ℓ, corresponding to a hidden ($\ell = 0.25M$) and a traversable ($\ell = 2.5M$) wormhole respectively. Recall that, since $\varrho = \sqrt{r^2 + \ell^2}$, the region $\varrho < \ell$ is unphysical and should be removed; for this reason it is shaded.

of ϱ. For reference, dotted lines mark the location of the wormhole mouth for two specific choices of ℓ, corresponding to a hidden and a traversable wormhole respectively.

We remind the reader that, although the plot extends to $\varrho = 0$, $\min(\varrho) = \ell$. Hence, for any given choice ℓ, the region $\varrho < \ell$ does not belong to the spacetime and should therefore be removed: in figure 29 this is rendered by shading. The curves should thus be cut off at $\varrho = \ell$ and joined smoothly with a mirror copy of themselves; moreover, they should be multiplied by ℓ^2.

The upshot of this analysis is that the deviations away from vacuum are sizeable only in a region close to the throat, but decay very fast as one moves away from the object. Therefore, the physics in the surrounding of the black bounce is well described by the equations of vacuum khronometric theory.

10.7 CHAPTER WRAP-UP

In this chapter, the arguments on RBHs presented in the previous parts of the thesis have been specified to the framework of Lorentz-violating gravity and, in particular, to Hořava gravity.

Specifically, since the low-energy version of Hořava gravity admits singular BHs, we have hypothesised that such BHs will be regularised when higher-order corrections are taken into account. Given that searching for regular solutions to the full theory is so far out of reach, we have built regular effective models that capture their key qualitative features. We have then analysed such effective models through the lenses of the low-energy theory.

These models consist of a regular metric and a regular æther field. They belong to either of two classes: simply connected and multiply connected spacetimes. They are remarkably simple and thus the perfect testbed for further inquiries on the phenomenology of Lorentz-violating alternatives to GR.

For instance, modified dispersion relations are known to slow down the mass inflation instability that arises at inner KHs; however, one may wonder whether an analogous instability will develop at an inner UH.

The most obvious follow-up to the discussion presented herein would be the inclusion of rotation. Unfortunately, we are unable to pursue such goal, at the moment, for a very simple reason on which we will elaborate in the following chapter.

Before moving on, we include two appendices that complement the material of this chapter.

10.8 APPENDICES

10.8.1 *Appendix: Optical scalars*

A coordinate-independent way to characterise the æther congruence is through the optical scalars:

$$\text{expansion} \quad \theta = \nabla_\mu u^\mu \,, \tag{349a}$$

$$\text{shear squared} \quad \sigma^2 \quad \text{with} \quad \sigma_{\mu\nu} = \nabla_{(\mu} u_{\nu)} - u_{(\mu} a_{\nu)} - \frac{\theta}{3} P_{\mu\nu} \,, \tag{349b}$$

$$\text{twist squared} \quad \omega^2 \quad \text{with} \quad \omega_{\mu\nu} = \nabla_{[\mu} u_{\nu]} - u_{[\mu} a_{\nu]} \,, \tag{349c}$$

where

$$P_{\mu\nu} = g_{\mu\nu} - u_\mu u_\nu \tag{350}$$

is the projector onto the hypersurfaces orthogonal to the æther.

Other interesting scalars are $u_\mu \chi^\mu$ and $a_\mu \chi^\mu$, as they are associated with properties of the UHs.

Since the æther is hypersurface-orthogonal, Frobenius' theorem implies that the twist vanishes. (Note that $\omega^2 \propto (u_{[\mu} \nabla_\nu u_{\rho]})^2$.) Moreover

$$a_\mu \chi^\nu = \sqrt{-a^2} = y \left(u_\mu \chi^\mu \right)' \,. \tag{351}$$

When evaluated on the Ansatz of eqs. (290) and (291), one finds

$$\theta = y' + y\frac{h'}{h} \tag{352}$$

and a similar, though lengthier, expression for σ^2. All this quantities thus depend algebraically on the functions $f(r)$, $h(r)$, $y(r)$ and their first derivatives, in a way that renders the following statement manifestly true: when $f(r)$, $h(r)$, $y(r)$ are of class $\mathcal{C}^1$ and bounded, all the scalars introduced above are $\mathcal{C}^1$ and bounded. We have computed them explicitly for the singular solution and found that they are ill-behaved at the origin; and then on the simply connected and on the multiply connected non-singular configurations, checking that they are indeed well-behaved everywhere — in particular, at the origin, at the UHs and at the KHs.

10.8.2 *Appendix: 2D expansions*

In order to make contact with the arguments of [100], we complement our analysis with a discussion on the local characterisation of horizons.

We start by considering a closed, spacelike 2-surface $\mathscr{S}^2$. The subspace of the tangent space that is orthogonal to the tangent space of $\mathscr{S}^2$ is spanned by two vectors that can be taken timelike, future-pointing and spacelike, outward-pointing — respectively. In our case, a simple choice for $\mathscr{S}^2$ is any sphere centred at the origin. The two vectors are then the æther and the vector s_μ of eq. (331) used to define the tangential pressure.

The induced metric on $\mathscr{S}^2$ is

$$h_{\mu\nu} = g_{\mu\nu} - u_\mu u_\nu + s_\mu s_\nu \tag{353}$$

and can be used to define the scalars

$$\theta^{(X)} = h^{\mu\nu}\nabla_\mu X_\nu \quad \text{with} \quad X = \{u, s\}\,. \tag{354}$$

These are expansions, but should not be confused with the optical scalar θ, which is defined in terms of a three-dimensional transverse metric. $\theta^{(u)}$ and $\theta^{(s)}$, and in particular their signs, determine whether $\mathscr{S}^2$ is a universal (marginally) trapped surface.

With our Ansätze of eqs. (290) and (291), we have

$$\theta^{(u)} = y\frac{h'}{h} \quad \text{and} \quad \theta^{(s)} = (u_\mu \chi^\mu)\frac{h'}{h}\,. \tag{355}$$

Recall that $y < 0$. Hence, on the singular solution eqs. (295) and (297), $\theta^{(u)}$ is always negative, i. e. the future-directed congruence is always converging, while $\theta^{(s)}$ has the sign of $u_\mu \chi^\mu$. Thus, $u_\mu \chi^\mu = 0$ marks a universal trapping horizon.

Note that both expansions diverge as $r \to 0$, meaning that $r = 0$ is a caustic. Penrose's theorem then implies that this is in fact a singularity, in the sense that the spacetime is not geodesically complete.

On the simply connected configurations of eqs. (309) and (310) we still have that $\theta^{(u)} < 0$ and that $\theta^{(s)}$ has the sign of $u_\mu \chi^\mu$, but we know that in this case $u_\mu \chi^\mu = 0$ has multiple roots and in particular it is positive in a neighbourhood of $r = 0$. Hence there exist multiple universal trapping horizons. Further note that in this case $r = 0$ is not a caustic anymore, since $\theta^{(u)} \to 0$ and $\theta^{(s)} \to 1$ as $r \to 0$.

In the multiply connected configuration the sign of the two expansions depends also on h'/h, which is positive in our universe but negative in the other. I. e. both congruences vanish and change sign at the wormhole mouth $r = 0$.

11

KERR BLACK HOLES IN EINSTEIN–ÆTHER THEORY

Having constructed static and spherically symmetric regular effective models of BHs and exotic ultracompact objects in khronometric theory, the obvious next step would be to investigate their rotating counterparts. Besides being coherent with the reasoning of this thesis, such step is necessary in moving closer to phenomenological applications.

Unfortunately, our best intentions are frustrated by a simple, yet substantial impediment: there are no known rotating BH solutions in khronometric theory. Slowly rotating solutions have been found numerically [37, 38], but extensions to high spins are still lacking. Most importantly, analytical solutions are unexpectedly elusive.

One might still be tempted to apply the NJP to the models presented in the previous chapter, but this would be rather imprudent. Indeed, as we said, the procedure never really has a strong justification, but in its standard uses one could at least gain some confidence by noting that the rotating metrics are very similar to Kerr — which is a solution of GR. Here, instead, vacuum solutions offer no guidance. Moreover, in this context constructing a rotating metric would be useless unless one finds a way to "spin up" the æther too. So, this strategy seems impracticable.

Interestingly, rotating BH solutions are known numerically in the closely related Einstein–æther theory. They were first constructed in the slow rotation regime [39], while the extension to higher spin is recent [7].

Although numerical solutions are not particularly suitable for our purposes, understanding them is nonetheless important. A notable feature of the results of [7] is that, at least in a regime in which the coupling constants are small, the solutions resemble GR BHs with an æther that is "painted" on top of them. However, the BHs of [7] have horizons that are not Killing.

A clear research programme thus seems to be emerging. In order to reach the long-term goal of investigating rotating (and hopefully regular) BH solutions in Hořava gravity, one would probably need to first build regular effective models of rotating BHs in khronometric theory. Reaching this intermediate goal is hindered by the lack of rotating BH solutions in khronometric theory, which are instead known numerically in the closely related Einstein–æther theory. These solutions however exhibit unexpected features that require understanding.

This chapter is a first step in this direction. We begin by noting that there exists a "minimal" corner of Einstein–æther's parameter space in which the Kerr metric is a solution of the equations of motion when complemented with a suitable æther. Then we analyse such solution.

This chapter reports on the first steps in this directions. The results presented here should be considered preliminary as they are subject of ongoing investigation.

11.1 EINSTEIN–ÆTHER THEORY

Einstein–æther theory [200, 204] is a generally covariant theory of gravity in which the metric is coupled to a vector field u^μ, the æther, which is constrained to be everywhere timelike and unit-norm. The æther can therefore never vanish and thus provides a preferred reference frame, in violation of Lorentz symmetry.

This theory is thus closely related to Hořava (and khronometric) gravity. It is however more general, in the sense that it is constructed following the spirit of effective field theories [14, 363]. Up to second order in derivatives, the Lagrangian reads

$$\mathcal{L} = R + \mathcal{L}_{æ} + \zeta \left(g_{\mu\nu} u^\mu u^\nu + 1 \right) , \tag{356}$$

where ζ is a Lagrange multiplier introduced to implement the unit-norm constraint, while the æther Lagrangian can be written as

$$\mathcal{L}_{æ} = -\frac{1}{3} c_\theta \, \theta^2 - c_\sigma \, \sigma^2 - c_\omega \, \omega^2 + c_a \, a^2 , \tag{357}$$

where

$$a_\mu = u^\nu \nabla_\nu u_\mu , \tag{358a}$$
$$\theta = \nabla_\mu u^\mu , \tag{358b}$$
$$\sigma_{\mu\nu} = \nabla_{(\mu} u_{\nu)} + u_{(\mu} a_{\nu)} - \frac{\theta}{3} P_{\mu\nu} , \tag{358c}$$
$$\omega_{\mu\nu} = \nabla_{[\mu} u_{\nu]} + u_{[\mu} a_{\nu]} \tag{358d}$$

are the æther's acceleration, expansion, shear, and twist — respectively. The tensor

$$P_{\mu\nu} = g_{\mu\nu} + u_\mu u_\nu \tag{359}$$

is a projector onto the subspace of the (co)tangent space orthogonal to the æther.

Several other parametrisations of the æther Lagrangian have appeared in the literature; here we follow [203], though we use the opposite signature for the metric: $(-,+,+,+)$ as in the rest of the thesis, but unlike chapter 10.

If the twist vanishes, $\omega_{\mu\nu} = 0$, then by Frobenius theorem the æther is hypersurface orthogonal. The Lagrangian eq. (357) can then

be rewritten as that of khronometric theory eq. (285) — modulo the signature change. Indeed, khronometric theory can be obtained as the limit $c_\omega \to \infty$ of Einstein–æther theory [203].

The couplings c_θ, c_σ, c_ω and c_a are tightly constrained by observations — see e. g. [7, 180] and references therein. In particular, the concomitant detection of the gravitational wave signal GW170817 [125], produced by the coalescence of two neutron stars, and of the gamma ray burst GRB 170817A [124] allowed to constrain the difference between the speed of gravitational waves and that of light to within 10^{-15}; this translates directly into a bound $c_\sigma \lesssim 10^{-15}$.

To date, only two regions of the parameter space have not been ruled out. In the first, c_ω is unconstrained and possibly large, while c_θ and c_a are small and equal up to even smaller corrections. In the second region, *both* c_ω and c_θ can be somewhat large, while c_a is very small. In either case, c_σ is constrained to be so small that it is usually set to zero in computations.

As said, there exist BH solutions in Einstein–æther theory. Spherically symmetric BHs can be found analytically for special values of the couplings [54], one of which was described in subsection 10.2.2; numerical solutions were reported in [36, 150]. The Schwarzschild spacetime with an appropriate æther flow is also a solution of a special class of Einstein–æther gravity [371].

Finding rotating solutions is more challenging. In the phenomenologically relevant sector, with small coupling constants, these solutions are expected to be parametrically "close" to the Kerr spacetime. This expectation is realised in the slow rotation limit [39]; and in the numerical rotating solutions found in [7]. Notably, these solutions exhibit metric horizons that are not Killing horizons.

To better understand the nature of rotating BHs in Einstein–æther theory, we may push this expectation to the extreme and look for solutions in which the metric is *exactly* Kerr. This strategy is motivated by the following remark: if one restricts the theory by setting

$$c_\omega = c_\sigma = c_a = 0\,, \tag{360}$$

i. e. by switching off all couplings except c_θ, then any vacuum solution of general relativity is a solution of this theory too, provided the expansion of the æther vanishes. Hence, in particular, the Kerr metric will be a solution if one can find an æther such that $\nabla_\mu u^\mu = 0$ (and possibly some further constraints). For the purpose of this chapter, we will refer to this restricted version of Einstein–æther theory as the "minimal æ-theory".

11.1.1 *The minimal æ-theory theory*

Setting $c_\omega = c_\sigma = c_a = 0$ is a drastic reduction of arbitrariness. One might wonder, therefore, if the resulting theory is still relevant and

viable. We argue that the answer is in the positive, although further investigation on the matter is required.

The full Einstein–æther theory contains gravitational modes of three kinds: the familiar helicity-2 mode, corresponding to the transverse and traceless part of the metric; a helicity-1 mode; and a helicity-0 mode. Each mode propagates at a speed (c_T, c_V, c_S for the tensor, vector and scalar mode respectively) that can be computed studying linear perturbations around flat spacetime and is set by the couplings of the theory.

A computation along the lines of [198] seemingly yields

$$c_T^2 = 1 \quad \text{and} \quad c_S^2 = 0\,, \tag{361}$$

i. e. the tensor mode moves at the speed of light, while the scalar is "frozen" and does not propagate.

The vector mode instead is non-dynamical and can be gauged away. Roughly speaking, this is a consequence of the fact that, in the minimal theory, the æther only couples through the expansion scalar and the æther's "gauge freedom" is correspondingly enlarged with respect to the non-minimal theory.

The minimal æ-theory is highly reminiscent of what the authors of [163] have called minimal *khronometric* theory — the phenomenologically motivated restriction of khronometric theory whereby (cf. eq. (285)) $\alpha = \beta = 0$. The difference between the two minimal theories is that in the æ-theory the twist coupling c_ω is set to zero, while in the khronometric theory the æther is hypersurface orthogonal and its twist therefore vanishes by construction.

Such minimal khronometric theory has been shown to be indistinguishable from GR in all phenomenological applications so far considered. In particular, in spherically symmetric stars and BHs the khronon is found to have a non-trivial profile and yet not to backreact on the geometry. See the relevant discussion in [163] and references therein.

Hence, our preliminary conclusion is that the minimal æ-theory is motivated and phenomenologically viable, though caution is advised. For the purpose of this chapter, however, the simplifications of the minimal theory are only needed insofar as they render the equations tractable analytically. More generally, one could think of these solutions as the zeroth order of an expansion in the other coupling constants. Thus, the pressing question becomes to understand if the solutions of the full theory *can* in fact be expressed in such a Taylor-series fashion; or, alternatively, if e. g. the limit $c_\omega \to 0$ is continuous on the solutions.

These questions are matter of ongoing investigation.

11.2 THE SOLUTION

Henceforth we focus on the minimal æ-theory and assume the metric is that of Kerr. We choose Boyer–Lindquist coordinates, so that the spacetime's two Killing vectors are

$$\chi^\mu = (1,0,0,0)\,, \tag{362}$$
$$\psi^\mu = (0,0,0,1)\,. \tag{363}$$

Explicitly, the metric reads

$$ds^2 = -\left(1-\frac{2Mr}{\Sigma}\right)\mathrm{d}t^2 - \frac{4Mra\sin^2\theta}{\Sigma}\,\mathrm{d}t\,\mathrm{d}\phi + \frac{\Sigma}{\Delta}\,\mathrm{d}r^2 + \Sigma\,\mathrm{d}\theta^2 + \frac{A\sin^2\theta}{\Sigma}\,\mathrm{d}\phi^2\,, \tag{364}$$

where

$$\Delta = r^2 + a^2 - 2Mr\,, \quad \Sigma = r^2 + a^2\cos^2\theta\,,$$
$$A = (r^2+a^2)^2 - \Delta a^2\sin^2\theta\,. \tag{365}$$

We wish to find an æther whose expansion vanishes:

$$\nabla_\mu u^\mu = 0\,. \tag{366}$$

As argued, this will result in a solution of the minimal æ-theory. We assume that the components of the æther depend on r and θ only, so that u_μ is Lie-dragged along the Killing vectors. Then eq. (366) becomes

$$\partial_r\left(\Delta u_r\right) + \frac{1}{\sin\theta}\,\partial_\theta\left(u_\theta\sin\theta\right) = 0\,. \tag{367}$$

This equation is under-determined. Since separation of variables is possible, one can write a general solution and then constrain it by imposing suitable boundary conditions.

A particularly simple solution is given by

$$u_r = -\frac{M^2\Theta(\theta)}{\Delta}\,, \quad u_\theta = 0\,, \tag{368}$$

where $\Theta(\theta)$ is an arbitrary function. The factor M^2 is purely conventional, while the sign is such that if Θ is taken to be positive then u_r is negative at infinity. Note that, at infinity, $u_r \sim r^{-2}$.

With this æther it is impossible to satisfy the hypersurface-orthogonality constraint $u_{[\mu}\nabla_\nu u_{\rho]} = 0$. This solution therefore exhibits a non-vanishing twist.

We can then solve the unit-norm constraint to express one of the two remaining components in terms of the other. For simplicity, let $u_\phi = 0$, then

$$u_t^2 = \frac{\Sigma\Delta + M^4\Theta^2}{A} \tag{369}$$

and $u_t = \pm\sqrt{u_t^2}$: the minus sign ensures that the æther is aligned with the timelike Killing vector at infinity, as is usually assumed; however, if u_t has a zero somewhere, than it must change sign upon crossing it in order to ensure that the æther be of class $\mathcal{C}^1$.

The full solution thus reads

$$u_\mu = \left(\mp\sqrt{\frac{\Sigma\Delta + M^4\Theta^2}{A}}, -\frac{M^2\Theta}{\Delta}, 0, 0 \right) , \tag{370}$$

or, raising the index,

$$u^\mu = \left(-\frac{A}{\Delta\Sigma}u_t, -\frac{M^2\Theta}{\Sigma}, 0, -\frac{2Mra}{\Delta\Sigma}u_t \right) . \tag{371}$$

Note that the choice $u_\phi = 0$ means that an observer comoving with the æther has zero Killing angular momentum, $u_\mu \psi^\mu = 0$; still, this æther is rotating, in some sense, since $u^\phi \neq 0$. Note that

$$\frac{u^\phi}{u^t} = \frac{2Mra}{A} = \Omega(r) , \tag{372}$$

where $\Omega(r)$ is the angular velocity of frame dragging.

The component u_r appears singular at the Killing horizons, where $\Delta = 0$. As is well known, some components of the metric also appear ill-behaved at those points, but this singularity is merely a coordinate artefact and can be removed by changing coordinates. A coordinate chart in which the æther is manifestly regular at the outer KH is the one provided by ingoing Kerr coordinates, in which the metric is regular at the future Killing horizon. In these coordinates, however, the æther is still singular at the inner horizon; it becomes regular there when expressed in the closely related outgoing Kerr coordinates, which also render the metric regular at the past KH.

A further check that the æther flow is in fact regular consists in computing θ, σ^2, ω^2 and a^2. These quantities completely characterise the flow and, being scalars, do not depend on the particular choice of coordinates. Except for θ, which vanishes by construction, their explicit expressions are rather cumbersome and for this reason we omit them here; however, we have checked that they are finite at $\Delta = 0$.

These scalars do reveal the existence of a singularity, at which they diverge, located at $\Sigma = 0$. This is exactly the location of Kerr's ring-like singularity.

11.3 FIXING $\Theta(\theta)$

The function $\Theta(\theta)$ is arbitrary. Since it was introduced *via* separation of variables, it must not depend on any of the coordinates except for θ; however, it might depend on the spin a.

One might restrict the admissible forms of Θ by demanding that eq. (370) reduces to a known solution in the limit of vanishing spin. In spherical symmetry (and in general whenever the twist vanishes), the minimal æ-theory coincides with the minimal khronometric theory, a solution of which is given by the BH of eqs. (295) and (296), analysed in subsection 10.2.2, with $\beta = 0$.

Demanding that our solution reduces to that of eqs. (295) and (296) amounts to

$$\lim_{a\to 0} M^2\Theta(\theta) = r_{æ}^2 \,. \tag{373}$$

We remind the reader that, in the spherical solution, $r_{æ}$ is an integration constant, whose value had to satisfy an inequality in order for the æther to be real-valued; in particular, when its value is fine tuned to be proportional to the mass, the spacetime contains a UH.

In the rotating case, too, u_t^2 in eq. (369) could become negative despite being a square, thus rendering u_t complex. This may happen for $r > 0$, as we will discuss at length momentarily. Moreover, it will *necessarily* happen for $r < 0$, since there exists a domain in which the denominator A is negative while the numerator remains positive.

The region $r < 0$ corresponds to a portion of spacetime which one is forced to include when analytically extending past Kerr's ring singularity. Since $\psi_\mu \psi^\mu = A \sin^2\theta/\Sigma$, such region is associated to the existence of closed timelike curves. Thus, the fact that the æther cannot be real-valued there constitutes a natural motivation for discarding the entire negative-r region. This result, though somewhat serendipitous, agrees with the expectation that theories with a preferred time direction should not admit closed causal curves.

Coming back to the $r > 0$ region, we may ensure that $u_t^2 \geq 0$ by demanding that $\Theta(\theta)$ satisfies a certain bound, in complete analogy with the spherically symmetric case. Namely, we need

$$\min(M^4\Theta^2) \geq -\min(\Delta\Sigma) \,. \tag{374}$$

Remarkably, this bound is satisfied by the trivial choice

$$M^2\Theta = r_{æ}^2 \,, \tag{375}$$

if $r_{æ}$ satisfies the corresponding bound for the spherically symmetric case. When in particular $r_{æ} = 27^{1/4}M/2$, the zero-spin limit has a UH while $a \neq 0$ implies $u_t^2 > 0$ for all r. That is, the UH in this case is an "accident" of spherical symmetry.

However, we wish to consider a different choice — admittedly a more complicated but arguably more interesting one. A graphical inspection of the function $\Delta\Sigma$ reveals a Mexican-hat-like shape: at any given θ, the function has a minimum in the radial direction located at one of the roots of the cubic equation

$$\partial_r(\Delta\Sigma) = 0 \,. \tag{376}$$

The root corresponding to the minimum, which we will call $r_{\rm PT}$, is a continuous function of θ (actually, of $a^2\cos^2\theta$). Henceforth, we will use the subscript "PT" to indicate that a quantity is evaluated at $r = r_{\rm PT}(\theta)$ — the meaning of the acronym will become clear in due time.

We thus propose to choose

$$M^2\Theta = \sqrt{-\Sigma_{\rm PT}\Delta_{\rm PT}}\,. \tag{377}$$

In this way, $(\Sigma\Delta + M^4\Theta^2)_{\rm PT} = 0$ and therefore $(u_\mu\chi^\mu)_{\rm PT} = 0$.

Incidentally, note that

$$[\nabla_\mu(\Sigma\Delta + M^4\Theta)]_{\rm PT} = 0 \quad \text{but} \quad [\nabla_\mu(u_\nu\chi^\nu)]_{\rm PT} \neq 0\,. \tag{378}$$

11.4 INTERPRETING THE "PT" SURFACE

As mentioned in subsection 10.2.1, in theories with a preferred foliation, such as Hořava gravity, the condition

$$u_\mu\chi^\mu = 0 \tag{379}$$

locally characterises a UH.

In general, Einstein–æther is *not* endowed with a preferred foliation, but merely with a preferred threading, i. e. a preferred time direction. Indeed, the solution we are focusing on displays a non-vanishing twist and is therefore not hypersurface orthogonal.

Still, even in Einstein–æther theory one can envisage non-linear dispersion relations of the form of eq. (286). Hence, in order to salvage the concept of BH, UHs ought to exist in this context too. Whether the condition eq. (379) remains a meaningful characterisation of UHs in the absence of hypersurface orthogonality, however, is far from clear.

An argument in favour of eq. (379) relies, once again, on studying the behaviour of two-dimensional expansions, in line with subsection 10.8.2 and [100]. Consider a unit spacelike vector s_μ, orthogonal to u_μ and such that its integral curves are purely radial and "outgoing" at infinity. Explicitly

$$s_\mu = \left(-u_r\sqrt{-\frac{g^{rr}}{g^{tt}}}, -u_t\sqrt{-\frac{g^{tt}}{g^{rr}}}, 0, 0\right)\,. \tag{380}$$

The quantity

$$\theta^{(s)} = (g^{\mu\nu} + u^\mu u^\nu - s^\mu s^\nu)\,\nabla_\mu s_\nu \tag{381}$$

measures the rate of change, along s_μ, of the cross-sectional area of the two-surfaces that are orthogonal to both u_μ and s_μ. When $\theta^{(s)} < 0$, these surfaces are "trapped", since they shrink as one moves "outwards" in the æther frame. Hence, $\theta^{(s)} = 0$ is an alternative local characterisation of the UH which seems not to rely on hypersurface orthogonality, at least explicitly.

For any circular metric [190] and for any æther flow such that $u_\theta = u_\phi = 0$, we have

$$\theta^{(s)} = -(u_\mu \chi^\mu) \frac{\partial_r \sqrt{g_{\theta\theta} g_{\phi\phi}}}{\sqrt{-g}}\,, \tag{382}$$

so the zeroes of $\theta^{(s)}$ coincide with those of $u_\mu \chi^\mu$. The surface $r = r_{\rm PT}(\theta)$ thus seems a good candidate for a UH.

This interpretation is strengthened by inspecting the slowly rotating limit: eq. (376) gives

$$r_{\rm PT} = \frac{3}{2} M + \mathcal{O}(a^2) \tag{383}$$

and

$$u_\mu = \left(\mp \sqrt{1 - \frac{2M}{r} + \frac{27}{16} \frac{M^4}{r^4}}, -\frac{3\sqrt{3} M^2}{r(r-2M)}, 0, 0 \right) + \mathcal{O}(a^2)\,, \tag{384}$$

which coincide with the corresponding spherically symmetric analytical solution up to $\mathcal{O}(a^2)$.

A closed-form expression for $r_{\rm PT}(\theta)$ could be found, but since it is not particularly enlightening we omit it here. However, since the radial minimum of $\Delta\Sigma$ must be located where $\Delta < 0$, we can guess that $r_{\rm PT}$ will lie between Kerr's KHs — i. e. in a region that in GR would be trapped. More specifically, since eq. (376) can be written as

$$\Delta_{\rm PT} = -\Sigma_{\rm PT} \frac{r_{\rm PT} - M}{r_{\rm PT}}\,, \tag{385}$$

we deduce that $r_{\rm PT} \geq M$; moreover, yet another rewriting of eq. (376) tells us that

$$r_{\rm PT} = \frac{3}{2} M - a^2 \left(1 + \cos^2\theta \frac{r_{\rm PT} - M}{r_{\rm PT}} \right) \leq \frac{3}{2} M\,. \tag{386}$$

To summarise,

$$M = \lim_{a \to M} r_{\rm PT} < r_{\rm PT} \leq \lim_{a \to 0} r_{\rm PT} = \frac{3}{2} M\,. \tag{387}$$

For arbitrary values of the spin, the surface $r = r_{\rm PT}(\theta)$ acquires a non-trivial dependence on θ which introduces considerable complications. A plot of such surfaces for several values of the spin is presented in figure 30. Differentiating eq. (376) with respect to θ gives

$$\frac{{\rm d}r_{\rm PT}}{{\rm d}\theta} = -\frac{{\rm d}(a^2 \cos^2\theta)}{{\rm d}\theta} \left[\frac{4 r_{\rm PT} (r_{\rm PT} - M)^2 - M \Delta_{\rm PT}}{(r_{\rm PT} - M)^2} \right]\,, \tag{388}$$

which vanishes at $\theta = 0,\ \pi/2,\ \pi$ but is non-zero otherwise. (Note that the quantity in square brackets is positive).

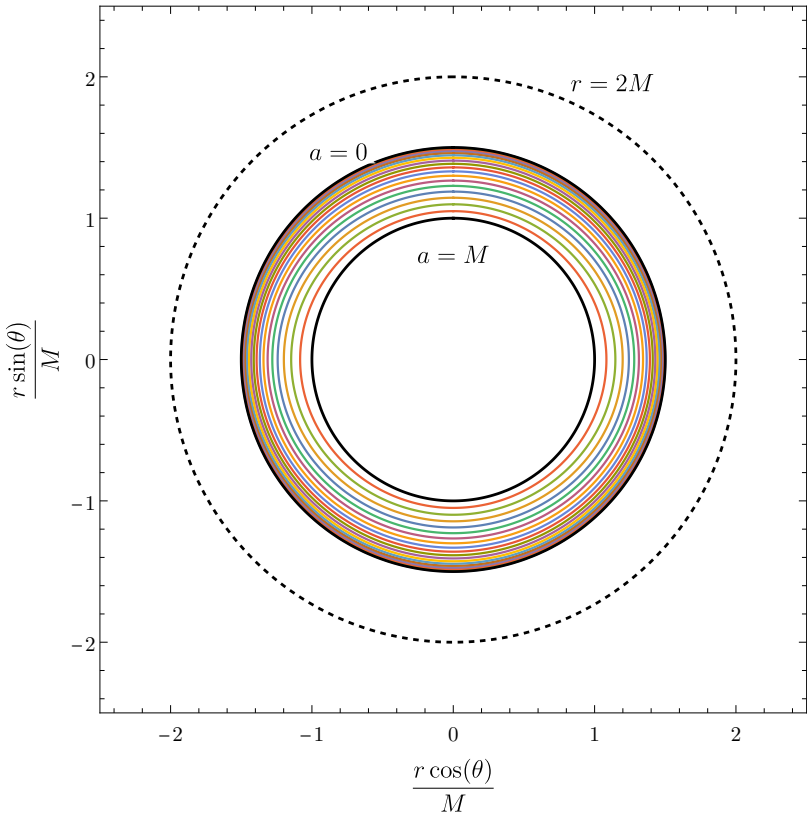

Figure 30: Plots of $r_{\rm PT}(\theta)$ for several values of the spin a. The north pole (south) is the uppermost (lowermost) point of each curve. The dotted line, which is reported for reference, corresponds to $r = 2M$, i.e. to the KH's radius of a Schwarzschild black hole of the same mass as our solution. Note that the curves look circles but, generically, they are not.

Crucially, however, the surface $r = r_{\rm PT}(\theta)$ is *not* orthogonal to the æther: its normal vector $n_\mu = \nabla_\mu(u_\nu\chi^\nu)$ can be written as

$$\begin{aligned} n_\mu &= 2\nabla_{[\mu}u_{\nu]}\chi^\nu \\ &= -\left(a_\nu\chi^\nu\right)u_\mu + \left(u_\nu\chi^\nu\right)a_\mu + 2\omega_{\mu\nu}\chi^\nu \\ &\overset{\rm PT}{=} -\left(a_\nu\chi^\nu\right)u_\mu + 2\omega_{\mu\nu}\chi^\nu\,. \end{aligned} \tag{389}$$

We have checked that $n_\mu n^\mu < 0$, so $r = r_{\rm PT}(\theta)$ is a spacelike hypersurface generated by the two Killing vectors χ^μ and ψ^μ, and by $\rho^\mu = (0, \frac{{\rm d}r_{\rm PT}}{{\rm d}\theta}, 1, 0)$.

Had the æther been hypersurface orthogonal, the normal vector would have been proportional to the æther itself and the proportionality constant could have been interpreted as a surface gravity (up to a conventional normalisation factor). In our case, instead, the normal is misaligned with the æther by an amount that is controlled by the twist.

This strongly suggests that $r = r_{\rm PT}(\theta)$ *cannot be interpreted as a* UH.

Indeed, the hypersurface generated by the integral curves of vectors that are orthogonal to the æther are hypersurfaces of simultaneity with respect to the preferred time. This is true by definition in khronometric theory, and also in Einstein–æther theory — the technical difference being that, in the absence of hypersurface orthogonality, these hypersurfaces do not constitute immersed submanifolds (cf. [359, app. B.3]). Heuristically, we might regard these surfaces as generated by "infinitely fast" trajectories, i. e. as ordinary causal trajectories in the limiting case in which their speed in the preferred frame goes to infinity.

The fact that the surface $r = r_{\mathrm{PT}}(\theta)$ is not one such hypersurface means that causal curves can cross it in both directions.

To better understand why, consider a generic curve $x^\mu(\sigma)$ with associated tangent vector $k^\mu = \mathrm{d}x^\mu/\mathrm{d}\sigma$. Assume that the curve has "infinite speed", in the sense that $u_\mu k^\mu = 0$. With an abuse of terminology, we will refer to it as a trajectory.

The vector s_μ (eq. (380)) can be complemented with

$$\begin{aligned}\left(e_{\hat\theta}\right)^\mu &= \frac{1}{\sqrt{g_{\theta\theta}}}(0,0,1,0) \quad \text{and}\\ \left(e_{\hat\phi}\right)^\mu &= \frac{1}{\sqrt{g_{\phi\phi}}}(0,0,0,1)\end{aligned} \tag{390}$$

to obtain an orthonormal basis of the subspace of the tangent space that is orthogonal to u_μ. Together with u_μ, these three vectors span the whole tangent space. We may thus decompose

$$k_\mu = k_s s_\mu + k_{\hat\theta}\left(e_{\hat\theta}\right)_\mu + k_{\hat\phi}\left(e_{\hat\phi}\right)_\mu , \tag{391}$$

where k_s, $k_{\hat\theta}$, $k_{\hat\phi}$ are given by the scalar product of k^μ with s_μ, $\left(e_{\hat\theta}\right)_\mu$ and $\left(e_{\hat\phi}\right)_\mu$, respectively.

If $k^r \neq 0$, the map $r(\sigma)$ is invertible and r can be used as a coordinate along the trajectory *in lieu* of σ. We may focus on the (t,r)-plane, where the most interesting motion happens, and neglect the angular motion. The trajectory has tangent derivative

$$\frac{\mathrm{d}t}{\mathrm{d}r} = \frac{\mathrm{d}t}{\mathrm{d}\sigma}\frac{\mathrm{d}\sigma}{\mathrm{d}r} = \frac{k^t}{k^r}\,. \tag{392}$$

Specifically, since $\left(e_{\hat\theta}\right)^t = \left(e_{\hat\phi}\right)^t = 0$,

$$\begin{aligned}\frac{k^t}{k^r} &= \frac{k_s s^t}{k_s s^r}\\ &= -\frac{u_r}{u_t}\,;\end{aligned} \tag{393}$$

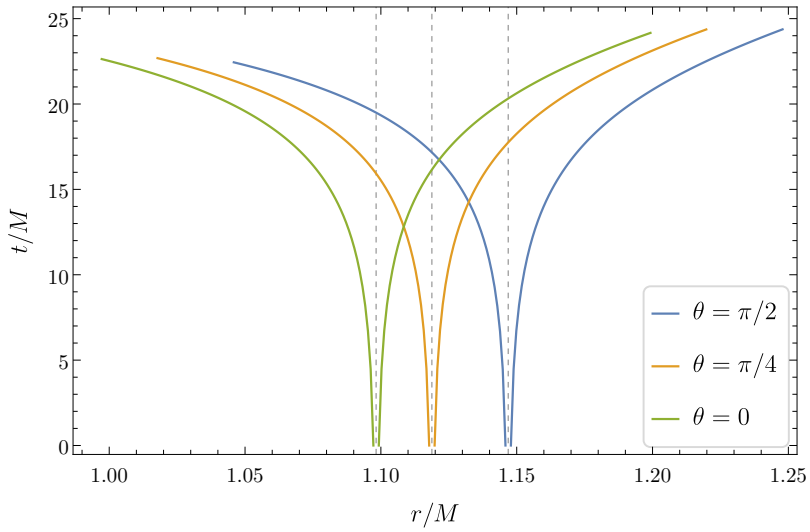

Figure 31: Integral lines of the vector s^μ, at different angles θ. The vertical lines mark $r = r_{\rm PT}(\theta)$. The spin is $a = 0.9M$.

in passing from the first to the second line, we have used the fact that

$$u_\mu s^\mu = 0 \Rightarrow \frac{s^t}{s^r} = -\frac{u_r}{u_t}\,. \tag{394}$$

Hence, the trajectory has an asymptote at $u_t = 0$, which is universal in the sense that it does not depend on k_μ as long as $k^r \neq 0$. In particular, curves starting in the region $u_t > 0$, i. e. at $r < r_{\rm PT}$, can never cross $r = r_{\rm PT}(\theta)$ it in the outward direction.

Figure 31 displays the integral curves of s^μ in the (t, r) plane in the vicinity of $r = r_{\rm PT}$ (since these coordinates are ill-behaved at the KHs, a coordinate change is needed if one wishes to extend these plots beyond those surfaces).

The remaining case $k^r = 0$, corresponds to "particles" moving only in the angular directions. There exist curves that start at $r < r_{\rm PT}$ and, moving only in the direction of $\left(e_{\hat\theta}\right)^\mu$, cross $r = r_{\rm PT}$ outwards. By continuity, it seems possible that there also exist causal curves that similarly exit $r = r_{\rm PT}$.

Let us characterise these instantaneous trajectories. First of all, note that

$$k^r = k_s s^r\,. \tag{395}$$

Since $s^r \propto u_t$, this component can be zero at $r = r_{\rm PT}$ even if $k_s \neq 0$. Leaving this particular case aside, for all $r \neq r_{\rm PT}$ we have that $k^r = 0 \Leftrightarrow k_s = 0$.

Because of the symmetries of the spacetime, there are two constants of the motion, each associated to one of the Killing vectors.[1] The two

1 This point is subtle. These trajectories are not geodesics, so it is not obvious that the Killing vectors generate conserved quantities. In the present case, they do in a sense that is made precise in [129].

quantities are $k_\mu \chi^\mu = k_t = -E$ and $k_\mu \psi^\mu = k_\phi = L$. Note that $k_{\hat{\phi}} = k_\phi / \sqrt{g_{\phi\phi}}$.

Consider in particular the conservation equation for $k_t = -E$:

$$\begin{aligned} -E &= k_s s_t + k_{\hat{\phi}} \left(e_{\hat{\phi}} \right)_\mu \\ &= k_s s_t - L\Omega \,, \end{aligned} \tag{396}$$

where $\Omega = -g_{t\phi}/g_{\phi\phi}$ as above. If we set $k_s = 0$ at some point, since E and L are constant while Ω is a function of θ (and r, which however we assume fixed), the only option is that $L = 0$ and therefore also $E = 0$. But this entails that k_s must vanish everywhere along the curve and therefore the curve can never reach infinity. Moreover, if k_s vanishes, then $k^t = 0$ everywhere too, i. e. this curve never advances in the Killing time.

The upshot of this discussion is that the status of the surface $r = r_{\mathrm{PT}}(\theta)$ is unclear. It is not a UH, yet it exhibits some characteristic features of one. For this reason, and for lack of a better terminology, we have called this surface "PT" as in "partially trapping".

11.5 A NOTE ON THE SURFACE GRAVITY

UHs in globally foliated manifolds seem to emit Hawking radiation in a way similar to horizons in GR. The temperature of such radiation is set by the horizon's surface gravity, defined as

$$-2\kappa_{\mathrm{h.o.}} = (a_\mu \chi^\mu)_{\mathrm{UH}} \tag{397}$$

(the suffix "h.o." stands for "hypersurface-orthogonal"). Since, in that context, UHs are leaves of the preferred foliation, their surface gravity is necessarily constant and a zeroth law of BH mechanics automatically holds.

Clearly, it is not obvious that the surface gravity of a UH with non-vanishing twist — supposing it exists — should be defined in the same way. Indeed, not surprisingly, the quantity $\kappa_{\mathrm{h.o.}}$ computed for our solution is *not* constant on the surface $r = r_{\mathrm{PT}}$.

The decomposition of the normal vector eq. (389) suggests an alternative definition

$$2\kappa_n = \left[\left(\frac{n^\mu}{\sqrt{-n^\alpha n_\alpha}} \right) \nabla_\mu (u_\nu \chi^\nu) \right]_{\mathrm{PT}} = \sqrt{-n^\nu n_\nu}_{\mathrm{PT}} \tag{398}$$

(the suffix "n" now stands for "normal"). Clearly,

$$\kappa_n^2 = \kappa_{\mathrm{h.o.}}^2 - \kappa_\omega^2 \tag{399}$$

where

$$\kappa_\omega^2 = \left[\omega_{\mu\nu} \chi^\nu \omega^\mu{}_\rho \chi^\rho \right]_{\mathrm{PT}} \,. \tag{400}$$

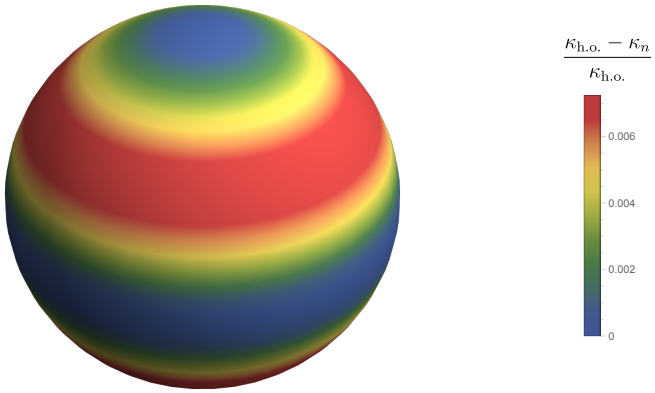

Figure 32: Relative difference of the two definitions of surface gravity, as a function of position on the surface $r = r_{\text{PT}}(\theta)$. The spin is $a = 0.9M$.

In the slowly rotating limit, we find

$$-2\kappa_{\text{h.o.}} = \frac{2}{3M}\sqrt{\frac{2}{3}}\left[1 + \frac{-17 + \cos^2\theta}{27M^2}a^2 + \mathcal{O}\left(a^4\right)\right] \tag{401}$$

$$-2\kappa_n = -2\kappa_{\text{h.o.}} + \mathcal{O}\left(a^4\right), \tag{402}$$

while

$$\kappa_\omega = \mathcal{O}\left(a^2\right). \tag{403}$$

The definition (398) is not constant along $r = r_{\text{PT}}$ either, but it has the advantage of encoding information on the twist in an obvious way. The two definitions coincide at the poles and at the equator, where the twist vanishes. For arbitrary angles, their difference can be computed numerically: though growing with the spin, the relative difference is always $\lesssim 1\%$. An example for $a = 0.9M$ is plotted in figure 32.

11.6 CHAPTER WRAP-UP

In this chapter, he have constructed a solution of a restricted version of Einstein–æther theory that we called minimal æ-theory. The solutions is such that the metric is exactly that of Kerr and the æther has vanishing expansion scalar. The solution has a free function, $\Theta(\theta)$, that only depends on the polar angle. We proposed to fix such free

function in a somewhat involved but consequential way. The resulting æther flow happens to be orthogonal to the Killing vector of staticity at a surface $r = r_{\mathrm{PT}}(\theta)$, which exhibits features characteristic of UHs without being one. Namely, it displays somewhat universal peeling properties.

Admittedly, the preceding discussion has opened up more questions than it has answered. In the present author's view, this is partially due to the fact that the results presented herein are preliminary; and partially a consequence of the relatively unexplored nature of rotating BHs in Lorentz-violating theories of gravity.

Indeed, although Hořava gravity and Einstein–æther theory can hardly be considered *new* proposals, the relevance of some of their implications — particularly in regards to BHs — is just starting to be appreciated. This is not surprising, since the very existence of BHs is, in such theories, serendipitous. It remains to be understood, therefore, to what extent the physics of GR BHs carries over to this context.

12

CONCLUSIONS AND OUTLOOK

The narrative of this thesis revolves around a single unifying theme: the construction of *regular effective models* for describing the dark and compact objects that we observe in the sky and that we call BHs. These models are motivated by the idea that new physics beyond GR will "regularise" spacetime singularities by preventing their formation.

We have been deliberately vague on what such new physics might be. Clearly, however, the most natural candidate is quantum gravity, in any of its many proposed realisations. Thus, the natural context in which this thesis should be collocated is that of quantum gravity phenomenology [8, 10].

Quantum gravity phenomenology is a relatively new framework whereby features that are common to multiple approaches to quantum gravity, e. g. violations of Lorentz invariance, are parametrised and tested. In the author's very partial opinion, this programme is already reshaping the general disposition towards quantum-gravity research.

Figuratively speaking, a pervasive attitude had quantum gravity labelled as *hic sunt dracones*:[1] a remote territory, stretching beyond the borders of current understanding, insidious and perilous to the occasional wanderer; but one whose affairs are ultimately inconsequential to the world's History — since quantum-gravitational effects supposedly become sizeable only at the Planck scale. Thus, in this perspective quantum gravity would easily become a sort of *Arcadia felix*:[2] a mythical land where all the problems and currently open issues in high-energy physics necessarily find their solution. (The two views seem in contradiction but are, in fact, quite coherent.)

The contents of this thesis challenge this point of view, since they demonstrate that it is possible to formulate reasonably precise assumptions concerning the behaviour of quantum gravity and translate them into concrete models whose theoretical consistency and phenomenological viability can then be tested.

Namely, we have argued that if quantum gravity is such that spacetime singularities are regularised in a way that can be captured in terms of pseudo-Riemannian geometry, then gravitational collapse necessarily results in any of a few qualitatively different classes of objects: simply connected RBHs with multiple horizons, simply connec-

1 *Hic sunt dracones* (or *leones*) is a phrase apocryphally attributed to medieval cartographers, who purportedly used it to mark uncharted territories.

2 Arcadia is a popular utopia whose inhabitants live in a perennial state of bliss and harmony with nature. (It is also a region of Greece, whose inhabitants probably face hurdles as all human beings.)

ted horizonless (exotic) compact objects, multiply connected hidden wormholes, and multiply connected naked wormholes.

We reviewed the rationale of such taxonomy, along with other preliminary notions on the topic of spacetime singularities, in chapter 2. In chapter 3, we presented general prescriptions for building metrics that describe simply and multiply connected regular geometries under the assumption of staticity and spherical symmetry; then discussed a common strategy for endowing such models with rotation in chapter 4.

With part ii, we focused on a particular family of multiply connected models known as black bounces. These represent wormholes whose throat may or may not be cloaked by horizons, depending on the value of a parameter ℓ.

In chapter 5, we built the black-bounce analogue of the Kerr metric by applying the NJP to the prototypical static and spherically symmetric black bounce — also known as SV metric. We described the causal structure of the resulting spacetime by investigating the trajectories of null rays and by drawing Carter–Penrose diagrams. Since the spacetime is not a solution of vacuum GR, we characterised the effective matter content in two complementary ways. Finally, we compared this object with a Kerr BH by detailing the extent to which the ergoregion, the light ring and the ISCO differ in the two cases.

In chapter 6 we extended the analysis of the previous chapter by building the black-bounce analogue of the Kerr–Newman spacetime — i. e. by adding an electric charge to the black-bounce–Kerr. We then investigated the ensuing spacetime in a way similar to what had been done for the electrically neutral case. Notably, we proposed a regularised version of the electromagnetic potential and suggested two alternative interpretations for the stress-energy tensor.

In chapter 7 we investigated the phenomenological viability of the black-bounce–Kerr as a Kerr-BH mimicker by studying scalar test-field perturbations. Specifically, we computed the fundamental (massless) QNMs and tracked its variation under changes in the parameter ℓ: in the BH branch, the results, obtained with two independent methods, are in qualitative accord with those of Kerr; in the naked wormhole branch, instead, we found evidence for unstable modes. This lead us to conjecture that rapidly rotating and very compact wormholes might generically be unstable. Finally, we computed the superradiance amplification factors, in both the massless and massive case, and found that they are suppressed by the increase of ℓ.

In chapter 9 we departed from the black-bounce family to consider another generic source of instability: mass inflation. Since the timescale of such instability is set by the inner horizon's surface gravity, we built a simply connected rotating RBH whose inner horizon is engineered so to have vanishing surface gravity and hence avoid mass inflation. This proposal should be considered as a proof of concept

that mass inflation can be quenched even in the presence of rotation; however, this example reiterates the argument that stability is generically an issue for all these effective models.

The upshot of the discussion, up to that point in the thesis, is thus that building regular models that mimic GR BHs is simple *in theory*; however, self consistency and phenomenology heavily constrain possible alternatives. Moreover, these models will generically sport deviations from vacuum GR at scales possibly much larger than the Planck scale — e. g. outside of the horizon, if there is one. Improving the accuracy of horizon-scale observations of astrophysical BHs is therefore of paramount importance.

In order to build models that are even more realistic, however, it will be necessary to go beyond the assumption of stationarity and consider situations that are truly dynamical. In this way, it will become possible to describe e. g. the formation process of such regular objects — a largely unexplored issue.

Note, incidentally, that these models are already being constrained through real observational data. For instance, shadow images, X-ray emission spectra and gravitational-wave inspirals have been used to bound the value of the parameter ℓ in black-bounce–Kerr spacetimes. Although these models were not quite built with this intent, analyses of this kind are extremely informative on the constraining power of current observations.

The thesis then continued with part iii, which is dedicated to putting the discussion on regular effective models in the context of some specific alternative theories of gravity. Namely, we focused on the quantum-gravity motivated Hořava gravity: since its infrared limit admits BH solutions that are singular, we conjectured that these would be regularised in the full theory.

Searching for such regular solutions by solving the theory's equations of motion is out of reach at the moment. For this reason, we resolved to apply the general prescriptions of chapter 3 to build effective regular models in the context of the infrared theory. The difference with respect to the standard case is that Hořava gravity is built in terms of an æther field which specifies a preferred foliation and needs to be regularised together with the metric.

The construction and investigation of these models was carried out in chapter 10. Their overall structure was found to be similar to what one has in metric theories of gravity — a conclusion that is not entirely trivial since KHs do not constitute causal horizons when Lorentz invariance is broken. Rather, the role of event horizons is played by UHs. Notably, the classification in terms of simply and multiply connected geometries remains relevant in this case too.

Logically, the most immediate extension of the results of chapter 10 would be the addition of rotation. However, since no rotating solu-

tion is known in the infrared limit of Hořava gravity, such extension could not be carried out right away. We thus turned our attention to a closely related theory, Einstein–æther gravity, for which rotating BHs have been found numerically. We focused on a narrow corner in the theory's parameter space and investigated, in chapter 11, a solution in which the metric is that of Kerr and the æther has vanishing expansion.

Several questions remain unanswered and deserve further scrutiny. For instance, the analysis of the rotating solution brought to light a possible limit in the usual characterisation of UHs, as this fails to capture cases in which the æther is hypersurface orthogonal: it is not clear that UHs exist in this case, although one would expect they did. More generally, the stability of UHs is far from ascertained in both Einstein–æther and Hořava gravity. Concerning Hořava gravity, in particular, it would be extremely important to check the validity of the conjecture that motivated chapter 10 and understand whether the inclusion of $\mathcal{L}_4$ and $\mathcal{L}_6$ really leads to the regularisation of the singularity. Hopefully, the effective models of chapter 10 will facilitate such investigation.

This last remark, in particular, alludes to what is probably the most ambitious goal of the quantum gravity phenomenology programme: providing guidance to aid the search for a quantum theory of gravity. This question, perhaps the most important of all, remains entirely open.

BIBLIOGRAPHY

[1] Gerard 't Hooft and M. J. G. Veltman. 'One Loop Divergencies in the Theory of Gravitation'. Ann. Inst. H. Poincare Phys. Theor. A **20** (1974), pp. 69–94 (cit. on p. 131).

[2] R. Abbott et al. 'GWTC-2: Compact Binary Coalescences Observed by LIGO and Virgo During the First Half of the Third Observing Run'. Phys. Rev. X **11**.2 (2021), p. 021053. arXiv:2010.14527 (cit. on p. 1).

[3] Ahmadjon Abdujabbarov, Muhammed Amir, Bobomurat Ahmedov and Sushant G. Ghosh. 'Shadow of Rotating Regular Black Holes'. Phys. Rev. D **93**.10 (2016), p. 104004. arXiv:1604.03809 (cit. on p. 41).

[4] Jahed Abedi and Niayesh Afshordi. 'Echoes from the Abyss: A Highly Spinning Black Hole Remnant for the Binary Neutron Star Merger GW170817'. J. Cosmol. Astropart. Phys. **2019**.11 (2019), pp. 010–010. arXiv:1803.10454 (cit. on p. 82).

[5] Jahed Abedi, Niayesh Afshordi, Naritaka Oshita and Qingwen Wang. 'Quantum Black Holes in the Sky'. Universe **6**.3 (2020), p. 43. arXiv:2001.09553 (cit. on p. 82).

[6] Marek A. Abramowicz and P. Chris Fragile. 'Foundations of Black Hole Accretion Disk Theory'. Living Rev. Relativ. **16**.1 (2013), p. 1. arXiv:1104.5499 (cit. on p. 1).

[7] Alexander Adam, Pau Figueras, Ted Jacobson and Toby Wiseman. 'Rotating Black Holes in Einstein-aether Theory'. Class. Quantum Grav. **39**.12 (2022), p. 125001. arXiv:2108.00005 (cit. on pp. 161, 163).

[8] A. Addazi et al. 'Quantum Gravity Phenomenology at the Dawn of the Multi-Messenger Era – A Review'. arXiv:2111.05659 [astro-ph, physics:gr-qc, physics:hep-ph, physics:hep-th] (2021). arXiv:2111.05659 (cit. on pp. 2, 177).

[9] Andrea Addazi, Antonino Marciano and Nicolas Yunes. 'Gravitational Instability of Exotic Compact Objects'. Eur. Phys. J. C **80**.1 (2020), p. 36. arXiv:1905.08734 (cit. on p. 81).

[10] Giovanni Amelino-Camelia. 'Quantum Spacetime Phenomenology'. Living Rev. Relativ. **16**.1 (2013), p. 5. arXiv:0806.0339 (cit. on p. 177).

[11] Lorenzo Annulli, Vitor Cardoso and Leonardo Gualtieri. 'Applications of the Close-Limit Approximation: Horizonless Compact Objects and Scalar Fields'. Class. Quantum Grav. **39**.10 (2022), p. 105005. arXiv:2104.11236 (cit. on p. 82).

[12] Stefano Ansoldi. 'Spherical Black Holes with Regular Center: A Review of Existing Models Including a Recent Realization with Gaussian Sources' (2008). arXiv:0802.0330 (cit. on pp. 19, 142).

[13] Nima Arkani-Hamed, Yu-tin Huang and Donal O'Connell. 'Kerr Black Holes as Elementary Particles'. J. High Energ. Phys. **2020**.1 (2020), p. 46. arXiv:1906.10100 (cit. on p. 36).

[14] Cristian Armendariz-Picon, Alberto Diez-Tejedor and Riccardo Penco. 'Effective Theory Approach to the Spontaneous Breakdown of Lorentz Invariance'. J. High Energ. Phys. **2010**.10 (2010), p. 79. arXiv:1004.5596 (cit. on p. 162).

[15] Julio Arrechea and Carlos Barceló. *Stellar Equilibrium on a Physical Vacuum Soil*. 2023. arXiv:2305.07939 (cit. on pp. 14, 33).

[16] Julio Arrechea, Carlos Barceló, Raúl Carballo-Rubio and Luis J. Garay. 'Schwarzschild Geometry Counterpart in Semiclassical Gravity'. Phys. Rev. D **101**.6 (2020), p. 064059. arXiv:1911.03213 (cit. on pp. 14, 33).

[17] Julio Arrechea, Carlos Barceló, Raúl Carballo-Rubio and Luis J. Garay. 'Reissner-Nordstr\"om Geometry Counterpart in Semiclassical Gravity' (2021). arXiv:2102.03544 (cit. on pp. 14, 33).

[18] K. G. Arun et al. 'New Horizons for Fundamental Physics with LISA'. Living Rev Relativ **25**.1 (2022), p. 4. arXiv:2205.01597 (cit. on p. 1).

[19] Eloy Ayón-Beato and Alberto García. 'The Bardeen Model as a Nonlinear Magnetic Monopole'. Physics Letters B **493**.1-2 (2000), pp. 149–152. arXiv:gr-qc/0009077 (cit. on pp. 24, 26).

[20] Eloy Ayón-Beato and Alberto García. 'Four Parametric Regular Black Hole Solution'. Gen Relativ Gravit **37**.4 (2005), pp. 635–641. arXiv:hep-th/0403229 (cit. on pp. 24, 26).

[21] Mustapha Azreg-Aïnou. 'From Static to Rotating to Conformal Static Solutions: Rotating Imperfect Fluid Wormholes with(out) Electric or Magnetic Field'. Eur. Phys. J. C **74**.5 (2014), p. 2865. arXiv:1401.4292 (cit. on pp. 39, 40, 111, 118).

[22] Mustapha Azreg-Aïnou. 'Generating Rotating Regular Black Hole Solutions without Complexification'. Phys. Rev. D **90**.6 (2014), p. 064041. arXiv:1405.2569 (cit. on pp. 39, 40, 111, 118).

[23] Mustapha Azreg-Aïnou. 'Regular and Conformal Regular Cores for Static and Rotating Solutions'. Physics Letters B **730** (2014), pp. 95–98. arXiv:1401.0787 (cit. on pp. 39, 111, 118).

[24] Joshua Baines, Thomas Berry, Alex Simpson and Matt Visser. 'Killing Tensor and Carter Constant for Painleve-Gullstrand Form of Lense-Thirring Spacetime'. Universe **7**.12 (2021), p. 473. arXiv:2110.01814 (cit. on p. 77).

[25] Leonardo Balart and Elias C. Vagenas. 'Regular Black Holes with a Nonlinear Electrodynamics Source'. Phys. Rev. D **90**.12 (2014), p. 124045. arXiv:1408.0306 (cit. on pp. 24, 26).

[26] Parth Bambhaniya, Saurabh K, Kimet Jusufi and Pankaj S. Joshi. 'Thin Accretion Disk in the Simpson-Visser Black-Bounce and Wormhole Spacetime' (2021). arXiv:2109.15054 (cit. on p. 63).

[27] Cosimo Bambi. 'Can the Supermassive Objects at the Centers of Galaxies Be Traversable Wormholes? The First Test of Strong Gravity for Mm/Sub-Mm VLBI Facilities'. Phys. Rev. D **87**.10 (2013), p. 107501. arXiv:1304.5691 (cit. on p. 22).

[28] Cosimo Bambi. 'Astrophysical Black Holes: A Review'. *Proceedings of Multifrequency Behaviour of High Energy Cosmic Sources - XIII — PoS(MULTIF2019)*. 2020, p. 028. arXiv:1906.03871 (cit. on p. 1).

[29] Cosimo Bambi, ed. *Regular Black Holes: Towards a New Paradigm of Gravitational Collapse*. Springer Series in Astrophysics and Cosmology. Singapore: Springer Nature, 2023 (cit. on p. 19).

[30] Cosimo Bambi. *X-Ray Tests of General Relativity with Black Holes*. 2023. arXiv:2305.10715 (cit. on p. 1).

[31] Cosimo Bambi and Leonardo Modesto. 'Rotating Regular Black Holes'. Physics Letters B **721**.4-5 (2013), pp. 329–334. arXiv:1302.6075 (cit. on pp. 36, 41).

[32] Cosimo Bambi, Leonardo Modesto and Leslaw Rachwal. 'Spacetime Completeness of Non-Singular Black Holes in Conformal Gravity'. JCAP **05** (2017), p. 003. arXiv:1611.00865 (cit. on pp. 109, 112).

[33] Cosimo Bambi and Dejan Stojkovic. 'Astrophysical Wormholes'. Universe **7**.5 (2021), p. 136. arXiv:2105.00881 (cit. on p. 22).

[34] Indrani Banerjee, Subhadip Sau and Soumitra SenGupta. *Signatures of Regular Black Holes from the Shadow of Sgr A* and M87**. 2022. arXiv:2206.12125 (cit. on p. 41).

[35] Leor Barack et al. 'Black Holes, Gravitational Waves and Fundamental Physics: A Roadmap'. Class. Quantum Grav. **36**.14 (2019), p. 143001. arXiv:1806.05195 (cit. on p. 2).

[36] Enrico Barausse, Ted Jacobson and Thomas P. Sotiriou. 'Black Holes in Einstein-aether and Horava-Lifshitz Gravity'. Phys. Rev. D **83**.12 (2011), p. 124043. arXiv:1104.2889 (cit. on pp. 134, 163).

[37] Enrico Barausse and Thomas P. Sotiriou. 'A No-Go Theorem for Slowly Rotating Black Holes in Horava-Lifshitz Gravity'. Phys. Rev. Lett. **109**.18 (2012), p. 181101. arXiv:1207.6370 (cit. on pp. 134, 161).

[38] Enrico Barausse and Thomas P. Sotiriou. 'Slowly Rotating Black Holes in Horava-Lifshitz Gravity'. Phys. Rev. D **87**.8 (2013), p. 087504. arXiv:1212.1334 (cit. on pp. 134, 161).

[39] Enrico Barausse, Thomas P. Sotiriou and Ian Vega. 'Slowly Rotating Black Holes in Einstein-{\ae}ther Theory'. Phys. Rev. D **93**.4 (2016), p. 044044. arXiv:1512.05894 (cit. on pp. 134, 161, 163).

[40] Enrico Barausse et al. 'Prospects for Fundamental Physics with LISA'. Gen Relativ Gravit **52**.8 (2020), p. 81. arXiv:2001.09793 (cit. on p. 1).

[41] Carlos Barceló, Valentin Boyanov, Raúl Carballo-Rubio and Luis J. Garay. 'Black Hole Inner Horizon Evaporation in Semiclassical Gravity'. Class. Quantum Grav. **38**.12 (2021), p. 125003. arXiv:2011.07331 (cit. on p. 108).

[42] Carlos Barceló, Valentin Boyanov, Raúl Carballo-Rubio and Luis J. Garay. 'Classical Mass Inflation vs Semiclassical Inner Horizon Inflation'. Phys. Rev. D **106**.12 (2022), p. 124006. arXiv:2203.13539 (cit. on p. 108).

[43] James M. Bardeen. 'Non-Singular General Relativistic Gravitational Collapse'. *Proceedings of the International Conference GR5*. Tblisi, Georgia: Tbilisi University Press, 1968 (cit. on pp. 27, 142).

[44] James M. Bardeen, William H. Press and Saul A. Teukolsky. 'Rotating Black Holes: Locally Nonrotating Frames, Energy Extraction, and Scalar Synchrotron Radiation'. The Astrophysical Journal **178** (1972), pp. 347–370 (cit. on pp. 93, 123).

[45] Andrei O. Barvinsky, Diego Blas, Mario Herrero-Valea, Sergey M. Sibiryakov and Christian F. Steinwachs. 'Renormalization of Horava Gravity'. Phys. Rev. D **93**.6 (2016), p. 064022. arXiv:1512.02250 (cit. on p. 132).

[46] Andrei O. Barvinsky, Diego Blas, Mario Herrero-Valea, Sergey M. Sibiryakov and Christian F. Steinwachs. 'Ho\v{r}ava Gravity Is Asymptotically Free (in 2+1 Dimensions)'. Phys. Rev. Lett. **119**.21 (2017), p. 211301. arXiv:1706.06809 (cit. on p. 132).

[47] Andrei O. Barvinsky, Mario Herrero-Valea and Sergey M. Sibiryakov. 'Towards the Renormalization Group Flow of Horava Gravity in $(3+1)$ Dimensions'. Phys. Rev. D **100**.2 (2019), p. 026012. arXiv:1905.03798 (cit. on p. 132).

[48] Andrei O. Barvinsky, Alexander V. Kurov and Sergey M. Sibiryakov. 'Beta Functions of $(3+1)$-Dimensional Projectable Horava Gravity'. Phys. Rev. D **105**.4 (2022), p. 044009. arXiv:2110.14688 (cit. on p. 132).

[49] Jorge Bellorin, Claudio Borquez and Byron Droguett. *BRST Symmetry and Unitarity of the Horava Theory*. 2022. arXiv:2212.14079 (cit. on p. 132).

[50] Jorge Bellorin, Claudio Borquez and Byron Droguett. 'Cancellation of Divergences in the Nonprojectable Horava Theory'. Phys. Rev. D **106**.4 (2022), p. 044055. arXiv:2207.08938 (cit. on p. 132).

[51] Philip Beltracchi and Paolo Gondolo. 'Physical Interpretation of Newman-Janis Rotating Systems. II. General Systems'. Phys. Rev. D **104**.12 (2021), p. 124067. arXiv:2108.02841 (cit. on p. 36).

[52] Philip Beltracchi and Paolo Gondolo. 'Physical Interpretation of Newman-Janis Rotating Systems. PartI : A Unique Family of Kerr-Schild Systems' (2021). arXiv:2104.02255 (cit. on p. 36).

[53] Carl M Bender and Steven A Orszag. *Advanced Mathematical Methods for Scientists and Engineers I*. 1st ed. New York, NY: Springer, New York, NY, 1999 (cit. on p. 104).

[54] Per Berglund, Jishnu Bhattacharyya and David Mattingly. 'Mechanics of Universal Horizons'. Phys. Rev. D **85**.12 (2012), p. 124019. arXiv:1202.4497 (cit. on pp. 134, 136, 137, 163).

[55] Clément Berthiere, Debajyoti Sarkar and Sergey N. Solodukhin. 'The Fate of Black Hole Horizons in Semiclassical Gravity'. Physics Letters B **786** (2018), pp. 21–27 (cit. on pp. 14, 33).

[56] Emanuele Berti, Victor Cardoso and Andrei O. Starinets. 'Quasinormal Modes of Black Holes and Black Branes'. Class. Quantum Grav. **26**.10 (2009), p. 163001 (cit. on p. 81).

[57] Emanuele Berti, Vitor Cardoso and Marc Casals. 'Eigenvalues and Eigenfunctions of Spin-Weighted Spheroidal Harmonics in Four and Higher Dimensions'. Phys. Rev. D **73**.10 (2006), p. 109902. arXiv:gr-qc/0511111 (cit. on p. 83).

[58] Emanuele Berti, Vitor Cardoso, Mark Ho-Yeuk Cheung, Francesco Di Filippo, Francisco Duque, Paul Martens and Shinji Mukohyama. 'Stability of the Fundamental Quasinormal Mode in Time-Domain Observations against Small Perturbations'. Phys. Rev. D **106**.8 (2022), p. 084011. arXiv:2205.08547 (cit. on p. 82).

[59] Emanuele Berti et al. 'Testing General Relativity with Present and Future Astrophysical Observations'. Class. Quantum Grav. **32**.24 (2015), p. 243001. arXiv:1501.07274 (cit. on p. 2).

[60] Swetha Bhagwat and Costantino Pacilio. 'Merger-Ringdown Consistency: A New Test of Strong Gravity Using Deep Learning'. Phys. Rev. D **104**.2 (2021), p. 024030. arXiv:2101.07817 (cit. on p. 82).

[61] Madhurima Bhattacharjee, Shinji Mukohyama, Mew-Bing Wan and Anzhong Wang. 'Gravitational Collapse and Formation of Universal Horizons in Einstein-æther Theory'. Phys. Rev. D **98**.6 (2018), p. 064010. arXiv:1806.00142 (cit. on p. 134).

[62] Jishnu Bhattacharyya, Mattia Colombo and Thomas P. Sotiriou. 'Causality and Black Holes in Spacetimes with a Preferred Foliation'. Class. Quantum Grav. **33**.23 (2016), p. 235003. arXiv:1509.01558 (cit. on p. 134).

[63] D. Blas, O. Pujolas and S. Sibiryakov. 'On the Extra Mode and Inconsistency of Horava Gravity'. J. High Energy Phys. **2009**.10 (2009), pp. 029–029. arXiv:0906.3046 (cit. on p. 132).

[64] D. Blas, O. Pujolas and S. Sibiryakov. 'Consistent Extension of Horava Gravity'. Phys. Rev. Lett. **104**.18 (2010), p. 181302. arXiv:0909.3525 (cit. on p. 132).

[65] D. Blas and S. Sibiryakov. 'Horava Gravity vs. Thermodynamics: The Black Hole Case'. Phys. Rev. D **84**.12 (2011), p. 124043. arXiv:1110.2195 (cit. on p. 134).

[66] Diego Blas, Oriol Pujolas and Sergey Sibiryakov. 'Models of Non-Relativistic Quantum Gravity: The Good, the Bad and the Healthy'. J. High Energ. Phys. **2011**.4 (2011), p. 18. arXiv:1007.3503 (cit. on pp. 132, 134).

[67] Alexander S. Blum, Roberto Lalli and Jürgen Renn. 'The Renaissance of General Relativity: How and Why It Happened'. Annalen der Physik **528**.5 (2016), pp. 344–349 (cit. on p. 10).

[68] Ana Bokulić, Tajron Jurić and Ivica Smolić. 'Constraints on Singularity Resolution by Nonlinear Electrodynamics' (2022). arXiv:2206.07064 (cit. on p. 24).

[69] S. V. Bolokhov, K. A. Bronnikov and M. V. Skvortsova. 'Magnetic Black Universes and Wormholes with a Phantom Scalar'. Class. Quantum Grav. **29**.24 (2012), p. 245006. arXiv:1208.4619 (cit. on pp. 24, 26, 30).

[70] A. Bonanno and M. Reuter. 'Renormalization Group Improved Black Hole Spacetimes'. Phys. Rev. D **62**.4 (2000), p. 043008. arXiv:hep-th/0002196 (cit. on p. 14).

[71] Alfio Bonanno, Amir-Pouyan Khosravi and Frank Saueressig. 'Regular Black Holes with Stable Cores'. Phys. Rev. D **103**.12 (2021), p. 124027. arXiv:2010.04226 (cit. on p. 108).

[72] Alfio Bonanno, Amir-Pouyan Khosravi and Frank Saueressig. 'Regular Evaporating Black Holes with Stable Cores'. Phys. Rev. D **107**.2 (2023), p. 024005. arXiv:2209.10612 (cit. on p. 108).

[73] Alfio Bonanno and Frank Saueressig. *Stability Properties of Regular Black Holes*. 2022. arXiv:2211.09192 (cit. on p. 108).

[74] Arvind Borde. 'Regular Black Holes and Topology Change'. Phys. Rev. D **55**.12 (1997), pp. 7615–7617. arXiv:gr-qc/9612057 (cit. on p. 16).

[75] Suddhasattwa Brahma, Che-Yu Chen and Dong-han Yeom. 'Testing Loop Quantum Gravity from Observational Consequences of Non-Singular Rotating Black Holes' (2020). arXiv:2012.08785 (cit. on p. 48).

[76] Marica Branchesi et al. 'Science with the Einstein Telescope: A Comparison of Different Designs'. J. Cosmol. Astropart. Phys. **2023**.07 (2023), p. 068. arXiv:2303.15923 (cit. on p. 1).

[77] Richard Brito, Vitor Cardoso and Paolo Pani. 'Superradiance – the 2020 Edition'. Lecture Notes in Physics, Berlin Springer Verlag **971** (2020). arXiv:1501.06570 (cit. on pp. 81, 94).

[78] David Brizuela, José M. Martín-García and Guillermo A. Mena Marugán. 'xPert: Computer Algebra for Metric Perturbation Theory'. General Relativity and Gravitation **41**.10 (2009), p. 2415 (cit. on p. 4).

[79] K. A. Bronnikov. 'Nonlinear Electrodynamics, Regular Black Holes and Wormholes'. Int. J. Mod. Phys. D **27**.06 (2018), p. 1841005. arXiv:1711.00087 (cit. on pp. 24, 26).

[80] K. A. Bronnikov. 'On Black Bounces, Wormholes and Partly Phantom Scalar Fields'. Phys. Rev. D **106**.6 (2022), p. 064029. arXiv:2206.09227 (cit. on pp. 24, 29).

[81] K. A. Bronnikov, H. Dehnen and V. N. Melnikov. 'Regular Black Holes and Black Universes'. Gen Relativ Gravit **39**.7 (2007), pp. 973–987. arXiv:gr-qc/0611022 (cit. on pp. 30, 65).

[82] K. A. Bronnikov and J. C. Fabris. 'Regular Phantom Black Holes'. Phys. Rev. Lett. **96** (2006), p. 251101. arXiv:gr-qc/0511109 (cit. on pp. 30, 65).

[83] Kirill A. Bronnikov. 'Regular Magnetic Black Holes and Monopoles from Nonlinear Electrodynamics'. Phys. Rev. D **63**.4 (2001), p. 044005. arXiv:gr-qc/0006014 (cit. on pp. 24, 26).

[84] Kirill A. Bronnikov and Roman A. Konoplya. 'Echoes in Brane Worlds: Ringing at a Black Hole–Wormhole Transition'. Phys. Rev. D **101**.6 (2020), p. 064004. arXiv:1912.05315 (cit. on p. 82).

[85] Kirill A. Bronnikov, Roman A. Konoplya and Thomas D. Pappas. 'General Parametrization of Wormhole Spacetimes and Its Application to Shadows and Quasinormal Modes' (2021). arXiv:2102.10679 (cit. on p. 22).

[86] Kirill A. Bronnikov and Rahul Kumar Walia. 'Field Sources for Simpson-Visser Spacetimes'. Phys. Rev. D **105**.4 (2022), p. 044039. arXiv:2112.13198 (cit. on pp. 24, 31).

[87] Pablo Bueno, Pablo A. Cano, Frederik Goelen, Thomas Hertog and Bert Vercnocke. 'Echoes of Kerr-like Wormholes'. Phys. Rev. D **97**.2 (2018), p. 024040. arXiv:1711.00391 (cit. on p. 82).

[88] C. P. Burgess. 'Quantum Gravity in Everyday Life: General Relativity as an Effective Field Theory'. Living Rev. Relativ. **7**.1 (2004), p. 5. arXiv:gr-qc/0311082 (cit. on p. 131).

[89] Pedro Cañate and Santiago Esteban Perez Bergliaffa. 'Transforming Singular Black Holes into Regular Black Holes Sourced by Nonlinear Electrodynamics'. Annals of Physics **454** (2023), p. 169358. arXiv:2203.03088 (cit. on pp. 24, 109).

[90] Rosangela Canonico, Luca Parisi and Gaetano Vilasi. 'The Newman Janis Algorithm: A Review of Some Results'. *Proceedings of the Twelfth International Conference on Geometry, Integrability and Quantization*. Institute of Biophysics and Biomedical Engineering, Bulgarian Academy of Sciences, 2011, pp. 159–169 (cit. on p. 36).

[91] Salvatore Capozziello, Francisco S. N. Lobo and José P. Mimoso. 'Energy Conditions in Modified Gravity'. Physics Letters B **730** (2014), pp. 280–283. arXiv:1312.0784 (cit. on p. 13).

[92] Raúl Carballo-Rubio. 'Stellar Equilibrium in Semiclassical Gravity'. Phys. Rev. Lett. **120**.6 (2018), p. 061102. arXiv:1706.05379 (cit. on pp. 14, 33).

[93] Raul Carballo-Rubio, Francesco Di Filippo, Stefano Liberati and Matt Visser. 'Causal Hierarchy in Modified Gravity'. J. High Energ. Phys. **2020**.12 (2020), p. 55. arXiv:2005.08533 (cit. on pp. 134, 143).

[94] Raúl Carballo-Rubio, Francesco Di Filippo, Stefano Liberati, Costantino Pacilio and Matt Visser. 'On the Viability of Regular Black Holes'. J. High Energ. Phys. **2018**.7 (2018), p. 23. arXiv:1805.02675 (cit. on p. 108).

[95] Raúl Carballo-Rubio, Francesco Di Filippo, Stefano Liberati, Costantino Pacilio and Matt Visser. 'Inner Horizon Instability and the Unstable Cores of Regular Black Holes'. J. High Energ. Phys. **2021**.5 (2021), p. 132. arXiv:2101.05006 (cit. on p. 108).

[96] Raúl Carballo-Rubio, Francesco Di Filippo, Stefano Liberati, Costantino Pacilio and Matt Visser. 'Regular Black Holes without Mass Inflation Instability' (2022). arXiv:2205.13556 (cit. on pp. 109, 114).

[97] Raúl Carballo-Rubio, Francesco Di Filippo, Stefano Liberati and Matt Visser. 'Geodesically Complete Black Holes'. Phys. Rev. D **101**.8 (2020), p. 084047. arXiv:1911.11200 (cit. on pp. 14, 15).

[98] Raúl Carballo-Rubio, Francesco Di Filippo, Stefano Liberati and Matt Visser. 'Opening the Pandora's Box at the Core of Black Holes'. Class. Quantum Grav. **37**.14 (2020), p. 145005. arXiv:1908.03261 (cit. on p. 14).

[99] Raúl Carballo-Rubio, Francesco Di Filippo, Stefano Liberati and Matt Visser. *A Connection between Regular Black Holes and Horizonless Ultracompact Stars*. 2022. arXiv:2211.05817 (cit. on p. 28).

[100] Raúl Carballo-Rubio, Francesco Di Filippo, Stefano Liberati and Matt Visser. 'Geodesically Complete Black Holes in Lorentz-violating Gravity'. J. High Energ. Phys. **2022**.2 (2022), p. 122. arXiv:2111.03113 (cit. on pp. 14, 144, 159, 168).

[101] Vitor Cardoso, João L. Costa, José Natário and Zhen Zhong. 'Energy Extraction from Bouncing Geometries'. Phys. Rev. D **108**.2 (2023), p. 024071. arXiv:2304.08520 (cit. on p. 107).

[102] Vitor Cardoso, Oscar J. C. Dias, Jose' P. S. Lemos and Shijun Yoshida. 'The Black Hole Bomb and Superradiant Instabilities'. Phys. Rev. D **70**.4 (2004), p. 049903. arXiv:hep-th/0404096 (cit. on p. 81).

[103] Vitor Cardoso, Edgardo Franzin and Paolo Pani. 'Is the Gravitational-Wave Ringdown a Probe of the Event Horizon?' Phys. Rev. Lett. **116**.17 (2016), p. 171101. arXiv:1602.07309 (cit. on p. 82).

[104] Vitor Cardoso, Seth Hopper, Caio F. B. Macedo, Carlos Palenzuela and Paolo Pani. 'Echoes of ECOs: Gravitational-Wave Signatures of Exotic Compact Objects and of Quantum Corrections at the Horizon Scale'. Phys. Rev. D **94**.8 (2016), p. 084031. arXiv:1608.08637 (cit. on p. 82).

[105] Vitor Cardoso, Seth Hopper, Caio F. B. Macedo, Carlos Palenzuela and Paolo Pani. 'Gravitational-Wave Signatures of Exotic Compact Objects and of Quantum Corrections at the Horizon Scale'. Phys. Rev. D **94**.8 (2016), p. 084031 (cit. on p. 82).

[106] Vitor Cardoso and Paolo Pani. 'Tests for the Existence of Horizons through Gravitational Wave Echoes'. Nat Astron **1**.9 (2017), pp. 586–591. arXiv:1709.01525 (cit. on p. 82).

[107] Vitor Cardoso and Paolo Pani. 'Testing the Nature of Dark Compact Objects: A Status Report'. Living Reviews in Relativity **22**.1 (2019), p. 4 (cit. on pp. 2, 14, 82).

[108] Vitor Cardoso, Paolo Pani, Mariano Cadoni and Marco Cavaglia. 'Ergoregion Instability of Ultra-Compact Astrophysical Objects'. Phys. Rev. D **77**.12 (2008), p. 124044. arXiv:0709.0532 (cit. on p. 81).

[109] Vitor Cardoso, Paolo Pani, Mariano Cadoni and Marco Cavaglia. 'Instability of Hyper-Compact Kerr-like Objects'. Class. Quantum Grav. **25**.19 (2008), p. 195010. arXiv:0808.1615 (cit. on pp. 81, 91).

[110] Zack Carson and Kent Yagi. 'Parameterized and Inspiral-Merger-Ringdown Consistency Tests of Gravity with Multi-Band Gravitational Wave Observations'. Phys. Rev. D **101**.4 (2020), p. 044047. arXiv:1911.05258 (cit. on p. 82).

[111] Brandon Carter. 'Global Structure of the Kerr Family of Gravitational Fields'. Phys. Rev. **174** (1968), pp. 1559–1571 (cit. on p. 76).

[112] Sumanta Chakraborty, Elisa Maggio, Anupam Mazumdar and Paolo Pani. 'Implications of the Quantum Nature of the Black Hole Horizon on the Gravitational-Wave Ringdown'. Phys. Rev. D **106**.2 (2022), p. 024041. arXiv:2202.09111 (cit. on p. 82).

[113] S. Chandrasekhar. *The Mathematical Theory of Black Holes*. Walton Street, Oxford: Oxford University Press, 1983 (cit. on pp. 49, 93, 101).

[114] S. Chandrasekhar and Steven L. Detweiler. 'The Quasi-Normal Modes of the Schwarzschild Black Hole'. Proc.Roy.Soc.Lond.A **344** (1975), pp. 441–452 (cit. on p. 86).

[115] Mark Ho-Yeuk Cheung, Kyriakos Destounis, Rodrigo Panosso Macedo, Emanuele Berti and Vitor Cardoso. 'The Elephant and the Flea: Destabilizing the Fundamental Mode of Black Holes' (2021). arXiv:2111.05415 (cit. on p. 82).

[116] Jan Chojnacki and Jan Kwapisz. 'Finite Action Principle and Hořava-Lifshitz Gravity: Early Universe, Black Holes, and Wormholes'. Phys. Rev. D **104**.10 (2021), p. 103504. arXiv:2102.13556 (cit. on p. 141).

[117] Piotr T. Chruściel, João Lopes Costa and Markus Heusler. 'Stationary Black Holes: Uniqueness and Beyond'. Living Rev Relativ **15**.1 (2012), p. 7 (cit. on p. 22).

[118] M. S. Churilova and Z. Stuchlik. 'Ringing of the Regular Black-Hole/Wormhole Transition'. Class. Quantum Grav. **37**.7 (2020), p. 075014. arXiv:1911.11823 (cit. on pp. 63, 88).

[119] C. J. S. Clarke. 'Singularities in Globally Hyperbolic Space-Time'. Commun.Math. Phys. **41**.1 (1975), pp. 65–78 (cit. on p. 9).

[120] C. J. S. Clarke. *The Analysis of Space-Time Singularities*. Cambridge Lecture Notes in Physics. Cambridge: Cambridge University Press, 1994 (cit. on p. 7).

[121] GRAVITY Collaboration et al. 'Detection of the Gravitational Redshift in the Orbit of the Star S2 near the Galactic Centre Massive Black Hole'. A&A **615** (2018), p. L15. arXiv:1807.09409 (cit. on p. 2).

[122] GRAVITY Collaboration et al. 'Detection of the Schwarzschild Precession in the Orbit of the Star S2 near the Galactic Centre Massive Black Hole'. A&A **636** (2020), p. L5. arXiv:2004.07187 (cit. on p. 2).

[123] LIGO Scientific Collaboration, Virgo Collaboration, Fermi Gamma-Ray Burst Monitor and INTEGRAL. 'Gravitational Waves and Gamma-rays from a Binary Neutron Star Merger: GW170817 and GRB 170817A'. ApJ **848**.2 (2017), p. L13. arXiv:1710.05834 (cit. on p. 1).

[124] LIGO Scientific Collaboration et al. 'Multi-Messenger Observations of a Binary Neutron Star Merger'. ApJ **848**.2 (2017), p. L12. arXiv:1710.05833 (cit. on pp. 1, 163).

[125] The LIGO Scientific Collaboration and The Virgo Collaboration. 'GW170817: Observation of Gravitational Waves from a Binary Neutron Star Inspiral'. Phys. Rev. Lett. **119**.16 (2017), p. 161101. arXiv:1710.05832 (cit. on pp. 1, 163).

[126] The LIGO Scientific Collaboration and the Virgo Collaboration. 'Observation of Gravitational Waves from a Binary Black Hole Merger'. Phys. Rev. Lett. **116**.6 (2016), p. 061102. arXiv:1602.03837 (cit. on p. 1).

[127] The LIGO Scientific Collaboration et al. 'GWTC-1: A Gravitational-Wave Transient Catalog of Compact Binary Mergers Observed by LIGO and Virgo during the First and Second Observing Runs'. Phys. Rev. X **9**.3 (2019), p. 031040. arXiv:1811.12907 (cit. on p. 1).

[128] The LIGO Scientific Collaboration et al. *GWTC-3: Compact Binary Coalescences Observed by LIGO and Virgo During the Second Part of the Third Observing Run*. 2021. arXiv:2111.03606 (cit. on p. 1).

[129] Bethan Cropp, Stefano Liberati, Arif Mohd and Matt Visser. 'Ray Tracing Einstein-{\AE}ther Black Holes: Universal versus Killing Horizons'. Phys. Rev. D **89**.6 (2014), p. 064061. arXiv:1312.0405 (cit. on p. 172).

[130] Bethan Cropp, Stefano Liberati and Matt Visser. 'Surface Gravities for Non-Killing Horizons'. Class. Quantum Grav. **30**.12 (2013), p. 125001. arXiv:1302.2383 (cit. on p. 55).

[131] Erik Curiel. 'The Analysis of Singular Spacetimes'. Philosophy of Science **66** (1999), S119–S145. JSTOR: 188766 (cit. on p. 11).

[132] Erik Curiel. 'Singularities and Black Holes'. *The Stanford Encyclopedia of Philosophy*. Ed. by Edward N. Zalta and Uri Nodelman. Summer 2023. Metaphysics Research Lab, Stanford University, 2023 (cit. on p. 11).

[133] De-Chang Dai, Djordje Minic and Dejan Stojkovic. 'How to Form a Wormhole'. arXiv:2010.03947 [gr-qc, physics:hep-th] (2020). arXiv:2010.03947 (cit. on p. 22).

[134] Thibault Damour and Sergey N. Solodukhin. 'Wormholes as Black Hole Foils'. Phys. Rev. D **76**.2 (2007), p. 024016. arXiv:0704.2667 (cit. on p. 22).

[135] Marco A. A. de Paula, Haroldo C. D. Lima Junior, Pedro V. P. Cunha and Luís C. B. Crispino. *Electrically Charged Regular Black Holes in Nonlinear Electrodynamics: Light Rings, Shadows and Gravitational Lensing*. 2023. arXiv:2305.04776 (cit. on p. 24).

[136] F. Del Porro, M. Herrero-Valea, S. Liberati and M. Schneider. 'Gravitational Tunneling in Lorentz Violating Gravity'. Phys. Rev. D **106**.6 (2022), p. 064055. arXiv:2207.08848 (cit. on p. 137).

[137] Francesco Del Porro, Mario Herrero-Valea, Stefano Liberati and Marc Schneider. 'Time Orientability and Particle Production from Universal Horizons'. Phys. Rev. D **105**.10 (2022), p. 104009. arXiv:2201.03584 (cit. on pp. 135, 137).

[138] Riccardo Della Monica and Ivan de Martino. 'Unveiling the Nature of SgrA* with the Geodesic Motion of S-stars'. J. Cosmol. Astropart. Phys. **2022**.03 (2022), p. 007. arXiv:2112.01888 (cit. on p. 63).

[139] Ramit Dey, Shauvik Biswas and Sumanta Chakraborty. 'Ergoregion Instability and Echoes for Braneworld Black Holes: Scalar, Electromagnetic and Gravitational Perturbations'. Phys. Rev. D **103**.8 (2021), p. 084019. arXiv:2010.07966 (cit. on p. 81).

[140] Francesco Di Filippo. 'Beyond General Relativity: Modified Theories and Non-Singular Black Holes'. PhD thesis. SISSA, SISSA, Trieste, 2020 (cit. on p. 14).

[141] Francesco Di Filippo, Raúl Carballo-Rubio, Stefano Liberati, Costantino Pacilio and Matt Visser. 'On the Inner Horizon Instability of Non-Singular Black Holes'. Universe **8**.4 (2022), p. 204 (cit. on p. 108).

[142] Tuan Do et al. 'Relativistic Redshift of the Star So-2 Orbiting the Galactic Center Supermassive Black Hole'. Science **365**.6454 (2019), pp. 664–668. arXiv:1907.10731 (cit. on p. 2).

[143] John F. Donoghue. 'Quantum Gravity as a Low Energy Effective Field Theory'. Scholarpedia **12**.4 (2017), p. 32997 (cit. on p. 131).

[144] Irina Dymnikova. 'Vacuum Nonsingular Black Hole'. General Relativity and Gravitation **24** (1992), pp. 235–242 (cit. on pp. 27, 142).

[145] Irina Dymnikova and Evgeny Galaktionov. 'Regular Rotating Electrically Charged Black Holes and Solitons in Non-Linear Electrodynamics Minimally Coupled to Gravity'. Class. Quantum Grav. **32**.16 (2015), p. 165015. arXiv:1510.01353 (cit. on p. 41).

[146] Irina Dymnikova and Evgeny Galaktionov. 'Basic Generic Properties of Regular Rotating Black Holes and Solitons'. Advances in Mathematical Physics **2017** (2017), e1035381 (cit. on p. 41).

[147] Astrid Eichhorn and Aaron Held. 'From a Locality-Principle for New Physics to Image Features of Regular Spinning Black Holes with Disks'. J. Cosmol. Astropart. Phys. **2021**.05 (2021), p. 073. arXiv:2103.13163 (cit. on pp. 25, 41).

[148] Astrid Eichhorn and Aaron Held. 'Image Features of Spinning Regular Black Holes Based on a Locality Principle'. Eur. Phys. J. C **81**.10 (2021), p. 933. arXiv:2103.07473 (cit. on p. 41).

[149] Astrid Eichhorn, Aaron Held and Philipp-Vincent Johannsen. 'Universal Signatures of Singularity-Resolving Physics in Photon Rings of Black Holes and Horizonless Objects'. J. Cosmol. Astropart. Phys. **2023**.01 (2023), p. 043. arXiv:2204.02429 (cit. on p. 41).

[150] Christopher Eling and Ted Jacobson. 'Black Holes in Einstein-Aether Theory'. Class. Quantum Grav. **23**.18 (2006), p. 5643. arXiv:gr-qc/0604088 (cit. on pp. 134, 163).

[151] Christopher Eling and Ted Jacobson. 'Spherical Solutions in Einstein-Aether Theory: Static Aether and Stars'. Class. Quantum Grav. **23**.18 (2006), p. 5625. arXiv:gr-qc/0603058 (cit. on p. 136).

[152] Homer G. Ellis. 'Ether Flow through a Drainhole: A Particle Model in General Relativity'. Journal of Mathematical Physics **14**.1 (1973), pp. 104–118 (cit. on p. 30).

[153] Harold Erbin. 'Janis-Newman Algorithm: Generating Rotating and NUT Charged Black Holes'. Universe **3**.1 (2017), p. 19. arXiv:1701.00037 (cit. on pp. 36, 72).

[154] Milko Estrada and Rodrigo Aros. 'A New Class of Regular Black Holes in Einstein Gauss Bonnet Gravity with Localized Sources of Matter'. Physics Letters B **844** (2023), p. 138090. arXiv:2305.17233 (cit. on p. 24).

[155] Event Horizon Telescope Collaboration et al. 'First Sagittarius A* Event Horizon Telescope Results. I. The Shadow of the Supermassive Black Hole in the Center of the Milky Way'. ApJL **930**.2 (2022), p. L12 (cit. on p. 1).

[156] Event Horizon Telescope Collaboration et al. 'First Sagittarius A* Event Horizon Telescope Results. II. EHT and Multiwavelength Observations, Data Processing, and Calibration'. ApJL **930**.2 (2022), p. L13 (cit. on p. 1).

[157] Event Horizon Telescope Collaboration et al. 'First Sagittarius A* Event Horizon Telescope Results. III. Imaging of the Galactic Center Supermassive Black Hole'. ApJL **930**.2 (2022), p. L14 (cit. on p. 1).

[158] Event Horizon Telescope Collaboration et al. 'First Sagittarius A* Event Horizon Telescope Results. IV. Variability, Morphology, and Black Hole Mass'. ApJL **930**.2 (2022), p. L15 (cit. on p. 1).

[159] Event Horizon Telescope Collaboration et al. 'First Sagittarius A* Event Horizon Telescope Results. V. Testing Astrophysical Models of the Galactic Center Black Hole'. ApJL **930**.2 (2022), p. L16 (cit. on p. 1).

[160] Event Horizon Telescope Collaboration et al. 'First Sagittarius A* Event Horizon Telescope Results. VI. Testing the Black Hole Metric'. ApJL **930**.2 (2022), p. L17 (cit. on p. 1).

[161] Zhong-Ying Fan and Xiaobao Wang. 'Construction of Regular Black Holes in General Relativity'. Phys. Rev. D **94**.12 (2016), p. 124027. arXiv:1610.02636 (cit. on pp. 26, 27).

[162] Rafael Ferraro. 'Untangling the Newman-Janis Algorithm'. Gen Relativ Gravit **46**.4 (2014), p. 1705. arXiv:1311.3946 (cit. on p. 36).

[163] Nicola Franchini, Mario Herrero-Valea and Enrico Barausse. 'The Relation between General Relativity and a Class of Ho\v{r}ava Gravity Theories'. Phys. Rev. D **103**.8 (2021), p. 084012. arXiv:2103.00929 (cit. on pp. 133, 164).

[164] Nicola Franchini, Mehdi Saravani and Thomas P. Sotiriou. 'Black Hole Horizons at the Extremal Limit in Lorentz-violating Gravity'. Phys. Rev. D **96**.10 (2017), p. 104044. arXiv:1707.09283 (cit. on p. 134).

[165] Edgardo Franzin, Stefano Liberati, Jacopo Mazza, Ramit Dey and Sumanta Chakraborty. 'Scalar Perturbations around Rotating Regular Black Holes and Wormholes: Quasi-Normal Modes, Ergoregion Instability and Superradiance'. Phys. Rev. D **105**.12 (2022), p. 124051. arXiv:2201.01650 (cit. on pp. 3, 99).

[166] Edgardo Franzin, Stefano Liberati, Jacopo Mazza, Alex Simpson and Matt Visser. 'Charged Black-Bounce Spacetimes'. J. Cosmol. Astropart. Phys. **2021**.07 (2021), p. 036. arXiv:2104.11376 (cit. on pp. 3, 65, 77, 99).

[167] Edgardo Franzin, Stefano Liberati, Jacopo Mazza and Vania Vellucci. 'Stable Rotating Regular Black Holes'. Phys. Rev. D **106**.10 (2022), p. 104060. arXiv:2207.08864 (cit. on p. 4).

[168] Edgardo Franzin, Stefano Liberati and Mauro Oi. 'Superradiance in Kerr-like Black Holes'. Phys. Rev. D **103**.10 (2021), p. 104034. arXiv:2102.03152 (cit. on pp. 81, 91).

[169] V. Frolov and I. Novikov. *Black Hole Physics: Basic Concepts and New Developments*. Fundamental Theories of Physics. Springer Netherlands, 1998 (cit. on pp. 75, 101).

[170] Valeri P. Frolov. 'Notes on Non-Singular Models of Black Holes'. Phys. Rev. D **94**.10 (2016), p. 104056. arXiv:1609.01758 (cit. on p. 142).

[171] Valeri P. Frolov, Pavel Krtouš and David Kubizňák. 'Black Holes, Hidden Symmetries, and Complete Integrability'. Living Rev Relativ **20**.1 (2017), p. 6 (cit. on pp. 78, 79).

[172] Ke Gao and Lei-Hua Liu. *Can Wormholes and Black Holes Be Distinguished by Magnification?* 2023. arXiv:2307.16627 (cit. on p. 63).

[173] Sushant G. Ghosh. 'A Nonsingular Rotating Black Hole'. Eur. Phys. J. C **75**.11 (2015), p. 532. arXiv:1408.5668 (cit. on p. 27).

[174] Sushant G. Ghosh, Muhammed Amir and Sunil D. Maharaj. 'Ergosphere and Shadow of a Rotating Regular Black Hole'. Nuclear Physics B **957** (2020), p. 115088. arXiv:2006.07570 (cit. on p. 41).

[175] Elena Giorgi. *The Carter Tensor and the Physical-Space Analysis in Perturbations of Kerr-Newman Spacetime*. 2021. arXiv:2105.14379 (cit. on p. 77).

[176] Marc H. Goroff and Augusto Sagnotti. 'The Ultraviolet Behavior of Einstein Gravity'. Nucl. Phys. B **266** (1986), pp. 709–736 (cit. on p. 131).

[177] Merce Guerrero, Gonzalo J. Olmo, Diego Rubiera-Garcia and Diego Sáez-Chillón Gómez. 'Light Ring Images of Double Photon Spheres in Black Hole and Wormhole Space-Times'. Phys. Rev. D **105**.8 (2022), p. 084057. arXiv:2202.03809 (cit. on p. 63).

[178] Alfredo Guevara, Ben Maybee, Alexander Ochirov, Donal O'Connell and Justin Vines. 'A Worldsheet for Kerr' (2020). arXiv:2012.11570 (cit. on p. 36).

[179] Carsten Gundlach and José M. Martín-García. 'Critical Phenomena in Gravitational Collapse'. Living Rev. Relativ. **10**.1 (2007), p. 5 (cit. on p. 32).

[180] Toral Gupta, Mario Herrero-Valea, Diego Blas, Enrico Barausse, Neil Cornish, Kent Yagi and Nicolás Yunes. 'New Binary Pulsar Constraints on Einstein-{\ae}ther Theory after GW170817'. Class. Quantum Grav. **38**.19 (2021), p. 195003. arXiv:2104.04596 (cit. on p. 163).

[181] Metin Gürses and Feza Gürsey. 'Lorentz Covariant Treatment of the Kerr–Schild Geometry'. Journal of Mathematical Physics **16**.12 (2008), pp. 2385–2390 (cit. on p. 41).

[182] Hal M. Haggard and Carlo Rovelli. 'Black Hole Fireworks: Quantum-Gravity Effects Outside the Horizon Spark Black to White Hole Tunneling'. Phys. Rev. D **92**.10 (2015), p. 104020. arXiv:1407.0989 (cit. on pp. 14, 32).

[183] Devin Hansen and Nicolas Yunes. 'Applicability of the Newman-Janis Algorithm to Black Hole Solutions of Modified Gravity Theories'. Phys. Rev. D **88**.10 (2013), p. 104020. arXiv:1308.6631 (cit. on p. 36).

[184] S. W. Hawking and G. F. R. Ellis. *The Large Scale Structure of Space-Time*. Cambridge Monographs on Mathematical Physics. Cambridge: Cambridge University Press, 1973 (cit. on pp. 7, 10, 24, 70, 75, 120, 149).

[185] Sean A. Hayward. 'General Laws of Black-Hole Dynamics'. Phys. Rev. D **49**.12 (1994), pp. 6467–6474. arXiv:gr-qc/9303006 (cit. on p. 21).

[186] Sean A. Hayward. 'Dynamic Wormholes'. Int. J. Mod. Phys. D **08**.03 (1999), pp. 373–382. arXiv:gr-qc/9805019 (cit. on p. 22).

[187] Sean A. Hayward. 'Formation and Evaporation of Non-Singular Black Holes'. Phys. Rev. Lett. **96**.3 (2006), p. 031103. arXiv:gr-qc/0506126 (cit. on pp. 27, 28, 142).

[188] M. Herrero-Valea. *The Status of Horava Gravity*. 2023. arXiv:2307.13039 (cit. on p. 132).

[189] Mario Herrero-Valea, Stefano Liberati and Raquel Santos-Garcia. 'Hawking Radiation from Universal Horizons'. J. High Energ. Phys. **2021**.4 (2021), p. 255. arXiv:2101.00028 (cit. on p. 137).

[190] Markus Heusler. *Black Hole Uniqueness Theorems*. Cambridge Lecture Notes in Physics. Cambridge: Cambridge University Press, 1996 (cit. on p. 169).

[191] Shahar Hod. 'Onset of Superradiant Instabilities in Rotating Spacetimes of Exotic Compact Objects'. J. High Energ. Phys. **2017**.6 (2017), p. 132. arXiv:1704.05856 (cit. on p. 81).

[192] Petr Horava. 'Quantum Gravity at a Lifshitz Point'. Phys. Rev. D **79**.8 (2009), p. 084008. arXiv:0901.3775 (cit. on p. 132).

[193] Gary T. Horowitz, Don Marolf, Jorge E. Santos and Diandian Wang. 'Creating a Traversable Wormhole'. Class. Quantum Grav. **36**.20 (2019), p. 205011. arXiv:1904.02187 (cit. on p. 22).

[194] Gary T. Horowitz and Robert Myers. 'The Value of Singularities'. Gen Relat Gravit **27**.9 (1995), pp. 915–919. arXiv:gr-qc/9503062 (cit. on p. 14).

[195] Shafqat Ul Islam, Jitendra Kumar and Sushant G. Ghosh. 'Strong Gravitational Lensing by Rotating Simpson-Visser Black Holes'. JCAP **10** (2021), p. 013. arXiv:2104.00696 (cit. on p. 63).

[196] Sai Iyer. 'Black-Hole Normal Modes: A WKB Approach. II. Schwarzschild Black Holes'. Phys. Rev. D **35**.12 (1987), pp. 3632–3636 (cit. on p. 87).

[197] Sai Iyer and Clifford M. Will. 'Black-Hole Normal Modes: A WKB Approach. I. Foundations and Application of a Higher-Order WKB Analysis of Potential-Barrier Scattering'. Phys. Rev. D **35**.12 (1987), pp. 3621–3631 (cit. on pp. 86, 87).

[198] T. Jacobson and D. Mattingly. 'Einstein-Aether Waves'. Phys. Rev. D **70**.2 (2004), p. 024003. arXiv:gr-qc/0402005 (cit. on p. 164).

[199] Ted Jacobson. 'When Is G_{tt} G_{rr} = -1?' Class. Quantum Grav. **24**.22 (2007), pp. 5717–5719. arXiv:0707.3222 (cit. on pp. 20, 21).

[200] Ted Jacobson. 'Einstein-Æther Gravity: A Status Report'. *Proceedings of From Quantum to Emergent Gravity: Theory and Phenomenology — PoS(QG-Ph)*. Vol. 43. SISSA Medialab, 2008, p. 020 (cit. on pp. 133, 162).

[201] Ted Jacobson. 'Extended Horava Gravity and Einstein-aether Theory'. Phys. Rev. D **81**.10 (2010), p. 101502. arXiv:1001.4823 (cit. on p. 133).

[202] Ted Jacobson. 'Initial Value Constraints with Tensor Matter'. Class. Quant. Grav. **28** (2011), p. 245011. arXiv:1108.1496 (cit. on p. 135).

[203] Ted Jacobson. 'Undoing the Twist: The Ho\v{r}ava Limit of Einstein-aether'. Phys. Rev. D **89**.8 (2014), p. 081501. arXiv:1310.5115 (cit. on pp. 133, 162, 163).

[204] Ted Jacobson and David Mattingly. 'Gravity with a Dynamical Preferred Frame'. Phys. Rev. D **64**.2 (2001), p. 024028. arXiv:gr-qc/0007031 (cit. on pp. 133, 162).

[205] Khadije Jafarzade, Mahdi Kord Zangeneh and Francisco S. N. Lobo. 'Observational Optical Constraints of Regular Black Holes'. Annals of Physics **446** (2022), p. 169126. arXiv:2106.13893 (cit. on p. 63).

[206] Stefan Janiszewski, Andreas Karch, Brandon Robinson and David Sommer. 'Charged Black Holes in Horava Gravity'. J. High Energ. Phys. **2014**.4 (2014), p. 163. arXiv:1401.6479 (cit. on p. 134).

[207] José Luis Jaramillo, Rodrigo Panosso Macedo and Lamis Al Sheikh. 'Gravitational Wave Signatures of Black Hole Quasi-Normal Mode Instability' (2021). arXiv:2105.03451 (cit. on p. 82).

[208] José Luis Jaramillo, Rodrigo Panosso Macedo and Lamis Al Sheikh. 'Pseudospectrum and Black Hole Quasi-Normal Mode (in)Stability'. Phys. Rev. X **11**.3 (2021), p. 031003. arXiv:2004.06434 (cit. on p. 82).

[209] Sohan Kumar Jha and Anisur Rahaman. 'Superradiance Scattering off Rotating Simpson-Visser Black Hole and Its Shadow in the Non-Commutative Setting' (2022). arXiv:2208.13176 (cit. on p. 63).

[210] Tim Johannsen. 'Regular Black Hole Metric with Three Constants of Motion'. Phys. Rev. D **88**.4 (2013), p. 044002. arXiv:1501.02809 (cit. on p. 82).

[211] Tim Johannsen. 'Sgr A* and General Relativity'. Class. Quantum Grav. **33**.11 (2016), p. 113001. arXiv:1512.03818 (cit. on p. 82).

[212] Pankaj S. Joshi. *Gravitational Collapse and Spacetime Singularities*. Cambridge Monographs on Mathematical Physics. Cambridge: Cambridge University Press, 2007 (cit. on p. 7).

[213] Haroldo C. D. Lima Junior, Carolina L. Benone and Luís C. B. Crispino. 'Scalar Scattering by Black Holes and Wormholes'. Eur. Phys. J. C **82**.7 (2022), p. 638 (cit. on p. 63).

[214] José Tarciso S. S. Junior and Manuel E. Rodrigues. 'Coincident f(Q) Gravity: Black Holes, Regular Black Holes and Black Bounces'. Eur. Phys. J. C **83**.6 (2023), p. 475. arXiv:2306.04661 (cit. on p. 24).

[215] Kimet Jusufi. 'Regular Black Holes in Verlinde's Emergent Gravity' (2022). arXiv:2208.12979 (cit. on p. 24).

[216] Kimet Jusufi, Mubasher Jamil, Hrishikesh Chakrabarty, Qiang Wu, Cosimo Bambi and Anzhong Wang. 'Rotating Regular Black Holes in Conformal Massive Gravity'. Phys. Rev. D **101**.4 (2020), p. 044035. arXiv:1911.07520 (cit. on p. 109).

[217] Vicky Kalogera et al. *The Next Generation Global Gravitational Wave Observatory: The Science Book*. 2021. arXiv:2111.06990 (cit. on p. 1).

[218] Alexander Kamenshchik and Polina Petriakova. 'Newman-Janis Algorithm's Application to Regular Black Hole Models'. Phys. Rev. D **107**.12 (2023), p. 124020. arXiv:2305.04697 (cit. on p. 41).

[219] Sayan Kar, Naresh Dadhich and Matt Visser. 'Quantifying Energy Condition Violations in Traversable Wormholes'. Pramana - J Phys **63**.4 (2004), pp. 859–864 (cit. on p. 58).

[220] Roy P. Kerr. *Discovering the Kerr and Kerr-Schild Metrics*. 2008. arXiv:0706.1109 (cit. on p. 35).

[221] K. D. Kokkotas. 'Normal Modes of the Kerr Black Hole'. Class. Quant. Grav. **8** (1991), pp. 2217–2224 (cit. on p. 86).

[222] Kostas D. Kokkotas and Bernd G. Schmidt. 'Quasi-Normal Modes of Stars and Black Holes'. Living Rev. Relativ. **2**.1 (1999), p. 2 (cit. on p. 81).

[223] R. A. Konoplya. 'Quasinormal Behavior of the D-dimensional Schwarzshild Black Hole and Higher Order WKB Approach'. Phys. Rev. D **68**.2 (2003), p. 024018. arXiv:gr-qc/0303052 (cit. on p. 87).

[224] R. A. Konoplya and A. Zhidenko. 'Passage of Radiation through Wormholes of Arbitrary Shape'. Phys. Rev. D **81**.12 (2010), p. 124036. arXiv:1004.1284 (cit. on p. 92).

[225] R. A. Konoplya and A. Zhidenko. 'Quasinormal Modes of Black Holes: From Astrophysics to String Theory'. Rev. Mod. Phys. **83**.3 (2011), pp. 793–836. arXiv:1102.4014 (cit. on p. 81).

[226] R. A. Konoplya, A. Zhidenko and A. F. Zinhailo. 'Higher Order WKB Formula for Quasinormal Modes and Grey-Body Factors: Recipes for Quick and Accurate Calculations'. Class. Quantum Grav. **36**.15 (2019), p. 155002. arXiv:1904.10333 (cit. on pp. 87, 88).

[227] Roman Konoplya and Alexander Zhidenko. 'Detection of Gravitational Waves from Black Holes: Is There a Window for Alternative Theories?' Physics Letters B **756** (2016), pp. 350–353. arXiv:1602.04738 (cit. on p. 82).

[228] A. Kovetz and T. Piran. 'The Efficiency of the Penrose Process'. Lett. Nuovo Cimento **12**.2 (1975), pp. 39–42 (cit. on pp. 93, 123).

[229] Rahul Kumar and Sushant G. Ghosh. 'Black Hole Parameter Estimation from Its Shadow'. ApJ **892**.2 (2020), p. 78. arXiv:1811.01260 (cit. on p. 27).

[230] Rahul Kumar, Amit Kumar and Sushant G. Ghosh. 'Testing Rotating Regular Metrics as Candidates for Astrophysical Black Holes'. ApJ **896**.1 (2020), p. 89. arXiv:2006.09869 (cit. on pp. 27, 41).

[231] Chen Lan and Yi-Fan Wang. 'Singularities of Regular Black Holes and the Monodromy Method for Asymptotic Quasinormal Modes'. Chinese Phys. C (2022). arXiv:2205.05935 (cit. on pp. 27, 42).

[232] Chen Lan, Hao Yang, Yang Guo and Yan-Gang Miao. *Regular Black Holes: A Short Topic Review*. 2023. arXiv:2303.11696 (cit. on p. 19).

[233] Guillermo Lara, Mario Herrero-Valea, Enrico Barausse and Sergey M. Sibiryakov. 'Black Holes in Ultraviolet-Complete Horava Gravity'. Phys. Rev. D **103**.10 (2021), p. 104007. arXiv:2103.01975 (cit. on p. 140).

[234] E. W. Leaver and Subrahmanyan Chandrasekhar. 'An Analytic Representation for the Quasi-Normal Modes of Kerr Black Holes'. Proceedings of the Royal Society of London. A. Mathematical and Physical Sciences **402**.1823 (1985), pp. 285–298 (cit. on p. 83).

[235] Stefano Liberati. 'Tests of Lorentz Invariance: A 2013 Update'. Class. Quantum Grav. **30**.13 (2013), p. 133001. arXiv:1304.5795 (cit. on p. 131).

[236] Stefano Liberati, Luca Maccione and Thomas P. Sotiriou. 'Scale Hierarchy in Horava-Lifshitz Gravity: A Strong Constraint from Synchrotron Radiation in the Crab Nebula'. Phys. Rev. Lett. **109**.15 (2012), p. 151602. arXiv:1207.0670 (cit. on p. 131).

[237] A. Lima, G. Alencar and J. Furtado. *Black String Bounce to Traversable Wormhole*. 2022. arXiv:2211.12349 (cit. on p. 31).

[238] Arthur Lima, Geová Alencar and Diego Sáez-Chillon Gómez. *Regularizing Rotating Black Strings: A New Black Bounce Solution*. 2023. arXiv:2307.07404 (cit. on p. 31).

[239] Haroldo C. D. Lima Junior, Carolina L. Benone and Luís C. B. Crispino. 'Scalar Absorption: Black Holes versus Wormholes'. Phys. Rev. D **101**.12 (2020), p. 124009. arXiv:2006.03967 (cit. on pp. 63, 96).

[240] Haroldo C. D. Lima Junior, Lu\'ıs C. B. Crispino and Atsushi Higuchi. 'On-Axis Tidal Forces in Kerr Spacetime'. Eur. Phys. J. Plus **135**.3 (2020), p. 334. arXiv:2003.09506 (cit. on p. 65).

[241] Haroldo C. D. Lima Junior, Luís C. B. Crispino, Pedro V. P. Cunha and Carlos A. R. Herdeiro. 'Spinning Black Holes with a Separable Hamilton-Jacobi Equation from a Modified Newman-Janis Algorithm'. Eur. Phys. J. C **80**.11 (2020), p. 1036. arXiv:2011.07301 (cit. on p. 40).

[242] Haroldo C. D. Lima Junior, Luís C. B. Crispino, Pedro V. P. Cunha and Carlos A. R. Herdeiro. 'Can Different Black Holes Cast the Same Shadow?' Phys. Rev. D **103**.8 (2021), p. 084040. arXiv:2102.07034 (cit. on p. 63).

[243] Kai Lin and Wei-Liang Qian. 'Ellis Drainhole Solution in Einstein-{\AE}ther Gravity and the Axial Gravitational Quasinormal Modes'. Eur. Phys. J. C **82**.6 (2022), p. 529. arXiv:2203.03081 (cit. on p. 141).

[244] Francisco S. N. Lobo and Aaron V. B. Arellano. 'Gravastars Supported by Nonlinear Electrodynamics'. Class. Quantum Grav. **24**.5 (2007), pp. 1069–1088. arXiv:gr-qc/0611083 (cit. on pp. 14, 24).

[245] Francisco S. N. Lobo, Manuel E. Rodrigues, Marcos V. de S. Silva, Alex Simpson and Matt Visser. 'Novel Black-Bounce Spacetimes: Wormholes, Regularity, Energy Conditions, and Causal Structure'. Phys. Rev. D **103**.8 (2021), p. 084052. arXiv:2009.12057 (cit. on pp. 25, 31, 65).

[246] Francisco S. N. Lobo, Alex Simpson and Matt Visser. 'Dynamic Thin-Shell Black-Bounce Traversable Wormholes'. Phys. Rev. D **101**.12 (2020), p. 124035. arXiv:2003.09419 (cit. on pp. 31, 65).

[247] R. Loll, G. Fabiano, D. Frattulillo and F. Wagner. *Quantum Gravity in 30 Questions*. 2022. arXiv:2206.06762 (cit. on p. 131).

[248] Malcolm A. H. MacCallum. 'Computer Algebra in Gravity Research'. Living Rev Relativ **21**.1 (2018), p. 6 (cit. on p. 4).

[249] Hideki Maeda. 'Quest for Realistic Non-Singular Black-Hole Geometries: Regular-center Type'. J. High Energ. Phys. **2022**.11 (2022), p. 108. arXiv:2107.04791 (cit. on pp. 19, 41, 142).

[250] Elisa Maggio, Vitor Cardoso, Sam R. Dolan and Paolo Pani. 'Ergoregion Instability of Exotic Compact Objects: Electromagnetic and Gravitational Perturbations and the Role of Absorption'. Phys. Rev. D **99**.6 (2019), p. 064007. arXiv:1807.08840 (cit. on p. 81).

[251] Elisa Maggio, Paolo Pani and Valeria Ferrari. 'Exotic Compact Objects and How to Quench Their Ergoregion Instability'. Phys. Rev. D **96**.10 (2017), p. 104047. arXiv:1703.03696 (cit. on p. 81).

[252] Elisa Maggio, Paolo Pani and Guilherme Raposo. 'Testing the Nature of Dark Compact Objects with Gravitational Waves'. 2021, pp. 1–37. arXiv:2105.06410 (cit. on p. 82).

[253] M. Maggiore. *Gravitational Waves: Volume 2: Astrophysics and Cosmology*. Oxford University Press, 2018 (cit. on p. 81).

[254] Michele Maggiore et al. 'Science Case for the Einstein Telescope'. J. Cosmol. Astropart. Phys. **2020**.03 (2020), pp. 050–050. arXiv:1912.02622 (cit. on pp. 1, 82).

[255] Daniele Malafarina. 'Classical Collapse to Black Holes and Quantum Bounces: A Review'. Universe **3**.2 (2017), p. 48. arXiv:1703.04138 (cit. on pp. 29, 32).

[256] Daniele Malafarina and Sabina Sagynbayeva. 'What a Difference a Quadrupole Makes?' (2020). arXiv:2009.12839 (cit. on p. 35).

[257] Juan Maldacena and Alexey Milekhin. 'Humanly Traversable Wormholes' (2020). arXiv:2008.06618 (cit. on p. 22).

[258] Jose M. Martin-Garcia, Renato Portugal and Leon R. U. Mansur. 'The Invar Tensor Package'. Computer Physics Communications **177**.8 (2007), pp. 640–648. arXiv:0704.1756 (cit. on p. 4).

[259] Jose M. Martin-Garcia, David Yllanes and Renato Portugal. 'The Invar Tensor Package: Differential Invariants of Riemann'. Computer Physics Communications **179**.8 (2008), pp. 586–590. arXiv:0802.1274 (cit. on p. 4).

[260] José M. Martín-García. *xAct: Efficient Tensor Computer Algebra for the Wolfram Language*. 2002 (cit. on p. 4).

[261] Prado Martin-Moruno and Matt Visser. 'Essential Core of the Hawking–Ellis Types'. Class. Quantum Grav. **35**.12 (2018), p. 125003. arXiv:1802.00865 (cit. on p. 70).

[262] Prado Martin-Moruno and Matt Visser. 'Hawking-Ellis Classification of Stress-Energy: Test-Fields versus Back-Reaction'. Phys. Rev. D **103**.12 (2021), p. 124003. arXiv:2102.13551 (cit. on pp. 24, 70).

[263] Prado Martín-Moruno and Matt Visser. 'Generalized Rainich Conditions, Generalized Stress-Energy Conditions, and the Hawking-Ellis Classification'. Class. Quantum Grav. **34**.22 (2017), p. 225014. arXiv:1707.04172 (cit. on p. 70).

[264] Angel D. Masa and Vilson T. Zanchin. 'Rotating Regular Black Holes and Rotating Stars with a Tolman Type Potential as a Regular Interior for the Kerr Metric' (2022). arXiv:2204.08113 (cit. on p. 41).

[265] David Mattingly. 'Modern Tests of Lorentz Invariance'. Living Rev. Relativ. **8**.1 (2005), p. 5. arXiv:gr-qc/0502097 (cit. on p. 131).

[266] Jerzy Matyjasek and Michał Opala. 'Quasinormal Modes of Black Holes. The Improved Semianalytic Approach'. Phys. Rev. D **96**.2 (2017), p. 024011. arXiv:1704.00361 (cit. on p. 87).

[267] Pawel O. Mazur and Emil Mottola. *Dark Energy and Condensate Stars: Casimir Energy in the Large*. 2004. arXiv:gr-qc/0405111 (cit. on p. 14).

[268] Pawel O. Mazur and Emil Mottola. 'Gravitational Vacuum Condensate Stars'. Proc. Natl. Acad. Sci. U.S.A. **101**.26 (2004), pp. 9545–9550. arXiv:gr-qc/0407075 (cit. on pp. 14, 28).

[269] Pawel O. Mazur and Emil Mottola. 'Gravitational Condensate Stars: An Alternative to Black Holes'. Universe **9**.2 (2023), p. 88. arXiv:gr-qc/0109035 (cit. on p. 14).

[270] Jacopo Mazza, Edgardo Franzin and Stefano Liberati. 'A Novel Family of Rotating Black Hole Mimickers'. J. Cosmol. Astropart. Phys. **2021**.04 (2021), p. 082. arXiv:2102.01105 (cit. on pp. 3, 54, 65, 99).

[271] Jacopo Mazza and Stefano Liberati. 'Regular Black Holes and Horizonless Ultra-Compact Objects in Lorentz-Violating Gravity'. J. High Energ. Phys. **2023**.3 (2023), p. 199. arXiv:2301.04697 (cit. on p. 4).

[272] A. J. M. Medved, Damien Martin and Matt Visser. 'Dirty Black Holes: Spacetime Geometry and near-Horizon Symmetries'. Class. Quantum Grav. **21**.13 (2004), pp. 3111–3125. arXiv:gr-qc/0402069 (cit. on p. 70).

[273] A. J. M. Medved, Damien Martin and Matt Visser. 'Dirty Black Holes: Symmetries at Stationary Non-Static Horizons'. Phys. Rev. D **70**.2 (2004), p. 024009. arXiv:gr-qc/0403026 (cit. on p. 70).

[274] Luis Felipe Longo Micchi, Niayesh Afshordi and Cecilia Chirenti. 'How Loud Are Echoes from Exotic Compact Objects?' arXiv:2010.14578 [gr-qc] (2020). arXiv:2010.14578 (cit. on p. 82).

[275] Charles W. Misner, K. S. Thorne and J. A. Wheeler. *Gravitation*. San Francisco: W. H. Freeman, 1973 (cit. on p. 71).

[276] Michael S. Morris and Kip S. Thorne. 'Wormholes in Spacetime and Their Use for Interstellar Travel: A Tool for Teaching General Relativity'. American Journal of Physics **56**.5 (1988), pp. 395–412 (cit. on p. 22).

[277] Michael S. Morris, Kip S. Thorne and Ulvi Yurtsever. 'Wormholes, Time Machines, and the Weak Energy Condition'. Phys. Rev. Lett. **61**.13 (1988), pp. 1446–1449 (cit. on p. 22).

[278] Emil Mottola. 'The Effective Theory of Gravity and Dynamical Vacuum Energy'. J. High Energ. Phys. **2022**.11 (2022), p. 37. arXiv:2205.04703 (cit. on pp. 14, 28).

[279] Emil Mottola. 'Gravitational Vacuum Condensate Stars'. *Regular Black Holes: Towards a New Paradigm of Gravitational Collapse*. Ed. by Cosimo Bambi. Springer Series in Astrophysics and Cosmology. Singapore: Springer Nature, 2023, pp. 283–352. arXiv:2302.09690 (cit. on p. 28).

[280] Yerlan Myrzakulov, Kairat Myrzakulov, Sudhaker Upadhyay and Dharm Veer Singh. 'Quasinormal Modes and Phase Structure of Regular AdS Einstein-Gauss-Bonnet Black Holes'. Int. J. Geom. Methods Mod. Phys. **20**.07 (2023), p. 2350121. arXiv:2305.11201 (cit. on p. 24).

[281] Hiroyuki Nakano, Norichika Sago, Hideyuki Tagoshi and Takahiro Tanaka. 'Black Hole Ringdown Echoes and Howls'. Progress of Theoretical and Experimental Physics **2017**.7 (2017) (cit. on p. 82).

[282] Kamal Kanti Nandi, Yuan-Zhong Zhang and K. B. Vijaya Kumar. 'Volume Integral Theorem for Exotic Matter'. Phys. Rev. D **70**.12 (2004), p. 127503. arXiv:gr-qc/0407079 (cit. on p. 58).

[283] J. V. Narlikar and A. K. Kembhavi. 'Space-Time Singularities and Conformal Gravity'. Lett. Nuovo Cim. **19** (1977), pp. 517–520 (cit. on p. 109).

[284] Deloshan Nawarajan and Matt Visser. 'Global Properties of Physically Interesting Lorentzian Spacetimes'. Int. J. Mod. Phys. D **25**.14 (2016), p. 1650106. arXiv:1601.03355 (cit. on p. 69).

[285] E. T. Newman, E. Couch, K. Chinnapared, A. Exton, A. Prakash and R. Torrence. 'Metric of a Rotating, Charged Mass'. Journal of Mathematical Physics **6**.6 (1965), pp. 918–919 (cit. on pp. 35, 76).

[286] E. T. Newman and A. I. Janis. 'Note on the Kerr Spinning-Particle Metric'. Journal of Mathematical Physics **6**.6 (1965), pp. 915–917 (cit. on p. 35).

[287] Ezra Newman and Tim Adamo. 'Kerr-Newman Metric'. Scholarpedia **9**.10 (2014), p. 31791 (cit. on p. 35).

[288] Shin'ichi Nojiri and G. G. L. Nashed. *Hayward Black Hole in Scalar-Einstein-Gauss-Bonnet Gravity in Four Dimensions*. 2023. arXiv:2306.14162 (cit. on p. 24).

[289] Hans-Peter Nollert. 'Quasinormal Modes: The Characteristic 'sound' of Black Holes and Neutron Stars'. Class. Quantum Grav. **16**.12 (1999), R159 (cit. on p. 81).

[290] Jacob Oost, Shinji Mukohyama and Anzhong Wang. 'Spherically Symmetric Exact Vacuum Solutions in Einstein-aether Theory'. Universe **7**.8 (2021), p. 272. arXiv:2106.09044 (cit. on p. 134).

[291] Amos Ori. 'Inner Structure of a Charged Black Hole: An Exact Mass-Inflation Solution'. Phys. Rev. Lett. **67**.7 (1991), pp. 789–792 (cit. on p. 108).

[292] Paolo Pani, Enrico Barausse, Emanuele Berti and Vitor Cardoso. 'Gravitational Instabilities of Superspinars'. Phys. Rev. D **82**.4 (2010), p. 044009. arXiv:1006.1863 (cit. on pp. 81, 104).

[293] Nicos Pelavas, Nicholas Neary and Kayll Lake. 'Properties of the Instantaneous Ergo Surface of a Kerr Black Hole'. Class. Quantum Grav. **18**.7 (2001), pp. 1319–1331. arXiv:gr-qc/0012052 (cit. on p. 103).

[294] R. Penrose and R. M. Floyd. 'Extraction of Rotational Energy from a Black Hole'. Nature Physical Science **229**.6 (1971), pp. 177–179 (cit. on pp. 93, 123).

[295] Roger Penrose. 'Gravitational Collapse and Space-Time Singularities'. Phys. Rev. Lett. **14**.3 (1965), pp. 57–59 (cit. on p. 10).

[296] E. Poisson and W. Israel. 'Inner-Horizon Instability and Mass Inflation in Black Holes'. Phys. Rev. Lett. **63**.16 (1989), pp. 1663–1666 (cit. on p. 108).

[297] I. Prasetyo, H. S. Ramadhan and A. Sulaksono. 'An Ultracompact Object from Semi-classical Gravity'. Phys. Rev. D **103**.12 (2021), p. 123536. arXiv:2105.11691 (cit. on pp. 14, 33).

[298] William H. Press and Saul A. Teukolsky. 'Floating Orbits, Superradiant Scattering and the Black-hole Bomb'. Nature **238** (1972), pp. 211–212 (cit. on p. 81).

[299] M. Punturo et al. 'The Einstein Telescope: A Third-Generation Gravitational Wave Observatory'. Class. Quantum Grav. **27**.19 (2010), p. 194002 (cit. on p. 1).

[300] Del Rajan. 'Complex Spacetimes and the Newman-Janis Trick'. MA thesis. Wellington, New Zeland: Victoria University of Wellington, 2015. arXiv:1601.03862 (cit. on p. 36).

[301] Del Rajan and Matt Visser. 'Cartesian Kerr-Schild Variation on the Newman-Janis Ansatz'. Int. J. Mod. Phys. D **26**.14 (2017), p. 1750167. arXiv:1601.03532 (cit. on p. 36).

[302] David Reitze et al. 'Cosmic Explorer: The U.S. Contribution to Gravitational-Wave Astronomy beyond LIGO'. Bull. Am. Astron. Soc. **51**.7 (2019), p. 035. arXiv:1907.04833 (cit. on p. 1).

[303] Christopher S. Reynolds. 'Observing Black Holes Spin'. Nat Astron **3**.1 (2019), pp. 41–47. arXiv:1903.11704 (cit. on p. 35).

[304] Shafqat Riaz, Askar B. Abdikamalov and Cosimo Bambi. *Testing Regular Black Holes with X-ray Data of GX~339–4*. 2023. arXiv:2306.09673 (cit. on p. 63).

[305] Shafqat Riaz, Swarnim Shashank, Rittick Roy, Askar B. Abdikamalov, Dimitry Ayzenberg, Cosimo Bambi, Zuobin Zhang and Menglei Zhou. 'Testing Regular Black Holes with X-ray and GW Data'. J. Cosmol. Astropart. Phys. **2022**.10 (2022), p. 040. arXiv:2206.03729 (cit. on p. 63).

[306] Manuel E. Rodrigues and Marcos V. de S. Silva. 'Bardeen Regular Black Hole With an Electric Source'. J. Cosmol. Astropart. Phys. **2018**.06 (2018), pp. 025–025. arXiv:1802.05095 (cit. on pp. 24, 26).

[307] Manuel E. Rodrigues and Marcos V. de S. Silva. 'Black Bounces with Multiple Throats and Anti-Throats' (2022). arXiv:2204.11851 (cit. on p. 31).

[308] Carlo Rovelli and Francesca Vidotto. 'Planck Stars'. Int. J. Mod. Phys. D **23**.12 (2014), p. 1442026. arXiv:1401.6562 (cit. on pp. 14, 32).

[309] Fintan D. Ryan. 'Gravitational Waves from the Inspiral of a Compact Object into a Massive, Axisymmetric Body with Arbitrary Multipole Moments'. Phys. Rev. D **52**.10 (1995), pp. 5707–5718 (cit. on p. 116).

[310] Alberto Salvio. 'Quadratic Gravity'. Front. Phys. **6** (2018), p. 77. arXiv:1804.09944 (cit. on p. 131).

[311] B. Sathyaprakash et al. 'Scientific Objectives of Einstein Telescope'. Class. Quantum Grav. **29**.12 (2012), p. 124013. arXiv:1206.0331 (cit. on p. 1).

[312] Bernard F. Schutz and Clifford M. Will. 'BLACK HOLE NORMAL MODES: A SEMIANALYTIC APPROACH'. Astrophys. J. Lett. **291** (1985), pp. L33–L36 (cit. on p. 86).

[313] Lorenzo Sebastiani and Sergio Zerbini. 'Some Remarks on Non-Singular Spherically Symmetric Space-Times' (2022). arXiv:2206.03814 (cit. on pp. 19, 142).

[314] Edward Seidel and Sai Iyer. 'Black-Hole Normal Modes: A WKB Approach. IV. Kerr Black Holes'. Phys. Rev. D **41**.2 (1990), pp. 374–382 (cit. on p. 86).

[315] José M. M. Senovilla. 'Singularity Theorems and Their Consequences'. General Relativity and Gravitation **30**.5 (1998), pp. 701–848. arXiv:1801.04912 (cit. on p. 10).

[316] José M. M. Senovilla and David Garfinkle. 'The 1965 Penrose Singularity Theorem'. Class. Quantum Grav. **32**.12 (2015), p. 124008. arXiv:1410.5226 (cit. on pp. 10, 11).

[317] Rajibul Shaikh, Kunal Pal, Kuntal Pal and Tapobrata Sarkar. 'Constraining Alternatives to the Kerr Black Hole'. Monthly Notices of the Royal Astronomical Society **506**.1 (2021), pp. 1229–1236. arXiv:2102.04299 (cit. on pp. 63, 65).

[318] B. Shakerin et al. *Scalar Curvature Invariants in Classical and Quantum Gravity*. 2021. arXiv:2106.05926 (cit. on p. 25).

[319] Alex Simpson. 'From Black-Bounce to Traversable Wormhole, and Beyond' (2021). arXiv:2110.05657 (cit. on pp. 31, 65).

[320] Alex Simpson. 'Excising Curvature Singularities from General Relativity'. PhD thesis. arXiv, 2023. arXiv:2304.07383 (cit. on pp. 25, 31).

[321] Alex Simpson, Prado Martin-Moruno and Matt Visser. 'Vaidya Spacetimes, Black-Bounces, and Traversable Wormholes'. Class. Quantum Grav. **36**.14 (2019), p. 145007. arXiv:1902.04232 (cit. on p. 31).

[322] Alex Simpson and Matt Visser. 'Black-Bounce to Traversable Wormhole'. J. Cosmol. Astropart. Phys. **2019**.02 (2019), pp. 042–042. arXiv:1812.07114 (cit. on pp. 30, 31, 53, 65, 70).

[323] Alex Simpson and Matt Visser. 'Regular Black Holes with Asymptotically Minkowski Cores'. Universe **6**.1 (2019), p. 8. arXiv:1911.01020 (cit. on p. 27).

[324] K. S. Stelle. 'Classical Gravity with Higher Derivatives'. Gen Relat Gravit **9**.4 (1978), pp. 353–371 (cit. on p. 131).

[325] Hans Stephani, Dietrich Kramer, Malcolm MacCallum, Cornelius Hoenselaers and Eduard Herlt. *Exact Solutions of Einstein's Field Equations*. 2nd ed. Cambridge Monographs on Mathematical Physics. Cambridge: Cambridge University Press, 2003 (cit. on pp. 25, 54).

[326] P. Szekeres and S.P. Drake. 'An Explanation of the Newman-Janis Algorithm'. General Relativity and Gravitation **32**.3 (2000), pp. 445–457. arXiv:gr-qc/9807001 (cit. on pp. 36, 38, 54).

[327] Edward Teo. 'Rotating Traversable Wormholes'. Phys. Rev. D **58**.2 (1998), p. 024014 (cit. on pp. 22, 61).

[328] S. A. Teukolsky and W. H. Press. 'Perturbations of a Rotating Black Hole. III - Interaction of the Hole with Gravitational and Electromagnet Ic Radiation'. Astrophys. J. **193** (1974), pp. 443–461 (cit. on p. 94).

[329] The Event Horizon Telescope Collaboration et al. 'First M87 Event Horizon Telescope Results. I. The Shadow of the Supermassive Black Hole'. ApJL **875**.1 (2019), p. L1 (cit. on p. 1).

[330] The Event Horizon Telescope Collaboration et al. 'First M87 Event Horizon Telescope Results. II. Array and Instrumentation'. ApJL **875**.1 (2019), p. L2 (cit. on p. 1).

[331] The Event Horizon Telescope Collaboration et al. 'First M87 Event Horizon Telescope Results. III. Data Processing and Calibration'. ApJL **875**.1 (2019), p. L3 (cit. on p. 1).

[332] The Event Horizon Telescope Collaboration et al. 'First M87 Event Horizon Telescope Results. IV. Imaging the Central Supermassive Black Hole'. ApJL **875**.1 (2019), p. L4 (cit. on p. 1).

[333] The Event Horizon Telescope Collaboration et al. 'First M87 Event Horizon Telescope Results. V. Physical Origin of the Asymmetric Ring'. ApJL **875**.1 (2019), p. L5 (cit. on p. 1).

[334] The Event Horizon Telescope Collaboration et al. 'First M87 Event Horizon Telescope Results. VI. The Shadow and Mass of the Central Black Hole'. ApJL **875**.1 (2019), p. L6 (cit. on p. 1).

[335] The Event Horizon Telescope Collaboration et al. 'First M87 Event Horizon Telescope Results. VII. Polarization of the Ring'. ApJL **910**.1 (2021), p. L12 (cit. on p. 1).

[336] The Event Horizon Telescope Collaboration et al. 'First M87 Event Horizon Telescope Results. VIII. Magnetic Field Structure near The Event Horizon'. ApJL **910**.1 (2021), p. L13 (cit. on p. 1).

[337] The NANOGrav Collaboration et al. 'The NANOGrav 15 Yr Data Set: Bayesian Limits on Gravitational Waves from Individual Supermassive Black Hole Binaries'. ApJL **951**.2 (2023), p. L50 (cit. on p. 1).

[338] The NANOGrav Collaboration et al. 'The NANOGrav 15 Yr Data Set: Detector Characterization and Noise Budget'. ApJL **951**.1 (2023), p. L10 (cit. on p. 1).

[339] The NANOGrav Collaboration et al. 'The NANOGrav 15 Yr Data Set: Evidence for a Gravitational-wave Background'. ApJL **951**.1 (2023), p. L8 (cit. on p. 1).

[340] The NANOGrav Collaboration et al. 'The NANOGrav 15 Yr Data Set: Observations and Timing of 68 Millisecond Pulsars'. ApJL **951**.1 (2023), p. L9 (cit. on p. 1).

[341] The NANOGrav Collaboration et al. 'The NANOGrav 15 Yr Data Set: Search for Signals from New Physics'. ApJL **951**.1 (2023), p. L11 (cit. on p. 1).

[342] Yoshimune Tomikawa, Keisuke Izumi and Tetsuya Shiromizu. 'New Definition of Wormhole Throat' (2015) (cit. on p. 22).

[343] Ramón Torres. 'Regular Rotating Black Holes'. *Regular Black Holes: Towards a New Paradigm of Gravitational Collapse*. Ed. by Cosimo Bambi. Springer Series in Astrophysics and Cosmology. Singapore: Springer Nature, 2023, pp. 421–446. arXiv:2208.12713 (cit. on pp. 10, 25, 41).

[344] Ramon Torres. *The Interiors of Singularity-Free Rotating Black Holes*. 2023. arXiv:2307.12096 (cit. on p. 42).

[345] Ramon Torres and Francesc Fayos. 'On Regular Rotating Black Holes'. Gen Relativ Gravit **49**.1 (2017), p. 2. arXiv:1611.03654 (cit. on pp. 10, 41).

[346] Bobir Toshmatov, Bobomurat Ahmedov, Ahmadjon Abdujabbarov and Zdeněk Stuchlík. 'Rotating Regular Black Hole Solution'. Phys. Rev. D **89**.10 (2014), p. 104017. arXiv:1404.6443 (cit. on p. 41).

[347] Naoki Tsukamoto. 'Black Hole Shadow in an Asymptotically-Flat, Stationary, and Axisymmetric Spacetime: The Kerr-Newman and Rotating Regular Black Holes'. Phys. Rev. D **97**.6 (2018), p. 064021. arXiv:1708.07427 (cit. on pp. 27, 41).

[348] Naoki Tsukamoto. 'Gravitational Lensing by Two Photon Spheres in a Black-Bounce Spacetime in Strong Deflection Limits'. Phys. Rev. D **104**.6 (2021), p. 064022. arXiv:2105.14336 (cit. on p. 63).

[349] Bobur Turimov. 'On Generic Rotating Regular Black Hole Solutions'. Annals Phys. **434** (2021), p. 168658 (cit. on p. 41).

[350] Sunny Vagnozzi et al. 'Horizon-Scale Tests of Gravity Theories and Fundamental Physics from the Event Horizon Telescope Image of Sagittarius A$\hat{*}$'. Class. Quantum Grav. **40**.16 (2023), p. 165007. arXiv:2205.07787 (cit. on p. 63).

[351] Vania Vellucci, Edgardo Franzin and Stefano Liberati. 'Echoes from Backreacting Exotic Compact Objects'. Phys. Rev. D **107**.4 (2023), p. 044027. arXiv:2205.14170 (cit. on p. 82).

[352] Matt Visser. 'Dirty Black Holes: Thermodynamics and Horizon Structure'. Phys. Rev. D **46**.6 (1992), pp. 2445–2451 (cit. on p. 70).

[353] Matt Visser. *Lorentzian Wormholes: From Einstein to Hawking*. AIP-Press, 1996 (cit. on pp. 16, 24, 55).

[354] Matt Visser. 'The Kerr Spacetime: A Brief Introduction'. *Kerr Fest: Black Holes in Astrophysics, General Relativity and Quantum Gravity*. 2007. arXiv:0706.0622 (cit. on pp. 65, 76).

[355] Matt Visser, Carlos Barcelo, Stefano Liberati and Sebastiano Sonego. 'Small, Dark, and Heavy: But Is It a Black Hole?' PoS **BHGRS** (2008), p. 010. arXiv:0902.0346 (cit. on p. 14).

[356] Matt Visser, Sayan Kar and Naresh Dadhich. 'Traversable Wormholes with Arbitrarily Small Energy Condition Violations'. Phys. Rev. Lett. **90**.20 (2003), p. 201102. arXiv:gr-qc/0301003 (cit. on p. 58).

[357] Matt Visser and David L. Wiltshire. 'Stable Gravastars - an Alternative to Black Holes?' Class. Quantum Grav. **21**.4 (2004), pp. 1135–1151. arXiv:gr-qc/0310107 (cit. on p. 14).

[358] Robert M. Wald. 'Energy Limits on the Penrose Process'. The Astrophysical Journal **191** (1974), pp. 231–234 (cit. on pp. 93, 123).

[359] Robert M. Wald. *General Relativity*. Chicago, USA: Chicago Univ. Pr., 1984 (cit. on pp. 4, 7, 9, 19, 171).

[360] Rahul Kumar Walia, Sushant G. Ghosh and Sunil D. Maharaj. 'Testing Rotating Regular Metrics with EHT Results of Sgr A*'. ApJ **939**.2 (2022), p. 77. arXiv:2207.00078 (cit. on p. 41).

[361] Steven Weinstein and Dean Rickles. 'Quantum Gravity'. *The Stanford Encyclopedia of Philosophy*. Ed. by Edward N. Zalta and Uri Nodelman. Summer 2023. Metaphysics Research Lab, Stanford University, 2023 (cit. on p. 131).

[362] David L. Wiltshire, Matt Visser and Susan M. Scott. *The Kerr Spacetime: Rotating Black Holes in General Relativity*. Cambridge University Press, 2009 (cit. on pp. 42, 65, 76).

[363] Benjamin Withers. 'Einstein-Aether as a Quantum Effective Field Theory'. Class. Quantum Grav. **26**.22 (2009), p. 225009. arXiv:0905.2446 (cit. on p. 162).

[364] R. P Woodard. 'Ostrogradsky's Theorem on Hamiltonian Instability'. Scholarpedia **10**.8 (2015), p. 32243 (cit. on p. 131).

[365] Kent Yagi and Leo C. Stein. 'Black Hole Based Tests of General Relativity'. Classical and Quantum Gravity **33**.5 (2016), p. 054001 (cit. on p. 1).

[366] Jinbo Yang and Hyat Huang. 'Trapping Horizons of the Evolving Charged Wormhole and Black Bounce' (2021). arXiv:2104.11134 (cit. on p. 65).

[367] Yi Yang, Dong Liu, Ali Övgün, Zheng-Wen Long and Zhaoyi Xu. 'Quasinormal Modes of Kerr-like Black Bounce Spacetime' (2022). arXiv:2205.07530 (cit. on p. 63).

[368] Yi Yang, Dong Liu, Zhaoyi Xu, Yujia Xing, Shurui Wu and Zheng-Wen Long. 'Echoes of Novel Black-Bounce Spacetimes'. Phys. Rev. D **104**.10 (2021), p. 104021. arXiv:2107.06554 (cit. on p. 63).

[369] Xu Ye, Chao-Hui Wang and Shao-Wen Wei. *Extracting Spinning Wormhole Energy via Magnetic Reconnection*. 2023. arXiv:2306.12097 (cit. on p. 63).

[370] E. Zakhary and C. B. G. Mcintosh. 'A Complete Set of Riemann Invariants'. General Relativity and Gravitation **29**.5 (1997), pp. 539–581 (cit. on p. 25).

[371] Chao Zhang, Xiang Zhao, Kai Lin, Shaojun Zhang, Wen Zhao and Anzhong Wang. 'Spherically Symmetric Static Black Holes in Einstein-aether Theory'. Phys. Rev. D **102**.6 (2020), p. 064043. arXiv:2004.06155 (cit. on p. 163).

[372] Lihang Zhou, Richard Brito, Zhan-Feng Mai and Lijing Shao. *Superradiant Instabilities of Massive Bosons around Exotic Compact Objects*. 2023. arXiv:2308.03091 (cit. on p. 81).

[373] Tian Zhou and Leonardo Modesto. *Geodesic Incompleteness of Some Popular Regular Black Holes*. 2022. arXiv:2208.02557 (cit. on pp. 27, 42).

COLOPHON

The cover is drawn over a still from a simulation by:
N. Fischer, H. Pfeiffer, A. Buonanno (Max Planck Institute for Gravitational Physics), Simulating eXtreme Spacetimes (SXS) Collaboration;

https://www.ligo.caltech.edu/image/ligo20200420a

This document was typeset using the typographical look-and-feel `classicthesis` developed by André Miede. The style was inspired by Robert Bringhurst's seminal book on typography "*The Elements of Typographic Style*". `classicthesis` is available for both LaTeX and LyX:

https://bitbucket.org/amiede/classicthesis/

Final Version as of 5th November 2023 (`classicthesis`).